EPA-600/4-76-016c
May 1976

Environmental Monitoring Series

CONTINUED RESEARCH IN MESOSCALE AIR POLLUTION SIMULATION MODELING: Volume III - Modeling of Microscale Phenomena

Environmental Sciences Research Laboratory
Office of Research and Development
U.S. Environmental Protection Agency
Research Triangle Park, North Carolina 27711

RESEARCH REPORTING SERIES

Research reports of the Office of Research and Development, U.S. Environmental Protection Agency, have been grouped into five series. These five broad categories were established to facilitate further development and application of environmental technology. Elimination of traditional grouping was consciously planned to foster technology transfer and a maximum interface in related fields. The five series are:

1. Environmental Health Effects Research
2. Environmental Protection Technology
3. Ecological Research
4. Environmental Monitoring
5. Socioeconomic Environmental Studies

This report has been assigned to the ENVIRONMENTAL MONITORING series. This series describes research conducted to develop new or improved methods and instrumentation for the identification and quantification of environmental pollutants at the lowest conceivably significant concentrations. It also includes studies to determine the ambient concentrations of pollutants in the environment and/or the variance of pollutants as a function of time or meteorological factors.

This document is available to the public through the National Technical Information Service, Springfield, Virginia 22161.

EPA 600/4-76-016 C
May 1976

CONTINUED RESEARCH IN MESOSCALE AIR POLLUTION SIMULATION MODELING: VOLUME III - MODELING OF MICROSCALE PHENOMENA

by

R. G. Lamb

Systems Applications, Incorporated
950 Northgate Drive
San Rafael, California 94903

68-02-1237

Project Officer

Kenneth L. Demerjian
Meteorology and Assessment Division
Enviromental Sciences Research Laboratory
Research Triangle Park, North Carolina 27711

U.S. ENVIRONMENTAL PROTECTION AGENCY
OFFICE OF RESEARCH AND DEVELOPMENT
ENVIRONMENTAL SCIENCES RESEARCH LABORATORY
RESEARCH TRIANGLE PARK, NORTH CAROLINA 27711

DISCLAIMER

This report has been reviewed by the Office of Research and Development, U.S. Environmental Protection Agency, and approved for publication. Mention of trade names or commercial products does not constitute endorsement or recommendation for use.

CONTENTS

ILLUSTRATIONS

TABLES

ACKNOWLEDGMENTS

The calculations of the optimal diffusivity profiles reported in Chapter II were performed in collaboration with Drs. W. Chen and J. H. Seinfeld of the Department of Chemical Engineering, California Institute of Technology. The author also wishes to thank Mr. Winston Shu of the California Institute of Technology for his assistance with the theory reported in Chapter III and for making available excerpts from his doctoral thesis, which is presently in preparation, for use in this report.

I OVERVIEW

In this report, the term "microscale" refers to all phenomena that have characteristic temporal or spatial scales that are too small to be resolvable in an explicit, deterministic manner in urban-scale air pollution simulation models. Turbulence, concentration fluctuations, and subgrid-scale concentration variations are examples of microscale phenomena. In this chapter, we outline theoretically the way in which each of these important microscale features arises; in subsequent chapters of this volume, we propose techniques for dealing with each in air pollution modeling studies.

Consider the case of two pollutant species, A and B, that undergo the reaction

$$A + B \rightarrow C \quad .$$

The fundamental equation governing the concentrations of each species is the so-called mass continuity equation, which in the case of A has the form

$$\frac{\partial A}{\partial t} + \frac{\partial}{\partial x_i}(u_i A) = \kappa \frac{\partial^2 A}{\partial x_i \partial x_i} + S_A - kAB \quad , \tag{1}$$

where

A = the instantaneous concentration of A at the point (x_1, x_2, x_3, t) ,

u_i = the i-th component of the instantaneous fluid velocity at the same point,

S_A = the source strength (mass/volume/time),

κ = the molecular diffusivity (of both A and B),

k = the rate constant of the chemical reaction.

In an application of Eq. (1) to a simulation of A in the atmosphere, information concerning the instantaneous fluid velocity, u, is available only from a few widely scattered meteorological stations. It can be shown using the sampling theorem that from such a finite set of discrete observations, only the features of the velocity field with spatial scales larger than about twice the average distance between sampling points can be described explicitly [see Lamb and Seinfeld (1973)]. All smaller features are unresolvable and must be treated as stochastic variables. Thus, in an atmospheric simulation, u_i must be expressed in the form

$$u_i = \bar{u}_i + u_i' \quad ,$$

where $\bar{u}_i$ is the mean velocity component, which embodies all of the large, resolvable features of the wind field, and u_i' represents all of the unresolvable features. The latter, which is usually called the turbulent velocity component, represents a microscale phenomenon according to our definition. Because of the stochastic nature of u_i', both A and B are stochastic; consequently, only their averaged properties have meaning. In air pollution studies, one of the most important averaged properties of the concentration is the mean, or first moment, which we denote by angular parentheses. Taking the mean of Eq. (1), we find that $\langle A \rangle$ is governed by the equation (assuming an incompressible atmosphere)

$$\frac{\partial \langle A \rangle}{\partial t} + u_i \frac{\partial \langle A \rangle}{\partial x_i} + \frac{\partial}{\partial x_i} \langle u_i' A \rangle = \kappa \frac{\partial^2 \langle A \rangle}{\partial x_i \partial x_i} + S_A - k \langle A \rangle \langle B \rangle - \langle A' B' \rangle \quad . \quad (2)$$

In this equation, we have taken $\langle\ \rangle$ to be an ensemble average, which can be regarded loosely as a time average. The quantities A' and B' represent instantaneous departures of the concentrations of species A and B, respectively, from each one's mean values. Induced by the velocity fluctuations u_i', both A' and B' are unresolvable and have definitions similar to that of u_i':

$$\begin{aligned} A' &= A - \langle A \rangle \quad , \\ B' &= B - \langle B \rangle \quad . \end{aligned} \quad (3)$$

It is readily apparent from Eq. (2) that the microscale velocity variations u_i' affect the mean concentration $\langle A \rangle$ both directly, through the transport term $\langle u_i' A' \rangle$, and indirectly, through the concentration fluctuation term $\langle A'B' \rangle$. Both of these effects must be expressed in terms of $\langle A \rangle$, $\langle B \rangle$, or other known variables before Eq. (2) can be solved, because otherwise the equation contains three unknown quantities: $\langle A \rangle$, $\langle u'A' \rangle$, and $\langle A'B' \rangle$.

In the case where u_i' is caused solely by turbulence in the planetary boundary layer, the most well-known method for approximating the fluctuating transport term $\langle u_i' A' \rangle$ is the so-called gradient transport approximation, proposed originally by Boussinesq in the nineteenth century. Under this hypothesis,

$$\langle u'_i \, A' \rangle = -K_{ij} \frac{\partial \langle A \rangle}{\partial x_j} \quad , \tag{4}$$

where K_{ij} is an empirical quantity called the turbulent diffusivity tensor. Theoretical expressions (based on similarity theory) are available for some of the components of K_{ij}, but these are restricted to the surface layer, which usually represents only a small portion of the layer into which pollutants mix under typical urban atmospheric conditions. In Chapter II, we discuss this diffusivity in more detail and present new expressions for the diffusivity--applicable to the entire mixed layer--which we derived using a new approach.

In cases where u_i' is caused both by ambient boundary layer turbulence and by perturbations of other origins, such as buoyancy forces (when the pollutant is hot) or turbulence generated in the wake of a large building or hill, methods other than the simple transport theory [Eq. (4)] must be used. The well-known plume rise formulas are examples of attempts to compensate for buoyancy effects on u_i'. In Chapter VI, we outline a technique for obtaining refined estimates of the transport term $\langle u_i' A' \rangle$ in problems where buoyancy forces play an important role.

Mathematical approximations for the fluctuation term $\langle A'B' \rangle$ have not been used heretofore in urban-scale air pollution models; such terms have simply been omitted. It is known, however, that this simplification is unjustified, especially for small-scale modeling and for fast chemical reactions. In Chapter III, we discuss some of the approximations that previous investigators have proposed for these terms, and we develop and test our own formulation. For the time being, let us write

$$\langle A'B' \rangle \simeq F_{AB} \quad . \tag{5}$$

Using Eqs. (4) and (5), we obtain the model equation:

$$\frac{\partial \langle A \rangle_m}{\partial t} + \bar{u}_i \frac{\partial \langle A \rangle_m}{\partial x_i} = \frac{\partial}{\partial x_i} K_{ij} \frac{\partial \langle A \rangle_m}{\partial x_j} + S_A - k \langle A \rangle_m \langle B \rangle_m - k F_{AB} \quad . \tag{6}$$

It is important to realize that this equation is actually a model of the "true" equation [Eq. (2)] because it contains approximations of the terms $\langle u_i' A' \rangle$ and $\langle A'B' \rangle$. To emphasize this point, we have designated the solution of Eq. (6) as $\langle A \rangle_m$ to distinguish it from the true mean value $\langle A \rangle$. These two quantities are related as follows:

$$\langle A \rangle_m = \langle A \rangle + \varepsilon (K_{ij}, F_{AB}) \quad , \tag{7}$$

where ε is an error term whose value is a function of the model approximations used for $\langle u_i' A' \rangle$ and $\langle A'B' \rangle$. Note also that we have dropped the molecular diffusivity term from Eq. (6) because it is known that relative to turbulent diffusion, molecular diffusion is negligible insofar as the mean $\langle A \rangle$ is concerned.

Figure 1, which summarizes the analyses presented up to this point, illustrates how A, $\langle A \rangle$, and $\langle A \rangle_m$ would relate to actual data gathered from pollution monitoring stations.

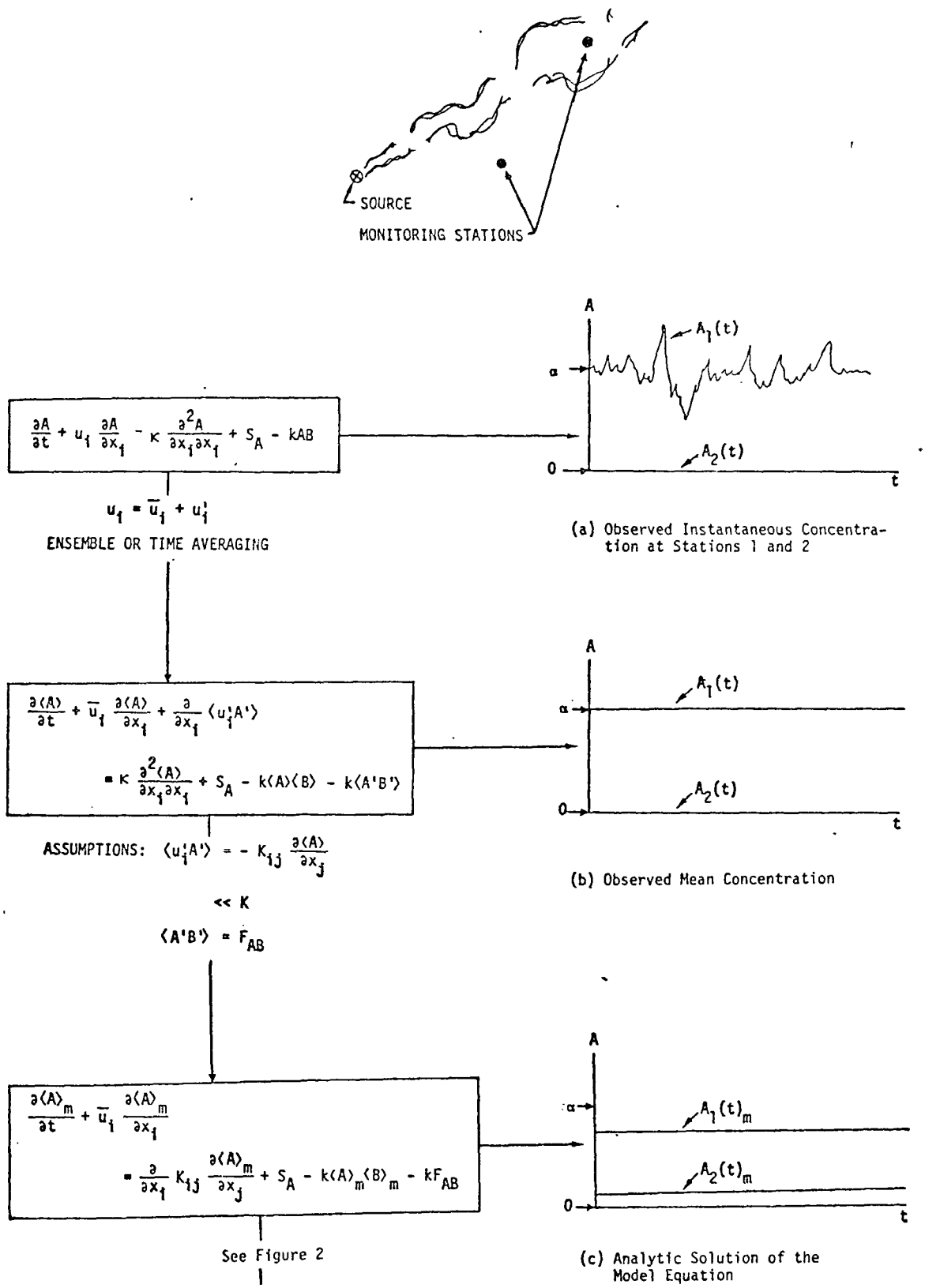

FIGURE 1. ILLUSTRATION OF THE RELATIONSHIPS AMONG THE SOLUTIONS OF VARIOUS GOVERNING EQUATIONS AND MEASURABLE POLLUTANT CONCENTRATIONS

Since Eq. (6) and its counterpart governing $\langle B \rangle_m$ are closed, and hence solvable, they can be used as the basis of an air pollution model. However, because these equations are nonlinear and because they contain variable coefficients, numerical integration methods must be used to obtain approximate forms of their solutions. To implement numerical techniques using a digital computer, we must first discretize the independent variables. But as we pointed out earlier, a finite set of samples of a continuous function is sufficient to describe only certain large-scale features of that function. Consequently, before Eq. (6) can be integrated numerically, it must first be "filtered" to remove all small-scale variations, both in $\langle A \rangle_m$ and in the independent parameters, such as K_{ij} and $\bar{u}_i$, that the grid system cannot resolve. The necessary filtering can be accomplished by averaging the equation at each point over a volume equivalent to that of the grid cells and over a period, Δt, equal to that of the time step used.

Let the required space averaging operation be denoted by the tilde (~) and be defined by

$$\tilde{f}(\underset{\sim}{x},t) = \frac{1}{8\Delta x \Delta y \Delta z} \int_{x-\Delta x}^{x+\Delta x} \int_{y-\Delta y}^{y+\Delta y} \int_{z-\Delta z}^{z+\Delta z} f(\underset{\sim}{x}',t)\,dx'\,dy'\,dz' \quad , \tag{8}$$

where $\underset{\sim}{x} = (x,y,z)$ and where Δx, Δy, and Δz represent the half-widths of the grid cell faces. Averaging Eq. (6) in this manner and assuming, as is usually true in practice, that neither $\bar{u}_i$ nor K_{ij} possesses spatial variations of a scale smaller than the grid, we obtain

$$\frac{\partial \langle \tilde{A} \rangle_m}{\partial t} + \bar{u}_i \frac{\partial \langle \tilde{A} \rangle_m}{\partial x_i} = \frac{\partial}{\partial x_i} K_{ij} \frac{\partial \langle \tilde{A} \rangle_m}{\partial x_j} + \tilde{S}_A - k \langle \tilde{A} \rangle_m \langle \tilde{B} \rangle_m - k\widetilde{A''B''} - k\tilde{F}_{AB} \quad , \tag{9}$$

where

$$A'' = \langle A \rangle_m - \langle \tilde{A} \rangle_m \quad ,$$

$$B'' = \langle B \rangle_m - \langle \tilde{B} \rangle_m \quad . \tag{10}$$

The variables A" and B" represent variations in $\langle A \rangle_m$ and $\langle B \rangle_m$, respectively, that are of a scale smaller than the grid size. Accordingly, A" and B" constitute a new microscale phenomenon with which we must deal in the development of an air pollution model. Note that A" and B" affect the chemical behavior of $\langle \tilde{A} \rangle_m$ in much the same way in which the turbulent concentration fluctuations A' and B' influence $\langle A \rangle$ [compare Eqs. (9) and (2)]. Hereafter we refer to A" and B" as subgrid-scale concentration variations (SSVs).

To complete our filtering of Eq. (6), we must next perform a time averaging of Eq. (9) over the period Δt of one time step. In practice, the size of the time step Δt required to maintain computational stability and to minimize truncation errors in the numerical integration of the model equations is much smaller than the characteristic time scale of any of the variables entering in Eq. (9). For this reason, the time average of $\langle \tilde{A} \rangle_m$ is equivalent to $\langle \tilde{A} \rangle_m$ itself. The same holds for $\tilde{S}_A$, K_{ij}, $\tilde{F}_{AB}$, and $\bar{u}_i$. Consequently, we can regard Eq. (9) as having been averaged in both space and time and as therefore representable in the required discrete form.

Like its analogue [Eq. (2)], Eq. (9) is not solvable because it contains, in addition to the dependent variable $\langle \tilde{A} \rangle_m$, the unknown quantity $\widetilde{A"B"}$. To our knowledge, this term has never before been considered in air pollution modeling studies. Apparently, this omission is due not to the belief that this term is small, but rather to a lack of awareness of the existence of the term. In Chapter IV, we consider this SSV term in more detail, both qualitatively and quantitatively, and we develop a mathematical method for representing it in pollution models. For the time being, let us write

$$G \approx \widetilde{A"B"} \quad , \tag{11}$$

where G denotes a known function. Equation (9) now takes the form

$$\frac{\partial \langle \tilde{A} \rangle_m}{\partial t} + \bar{u}_i \frac{\partial \langle \tilde{A} \rangle_m}{\partial x_i} = \frac{\partial}{\partial x_i} K_{ij} \frac{\partial \langle \tilde{A} \rangle_m}{\partial x_j} + \tilde{S}_A - k \langle \tilde{A} \rangle_m \langle \tilde{B} \rangle_m - kG - k\tilde{F}_{AB} \quad . \tag{12}$$

Through a series of operations and approximations, each motivated by necessity, we have arrived at an equation [Eq. (12)] that can feasibly be used as the basis for a simulation model of urban air pollution. A natural question at this point is whether the solution $\langle\tilde{A}\rangle_m$ of this equation provides an adequate representation of the desired mean concentration $\langle A\rangle$. To answer this questions, we plotted in Figure 2(b) the values of $\langle\tilde{A}\rangle_m$ that Eq. (12) would yield at the two sample sites under the conditions of the problem depicted in Figure 1(a) [and 2(a)]. After comparing these values with the corresponding values of $\langle A\rangle$ shown in Figure 1(b), one might conclude that $\langle\tilde{A}\rangle_m$ bears no resemblance to the desired quantity $\langle A\rangle$ and that, consequently, an air pollution model based on Eq. (12) would be of no value whatsoever. However, a totally different picture emerges when the global features of $\langle\tilde{A}\rangle_m$ are compared with those of $\langle A\rangle$. Figure 2(c), which presents this comparison, demonstrates that on scales that are large compared with the grid scale, a positive correlation exists between $\langle\tilde{A}\rangle_m$ and $\langle A\rangle$; $\langle\tilde{A}\rangle_m$ reproduces the overall features of the regional distribution of $\langle A\rangle$ quite well. Only on scales comparable to and smaller than the grid size does Eq. (12) break down. This fact raises a second question: What degree of spatial resolution is required of an airshed model?

The answer to this question must be inferred from the nature of the task for which the model is intended. For example, one such task is the delineation of long period trends and regional patterns in urban air quality. For this purpose, a model based on Eq. (12) should suffice. However, models are also required that assess whether particular control strategies can achieve air quality standards. To serve in this capacity, an airshed model must possess point spatial resolution, since the standards for some pollutants are currently expressed in terms of specific, short-period concentrations. Thus, techniques for simulating urban pollution are required that can reproduce the entire spectrum of spatial variations in the concentration field.

The basic model equation [Eq. (6)] from which Eq. (12) was derived possesses the desired range of resolution; but, as the reader will recall, the integration of this equation with point resolution over an entire urban

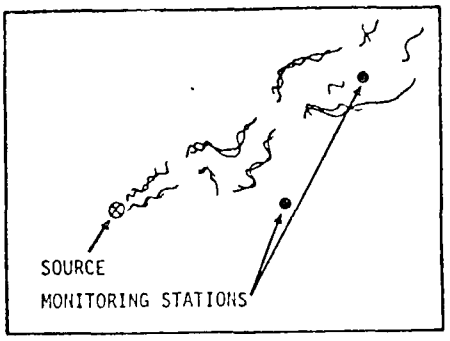

Horizontal Boundaries of One Grid Cell

Continued from Figure 1

$$\frac{\partial \langle A \rangle_m}{\partial t} + \bar{u}_i \frac{\partial \langle A \rangle_m}{\partial x_i} = \frac{\partial}{\partial x_i} K_{ij} \frac{\partial \langle A \rangle_m}{\partial x_j} + S_A - k \langle A \rangle_m \langle B \rangle_m - k F_{AB}$$

Averaging Over Time Step and Grid Cell

$$\frac{\partial \langle \tilde{A} \rangle_m}{\partial t} + \bar{u}_i \frac{\partial \langle \tilde{A} \rangle_m}{\partial x_i} = \frac{\partial}{\partial x_i} K_{ij} \frac{\partial \langle \tilde{A} \rangle_m}{\partial x_j} + \tilde{S}_A - k \langle \tilde{A} \rangle_m \langle \tilde{B} \rangle_m - k \widetilde{A''B''} - k \tilde{F}_{AB}$$

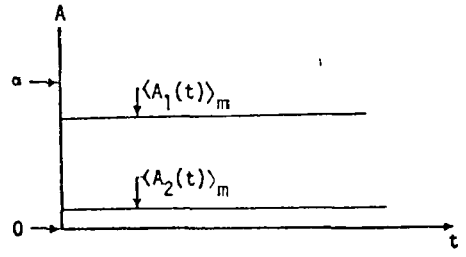

(a) Same as Figure 1(c)

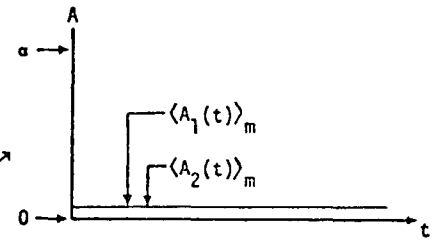

(b) Model Equation Adequate for Computer Simulation and Predicted Values at Stations 1 and 2

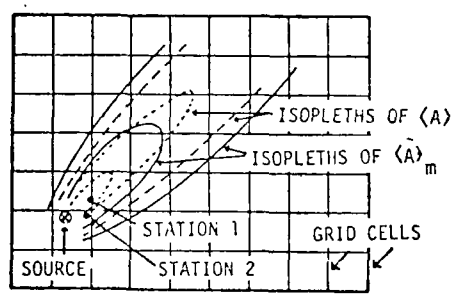

(c) Spatial Distributions of $\langle \tilde{A} \rangle_m$ and $\langle A \rangle$

FIGURE 2. ILLUSTRATION OF THE RELATIONSHIPS AMONG THE SOLUTIONS OF VARIOUS GOVERNING EQUATIONS AND MEASURABLE POLLUTANT CONCENTRATIONS

region would require a prohibitive amount of computer time and storage. This constraint is what motivated the spatial averaging, or small-scale filtering, process that led to Eq. (12). In Chapter V, we develop what we call a subgrid-scale model that can be used in conjunction with an airshed model based on Eq. (12) to obtain point resolution--in particular, the quantity $\langle A \rangle_m$--at any arbitrary point. An alternative to the approach presented in Chapter V (which we do not discuss in this report) is to calculate in addition to $\langle \tilde{A} \rangle_m$ the quantity $\widetilde{A''^2}$. By virtue of the definition of A" [Eq. (10)], the quantity $[\widetilde{A''^2}]^{1/2}$ is a measure of the amplitude of deviations of $\langle A \rangle_m$ from $\langle \tilde{A} \rangle_m$ that one can expect within the grid cell where $\widetilde{A''^2}$ is evaluated. From the modeling standpoint, this approach has certain operational advantages, but it does not provide the preciseness that is often required.

In summary, our research into microscale phenomena has focused on all aspects of air pollution modeling that are attributable to mechanisms whose spatial or temporal scales are too small to be resolvable in a simulation model of an urban-scale region. Figure 3 summarizes these research areas schematically. Because of the broad scope of this project, our efforts have not yet produced working solutions to all of the problems that we have considered. Our primary concern in this portion of our contract effort has been to explore each of the microscale problem areas in some detail, to assess the relative importance of each to the overall problem of air pollution modeling, and to design techniques for dealing with problem areas as needed. Only the implementation of our proposed techniques remains. We present a technical summary of the work described in this volume in Chapter VII and a discussion of the work and problems remaining in Chapter VIII.

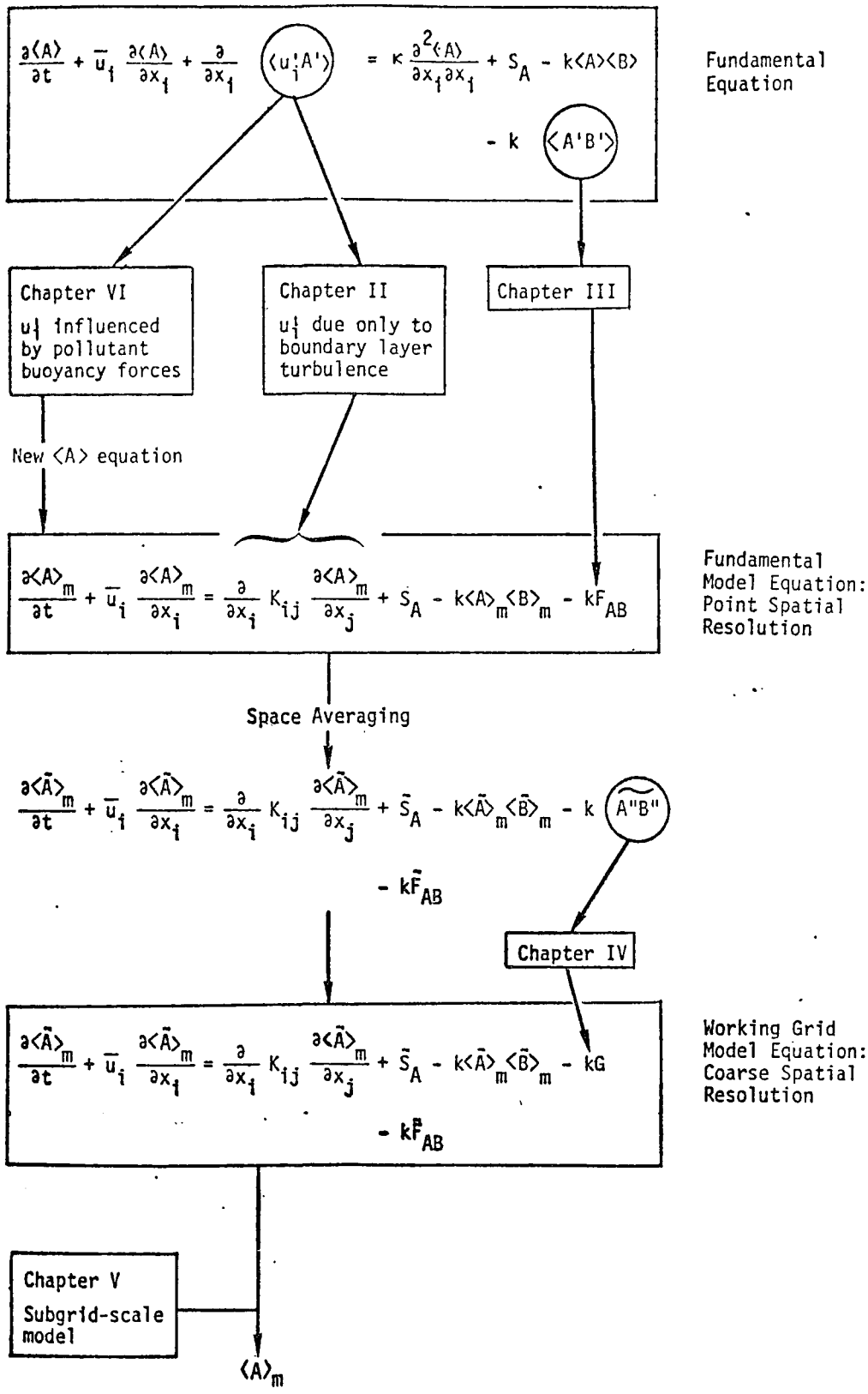

FIGURE 3. SCHEMATIC SUMMARY AND INDEX OF MICROSCALE RESEARCH

II ESTIMATION OF EDDY DIFFUSIVITY, WIND SHEAR PROFILES, AND DISPERSION PARAMETERS IN THE PLANETARY BOUNDARY LAYER

A. INTRODUCTION

The term $\overline{u_i' A'}$ entering into Eq. (2) represents the mean flux of the material A arising from turbulent fluctuations in the fluid velocity field. The physical significance of this flux can be illustrated by the following example.

Suppose that a fluid is placed in a closed container and that turbulent motions are subsequently induced in the fluid by some mechanical means. Suppose further that numerous infinitesimal velocity and concentration probes are placed uniformly throughout the fluid. Let $\underset{\sim}{u}(\underset{\sim}{x},t)$ denote the functional form of the expression that best describes the instantaneous signals gathered from all the velocity probes, and similarly let $c(\underset{\sim}{x},t)$ denote the expression that best represents the concentration measurements. Let us assume that at some instant t_0 a steady point source of unit strength of the material c is introduced into the fluid at the point $\underset{\sim}{x}_0$, and that no matter how many times the experiment is repeated, the measured field $c(\underset{\sim}{x},t)$ is always found to be identical to the solution of the continuity equation

$$\frac{\partial c}{\partial t} + u_i \frac{\partial c}{\partial x_i} = \delta(\underset{\sim}{x} - \underset{\sim}{x}_0) \quad ,$$

where u_i is the measured velocity field and where molecular diffusion does not affect c.

Suppose that many of the velocity probes are now withdrawn and that the velocity fields sensed by the remaining probes is described by the function U(x,t). If the above experiment were repeated, one would find that the measured concentration field $c(\underset{\sim}{x},t)$ spreads out more than is predicted by the equation

$$\frac{\partial c}{\partial t} + U_i \frac{\partial c}{\partial x_i} = \delta(\underset{\sim}{x} - \underset{\sim}{x}_0) \quad .$$

A greater degree of spreading would be observed if still fewer velocity probes were used to obtain $\underset{\sim}{U}$. This apparent spreading is the phenomenon known as turbulent diffusion.

Our example illustrates that turbulent diffusion is actually an artifact of our lack of knowledge of the true velocity field. The example also suggests that the magnitude of the diffusion phenomenon is related to the density of velocity probes with which the fluid motions are monitored. Since this aspect of diffusion and its potential significance to pollution modeling have been discussed by Lamb (1971), and we do not elaborate upon them here. The primary concern in this section is to develop a mathematical description of the diffusion phenomenon caused by turbulence in the planetary boundary layer.

There are basically two approaches to deriving such a description--Eulerian and Lagrangian. The starting point of the Eulerian method is the mass continuity equation:

$$\frac{\partial c}{\partial t} + \frac{\partial}{\partial x_i} u_i c = S \quad , \tag{13}$$

where S is a known function describing the distribution of sources of the scalar quantity. This same equation was introduced above but in a slightly less general form. In a turbulent fluid, such as the atmosphere, the lack of a total description of the velocity field u_i makes it necessary to treat u_i--and hence c--as stochastic variables. These are customarily decomposed into mean ($\langle u_i \rangle$ and $\langle c \rangle$) and fluctuating (u_i' and c') components. Then, from Eq. (13), one can see that $\langle c \rangle$ is governed by the equation

$$\frac{\partial \langle c \rangle}{\partial t} + \frac{\partial}{\partial x_i} \langle u_i \rangle \langle c \rangle + \frac{\partial}{\partial x_i} \langle u_i' c' \rangle = S \quad , \tag{14}$$

which is unsolvable because of the presence of the additional unknown quantity $\langle u_i' c' \rangle$.

This problem, known as the closure problem, is a fundamental obstacle that impedes the progress of all Eulerian-type approaches to the analytical study of turbulent diffusion. One of the oldest and best known attempts to circumvent the closure problem is the so-called gradient transport hypothesis, which dates back to Boussinesq in the nineteenth century. In the context of Eq. (14), this hypothesis states that

$$\langle u_i' c' \rangle = -K_{ij} \frac{\partial \langle c \rangle}{\partial x_j} \quad , \tag{15}$$

where K_{ij} is a turbulent diffusivity tensor that must be evaluated using empirical data. In Volume II, we discussed some of the attempts made by previous investigators to relate certain components of K_{ij} to measurable properties of the boundary layer. We review some of these later in this chapter.

Since Eq. (15) implies that turbulent diffusion behaves like molecular diffusion, the validity of this equation cannot be universal. In recent years, several more advanced closure schemes have been developed, primarily for the turbulent momentum and energy equations (see, for example, Hanjalic and Launder, 1972; Lumley, 1970; Donaldson , 1969); but none has yet been demonstrated to be widely applicable to problems of atmospheric diffusion.

In contrast, the Lagrangian approach, starting from basic principles, leads directly to the closed equation

$$\left\langle c(\underset{\sim}{r},t) \right\rangle = \int\int_0^t p(\underset{\sim}{r},t|\underset{\sim}{r}',t') \, S(\underset{\sim}{r}',t') \, dt' \, d\underset{\sim}{r}' \quad , \tag{16}$$

where $p(\underset{\sim}{r},t|\underset{\sim}{r}',t')$ is the conditional probability density that a particle of the scalar released at $(\underset{\sim}{r}',t')$ will be found at $(\underset{\sim}{r},t)$. [The derivations of Eq. (16) and the equations governing all of the higher order stochastic moments of c can be found in Lamb (1974)]. In principle, p is a measurable Lagrangian property of the turbulence velocity field and the molecular dif-

fusivity of the scalar particles, but in practice the exact form of p is virtually unattainable because of the extreme difficulty of tracking individual particles in turbulent fluid, especially the atmosphere. Consequently, just as the closure problem impairs the utility of Eq. (14), the lack of information regarding the exact form of p hampers the use of its Lagrangian counterpart, Eq. (16). And just as various schemes have been advanced for rendering Eq. (14) solvable, several hypotheses have been proposed for implementing Eq. (16). Among the latter, the most well known is the assumption that p is Gaussian. With this approximation and the assumptions that the turbulence is isotropic and stationary, it can be shown that the widely used Gaussian plume and puff models are derivable from Eq. (16). Similarly, under the assumption that p describes a Markov process, as would be true in a study of pure molecular diffusion, it can be shown that Eq. (16) reduces to the diffusion equation, represented by Eqs. (14) and (15) (see Chapter V of this volume). Unfortunately, none of these models in their current forms provide a wholly adequate description of atmospheric diffusion.

Recognizing the difficulties in obtaining actual field data to test and implement turbulence theories, some investigators pursued the problem of simulating turbulent flows computationally (Deardorff, 1970, 1972; Orszag and Israeli, 1974). In particular, Deardorff developed a model that simulates the turbulent planetary boundary layer, under various stability conditions, below an inversion base of constant height (Deardorff, 1970). This model opens up new avenues, through Eq. (16), to applied studies of atmospheric diffusion, because in the atmosphere, where molecular diffusion has a negligible effect on the distribution of the mean concentration $\langle c \rangle$, the probability density p that enters in Eq. (16) can be regarded as a function solely of the turbulence velocity field and can accordingly be calculated from the numerically simulated turbulence fields. In this chapter, we describe some of our preliminary work along these lines using the turbulence model of Deardorff described above.

The main objective of our study was to use the mean concentration profiles computed from the numerically derived values of p [referred to as the numerico-empirical profiles] to assess the adequacy of conventional atmospheric diffusion theories. First, we assessed the atmospheric diffusion

equation, Eq. (14) with Eq. (15), by determining the profile of vertical eddy diffusivity that produces the closest fit of the predicted mean concentrations with the numerico-empirical profiles. Second, we compared the numerico-empirical profiles with those predicted by (1) the Gaussian plume formula with Pasquill-Gifford dispersion parameters and (2) the Gaussian puff equation with McElroy-Pooler travel-time-dependent dispersion parameters. Additional studies of the plume and puff models that we carried out are relevant to the work described in some of the later chapters of this volume.

B. DESCRIPTION OF THE NUMERICAL EXPERIMENTS

We considered the three-dimensional dispersion of marked particles in an atmospheric flow between the ground ($\hat{z} = 0$) and an elevated boundary of constant height $\hat{h}$ as simulated by the planetary boundary layer model of Deardorff (1970). (In this chapter, we use the caret to distinguish dimensional variables from those that have been nondimensionalized.) In each of two experiments representing neutral ($\hat{h}/L = 0$) and slightly unstable ($\hat{h}/L = -4.5$) atmospheric conditions, where L is the Monin-Obukhov length, 800 particles were released from points on a horizontal plane and followed for a given period of time. Using the computed trajectories of each particle, we calculated the two-dimensional density function $p(\hat{x},\hat{z},t|\hat{x}',\hat{z}',t')$ in the following way. (The components of $\underset{\sim}{r}$ and $\underset{\sim}{r}'$ were taken to be $\hat{x}$, $\hat{z}$ and $\hat{x}'$, $\hat{z}'$, respectively.)

First, we transformed the coordinate system of each particle to a moving frame:

$$\xi_i(\tau) = \hat{x}_i(\tau) - [\hat{x}_i' + \bar{u}(\hat{z}_s)\tau] \quad ,$$

$$\zeta_i(\tau) = \hat{z}_i(\tau) - \hat{z}_s \quad , \tag{17}$$

$$i = 1, 2, \ldots, 800 \quad ,$$

where $\bar{u}(\hat{z}_s)$ is the mean value of the $\hat{x}$-component of the wind at the level of release of the particles and $\tau = t - t'$. Then we introduced a new function, $p_{\xi\zeta}$, such that

$$p_{\xi\zeta}(\xi,\zeta,\tau) = \begin{cases} N(\xi,\zeta,\tau)\left\{800h[2X(\tau)]\right\}^{-1} & , \quad |\xi| \le X(\tau) \quad , \\ 0, \quad \text{otherwise} & , \end{cases} \tag{18}$$

where $N(\xi,\zeta,\tau)$ is the number of particles at time τ that lie in the range $\xi - 1/2\ \Delta\xi \le \xi_i(\tau) \le \xi + 1/2\ \Delta\xi$ and $\zeta - 1/2\ \Delta\zeta \le \zeta_i(\tau) \le \zeta + 1/2\ \Delta\zeta$ and $X(\tau)$ is a distance that is exceeded by the $|\xi_i|$ of only a negligible fraction of the 800 particles. The intervals $\Delta\xi$ and $\Delta\zeta$ are also functions of τ and are sufficiently large that a minimum number of the intervals $\Delta\xi\Delta\zeta$ are void of particles at each τ. Clearly, we can approximate the desired transition probability density function $p(\hat{x},\hat{z},t|\hat{x}',\hat{z}',t')$ as follows:

$$p(\hat{x},\hat{z},t|\hat{x}',\hat{z}',t') \doteq p_{\xi\zeta}[\xi-\bar{u}(\hat{z}_s)\tau,\zeta,\tau] \quad . \tag{19a}$$

The accuracy of a probability density function derived in this manner is virtually impossible to assess using analytical error formulas alone. The best error estimates are obtained by repeating the calculations with a fresh set of data and then comparing the results. The limited data set available in this study precluded such a check, but we plan to examine this matter in more detail in future studies. Suffice it to say that random errors in the computed density function p are attenuated by the integration process, when used in Eq. (16), and that as a result the calculated mean concentrations are less erroneous than the p function on which they are based. The function $p(x,z,t|x',z_s,t') = p(x-x',z-z_s,t-t')$ is shown graphically in Figure 4 for several travel times and for each of the two stability conditions considered. The nondimensional space and time coordinates used here are defined by

$$x = \frac{\hat{x}}{\hat{h}} \quad , \quad z = \frac{\hat{z}}{\hat{h}} \quad , \quad t = \frac{\hat{t}u_*}{\hat{h}} \quad , \tag{19b}$$

where u_* is the friction velocity and h is a vertical length scale defined later.

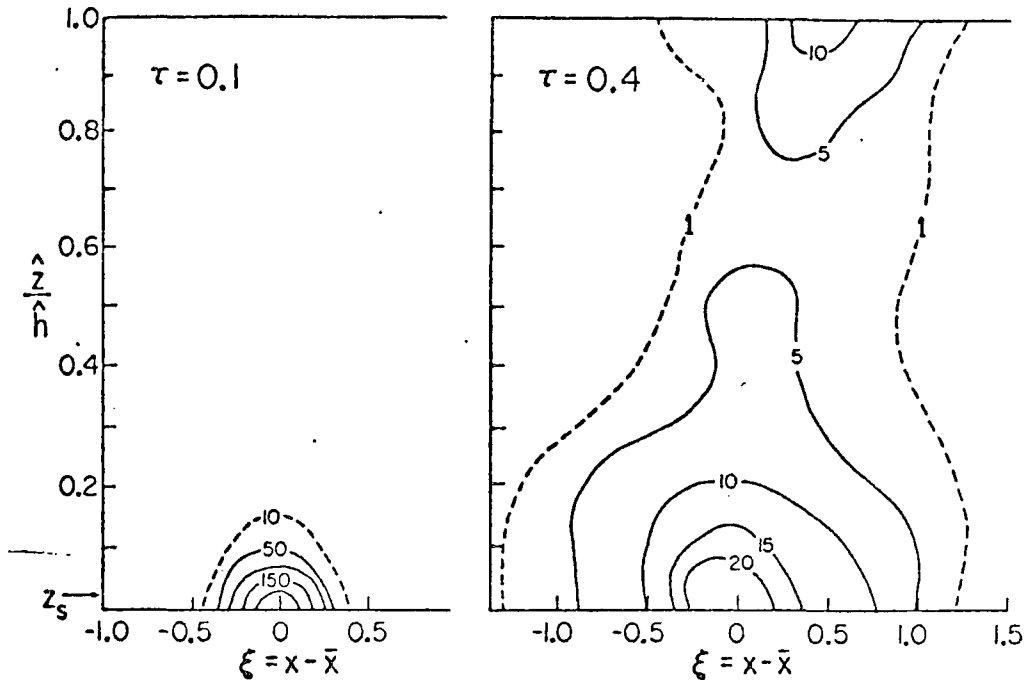

(a) Unstable Conditions

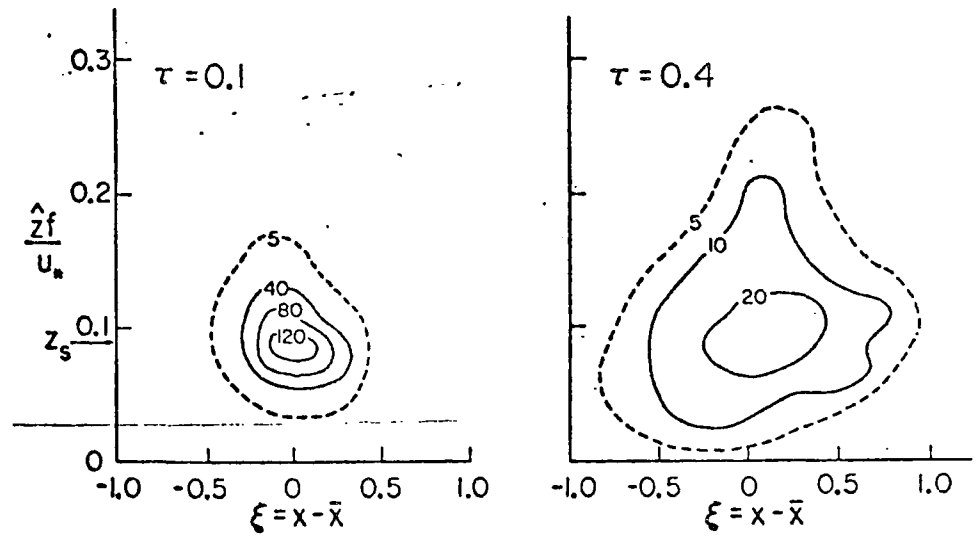

(b) Neutral Conditions

FIGURE 4. THE PROBABILITY DENSITY FUNCTION $p(\xi,z,\tau/Z_S)$--IN RELATIVE UNITS--DERIVED FROM THE MODEL OF DEARDORFF

We used the results of the above analyses for both the neutral and slightly unstable cases in Eq. (16) to compute the mean cross-wind integrated concentration, $\langle c(x,z)\rangle$, of a chemically inert substance arising from a continuously emitting point source. For $S(x,z,t) = M\delta(x - x_s)\delta(z - z_s)$, where M is the emission rate (a constant) and $\langle c(x,z,t_0)\rangle = 0$, Eq. (16) becomes

$$\langle c(x,z)\rangle = \lim_{t\to\infty} M \int_0^t p(x,z,t|x_s,z_s,t')\, dt' \quad . \qquad (20)$$

Section C presents the results of the calculations.

C. ASSESSMENT OF THE ATMOSPHERIC DIFFUSION EQUATION

In the introduction, we mentioned that the implications of the gradient transport hypothesis [Eq. (15)] regarding the nature of turbulent diffusion are generally incorrect. However, the so-called diffusion equation to which this hypothesis gives rise through Eq. (14) is an attractive equation from the standpoint of describing atmospheric diffusion. Specifically, this equation is simple and easily solvable using conventional finite differencing techniques, and it lumps the effects of the turbulence into the single function K_{ij} rather than into one or several additional differential equations. This last point is particularly significant in the context of photochemical pollution modeling, where the number of differential equations involved is already so large that the addition of more equations to handle the diffusion terms would make the computational burden prohibitive. Thus, a tacit constraint on our analysis was that the closure approximation we derived must require no additional equations.

These considerations therefore prompted the following question: Does a function K_{ij} exist that renders the differences between the solution of the diffusion equation and the solution of Eq. (16) acceptably small, and if so, how does this "optimal" diffusivity compare with the expressions in current use? As an added constraint, we insisted that the function K_{ij} depend only on spatial coordinates and not on travel time. Without this restriction,

which contradicts observations, K_{ij} would become a function of the source distribution S and would therefore acquire extremely unwieldly forms in problems such as urban pollution modeling, where one must deal with a multitude of widely scattered sources of various shapes and sizes and temporally variable strengths. In short, we attempted to determine whether turbulent diffusion can be described with acceptable accuracy in terms of some local, hypothetical property of the flow field.

To explore this question, we considered the two-dimensional steady-state form of the atmospheric diffusion equation, in which turbulent dispersion in the direction of the mean wind is neglected, i. e.,

$$\bar{u}(\hat{z}) \frac{\partial \langle c \rangle}{\partial \hat{x}} = \frac{\partial}{\partial \hat{z}} \left[\hat{K}_Z(\hat{z}) \frac{\partial \langle c \rangle}{\partial \hat{z}} \right] + M\hat{\delta}(\hat{x} - \hat{x}_s)\, \hat{\delta}(\hat{z} - \hat{z}_s) \quad . \tag{21}$$

Upon defining the dimensionless variables,

$$u = \frac{\bar{u}}{u_*} \quad , \quad K_Z = \frac{\hat{K}_Z}{u_* \hat{h}} \quad , \quad C = \frac{\langle c \rangle \bar{u}(\hat{z}_s)\hat{h}}{M} \quad , \tag{22}$$

where $\hat{h}$ is a vertical length scale and u_* is the friction velocity, we obtain the dimensionless form of Eq. (22):

$$u \frac{\partial C}{\partial x} = \frac{\partial}{\partial z} \left(K_Z \frac{\partial C}{\partial z} \right) + \left[\frac{\bar{u}(\hat{z}_s)}{u_*} \right] \delta(x - x_s)\, \delta(z - z_s) \quad , \tag{23}$$

where $\delta(\cdot) = \hat{\delta}(\cdot)\hat{h}$ and where x, z, and t are given by Eq. (19b). The boundary conditions for Eq. (23) are

$$C(z,0) = 0 \quad , \tag{24}$$

$$K_Z \frac{\partial C}{\partial z} = 0 \quad , \quad z = 0, 1 \quad . \tag{25}$$

In contrast to the neutral case, in which the depth of the planetary boundary layer is some fraction of u_*/f, where f is the Coriolis parameter, Deardorff found that the unstable boundary layer extends up to the height z_i

of the inversion base below which convective mixing is confined. Consequently, the proper choice of the length scale $\hat{h}$ is $\hat{h} = z_i$ in unstable cases and $\hat{h} = u_*/f$ in the neutral case.

Before proceeding with the calculation of the optimal diffusivity K_Z, we first consider the mean velocity profiles u that enter into Eq. (23) and also the diffusivity profiles K_Z in current use.

1. Wind Profiles from the Planetary Boundary Layer Model

Figure 5 shows u(z) computed by the planetary boundary layer model in the two cases of $\hat{h}/L = 0$ and $\hat{h}/L = -4.5$. It is of interest to compare these profiles with those predicted by conventional theories.

According to the Monin-Obukhov similarity theory, the mean velocity gradient in the surface layer is given by (Monin and Yaglom, 1971)

$$\frac{\partial \bar{u}}{\partial \hat{z}} = \frac{u_*}{\kappa \hat{z}} \hat{\phi}_m\left(\frac{\hat{z}}{L}\right) \quad , \tag{26}$$

where

$$\hat{\phi}_m\left(\frac{\hat{z}}{L}\right) = \begin{cases} 1 \quad , & \text{neutral } \hat{z} < \kappa u_*/f \quad ; \\ \left(1 - \beta \frac{\hat{z}}{L}\right)^{-0.25} \quad , & \text{unstable } -2 < \hat{z}/L < 0 \end{cases} \tag{27}$$

The commonly accepted value of β is 15. The mean surface layer velocity profiles obtained by integrating Eq. (26) from $\hat{z}_0$ to $\hat{z} + \hat{z}_0$ are given in Table 1, where the profiles are expressed in both dimensional and dimensionless form.

Above the surface layer, there is a change of wind direction with height (the Ekman layer). In the planetary boundary layer, $\bar{v} \cong 1/5\ \bar{u}$ at the geostrophic level, so that $|v| \cong \bar{u}$, even with turning. In the unstable case, i.e., $\hat{z}_i/L \lesssim -1.5$, both observational data and the numerical calculation show that the change of wind direction is strongly suppressed, resulting in

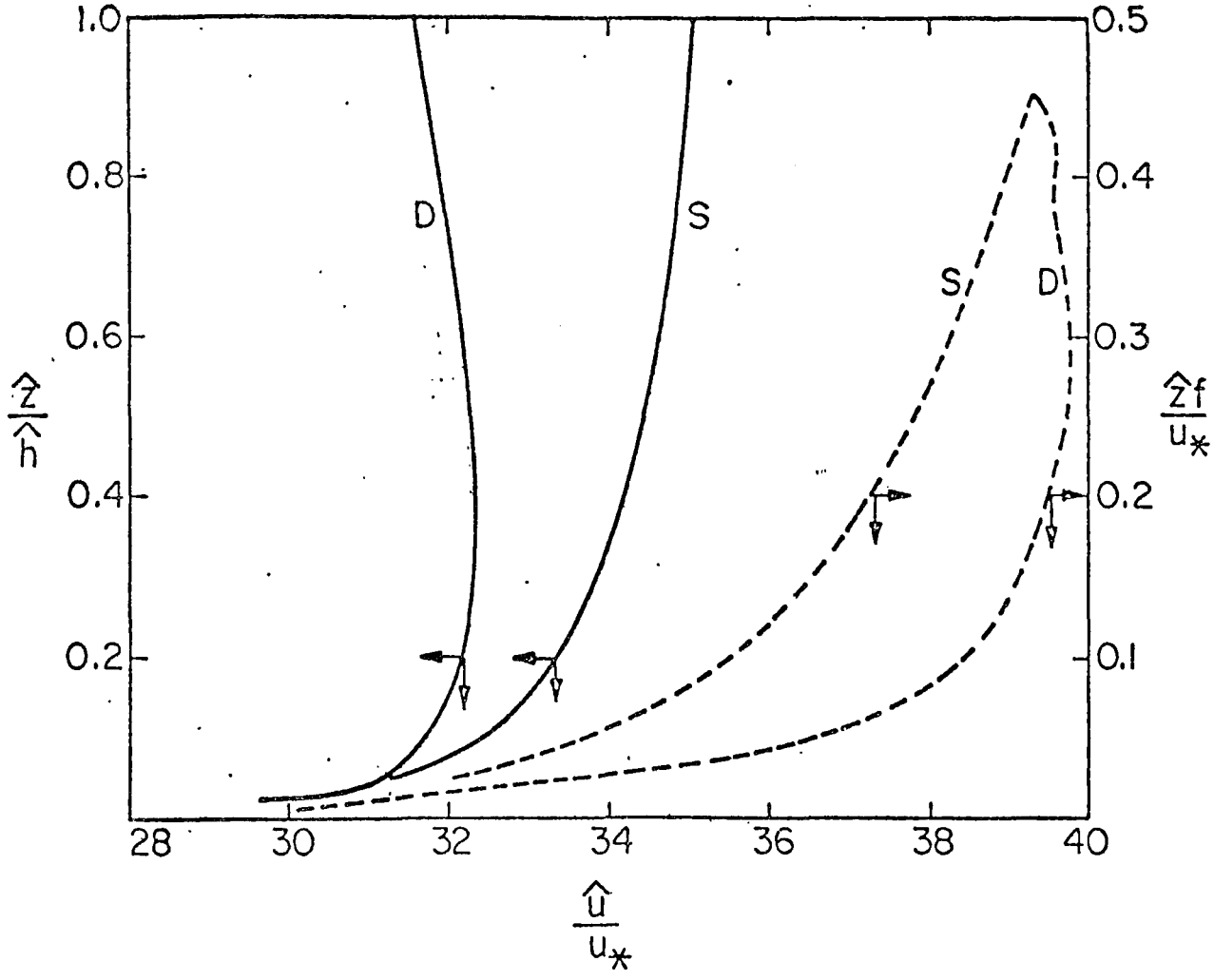

FIGURE 5. WIND PROFILES GIVEN BY SIMILARITY THEORY (S) AND DEARDORFF'S MODEL (D) FOR NEUTRAL (DASHED CURVES) AND UNSTABLE ($\hat{h}/L$ = -4.5) CONDITIONS

Table 1

WIND AND VERTICAL EDDY DIFFUSIVITY PROFILES IN THE SURFACE LAYER FROM SIMILARITY THEORY

	Neutral: $\hat{z} < \kappa u_*/f$	Unstable: $-2 < \hat{z}/L < 0$
$\bar{u}(\hat{z})$	$\frac{u_*}{\kappa} \ell n \left(1 + \frac{\hat{z}}{\hat{z}_0}\right)$	$\frac{u_*}{\kappa} \left[2 \left(\tan^{-1} \hat{\Psi} - \tan^{-1} \hat{\Psi}_0 \right) + \ell n \left(\frac{\hat{\Psi} + 1}{\hat{\Psi}_0 - 1} \right) - \ell n \left(\frac{\hat{\Psi} + 1}{\hat{\Psi}_0 + 1} \right) \right]$
$u(z)$	$\frac{1}{\kappa} \ell n \left(1 + \frac{z}{z_0}\right)$	$\frac{1}{\kappa} \left[2 \left(\tan^{-1} \Psi - \tan^{-1} \Psi_0 \right) + \ell n \left(\frac{\Psi - 1}{\Psi_0 - 1} \right) - \ell n \left(\frac{\Psi + 1}{\Psi_0 + 1} \right) \right]$
$\hat{K}_z(\hat{z})$	$\kappa u_* \hat{z}$	$\kappa u_* \hat{z} \left(1 - \beta \frac{\hat{z}}{L}\right)^{-0.25}$
$K_z(z)$	κz	$\kappa z \left(1 - \beta z \frac{\hat{h}}{L}\right)^{-0.25}$

Note: $\hat{\Psi} = \left[1 - \beta(\hat{z} + \hat{z}_0)/L\right]^{1/4}$, $\Psi_0 = (1 - \beta \hat{z}_0/L)^{1/4}$;

$\Psi = \left[1 - \beta(z + z_0)\hat{h}/L\right]^{1/4}$, $\Psi_0 = (1 - \beta z_0 \hat{h}/L)^{1/4}$.

a nearly unidirectional flow in the planetary boundary layer. Thus, in the diffusion calculations presented later, we neglected the turning of the wind with height in all situations. Although several approximate expressions have been proposed to describe the wind speed profile above the surface layer, none of these agrees as well with the numerically calculated wind as the profile obtained by simply extrapolating the surface layer formulation [Eqs. (26) and (27)] to the top of the boundary layer (see Figure 5).

2. Theoretical Forms for Eddy Diffusivities

The surface layer vertical eddy diffusivities corresponding to the mean wind profiles derived from similarity theory are given in Table 1. Considerably less is known about the behavior of K_Z above the surface layer than within it. In two recent studies, expressions for K_Z in the planetary boundary layer above the surface layer have been proposed.

Ragland (1973) suggested that $\hat{K}_Z$ be taken as constant above the surface layer at its value at the top of the surface layer. In contrast, Shir and Shieh (1973) assumed that in the planetary boundary layer under neutral conditions $\hat{K}_Z$ obeys the form

$$\hat{K}_Z = u_* \ell(\hat{z}), \quad \text{neutral} \quad , \tag{28}$$

where $\ell(\hat{z}) = \kappa \hat{z} \exp(-4\hat{z}/z_i)$, and that under nonneutral conditions, $\hat{K}_Z$ obeys the form

$$\hat{K}_Z(\hat{z}) = \hat{K}_Z(\hat{z}_1) \frac{\ell(\hat{z})}{\ell(\hat{z}_1)} \quad , \tag{29}$$

where $\hat{z}_1$ is taken to be 10 m. In these computations, $\hat{K}_Z(\hat{z}_1)$ is to be calculated assuming that $\hat{z}_1 (= 10 \text{ m})$ lies within the surface layer. In the dimensionless form adopted here, Eqs. (28) and (29) become

$$K_Z = \kappa z e^{-4z} \tag{30}$$

and

$$K_Z(z) = K_Z(z_1)\left[\frac{z}{z_1} e^{4(z_1-z)}\right] \quad , \quad \text{unstable} \quad . \tag{31}$$

We postpone further discussion of these proposed diffusivity profiles until after we have derived our "optimal" estimate of K_Z.

3. Estimation of the Optimal $K_Z(z)$ in the Atmospheric Diffusion Equation

In addressing the question of the existence of an optimal diffusivity K_Z, one faces the general problem of estimating the form of a functional parameter appearing in a partial differential equation [namely, Eq. (23)], such that the solution of that equation matches certain given data as closely as possible. If the data are available as continuous functions of x and z, denoted here by $C_\ell(x,z)$, then the customary criterion to be minimized by the choice of $K_Z(z)$ is

$$J = \int_0^{\ell_0}\int_0^1 [C_\ell(x,z) - C(x,z)]^2 \, dz \, dx \quad , \tag{32}$$

where ℓ_0 is the extent of x over which data are available.

This problem is known as an inverse problem. As Chen and Seinfeld (1972) and Chen et al. (1974) have shown, problems of this type can be solved efficiently by techniques of optimal control theory. The optimal control problem to be solved is the following: Determine the function $K_Z(z)$ that minimizes J, subject to Eqs. (23) through (25) and to $K_Z \geq 0$. For this problem, the necessary conditions for optimality assume the form of a two-point boundary value problem:

$$u \frac{\partial C}{\partial x} = \frac{\partial}{\partial z}\left(K_Z \frac{\partial C}{\partial z}\right) + \left(\frac{\hat{u}}{u_*}\right) \delta(x - x_s)\, \delta(z - z_s) \quad , \tag{33}$$

$$C(0,z) = 0 \quad , \tag{34}$$

$$K_Z \frac{\partial C}{\partial z} = 0 \quad , \quad z = 0,\ 1 \quad , \tag{35}$$

$$\frac{\partial \psi}{\partial x} = - \frac{\partial}{\partial z}\left[K_Z \frac{\partial}{\partial z}\left(\frac{\psi}{u}\right)\right] + 2[C_\ell(x,z) - C(x,z)] \quad , \tag{36}$$

$$\psi(\ell_0,z) = 0 \quad , \tag{37}$$

$$K_Z \frac{\partial}{\partial z}\left(\frac{\psi}{u}\right) = 0 \quad , \quad z = 0,\ 1 \quad , \tag{38}$$

$$\frac{\delta J}{\delta K_Z} = - \int_0^{\ell_0} \frac{\partial C}{\partial z} \frac{\partial}{\partial z}\left(\frac{\psi}{u}\right) dx = 0 \quad , \tag{39}$$

where $\delta J/\delta K_Z$ is the functional derivative of J with respect to K_Z and $\psi(x,z)$ is the adjoint variable to C (x,z) as shown, for example, by Lions (1971).

The two-point boundary value problem given by Eqs. (33) through (39) cannot be solved analytically and must therefore be solved iteratively. One straightforward means of determining the optimal value of K_Z numerically is to use the method of steepest descent. From the definition of the functional derivative, we can rewrite Eq. (39) as

$$\delta J = -\int_0^1 \left\{ \int_0^{\ell_0} \left[\frac{\partial}{\partial z}\left(\frac{\psi}{u}\right)\right]\left(\frac{\partial C}{\partial z}\right) dx \right\} \delta K_Z(z)\, dz \quad , \tag{40}$$

which is a direct expression for the effect of a perturbation in K_Z on the value of J. The basis of the method of steepest descent is to choose δK_Z such that δJ is negative. This can be accomplished by setting

$$\delta K_Z(z) = W(z) \int_0^{\ell_0} \left[\frac{\partial}{\partial x}\left(\frac{\psi}{u}\right)\right]\left(\frac{\partial C}{\partial z}\right) dx \quad , \tag{41}$$

where $W(z)$ is an arbitrary positive function of z.

The algorithm proceeds as follows:

(1) Make an initial guess of $K_Z(z)$, calling it $K_Z^0(z)$. Select $W(z)$.

(2) Integrate Eqs. (33) through (35) from $x = 0$ to $x = \ell_0$ using K_Z^0. Evaluate J.

(3) Integrate Eqs. (36) through (38) from $x = \ell_0$ to $x = 0$ using K_Z^0 and $C(x,z)$ from Step 2.

(4) Compute δK_Z from Eq. (41), and call it δK_Z^0.

(5) Revise the initial guess of K_Z by

$$K_Z^1 = K_Z^0 + \delta K_Z^0 \quad .$$

If $K_Z^1 < 0$, set $K_Z = 0$.

(6) Using K_Z^1, return to Step 2 and repeat.

(7) Continue until $(J^n - J^{n+1})/J^n < \varepsilon$, where ε is a preset convergence criterion.

In the steepest descent algorithm, the perturbations in K_Z are defined so as to seek the minimum of J by moving K_Z along the gradient of J with respect to K_Z. The length of the step, i.e., how far a distance one proceeds along the gradient in each direction, is controlled by the choice of the function $W(z)$. Although it is possible to choose $W(z)$ by an auxiliary optimization problem, it is generally simpler computationally to select a constant value of W initially equal, say, to some fraction of the initial guess of K_Z. If, during the iteration, an improved estimate of K_Z increases rather than decreases J, the minimum has been overstepped. One must then go back to the value from the previous iteration, and decrease W by a preset factor before

computing the new estimate. The convergent value of K_Z generally varies depending on the initial guess. Thus, it is desirable to try several different initial guesses to determine the variability of the convergent K_Z profiles. We carried out this procedure in the present study, and we substantially attained the profiles to be discussed subsequently, regardless of the initial guess. Nevertheless, results on the uniqueness of profiles determined by using optimal control theory are still unavailable.

The resulting optimal diffusivity profile $K_Z(z)$ for the neutral case is shown in Figure 6, which also shows the profiles given by similarity theory (listed in Table 1); the profile suggested by Shir and Shieh, Eq. (28), and the eddy viscosity calculated by Deardorff. The optimal profile agrees relatively well with that proposed by Shir and Shieh and shows also fairly close correspondence to the eddy viscosity profile computed by Deardorff. However, the diffusivity estimates given by similarity theory are consistently too large and differ from the optimal value by nearly a factor of 10 at the top of the boundary layer.

The opposite situation is found in the unstable case (Figure 7), where the optimal diffusivities are much larger than those given by similarity theory. When the latter values were used in Eq. (23), the resulting errors were a factor of 10 larger than those produced by the optimal K_Z profile. For all common values of $\hat{h}$, the Shir-Shieh profile for K_Z under unstable conditions (not shown in Figure 7) gives smaller diffusivities than does similarity theory.

The fact that the optimal K_Z profile does not drop to zero along the broken line shown in Figure 7 cannot be attributed to the algorithm that was used to compute K_Z, because we found that the smaller diffusivity values near the surface resulted in larger errors in the ground-level concentrations predicted by Eq. (23). A more likely cause is the larger truncation errors in the finite difference model of Eq. (23).

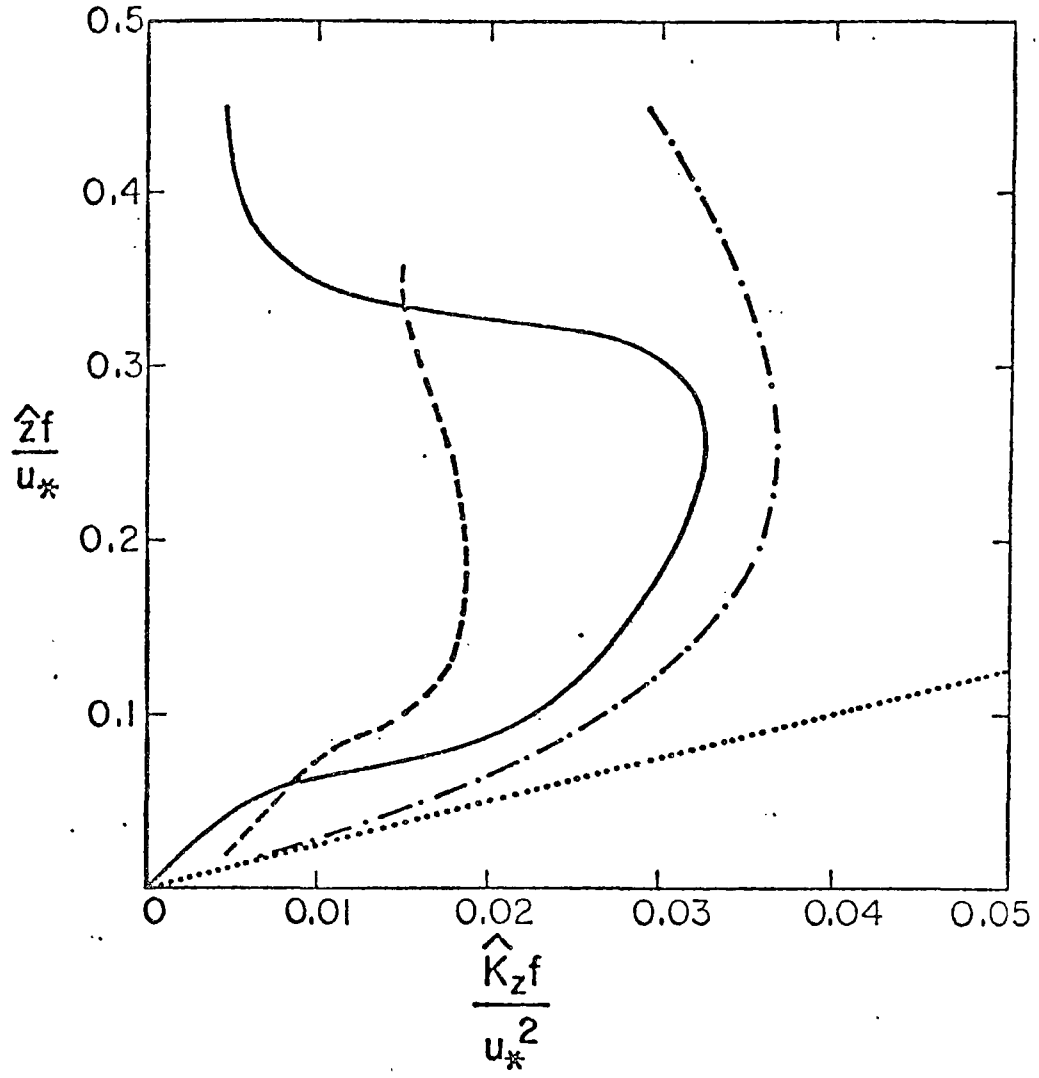

FIGURE 6. COMPARISON OF THE OPTIMAL K_Z PROFILE (SOLID CURVE) WITH THE PROFILE PROPOSED BY SHIR AND SHIEH (DASH-DOT LINE), THE PROFILE GIVEN BY SIMILARITY THEORY (DOTTED LINE), AND THE EDDY VISCOSITY CALCULATED BY DEARDORFF (DASHED LINE) IN THE NEUTRAL ($\hat{h}/L = 0$) BOUNDARY LAYER

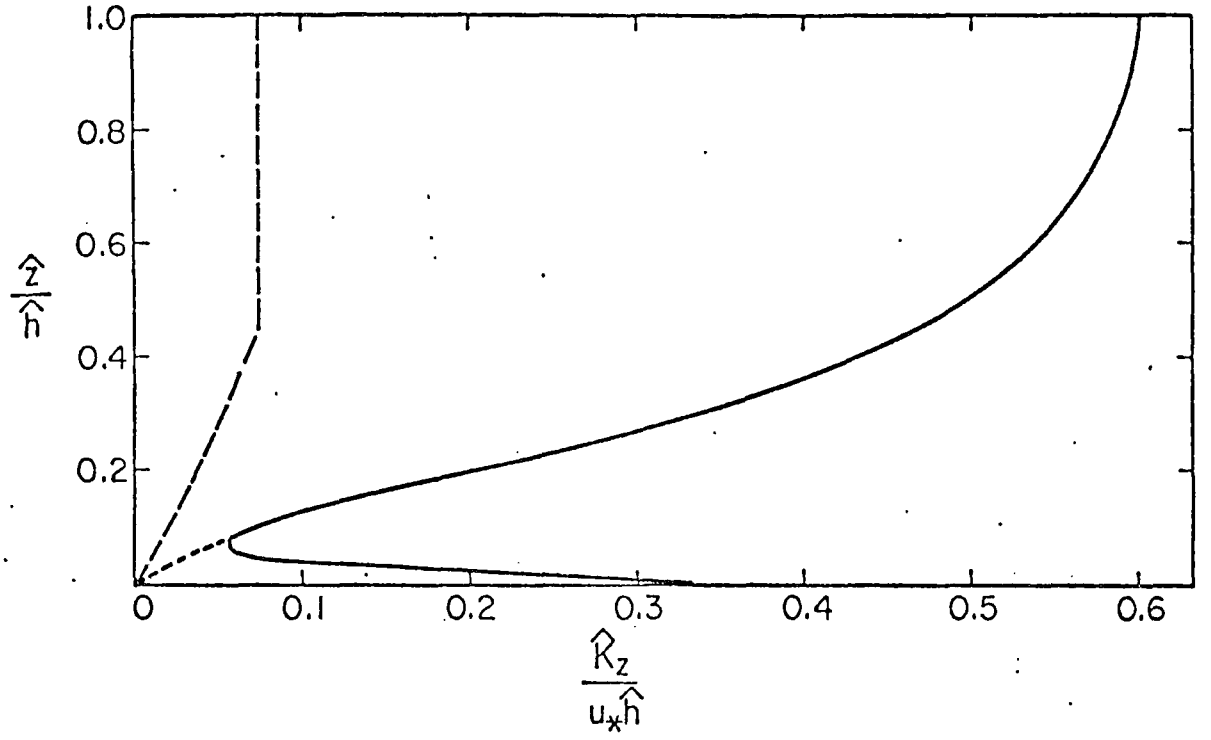

FIGURE 7. COMPARISON OF THE OPTIMAL K_Z PROFILE (SOLID CURVE) WITH THE PROFILE BASED ON SIMILARITY THEORY PROPOSED BY RAGLAND (DASHED) IN THE UNSTABLE ($\hat{h}/L$ = -4.5) BOUNDARY LAYER (See the text for an explanation of the short dashed line.)

Having described the differences between the optimal K_Z profile and some of the diffusivity formulas in current use, we turn now to the important question of how well the solutions of Eq. (23), using the optimal profiles, compare with the corresponding numerico-empirical solutions of Eq. (16). The latter are displayed in Figures 8(a) and 9(a) for the neutral and unstable cases, respectively. Note that in the neutral case the source height $z_s = 0.09$, and in the unstable case $z_s = 0.025$. To facilitate comparison of these solutions with those of Eq. (23), we plotted the latter in Figures 8(b) and 9(b) in the form of a fractional error

$$\varepsilon(x,z) = \frac{C(x,z) - C_0(x,z)}{C_0(x,z)} \quad , \tag{42}$$

where C denotes the solution of Eq. (23) and C_0 represents the corresponding value given by Eq. (16). These figures give the values of ε multiplied by 100 so that they can be interpreted as plots of the percentage error.

The figures reveal that the errors in Eq. (23) are nearly randomly distributed in space, except for the neutral case, in which rather large errors occur near the source. The larger errors in this region are consistent with the conclusion drawn from theoretical considerations that the gradient transport hypothesis should not hold when the length scale of the mean concentration distribution is comparable to or smaller than the Lagrangian length scale of the turbulence (Lamb, 1973). For the most part, however, this hypothesis appears to be reasonable. Errors in the calculated concentrations are no larger than about 20 percent at points farther than about $6u_*/f$ from the source in the neutral case and at nearly all points at ground level in the unstable case. Thus, if we find in future studies that the optimal K_Z profile is insensitive to the source height z_s and to the number, shapes, sizes, and distribution of particle sources, and that in such applications the errors in the diffusion equation do not increase significantly beyond those shown in Figures 8(b) and 9(b), then we will have succeeded, through the concept of optimal diffusivity, in transforming the diffusion equation into a model of atmospheric diffusion that is accurate enough to be useful in a wide range of applied problems.

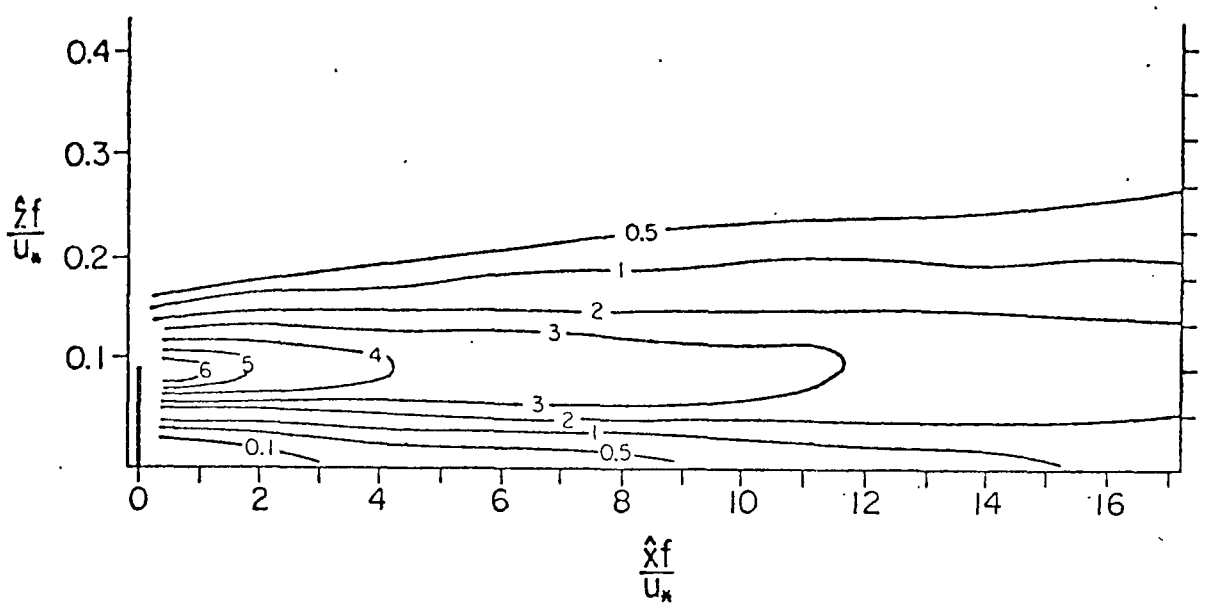

(a) Nondimensionalized Cross-Wind Integrated Concentrations Computed from Eq. (16) Using the Probability Density p Calculated from Deardorff's Data for Neutral (h/L = 0) Stability

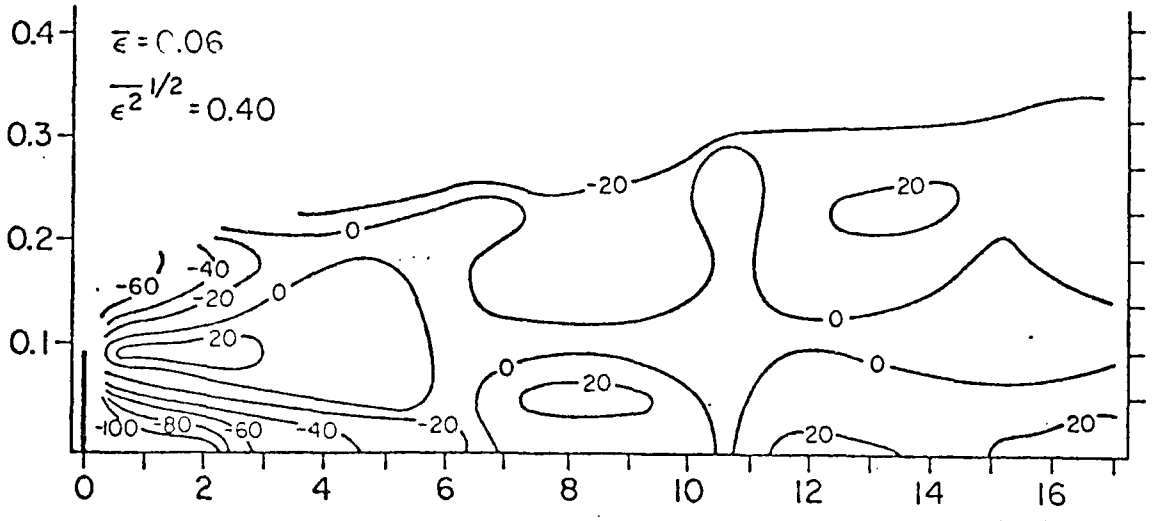

(b) Concentrations Given by the Diffusion Equation [Eq. (23)] Using the Optimum K_Z Profile Shown in Figure 6 and the Wind Profile (D) in Figure 5. Concentrations are expressed as the percentage deviation (i.e., 100ε) from those given in Part (a) above.

FIGURE 8. COMPARISON OF OPTIMAL PROFILE AND NUMERICO-EMPIRICAL SOLUTIONS FOR THE NEUTRAL CASE

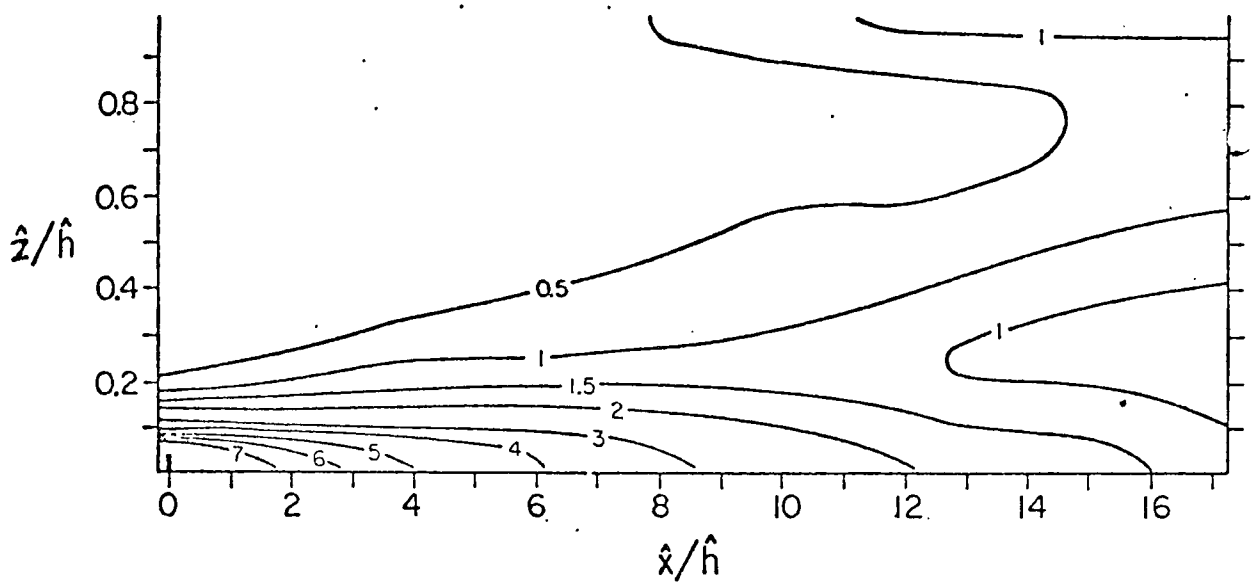

(a) Nondimensionalized Cross-Wind Integrated Concentrations Computed from Eq. (16) Using the Probability Density p Calculated from Deardorff's Data for the Unstable ($\hat{h}/L$ = -4.5) Case

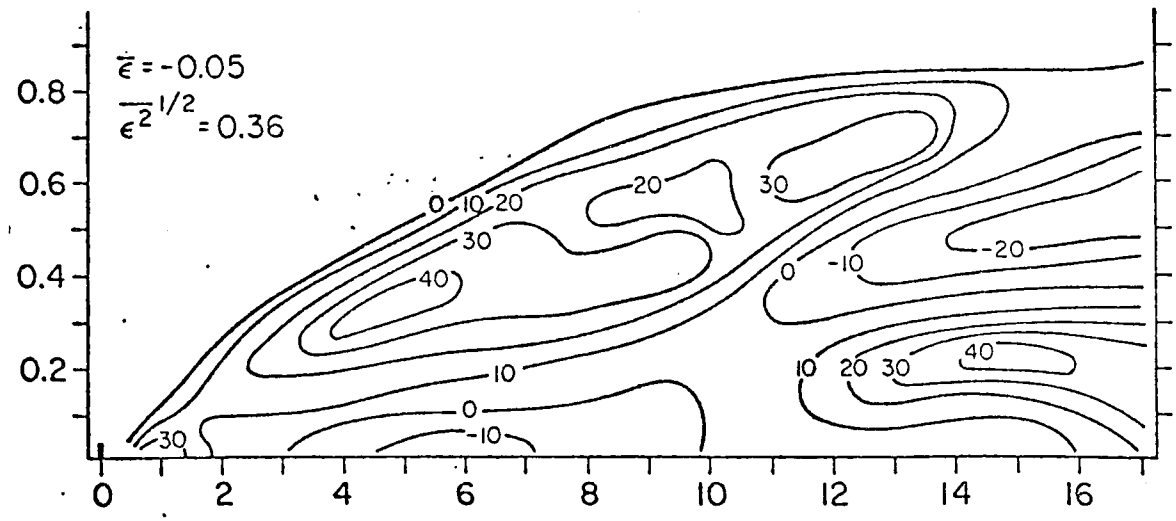

(b) Concentrations Given by the Diffusion Equation [Eq. (23)] Using the Optimum K_Z Profile Shown in Figure 6 and the Wind Wind Profile (D) in Figure 5. Concentrations are expressed as the percentage deviation (i.e., 100ϵ) from those given in Part (a) above.

FIGURE 9. COMPARISON OF OPTIMAL PROFILE AND NUMERICO-EMPIRICAL SOLUTIONS FOR THE UNSTABLE CASE

D. ANALYSIS OF THE DISPERSION PARAMETERS σ_z AND σ_x IN THE PLUME AND PUFF MODELS

Because we use the plume and puff models later, we attempt here to optimize the performance of these models. As previously mentioned, in both the plume and puff models, we assume that the probability density function p that enters in Eq. (16) has a Gaussian form that is completely determined by the mean $(\bar{x},\bar{z})$ and mean square $(\overline{x^2},\overline{z^2})$ displacements of fluid particles from their point of release. Recall that these quantities are properties of the turbulence. Because of the great difficulty of tracking particles in the atmosphere, past empirical studies of atmospheric diffusion have not attemped to measure the particle displacement statistics directly. Rather, $\overline{x^2}$ and $\overline{z^2}$ have been treated merely as free parameters to be used in fitting a Gaussian profile to concentration measurements made downwind from point sources of known strength under various atmospheric conditions. In this manner, the so-called dispersion parameters of Pasquill and Gifford and McElroy and Pooler were obtained. If the probability density p were actually Gaussian and if the assumptions involved in the empirical determination of the dispersion parameters were correct, then these parameters should be equivalent to the mean square particle displacements $\overline{x^2}$ and $\overline{z^2}$. Let us compare the profiles of $\overline{x^2}$ and $\overline{z^2}$ calculated from the particle trajectories given by Deardorff's model with the dispersion parameters measured in the two empirical studies just cited.

The Pasquill-Gifford data give a vertical dispersion parameter σ_z as a function of distance x from the source for various atmospheric stabilities. In principle, the parameter σ_z is related to the particle displacement statistics by

$$\sigma_z^2 = (\overline{z^2} - \bar{z}^2) \quad ,$$

and the distance x from the source is equivalent to $\bar{x}$. In all cases $\bar{z} = z_s$, where z_s is the height of release of the particles.

The computed values of $(\overline{z^2} - \bar{z}^2)^{\frac{1}{2}}$ as a function of $\bar{x}$ for both the neutral and unstable cases are represented in Figure 10 by the open triangles and open circles, respectively. In this figure, the nondimensionalized Pasquill-Gifford profiles of σ_z as a function of $\bar{x}$ for three different atmospheric stabilities are indicated by the curves. Since the positions, but not the slopes, of these curves depend on the value of the length scale $\hat{h}$ that is used to nondimensionalize σ_z and $\bar{x}$, we have indicated the extent to which each curve would be displaced by a different choice of $\hat{h}$.

Figure 10 clearly shows poor agreement between the calculated and measured σ's. The chief discrepancy is a systematic shift of the calculated values to the right of the measured ones. Thus, if we plot $(\overline{z^2} - \bar{z}^2)$ as a function of $0.24\bar{x}$, we obtain the closed circles and triangles shown in Figure 10, and these agree much better with the measurements. Note that in both the neutral and unstable cases, the slope of the computed σ_z profile conforms for small distances x to that of the Pasquill-Gifford profile for Class C stability (i.e., slightly unstable); but that at greater distances, the slopes become dissimilar, with the unstable case becoming parallel to the Class B profile and the neutral case becoming parallel to the Class D curve.

The closer agreement between the computed and measured data that results when a smaller value of $\bar{x}$, namely $0.24\bar{x}$, is used suggests that the Pasquill-Gifford data pertain to particles released from a lower level than that used in the numerical experiments. This conclusion follows from the fact that for a release height z', $d\bar{x}/dt \approx u(z')$; and, thus, with a strong wind shear near the ground (see Figure 5), $\bar{x}$ will increase with z' for a given value of the travel time t. This effect has apparently not been taken into account in routine diffusion estimates made with the plume formula (see Turner 1969). Consequently, one would expect those calculations to overestimate systematically the ground-level concentrations resulting from elevated sources, if (as appears likely) σ_z is less sensitive to z' than $\bar{x}$ is.

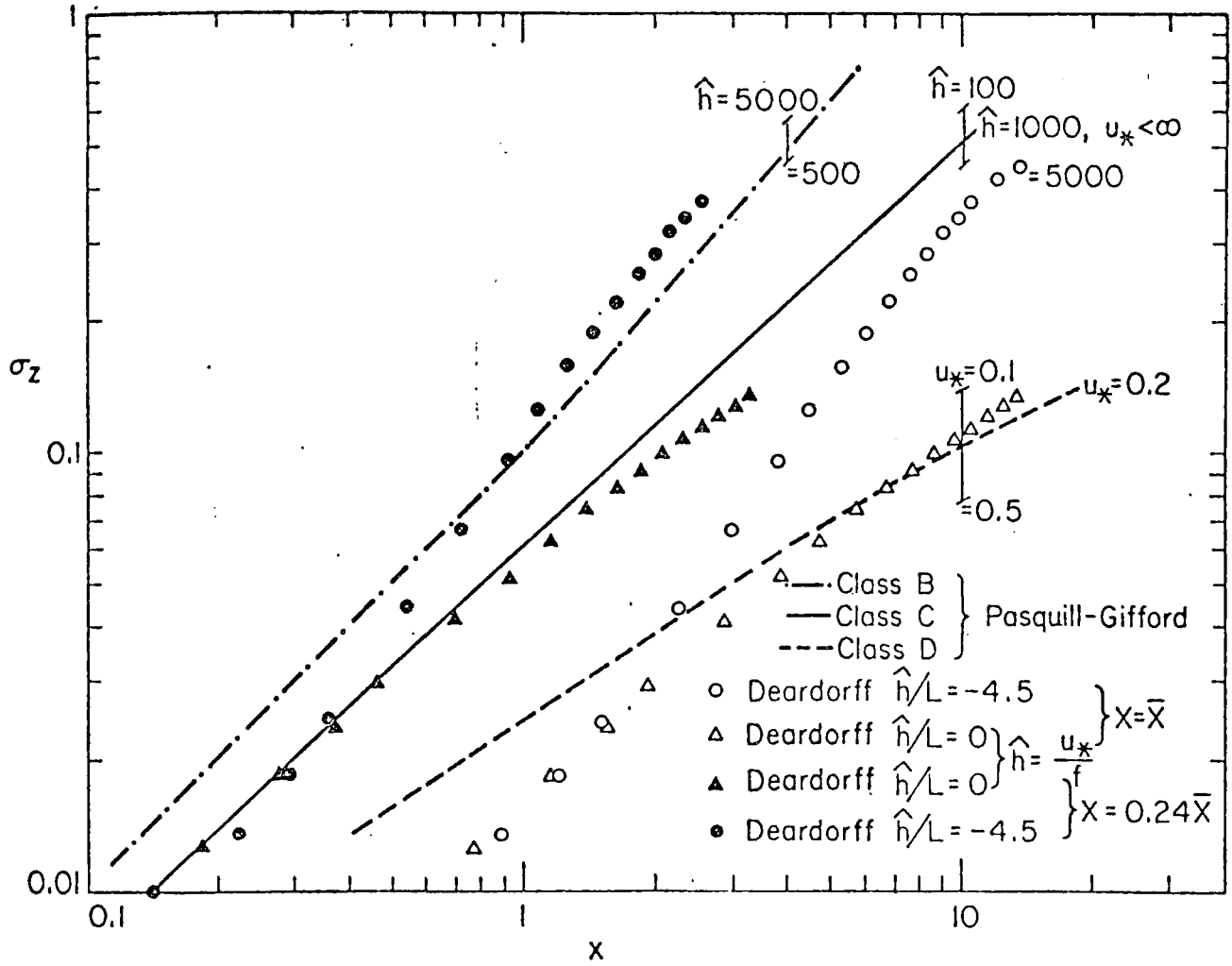

FIGURE 10. COMPARISON OF THE COMPUTED NONDIMENSIONALIZED ROOT-MEAN-SQUARE VERTICAL PARTICLE DISPLACEMENT σ_z (CIRCLES AND TRIANGLES) WITH THE PASQUILL-GIFFORD σ_z DISPERSION PARAMETER (CURVES) FOR NEUTRAL AND UNSTABLE CONDITIONS AS A FUNCTION OF DOWNWIND DISTANCE FROM THE SOURCE

The Pasquill-Gifford dispersion parameters are useful only in the plume formula. The puff model, however, requires σ's that are functions of travel time. Figure 11 presents data of this type, which have been collected by McElroy and Pooler in St. Louis. In this figure, the data are shown in nondimensional form, along with the computed values of $(\overline{z^2} - \bar{z}^2)$ for the same stability cases. Again, the positions, but not the slopes, of the empirical curves depend on the values of the length scale $\hat{h}$ and the time scale $\hat{h}/u_*$ that are used to nondimensionalize the data. Figure 11 shows that for a value of $u_* = 0.98$ m/sec, which is not unreasonable for the urban area in which the McElroy-Pooler data were collected, the computed and measured $\sigma_z(t)$ profiles are in excellent agreement in the unstable case and in good agreement for small t, under neutral conditions. (The downward turning of the computed σ_z profile at large t is a result of the effect of the simulated inversion base at z = 1 in the numerical model.)

Figure 12 compares the computed streamwise dispersion $\sigma_x = (\overline{x^2} - \bar{x}^2)^{\frac{1}{2}}$ with the lateral dispersion $\sigma_y = (\overline{y^2} - \bar{y}^2)^{\frac{1}{2}}$ observed by McElroy and Pooler as a function of travel time. (We did not compute σ_y originally because it is not needed in our problem.)

The McElroy-Pooler data for σ_y show little variation between neutral and unstable conditions, and the computed σ_x values exhibit the same behavior. In fact, Figure 12 shows that when the empirical data are nondimensionalized using a friction velocity of about 0.45 m/sec, about one-half the value used earlier with σ_z, the computed and observed dispersion curves are nearly superposed.

Recall that if the turbulence were such that the probability density p that enters in the generalized diffusion equation [Eq. (16)]--and in the puff equation--were actually Gaussian with joint moments $\overline{xy} = \overline{xz} = \overline{yz} = 0$, as is assumed in the puff model, then the empirical σ's would be equivalent to the root-mean-square second moments of p, i.e., $\overline{x^2}^{\frac{1}{2}}$, $\overline{z^2}^{\frac{1}{2}}$, and so forth, as described earlier, and the concentrations predicted by the puff model would agree exactly with those given by Eq. (16). It follows, therefore,

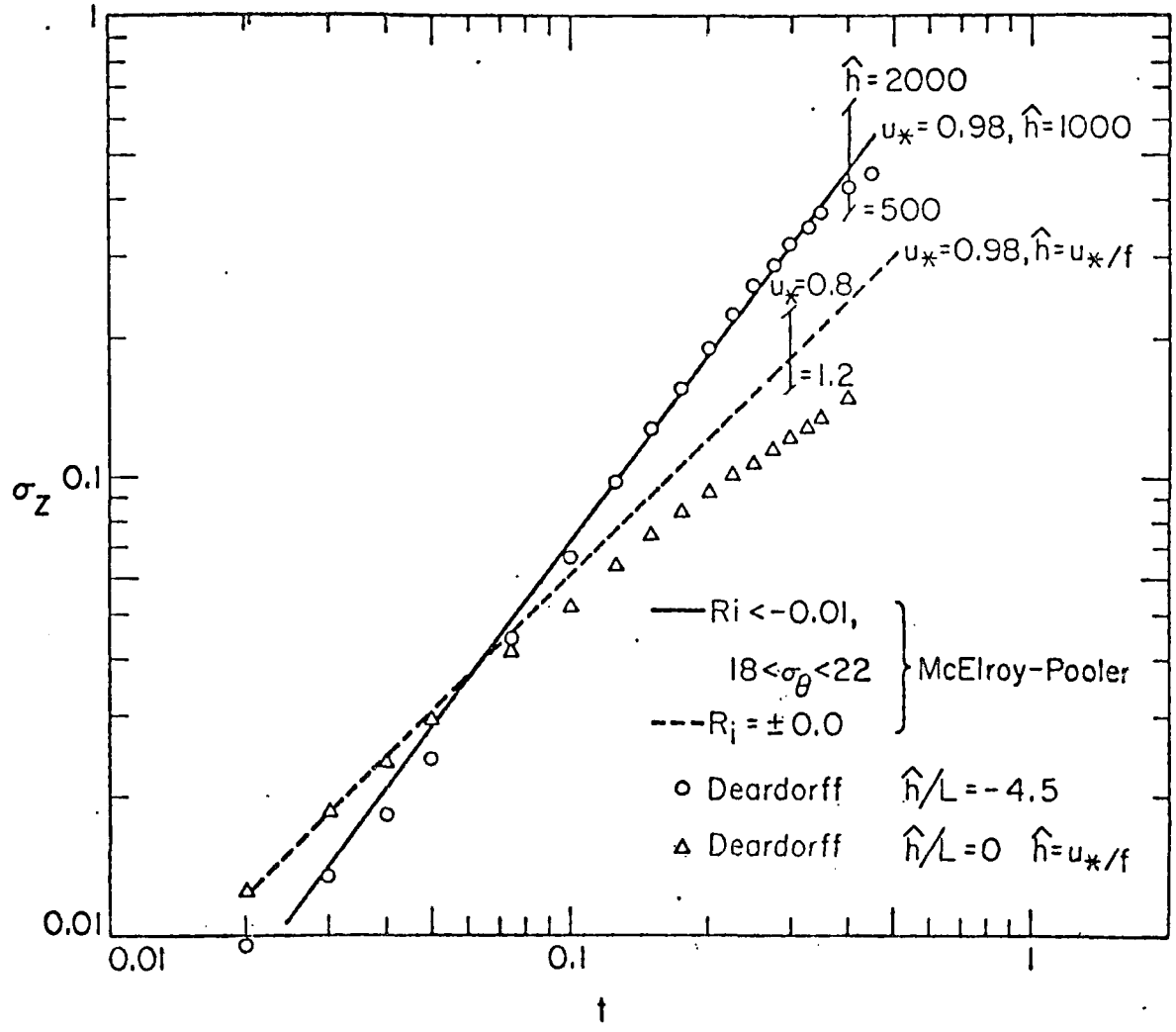

FIGURE 11. COMPARISON OF THE COMPUTED NONDIMENSIONALIZED ROOT-MEAN-SQUARE VERTICAL PARTICLE DISPLACEMENT σ_z (CIRCLES AND TRIANGLES) WITH THE MCELROY-POOLER σ_z DISPERSION PARAMETER UNDER NEUTRAL AND UNSTABLE CONDITIONS AS A FUNCTION OF TRAVEL TIME t

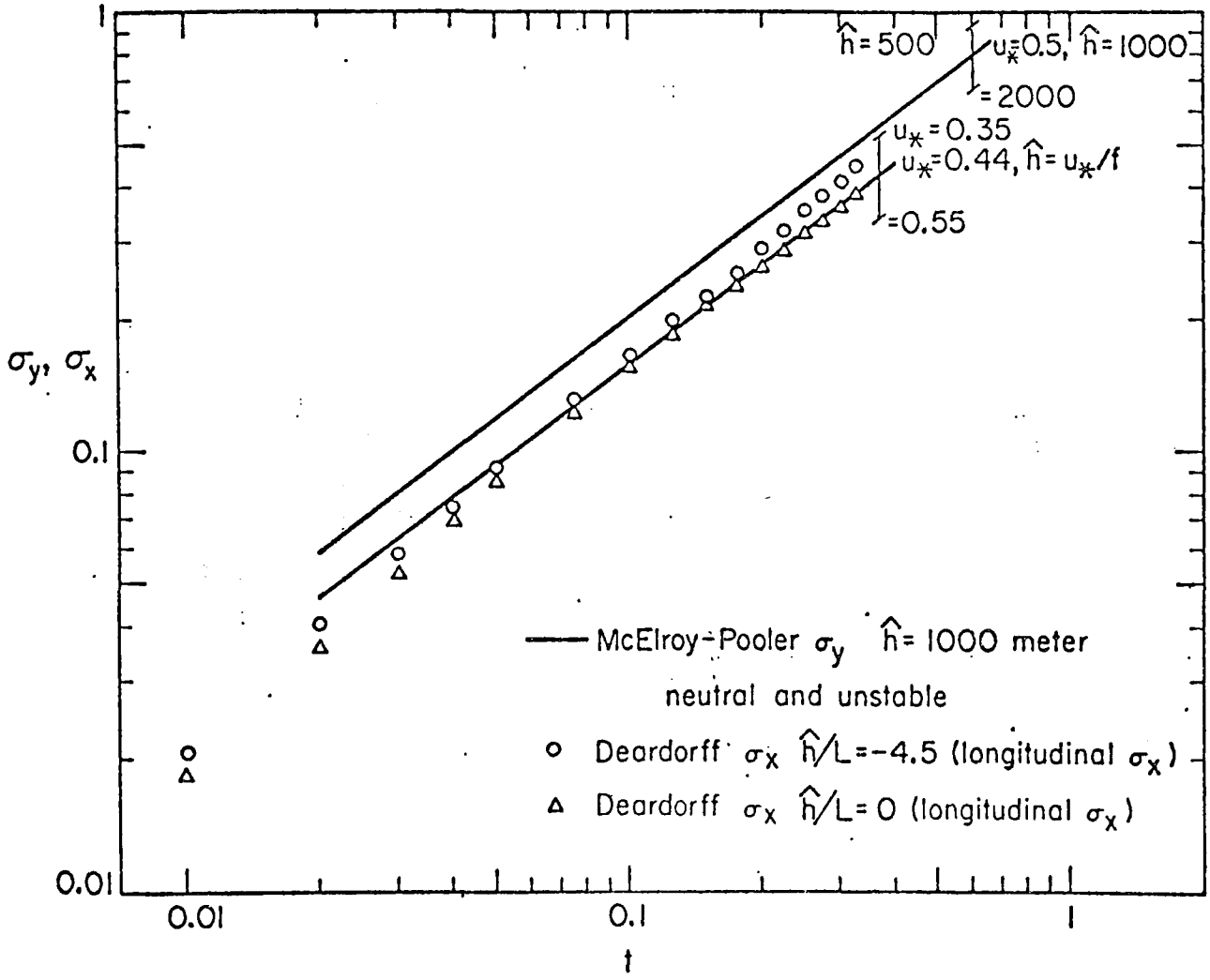

FIGURE 12. COMPARISON OF THE COMPUTED NONDIMENSIONALIZED STREAMWISE ROOT-MEAN-SQUARE PARTICLE DISPLACEMENT σ_x (CIRCLES AND TRIANGLES) WITH THE MCELROY-POOLER LATERAL DISPERSION PARAMETER σ_y FOR NEUTRAL AND UNSTABLE CONDITIONS AS A FUNCTION OF TRAVEL TIME t

that since the empirical σ's are in close agreement with the numerically calculated values of $\overline{x^2}^{1/2}$, $\overline{z^2}^{1/2}$, and so forth, major errors in the puff model predictions reflect departures of the turbulence characteristics from those consistent with the assumed Gaussian form of p. Similar arguments apply to the plume formula. Let us examine these errors.

For this purpose, we set up the standard plume model using Pasquill-Gifford dispersion data, and the puff model of Lamb and Neiburger (1971) using the McElroy-Pooler data, to simulate the same two-dimensional problem that was treated earlier in Section C. In each case, we nondimensionalized the empirical data in the manner portrayed in Figures 10, 11, and 12 so that each set was in closest agreement with the computed particle statistics $\overline{x^2}$, $\overline{z^2}$, and so forth. We should point out that the plume model does not account rigorously for the effects of the inversion layer present in this problem. However, in the trial calculations presented here, this deficiency is not serious, because within the range of downwind distances treated, the inversion layer has little overall influence on the concentration distributions.

Figure 13 presents the results of the calculations for the neutral case, and Figure 14 gives those for the unstable case. As in the previous figures, we have plotted the model predictions in terms of their fractional departure ε, Eq. (42), from the corresponding numerico-empirical solutions of Eq. (16). The latter are given in Figures 8(a) and 9(a). We consider only the puff model results here, because these results provide a better assessment of the accuracy of the assumed Gaussian form of p due to the closer agreement between the McElroy-Pooler data and the computed particle statistics.

As shown in Figure 11, for the neutral case the empirical σ_z and the calculated $\overline{z^2}^{1/2}$ profiles are nearly superposed for travel times $t \lesssim 0.1$, which corresponds to distances x from the source in the range $0 < x \lesssim 4$.

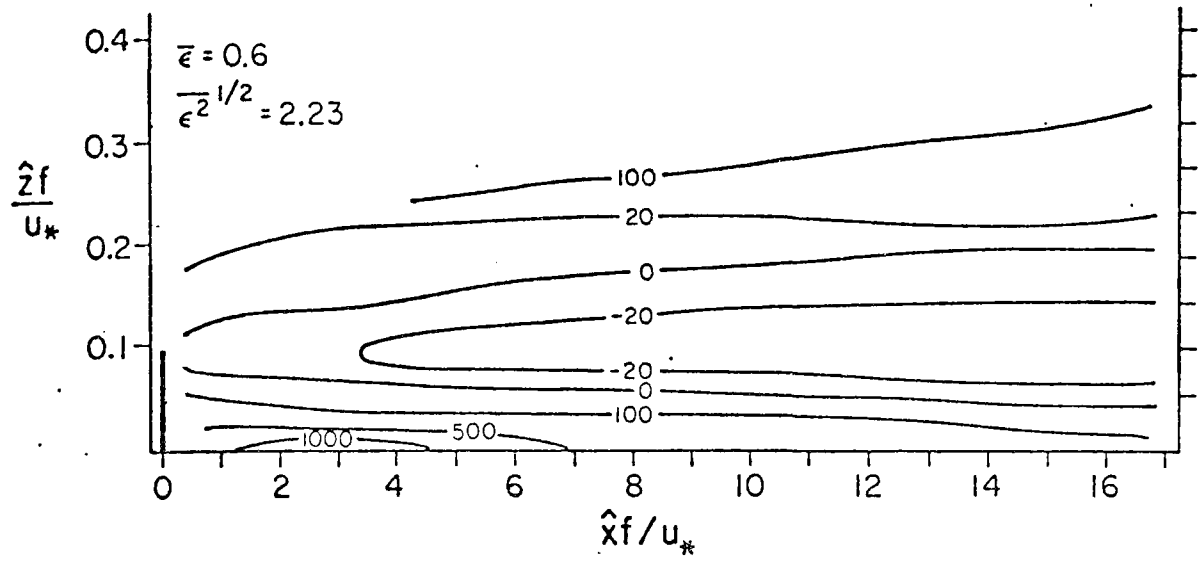

(a) Nondimensionalized Cross-Wind Integrated Concentrations Predicted by the Puff Model, Expressed as the Percentage Deviation (i.e., 100ε) from Those Shown in Figure 8(a) Which Were Obtained from Eq. (16) for the Case of Neutral Stability

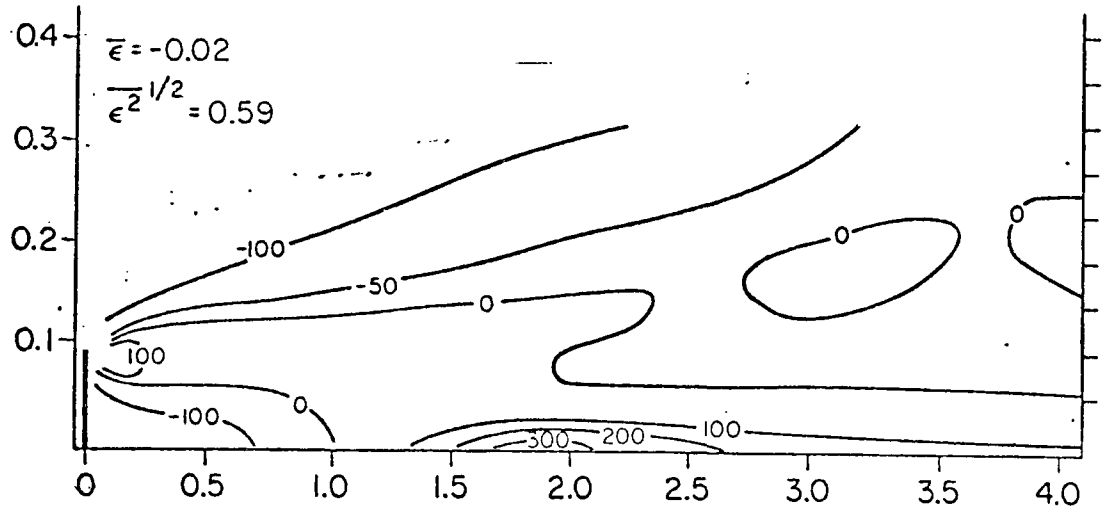

(b) Results of the Plume Model Calculations Expressed as in Part (a)

FIGURE 13. COMPARISON OF THE PREDICTIONS MADE BY THE PUFF MODEL AND THE PLUME MODEL FOR THE CASE OF NEUTRAL STABILITY. The puff model used neutral, travel-time-dependent McElroy-Pooler data; the plume model used Pasquill-Gifford Class C data and an expanded x-axis (see the text).

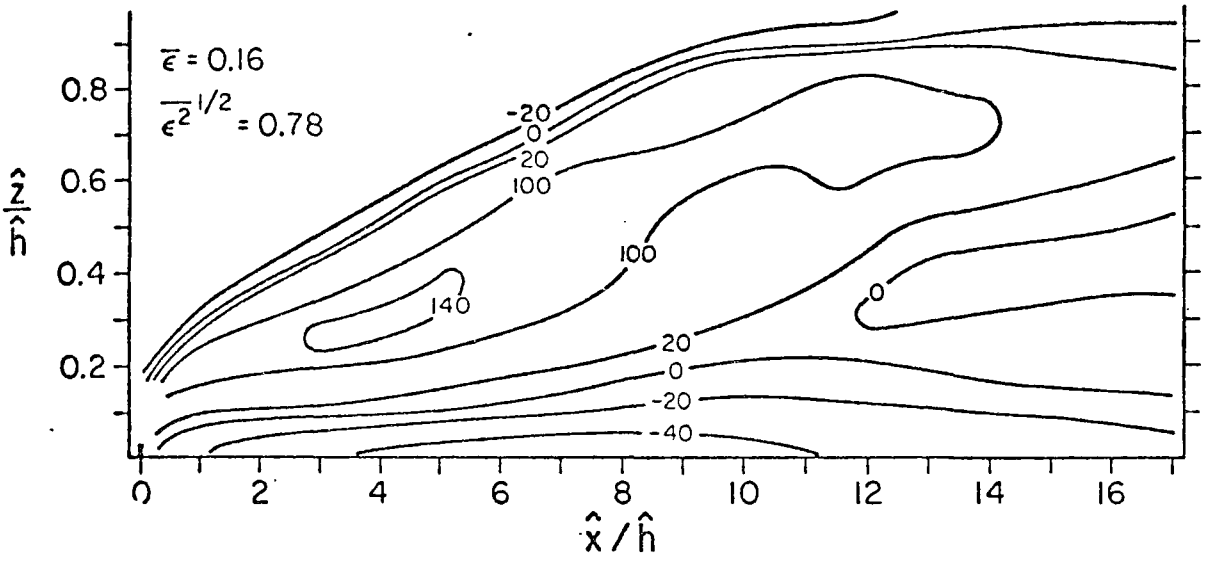

(a) Nondimensionalized Cross-Wind Integrated Concentrations Predicted by the Puff Model, Expressed as the Percentage Deviation (i.e., 100) from Those Shown in Figure 9(a), Which Were Obtained from Eq. (16) for the Unstable Case

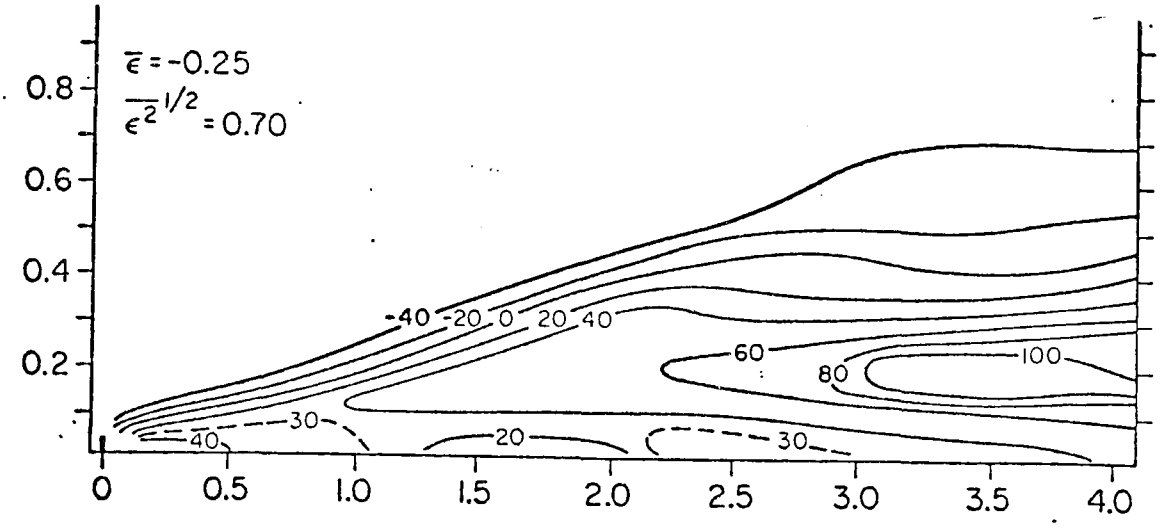

(b) Results of the Plume Model Calculations Expressed as in Part (a)

FIGURE 14. COMPARISON OF THE PREDICTIONS MADE BY THE PUFF MODEL AND THE PLUME MODEL FOR THE UNSTABLE CASE. The puff model used "slightly unstable" McElroy-Pooler data; the plume model used Pasquill-Gifford Class B data and an expanded x-axis (see the text).

However, Figure 13(a) reveals that in this range the predictions of the puff model are considerably in error. Concentrations are underestimated on the centerline of the plume and are greatly overestimated at the edges, especially along the plume edge that touches the ground. This behavior suggests that the diffusing particles behave as if a weak restoring force were preventing them from wandering too far away from their level of release, i.e., the plume axis. Thus, particles that have wandered a distance $\overline{z^2}^{1/2}$, say, from the plume axis have a larger probability of moving back toward the plume centerline than of continuing on to still more remote points. In contrast, the Gaussian density implies that at each instant the particles have equal probabilities of moving toward or away from the plume axis. In short, the Gaussian density has a much larger kurtosis or flatness factor than the true probability density p does under neutral conditions.

Turning next to the unstable case, we see in Figure 11 that the measured σ_z values and those computed for $\overline{z^2}^{1/2}$ are in excellent agreement at all travel times (and distances from the source), except those at the extreme upper limit of the range treated. Figure 14(a) reveals that the errors in the puff model predictions are smaller in this instance than those in the neutral case but that there is still a tendency for the predicted concentrations along the plume centerline to be too small and for those at the edges to be too large. One factor contributing to these errors is the assumption in the puff model that the joint moment $\overline{xz}$ is zero. Actually, this moment is strongly positive; because of the rapid increase in wind speed above the level of release (namely, $z_{REL} = 0.025\hat{h}$) of the particles in the unstable case (see Figure 5), particles that are displaced upward are also systematically displaced downstream. Consequently, at any distance x from the source, a significant fraction of the particles that normally would be found at the plume edge are found farther downstream, and in their places are particles from points upstream of x, which thus have smaller vertical displacements. As a result, the effective width of the plume is consistently smaller than one would predict on the basis of $\overline{z^2}^{1/2}$ alone. This phenomenon is not as pronounced in the neutral case, because the wind shear at the level of release ($z_{REL} = 0.1u_*/f$) of the particles is much smaller (see Figure 5).

The analyses just completed illustrate the inadequacy of the basic assumption underlying the plume and puff models that the probability density p entering in Eq. (16) is of a Gaussian form. However, despite these limitations, the plume and puff models remain attractive formulations in applied studies because of their mathematical simplicity. For this reason, it is useful to inquire whether profiles exist that will bring the errors in the predictions of these two models within the range of acceptability.

To explore this question, we used the variances $\sigma_x(\tau)$ and $\sigma_z(\tau)$ as adjustable parameters for obtaining a least-squares best fit of the Gaussian density function to the numerico-empirical expression p. Figures 15 and 16 present the resulting "optimal" profiles of σ_x and σ_z, respectively. In each case, the corresponding empirical data of McElroy and Pooler, presented earlier in Figures 11 and 12, are shown for comparison. Since the method used to obtain the empirical data is similar to that used here to obtain the optimal σ_x and σ_z values, it is surprising that the latter do not compare as well with the empirical data as do the computed root-mean-square particle displacements shown in Figures 11 and 12.

In a similar manner, we adjusted the dispersion parameter $\sigma_z(x)$ to obtain the least-squares best fit of the plume formula to the numerico-empirical concentration distributions given in Figures 8(a) and 9(a). Figure 17 presents the results, along with the empirical Pasquill-Gifford data for comparison. We subsequently inserted these "optimal" dispersion coefficients into the puff and plume models and performed new sets of calculations to compare with the numerico-empirical concentration profiles given in Figures 8(a) and 9(a). The results, given in terms of the fractional error ε used earlier, are presented in Figure 18 for the neutral case and in Figure 19 for the unstable case. Comparing Figures 13(a) and 14(a) with Figures 18(a) and 19(a), we find that although the optimal σ_x and σ_z profiles improved, the overall performance of the puff model, errors in the predicted values remain intolerably large in certain regions. This is especially true for the ground-level concentrations predicted in the neutral case [see Figure 18(a)].

Figures 13(b) and 18(b) reveal that using the "optimal" $\sigma_z(x)$ profiles, the plume model fails by a considerable margin to achieve the level of accuracy that was attained in the earlier calculations. The reader will recall that in the previous computations, we expanded the x-axis to account for

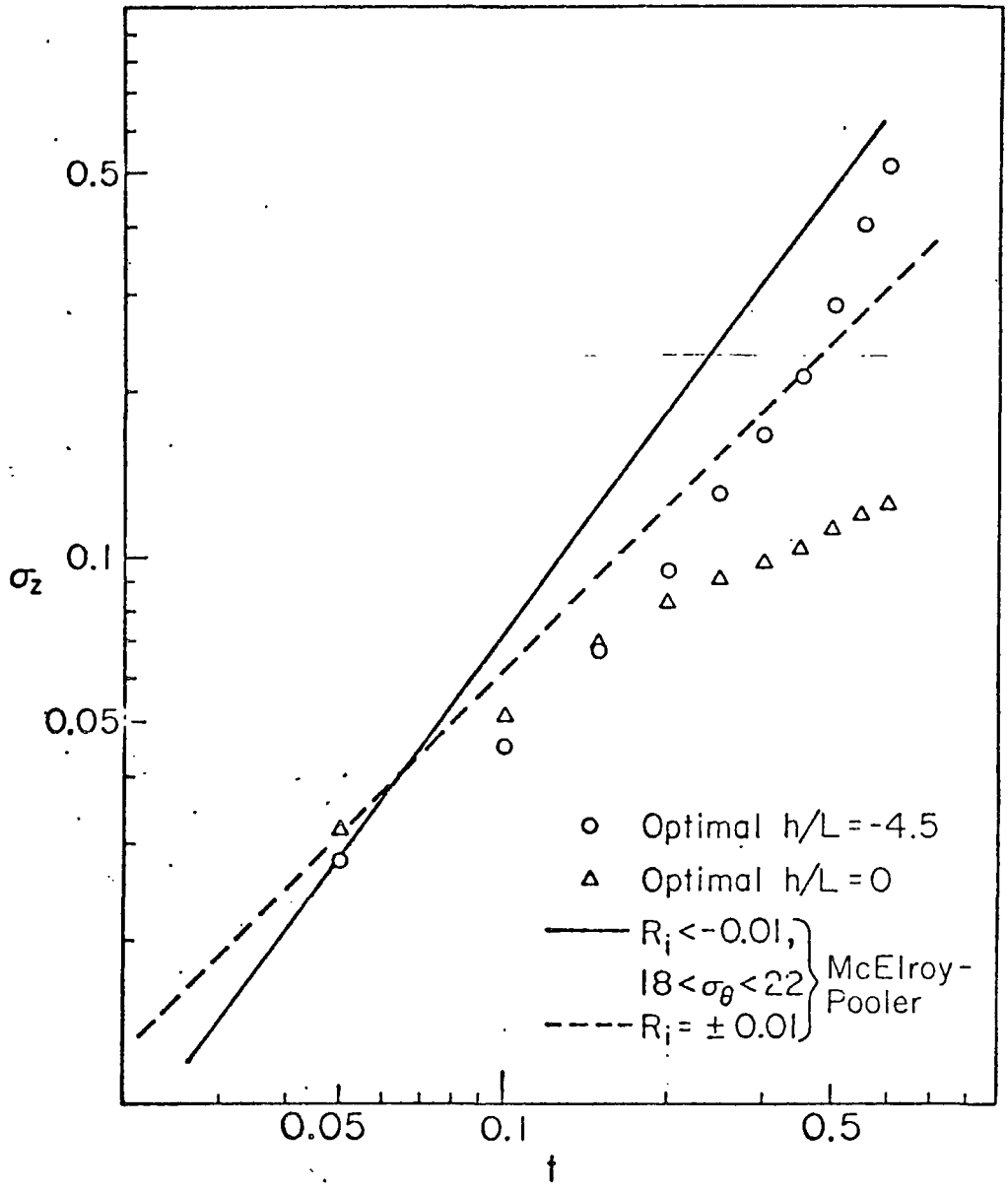

FIGURE 15. OPTIMAL $\sigma_z(t)$ PROFILES FOR USE IN THE PUFF MODEL COMPARED WITH THE EMPIRICAL DATA OF MCELROY AND POOLER

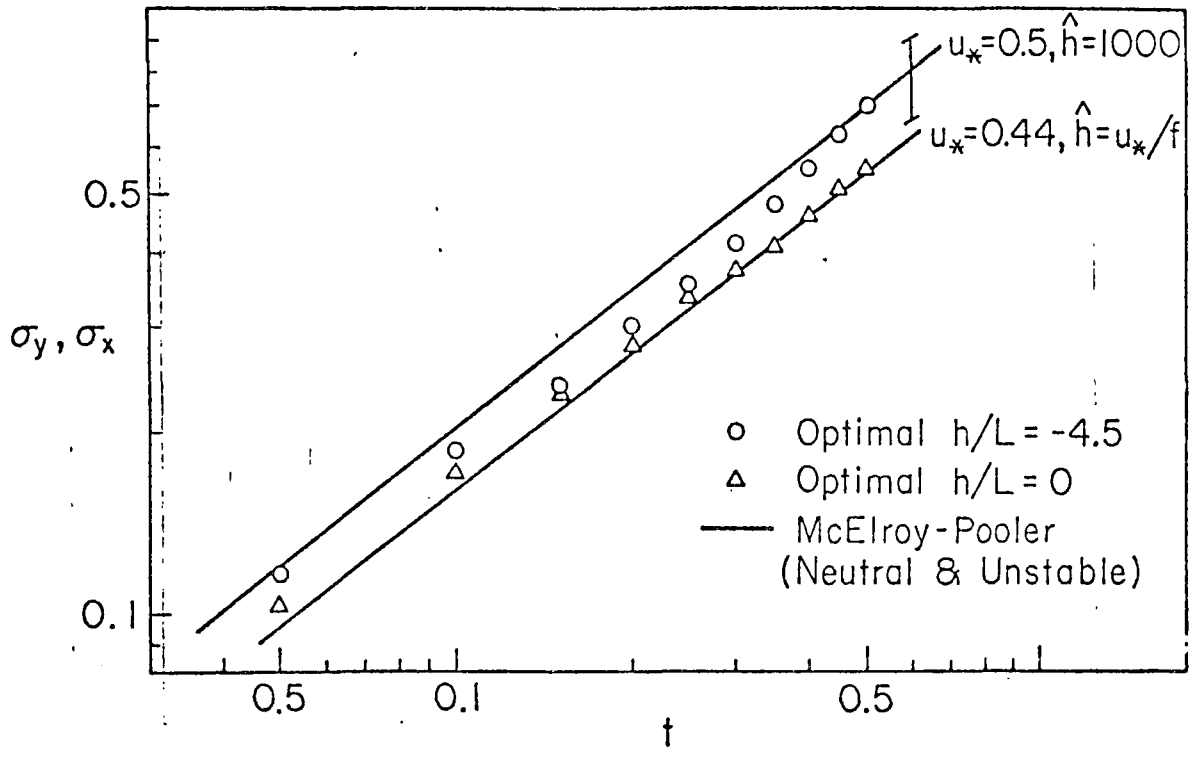

FIGURE 16. OPTIMAL STREAMWISE DISPERSION $\sigma_x(t)$ COMPARED WITH THE EMPIRICAL LATERAL DISPERSION DATA OF MCELROY AND POOLER

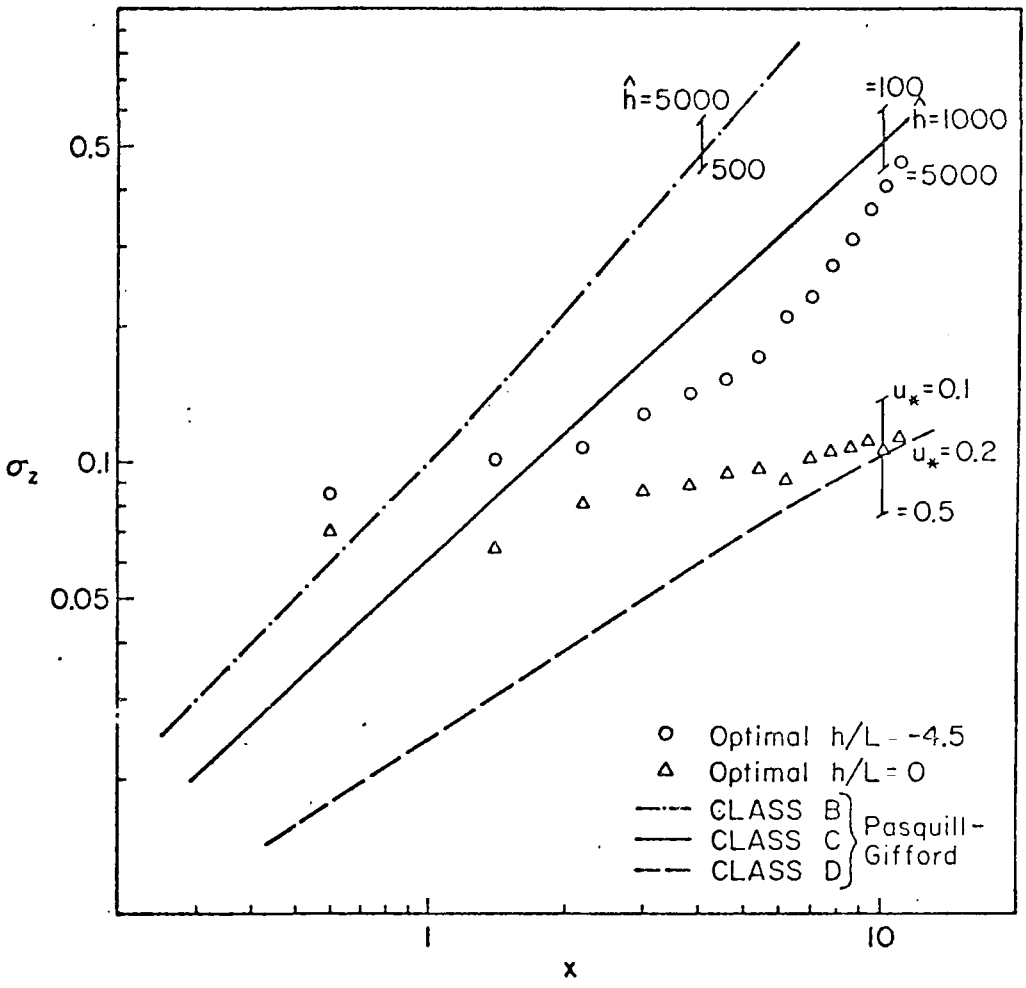

FIGURE 17. OPTIMAL $\sigma_z(x)$ PROFILES FOR USE IN THE PLUME FORMULA COMPARED WITH THE EMPIRICAL DATA OF PASQUILL AND GIFFORD

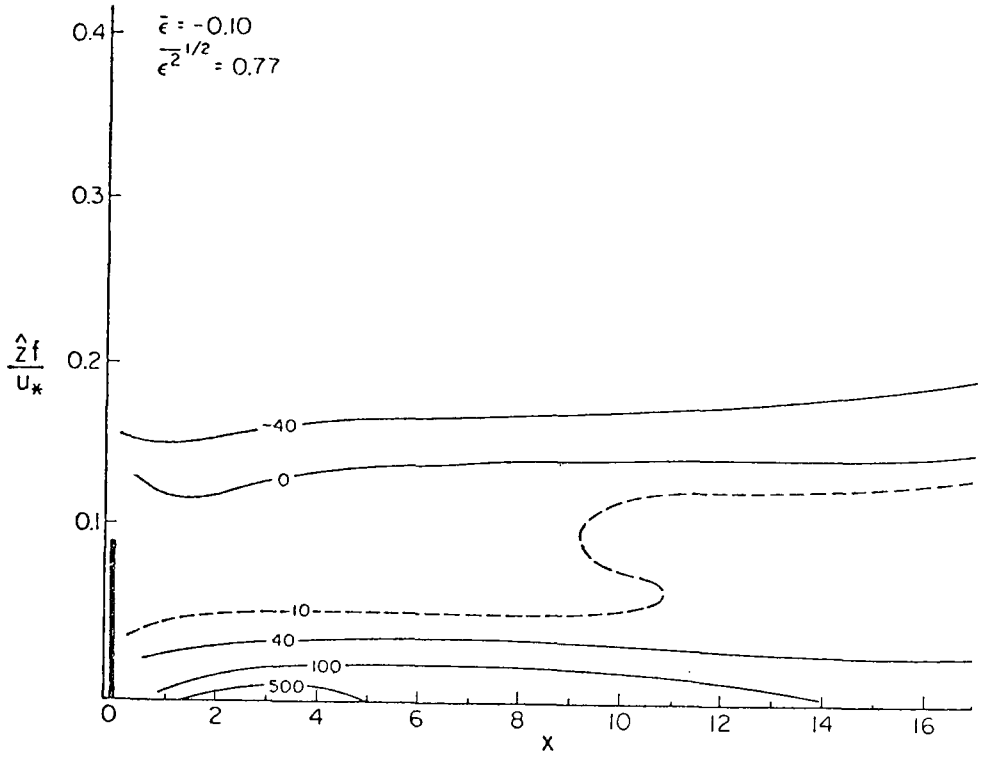

(a) Results of the Puff Model

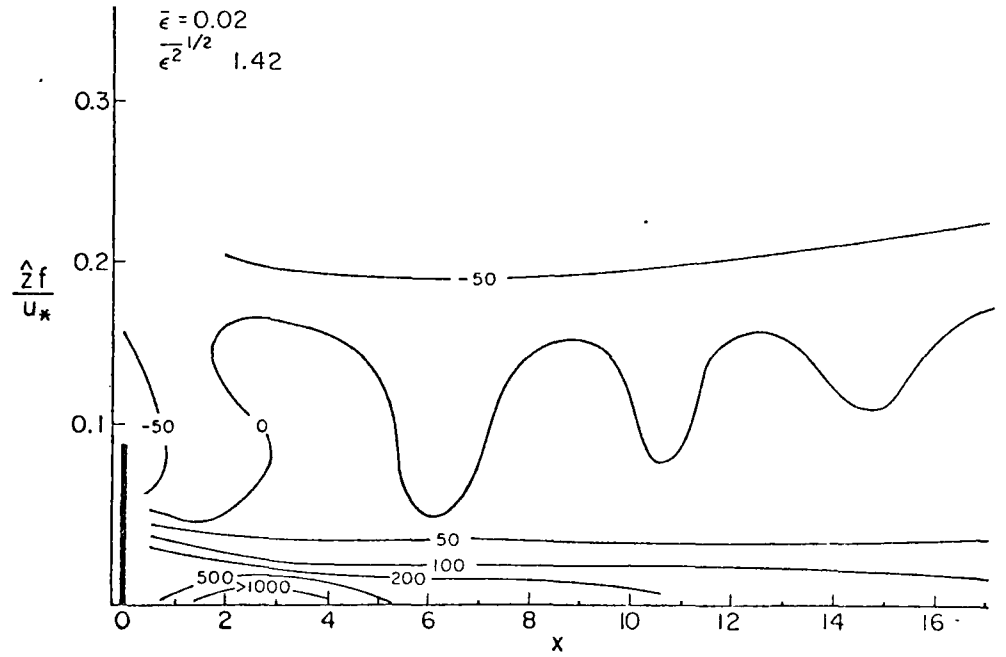

(b) Results of the Plume Model

FIGURE 18. THE FRACTIONAL ERROR (100ε) RESULTING IN THE PUFF MODEL AND THE PLUME MODEL USING THE OPTIMAL σ PROFILES SHOWN IN FIGURES 15 THROUGH 17 FOR THE NEUTRAL CASE. Errors are relative to numerico-empirical concentration distribution given in Figure 8(a).

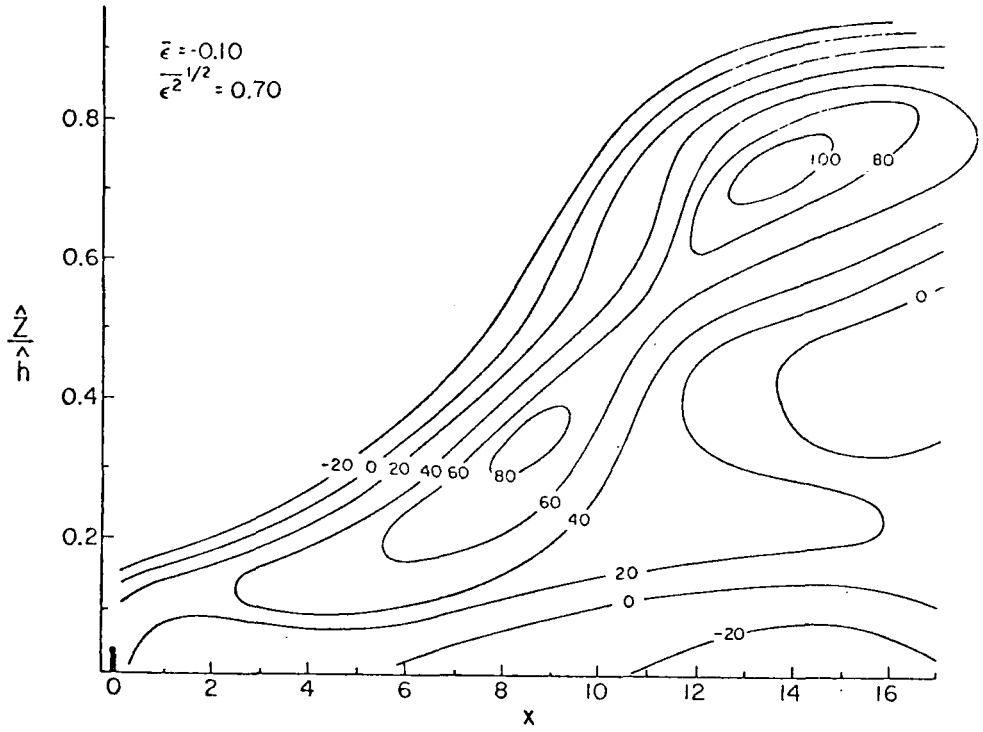

(a) Results of the Puff Model

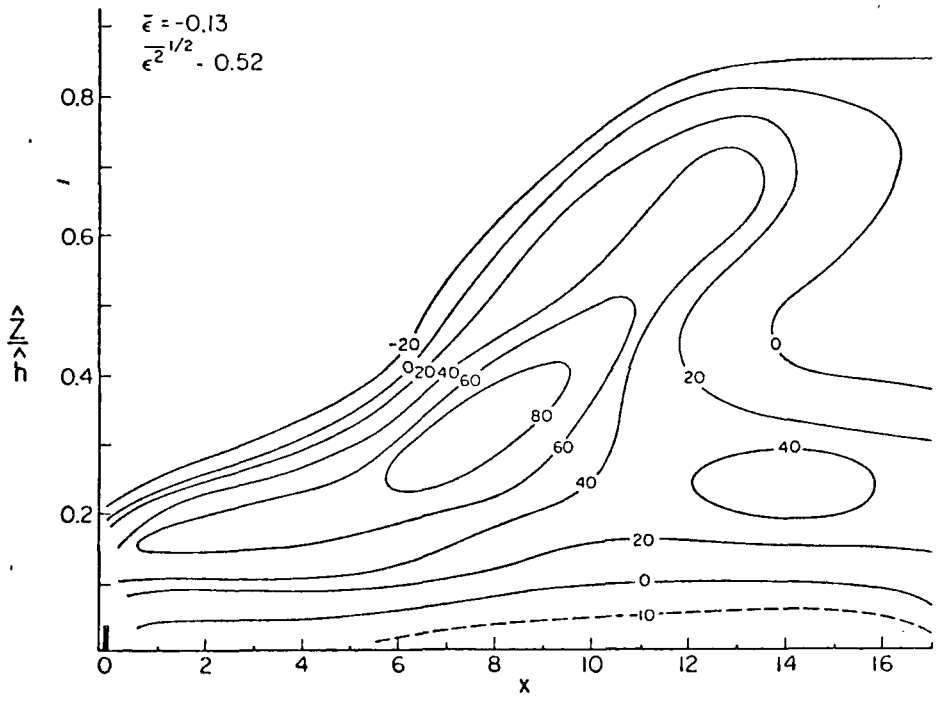

(b) Results of the Plume Model

FIGURE 19. THE FRACTIONAL ERROR (100ε) RESULTING IN THE PUFF MODEL AND THE PLUME MODEL USING THE OPTIMAL σ PROFILES SHOWN IN FIGURES 15 THROUGH 17 FOR THE UNSTABLE CASE. Errors are relative to the numerico-empirical concentration distribution given in Figure 9(a).

apparent differences in the mean particle velocities implicit in the empirical data and in the numerical turbulence model. We also made arbitrary adjustments of the atmospheric stability. In contrast, we did not employ any of these artifices in computing the optimal $\sigma_z(x)$ values. These facts, together with the error values given in Figure 18(b) suggest that the basic plume formula does not provide a wholly adequate description of atmospheric diffusion, at least under neutral stability conditions. However, under unstable conditions, the accuracy is better, as indicated by Figure 19(b).

E. IMPLEMENTATION OF THE OPTIMAL DIFFUSIVITY AND WIND SHEAR PROFILES IN AN AIRSHED MODEL

Since the optimal diffusivity profiles derived in Section C are based on a rather small ensemble of particle trajectories, the statistical significance of these profiles is limited. In addition, the question arises of whether the profiles vary significantly with changes in the source height. (In our studies, data from only one release height were available for each stability case.) The data needed to resolve these problems are currently being collected using Deardorff's newest model, and we plan to continue studies similar to those described above but with a much wider scope.

For the present, however, we are developing the methods necessary to implement these diffusivity and wind shear profiles in operational airshed models. For this purpose, we have fitted fourth-order polynomials to the wind shear and optimal diffusivity profiles derived earlier. Table 2 presents these in nondimensional form. The only task necessary to use these results in a diffusion model is to convert the profiles into dimensional forms. Thus, denoting dimensional variables by the caret (^), we have [cf Eq. (22)]

$$\hat{K}_z(\hat{z}) = \begin{cases} K_z\left(\dfrac{\hat{z}}{z_i}\right) u_* z_i & , \quad \text{unstable case } (z_i/L = -4.5) \quad ; \\ K_z\left(\dfrac{\hat{z}f}{u_*}\right) \dfrac{u_*^2}{f} & , \quad \text{neutral case } (z_i/L = 0) \quad . \end{cases} \tag{43}$$

Here $K_z(z)$ is the nondimensional diffusivity, given in Table 2, at height z (nondimensional) and u_*, z_i, f, and L are defined as before. Similarly, we have

$$\hat{\bar{u}}(\hat{z}) = \bar{u}\left(\frac{\hat{z}}{\hat{h}}\right)\hat{u}_* \quad , \tag{44}$$

where $\hat{u}_*$ is the friction velocity, $\bar{u}$ is the wind speed profile given in Table 2, and $\hat{h} = z_i$ in the unstable case and u_*/f under neutral conditions. Note that the wind profile $\bar{u}$ given in the table is for a particular value of $R = \hat{h}/\hat{z}_0$, where $\hat{z}_0$ is the surface roughness. For different values of R, the profiles must be adjusted as described below.

In air pollution modeling studies, one normally has available only z_i, f, z_0, and u_{10}, where the last term denotes the wind speed at 10 m*. Atmospheric stability data are seldom available from measurements. Rather, Pasquill's technique of categorizing the stability into Classes A through F using ground level wind speed and insolation observations is frequently employed. Recently, Golder (1972) obtained approximate relationships between Pasquill's stability classes and the Monin-Obukhov length L. Thus, we assume that estimates of $\hat{z}_i/L$ can be obtained using Golder's formulas and Pasquill's stability classes. The friction velocity u_* must be determined before the wind and diffusivity profiles can be converted into dimensional forms.

An often used formula for u_* is

$$u_* = C_D u_g \quad , \tag{45}$$

where C_D is a drag coefficient for the boundary layer and u_g is the geostrophic wind speed. Lettau (1959) proposed the formula

$$C_D = 0.16\left[\log_{10}\left(\frac{u_g}{fz_0}\right) - 1.8\right]^{-1} \quad , \quad \text{neutral case} \tag{46}$$

*A technique for estimating the surface roughness z_0 has been proposed by Lettau (1970).

Table 2

OPTIMAL PARAMETERS FOR USE IN THE DIFFUSION EQUATION AND IN THE GAUSSIAN PUFF AND PLUME MODELS (NONDIMENSIONAL VARIABLES†)

Model	Parameter	Stability: Neutral $\frac{\hat{h}}{L} = 0$ $\frac{u_*}{fz_0} = 1.5 \times 10^7$	Stability: Unstable $\frac{\hat{h}}{L} = -4.5$ $\frac{z_i}{z_0} = 6.8 \times 10^6$
Gaussian puff	$\sigma_z(\tau)$	$= 0.0045 + 0.4\tau$, $0.022 < \tau \leq 0.079$ $= 0.026 + 0.129\tau$, $0.079 < \tau \leq 0.32$	$= -0.0023 + 0.65\tau - 1.89\tau^2 + 5.32\tau^3$, $0.04 < \tau \leq 0.52$
	$\sigma_x(\tau)$	$= 1.85\tau$, $0 < \tau \leq 0.045$ $= 0.045 + 0.92\tau$, $0.045 < \tau \leq 0.32$	$= 0.045 + 1.307\tau$, $0.05 < \tau \leq 0.7$
Gaussian plume	$\sigma_z(x)$	$= 0.032 + 0.0044x$, $0.23 < x < 4.0$	$= 0.075 + 0.0167x$, $0.5 < x < 5.5$ $= -0.065 + 0.0435x$, $5.5 < x < 9.5$
Diffusion equation	$K_z(z)$§	$= 7.396 \times 10^{-4} + 6.082 \times 10^{-2}z + 2.532z^2 - 12.72z^3 + 15.17z^4$, $0 < z < 0.45$; $= 0$, $z > 0.45$.	$= -6.934 \times 10^{-3} + 0.6113z + 3.297z^2 - 6.442z^3 + 3.153z^4$, $0.02 < z < 1.0$
	$\bar{u}(z)$	$= 29.82 + 213.2z - 1989z^2 + 8743z^3 - 14670z^4$, $0.022 < z < 0.21$; $= u(0.21)$, $z \geq 0.21$.	$= 26.22 + 153.2z - 1428z^2 + 5541z^3 - 7523z^4$, $0.025 < z < 0.3$ $= u(0.3)$, $z \geq 0.3$.

† All lengths were made nondimensional by z_i = inversion height in the unstable case and by u_*/f in the neutral case. Times were made nondimensional by z_i/u_* (unstable) and $1/f$ (neutral).

§ The polynomial given for the neutral case is only qualitatively accurate. See Appendix A for a more precise formulation.

for neutral conditions. Our work with Deardorff's boundary layer model has led to a confirmation of this expression. We have also found that in the unstable case, the drag coefficient is given approximately by

$$C_D = 0.156\left[\log_{10}\left(\frac{L}{z_0}\right) - 1.18\right]^{-1} \quad , \text{ unstable case} \quad . \tag{47}$$

Because the geostrophic wind speed u_g is often not known in air pollution studies, Eq. (45) is difficult to use in diffusion modeling applications. Consequently, we attempt below to obtain u_* from the 10-m wind u_{10} and the wind speed profiles that we have available.

Consider first the unstable case $z_i/L = -4.5$, which is representative of the mixed layer over urban regions during much of the daylight period. For the unstable case, we have from Table 2,

$$\begin{aligned} \frac{\hat{\bar{u}}\left(\frac{z}{z_i}\right)}{u_*} = \bar{u}(z) &= 26.22 + 153.2z - 1428z^2 \\ &\quad + 5541z^3 - 7523z^4 \quad , \\ &\qquad 0.025 < \hat{z}/z_i < 0.3 \quad ; \\ = \bar{u}(0.3) \quad , &\quad z = \hat{z}/z_i \geq 0.3 \quad . \end{aligned} \tag{48}$$

Note that this profile is valid only for $z \geq 0.025$, $R = z_i/z_0 = 6.8 \times 10^6$, and $\hat{z}_i/L = -4.5$. For different values of R, the wind speed profile $\bar{u}(z,z_0)$ is (for a given z_0)

$$\bar{u}(z,z_0) = \bar{u}(z) - \frac{1}{k}\ell n\left(6.8 \times 10^6\, z_0\right) \quad , \quad \begin{matrix} 0.025 < z < 0.3 \, , \\ z_0 < .004 \quad ; \end{matrix} \tag{49}$$

where $\bar{u}(z)$ is given by Eq. (48) and k is the von Karman constant ($\simeq$,35). (Note the restriction on the size of z_0.)

Let

$$z_{10} = \frac{10}{\hat{z}_i} \tag{50}$$

represent the nondimensionalized 10-m anemometer height. Then we have from Eq. (49)

$$\bar{u}(z_{10},z_0) = \frac{\hat{\bar{u}}_{10}}{u_*} \quad .$$

Therefore,

$$u_* = \frac{\hat{\bar{u}}_{10}}{\bar{u}(z_{10},z_0)} \quad . \tag{51}$$

Note that the expression in Eq. (49) for $\bar{u}(z,z_0)$ is valid only for heights $z > 0.025$. If z_{10} is smaller than this value, we are in the surface layer, where similarity theory gives (see Table 1)

$$\bar{u}(z,z_0) = \frac{1}{k}\left[2\left(\tan^{-1}x - \tan^{-1}x_0\right) + \ell n\left(\frac{x-1}{x_0-1}\right) - \ell n\left(\frac{x+1}{x_0+1}\right)\right] \quad ,$$

$$z_0 < z < 0.025 \quad , \tag{52}$$

where

$$x = \left[1 - 15(z+z_0)\frac{z_i}{L}\right]^{1/4} \quad ,$$

$$x_0 = \left[1 - 15z_0\frac{z_i}{L}\right]^{1/4} \quad . \tag{53}$$

In summary, we obtain the friction velocity u_* in unstable cases from the formula

$$u_* = \frac{\hat{\bar{u}}_{10}}{\bar{u}(z_{10},z_0)}$$

where $\hat{\bar{u}}_{10}$ is the wind speed at the anemometer height and $\bar{u}$ is given by Eqs. (48) and (49) for z_{10} in the range $0.025 < z_{10} < 0.3$ and by Eqs. (52) and (53) when $z_0 < z_{10} < 0.025$. Note that the surface roughness $\hat{z}_0$, the mixing height $\hat{z}_i$, and the Monin-Obukhov length L must be known to obtain u_*.

In the neutral case ($z_i/L = 0$), the evaluation of u_* is somewhat simpler because the anemometer height is always within the surface layer. Here similarity theory gives (see Table 1)

$$\bar{u}(z,z_0) = \frac{1}{k} \ln\left(\frac{z + z_0}{z_0}\right) \quad , \quad \left(\frac{z_i}{L} = 0\right) \text{ neutral stability} \quad . \tag{54}$$

Thus, if $\hat{z}_{10} = 10$ meters and $\hat{\bar{u}}_{10}$ is the 10-m wind speed, we can assume that

$$u_* = \frac{k\hat{\bar{u}}_{10}}{\ln\left(\frac{\hat{z}_{10} + \hat{z}_0}{\hat{z}_0}\right)} \quad , \quad \text{neutral stability} \quad . \tag{55}$$

It is important to note that Eq. (54) is very accurate up to a height $z \simeq 0.03\, u_*/f$. Since $f \simeq 10^{-4}$ sec^{-1} for latitudes within the United States and $u_* \gtrsim 0.1$ m/sec over urban regions during most of the daylight hours, it is easy to see that 10 m is a value that is well within the range of validity of Eq. (54).

Having established formulas for the friction velocity u_*, we can convert the nondimensional wind speed and diffusivity profiles of Table 2 into physical forms quite easily using the computer. Our approach is to define FORTRAN functions USTAR, DKZ, and UBAR, which calculate the friction velocity, diffusivity, and wind speed, respectively, given the following data:

u_{10} = anemometer wind speed at height z_{10},

z_0 = local surface roughness,

z_i = local inversion height,

z_i/L = stability parameter (recall that the Monin-Obukhov length L is assumed to be known),

z = level at which the diffusivity or wind speed is required,

f = $2\Omega \sin \phi$ = Coriolis parameter.

In the execution of the pollution model, the function USTAR is called for each point on the horizontal plane to compute the local friction velocity. Thus, we have

$$u_* = \text{USTAR(U10,Z0,ZIOVL,ZI,ZI0)} \quad ,$$

where the arguments of USTAR are given the proper local values. Once u_* is determined, the functions DKZ and UBAR can be referenced as follows:

$$K_z(z) = \text{DKZ(Z,ZI,USTAR,F,ZIOVL)} \quad ,$$

$$\bar{u}(z) = \text{UBAR (Z,Z0,ZI,ZIOVL,F,USTAR)} \quad .$$

These functions merely use their arguments to translate the polynomials given in Table 2 into dimensional values. Note that the functions DKZ and UBAR simply replace the diffusivity and wind speed variables in the program.

Listings of the FORTRAN programs of each of these three functions are provided in Appendix A. Note in the listing of UBAR that in the portion of the surface layer not covered by the profiles given in Table 2, we use well-known analytical expressions for $\bar{u}(z)$. Equation (52) is an example of such an expression. Further information in this regard can be obtained from Ragland (1973).

At present, the three functions USTAR, DKZ, and UBAR are applicable only to the stability cases $z_i/L = 0$ (neutral) and $z_i/L = -4.5$ (slightly unstable). The data on which the profiles of Table 2 are based are currently restricted to these conditions. We hope to be able to extend the scope and accuracy of this work in the future. Deardorff (1972) has found, for example, that in all situations where $-z_i/L$ is greater than about 5, the proper velocity scale is

$$w_* = \left(-\frac{1}{k}\frac{z_i}{L}\right)^{1/3} u_*$$

rather than u_*. If this is true, then one K_z profile should suffice for all unstable conditions in the range $z_i/L < -5$, but this remains to be checked. Also, our K_z profiles were obtained for fixed source heights. In principle, the diffusivity should be independent of source height; but because of the heuristic nature of the concept of a turbulent diffusivity, this may not be the case. Further work is therefore needed to ascertain the influence of source height on the optimal K_z profiles.

III DEVELOPMENT OF A CLOSURE APPROXIMATION FOR THE CONCENTRATION FLUCTUATION TERMS IN THE GOVERNING EQUATIONS

A. INTRODUCTION

Snapshots of smoke plumes in the atmosphere always reveal an erratic distribution of smoke concentration within the local vicinity of the smoke source. In contrast, time exposures usually reveal a smooth distribution that closely resembles the classical Gaussian profile. If two such photographs of the same plume were superposed, the difference in apparent smoke concentration at any point would represent the instantaneous magnitude at that point of the so-called turbulent concentration fluctuation. That is, if A denotes the instantaneous concentration, portrayed by the snapshot, and $\overline{A}$ denotes the mean, revealed by the time exposure, then

$$A' = A - \overline{A} \tag{56}$$

is the concentration fluctuation.

In situations where nonlinear chemical reactions occur among constituents of the plume or between the plume's constituents and chemical species entrained from the ambient atmosphere, the presence of concentration fluctuations can have a profound impact on the behavior of the mean concentrations of all the reacting species. This can be demonstrated mathematically by the following simple example. Suppose that two species, A and B, undergo the bimolecular reaction

$$A + B \rightarrow C \quad ,$$

with rate constant k. The equation governing the instantaneous concentration of A is, therefore,

$$\frac{dA}{dt} = -kAB \quad . \tag{57}$$

If the two species are not homogeneously distributed, local fluctuations A' and B' exist. The mean concentration $\bar{A}$ is then governed by the equation

$$\frac{d\bar{A}}{dt} = -k\bar{A}\bar{B} - k\overline{A'B'} \quad . \tag{58}$$

This equation follows from Eqs. (57) and (56) and the assumption that $\overline{A'} = \overline{B'} = 0$. Equation (58) indicates that, depending on their amplitude, the concentration fluctuations can actually dominate the evolution of the mean concentration distribution.

Since the term $\overline{A'B'}$ is an additional unknown variable, Eq. (58) cannot be solved until another expression relating $\overline{A'B'}$ to $\bar{A}$ and $\bar{B}$ or to some other known quantities is found. This is known as the closure problem. The search for such relationships, or closure approximations as they are generally called, has been undertaken by several investigators. Of these, the most sophisticated work has been done by O'Brien (1968) and Hilst et al. (1973). Both of these studies, which are similar in nature, follow along the lines of the so-called invariant modeling approach. We outline this method below, using the work of Hilst et al. as an example.

In the context of the problem represented by Eq. (58), the first step is to formulate the equation governing $\overline{A'B'}$ and to add it to the system of equations governing $\bar{A}$ and $\bar{B}$. We then have [repeating Eq. (58)]

$$\frac{d\bar{A}}{dt} = -k\bar{A}\bar{B} - k\overline{A'B'} \tag{59a}$$

$$\frac{d\bar{B}}{dt} = -k\bar{A}\bar{B} - k\overline{A'B'} \tag{59b}$$

$$\frac{d\overline{A'B'}}{dt} = -k\left[\bar{A}\overline{B'^2} + \bar{B}\overline{A'B'} + \bar{B}\overline{A'^2} + \bar{A}\overline{A'B'} + \overline{A'B'^2} + \overline{B'A'^2}\right] \quad . \tag{59c}$$

The last equation involves the mean squares $\overline{A'^2}$ and $\overline{B'^2}$, and so their governing equations must also be considered:

$$\frac{d\overline{A'^2}}{dt} = -2k\left[\bar{B}\overline{A'^2} + \bar{A}\overline{A'B'} + \overline{A'^2B'}\right] \quad . \tag{59d}$$

$$\frac{d\overline{B'^2}}{dt} = -2k\left[\bar{A}\overline{B'^2} + \bar{B}\overline{A'B'} + \overline{A'B'^2}\right] \quad . \tag{59e}$$

The presence of third-order moments, such as $\overline{A'B'^2}$, in Eqs. (59c) through (59e) precludes a solution of the system of equations represented by Eqs. (59a) through (59e). Note that the problem here is identical to the one we faced with Eq. (58), i.e., too many unknowns for the available set of equations. It is apparent, therefore, that merely writing down the governing equation for each new unknown that appears does not in itself resolve the difficulty, for this process produces an infinite hierarchy of equations. At some point, a hypothetical expression must be introduced to circumvent the hierarchy and to produce a closed, finite set of equations. It is at the point represented by the system [Eqs. (59a) through (59e)] that Hilst et al. introduced their closure hypothesis in the form

$$\overline{A'^2B'} = \frac{\bar{A}^2\bar{B}}{M+1}\left(1 + \frac{\overline{A'^2}}{\bar{A}^2} + 2\,\frac{\overline{A'B'}}{\bar{A}\bar{B}}\right)\left(\frac{\overline{A'B'}}{\bar{A}\bar{B}} - M\right) \quad , \tag{59f}$$

$$\overline{A'B'^2} = \frac{\bar{A}\bar{B}^2}{M+1}\left(1 + \frac{\overline{B'^2}}{\bar{B}^2} + 2\,\frac{\overline{A'B'}}{\bar{A}\bar{B}}\right)\left(\frac{\overline{A'B'}}{\bar{A}\bar{B}} - M\right) \quad , \tag{59g}$$

where

$$M = \begin{cases} 0, & \text{if } (\overline{A'^2}/\overline{A}^2)\,(\overline{B'^2}/\overline{B}^2) \leq 1 \quad ; \\ 1, & \text{otherwise} \quad . \end{cases}$$

Equations (59f) and (59g) are not based on any physical concepts or on experimental observations. Rather, they are simply mathematical approximations that are designed to satisfy the following realizability conditions:

$$\left.\begin{aligned} &\overline{A^2B} = 0 \quad , \quad \text{if } \overline{A'B'} = -\overline{AB} \quad ; \\ &\overline{A^2B} = \overline{A}^2\overline{B} \quad , \quad \text{if } \overline{A'^2} = 0 \quad ; \\ &\overline{A^2B} = \overline{A}^2\overline{B} + \overline{A'^2}\,\overline{B} + 2\overline{A'B'A} \quad , \quad \text{if } \overline{A'^2B'} = 0 \quad ; \\ &\overline{A^2B} \geq 0 \quad . \end{aligned}\right\} \tag{60}$$

We should note that Eqs. (59f) and (59g) are not the only relationships that satisfy Conditions (60), nor are these conditions the only ones that the statistics of A and B satisfy.

Although Hilst et al. have found good agreement between the predictions of their model [Eq. (59)] and the corresponding analytic solutions of certain simplified chemical reactors, from the standpoint of urban pollution modeling, their approach is not altogether acceptable. The objection is that in a system involving m nonlinear reactions among n species, their technique introduced n + m additional differential equations into the existing set of n to be solved. Thus, in a typical case where there are five pollutants and five reactions (in which concentration fluctuations are important), the number of differential equations to be solved is 15 instead of 5. Needless to say, an increase in computational effort of this magnitude cannot be accommodated in urban diffusion models given present computer speed.

Since none of the existing closure approximations for the turbulent concentration fluctuation terms possess both the degree of accuracy and the ease of implementation that are required in pollution simulation studies, we set for ourselves the task of developing a new approximation that would more closely satisfy these needs. Our primary constraint was that the new scheme should involve no additional differential equations. The existence of such a scheme has been suggested by our work in the previous chapter with the analogous term $\overline{u_i'c'}$. In Chapter II, we found that by a proper choice of the functional form of the diffusivity K_z, the approximation

$$\overline{w'c'} = -K_z \frac{\partial \overline{c}}{\partial z}$$

could be made sufficiently accurate to be useful in diffusion modeling applications. Moreover, this formulation does not require that additional equations be solved. Using this work as a guide, we set out to find an expression of the form

$$\overline{A'B'} = f(\overline{A},\overline{B},\text{known parameters}) \quad .$$

We describe the expression that we have developed and our attempts to demonstrate its accuracy in the remainder of this chapter.

B. DERIVATION OF AN APPROXIMATION FOR CONCENTRATION FLUCTUATION TERMS SUCH AS $\overline{A'B'}$

The following simple example illustrates both the reasoning behind our approach and the essence of the closure problem itself.

Suppose that rectangular pulses or slugs of the species A and B are present in a one-dimensional system as shown in Figure 20. The mean concentration $\overline{A}$ of A is defined by

$$\overline{A} = \frac{1}{L}\int_{x_0}^{x_0+L} A\, dx = \frac{A_0 \ell_A}{L} \quad , \qquad (61)$$

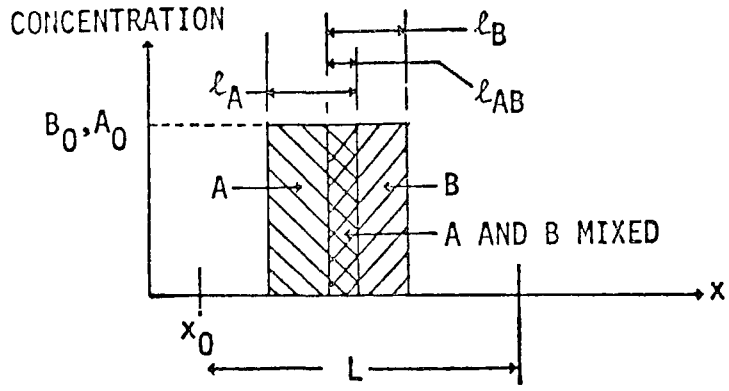

FIGURE 20. TWO INITIAL SLUGS OF SPECIES A AND B IN A ONE-DIMENSIONAL VESSEL

and a similar definition applies for $\overline{B}$. These results follow immediately from Figure 20. (Although in this example L represents an averaging length interval, it could just as well denote time or ensemble averaging domains because the results that we derive below are the same in all cases.) Since A and B are not uniformly distributed within L, concentration fluctuations exist. At points outside the slug of A, the fluctuation A' has a magnitude

$$A' = A - \overline{A} = -\frac{A_0 \ell_A}{L} \quad ; \tag{62}$$

and at points within the slug,

$$A' = A_0\left(1 - \frac{\ell_A}{L}\right) \quad . \tag{63}$$

Similar expressions pertain to the fluctuations B'.

Suppose that both A and B undergo first-order decay reactions whose rates are given by

$$\frac{dA}{dt} = -k_A A \quad ,$$

$$\frac{dB}{dt} = -k_B B \quad . \tag{64}$$

The concentrations within the slugs then become

$$A = A_0 e^{-k_A t} \quad ,$$
$$B = B_0 e^{-k_B t} \quad . \tag{65}$$

From these expressions and Eq. (61), we find that the mean concentration $\overline{A}$ is

$$\overline{A} = \frac{A_0 \ell_A}{L} e^{-k_A t} = \overline{A}_0 e^{-k_A t} \quad , \tag{66}$$

and a similar equation holds for $\overline{B}$. Here, $\overline{A}_0$ denotes the initial value of $\overline{A}$. Upon differentiating Eq. (66), we find that

$$\frac{d\overline{A}}{dt} = -k_A \overline{A} \quad . \tag{67}$$

Since this expression is not explicitly dependent upon ℓ_A or ℓ_{AB}, the temporal behavior of $\overline{A}$ is independent of the way in which A is distributed within L. We can conclude, therefore, that linear reactions are unaffected by the presence of concentration fluctuations.

Suppose, however, that A and B react with each other in the manner

$$A + B \rightarrow D$$

with rate constant k. In the example shown in Figure 20, it is clear that this reaction can occur only in the domain (of width ℓ_{AB}) where A and B are mixed. Outside this domain, the concentrations of A and B remain unchanged for all time. Let A_m and B_m denote the concentrations within the mixed zone ℓ_{AB}. Then

$$\frac{dA_m}{dt} = \frac{dB_m}{dt} = -kA_m B_m \quad , \tag{68}$$

and from the definition given by Eq. (61), we have

$$\overline{A} = \frac{1}{L}\left[A_0(\ell_A - \ell_{AB}) + A_m\ell_{AB}\right] \quad ,$$
$$\overline{B} = \frac{1}{L}\left[B_0(\ell_B - \ell_{AB}) + B_m\ell_{AB}\right] \quad . \tag{69}$$

Keeping in mind that all terms on the right side of Eq. (69) are constants except A_m and B_m, we obtain upon differentiating Eq. (69)

$$\frac{d\overline{A}}{dt} = \frac{\ell_{AB}}{L}\frac{dA_m}{dt} = -kA_mB_m\frac{\ell_{AB}}{L} \quad , \tag{70}$$

and

$$\frac{d\overline{B}}{dt} = -kA_mB_m\frac{\ell_{AB}}{L} \quad .$$

These equations show that in contrast to the linear reactions considered earlier, the behavior of $\overline{A}$ and $\overline{B}$ is now explicitly dependent upon ℓ_{AB}. In other words, because of the nonlinearity of the chemistry, temporal changes in $\overline{A}$ and $\overline{B}$ are sensitive to the manner in which the species of A and B are distributed in space and time.

This fact is obvious from Figure 20, which shows that the quantities of A and B that are consumed by the reaction A + B → D are determined by the extent to which the slugs of A and B overlap. Moreover, this figure indicates that the extent of overlap, i.e. ℓ_{AB}, is not expressible in terms of $\overline{A}$ and $\overline{B}$ alone because these variables are independent of the positions of the slugs within the interval L.

Herein lies the essence of the closure problem--the parameters that control $\overline{A}$ and $\overline{B}$, in this case A_m, B_m, and ℓ_{AB}, are not expressible in terms of only the variables $\overline{A}$ and $\overline{B}$ themselves. The origin of this difficulty lies in the loss of information about the details of the distribution of A and B within L when A and B are averaged over the interval L.

Consequently, in situations where these details play on explicit role (namely, where nonlinear processes are involved), the closure problem arises in equations governing mean values. This suggests that solving the closure problem means retrieving the information that is lost in the averaging process. This simple notion is the basic principle underlying our proposed closure approximation. Specifically, restricting ourselves to chemical reactions that do not perturb the fluid flow (all air pollution reactions fall into this group), we plan to show that most of the information contained in the term $\overline{A'B'}$ is also present in its counterpart $\overline{A_I'B_I'}$, which pertains to the case where the species A and B are inert, and since $\overline{A_I'B_I'}$ is determined solely by those processes that control the spatial distributions of A and B, then $\overline{A_I'B_I'}$, and hence $\overline{A'B'}$, are expressible in terms of measurable properties of the system.

To demonstrate this approach, we consider the problem described in Figure 20. Under the passive reaction assumption, the extents of the regions ℓ_A, ℓ_B, and ℓ_{AB} are the same, regardless of the chemical properties of the species A and B. Consequently, if inert materials A_I and B_I are released into this system in initial concentration A_0 and B_0, and if the same mechanisms that controlled the positions and sizes of the slugs of the reactive species A and B also act upon A_I and B_I, then we would observe

$$\overline{A}_I = \frac{A_0 \ell_A}{L} \quad , \tag{71a}$$

$$\overline{B}_I = \frac{B_0 \ell_B}{L} \quad ; \tag{71b}$$

and the second moments would be

$$\overline{A_I^2} = \frac{A_0^2 \ell_A}{L} \quad , \tag{71c}$$

$$\overline{B_I^2} = \frac{B_0^2 \ell_B}{L} \quad , \tag{71d}$$

$$\overline{A_I B_I} = \frac{A_0 B_0 \ell_{AB}}{L} \quad . \tag{71e}$$

All parameters on the right-hand side of Eqs. (71a) through (71e) are identical to the corresponding terms entering into Eq. (69), and all quantities on the left side of Eqs. (71a) through (71e) represent measurable parameters. If the latter are regarded as properties of the system and are specified along with the other parameters that describe the given problem, then the five equations comprising the set can be solved for the five unknowns A_0, B_0, ℓ_A, ℓ_B, and ℓ_{AB}. These results can then be substituted into Eq. (69) to obtain the variables A_m, B_m, and ℓ_{AB} that are required to achieve closure of the reaction rate equation [Eq. (70)].

The results of the solution of Eqs. (71a) through (71e) are

$$\begin{aligned}
\ell_{AB} &= \frac{L\hat{\Gamma}_{AB}}{\hat{\Gamma}_A \hat{\Gamma}_B} \quad , \\
\ell_A &= \frac{L}{\hat{\Gamma}_A} \quad , \\
A_0 &= \frac{\overline{A_I}}{\hat{\Gamma}_A} \quad , \\
B_0 &= \frac{\overline{B_I}}{\hat{\Gamma}_B} \quad ,
\end{aligned} \tag{72}$$

where

$$\hat{\Gamma}_{AB} = \frac{\overline{A_I B_I}}{\overline{A}_I \overline{B}_I} \quad , \tag{73a}$$

$$\hat{\Gamma}_A = \frac{\overline{A_I^2}}{\overline{A}_I^2} \quad , \tag{73b}$$

$$\hat{\Gamma}_B = \frac{\overline{B_I^2}}{\overline{B}_I^2} \quad . \tag{73c}$$

After substituting these results into Eq. (69) and solving for A_m and B_m, we can write Eq. (70) in the closed form

$$\frac{d\overline{A}}{dt} = -\frac{k\hat{\Gamma}_A\hat{\Gamma}_B}{\hat{\Gamma}_{AB}}\left[\overline{A} - \overline{A}_I\left(1 - \frac{\hat{\Gamma}_{AB}}{\hat{\Gamma}_B}\right)\right]\left[\overline{B} - \overline{B}_I\left(1 - \frac{\hat{\Gamma}_{AB}}{\hat{\Gamma}_A}\right)\right] \quad . \tag{74}$$

Since the right side of this equation is equivalent to

$$-k\overline{AB} = -k[\overline{A}\,\overline{B} + \overline{A'B'}] \quad , \tag{75}$$

our approximation for $\overline{A'B'}$ is given by

$$\overline{A'B'} = \frac{\hat{\Gamma}_A\hat{\Gamma}_B}{\hat{\Gamma}_{AB}}\left[\overline{A} - \overline{A}_I\left(1 - \frac{\hat{\Gamma}_{AB}}{\hat{\Gamma}_B}\right)\right]\left[\overline{B} - \overline{B}_I\left(1 - \frac{\hat{\Gamma}_{AB}}{\hat{\Gamma}_A}\right)\right] - \overline{A}\,\overline{B} \quad . \tag{76}$$

We emphasize that this relationship is <u>exact</u> in the case of the problem of two rectangular slugs of A and B shown in Figure 20.

Before we extend this technique to more generalized situations, it is of interest to test the accuracy of the Hilst et al. closure [Eqs. (59f) through 59g)] in the context of this simple problem.

To simplify the mathematics, let us assume that $\ell_{AB} = \ell_A = \ell_B = \ell$, i.e., that the species A and B are premixed. If A = B, then we find from the definitions of the bar average ($\bar{}$) and the fluctuation A', Eqs. (61) and (62), respectively, that

$$\overline{A'^3} = \frac{A^3 \ell}{L}\left[1 - 3\frac{\ell}{L} + 2\frac{\ell^2}{L^2}\right] \quad . \tag{77}$$

For this quantity, the Hilst et al. approximation [Eqs. (59f) through (59g)] gives

$$\overline{A'^3_{DH}} \begin{cases} = \dfrac{A^3 \ell}{L}\left[1.5 - \dfrac{4\ell}{L} + \dfrac{2\ell^2}{L^2}\right] & , \quad \ell < L/2 \quad ; \\ = \dfrac{A^3 \ell}{L}\left[3 - 5\dfrac{\ell}{L} + 2\dfrac{\ell^2}{L^2}\right] & , \quad L/2 < \ell < L \quad . \end{cases} \tag{78}$$

Figure 21 shows the behavior of the fractional error of this approximation, i.e.,

$$\varepsilon = \frac{\overline{A'^3} - \overline{A'^3_{DH}}}{\overline{A'^3}} \quad , \tag{79}$$

as a function of the normalized mean square fluctuation

$$\frac{\overline{A'^2}}{\bar{A}^2} = \frac{L}{\ell} - 1 \quad . \tag{80}$$

The large size of errors in this approximation, even for this elementary problem, emphasizes the extreme difficulty of finding a closure scheme based on hypothetical relationships among statistical moments that is accurate for a wide range of situations.

Consider now the extension of the closure scheme developed above for the simple problem shown in Figure 20 to the generalized situation exhibited in Figure 22. The disjointed volume v_{AB} represents the total volume where A and B particles are found together; and the volumes v_A and v_B denote those regions where A and B are found in isolation. If the averaging volume V implicit in the bar operator ($\bar{}$) encompasses all of v_A, v_B, and v_{AB}, then we have by definition

$$\overline{A} = \frac{1}{V}\left[\int_{v_A} A \, dv + \int_{v_{AB}} A \, dv\right] \quad , \tag{81}$$

$$\overline{B} = \frac{1}{V}\left[\int_{v_B} B \, dv + \int_{v_{AB}} B \, dv\right] \quad , \tag{82}$$

$$\overline{AB} = \frac{1}{V}\int_{v_{AB}} AB \, dv \quad . \tag{83}$$

Let the following variables be defined:

$$\hat{A} = \frac{1}{v_A}\int_{v_A} A \, dv \quad , \quad \hat{B} = \frac{1}{v_B}\int_{v_B} B \, dv \quad ; \tag{84}$$

$$\hat{a} = \frac{1}{v_{AB}}\int_{v_{AB}} A \, dv \quad , \quad \hat{b} = \frac{1}{v_{AB}}\int_{v_{AB}} B \, dv \quad . \tag{85}$$

In terms of these variables, $\overline{A}$ and $\overline{B}$ become

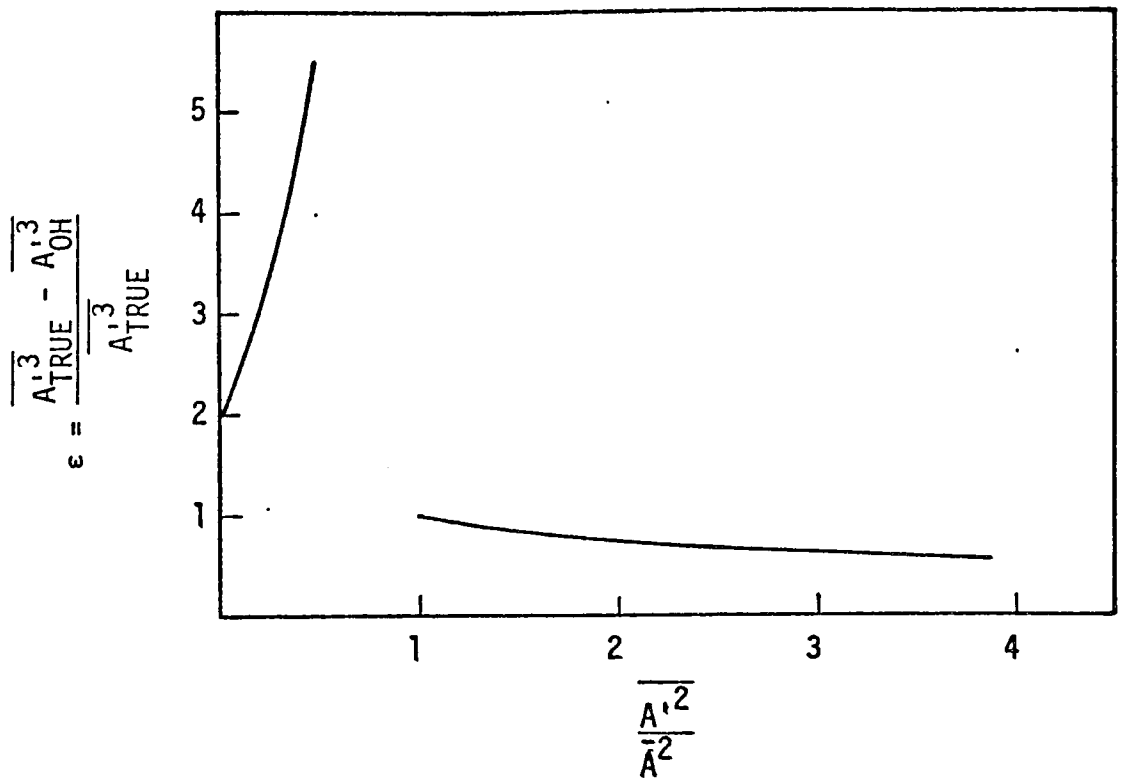

FIGURE 21. FRACTIONAL ERROR ε IN THE DONALDSON-HILST APPROXIMATION [EQ. (59f)] OF $\overline{A'^3}$ FOR THE CASE OF TWO PREMIXED SLUGS OF MATERIAL IN A ONE-DIMENSIONAL REACTOR (plotted as a function of the normalized mean square fluctuation $\overline{A'^2}/\bar{A}^2$)

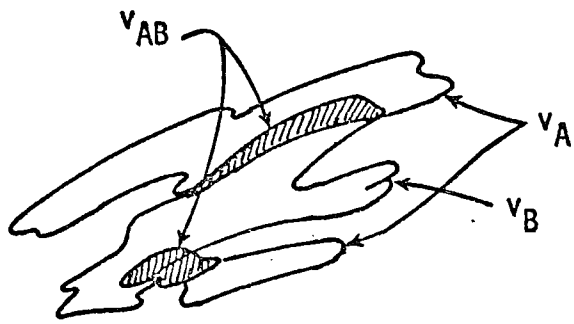

FIGURE 22. MIXING TURBULENT CLOUDS OF REACTING PARTICLE SPECIES A AND B

$$\overline{A} = \frac{1}{V}\left[\hat{A}v_A + \hat{a}v_{AB}\right] \quad , \tag{86}$$

$$\overline{B} = \frac{1}{V}\left[\hat{B}v_B + \hat{b}v_{AB}\right] \quad . \tag{87}$$

Recalling that the concentrations within and the extents of the zones v_A and v_B are the same regardless of the chemical nature of the reacting species, we find that the quantities corresponding to Eqs. (86) and (87) for inert particle species $\overline{A_I}$ and $\overline{B_I}$ are

$$\overline{A}_I = \frac{1}{V}\left[\hat{A}v_A + \hat{a}_I v_{AB}\right] \quad , \tag{88}$$

$$\overline{B}_I = \frac{1}{V}\left[\hat{B}v_B + \hat{b}_I v_{AB}\right] \quad , \tag{89}$$

where

$$\hat{a}_I = \frac{1}{v_{AB}} \int_{v_{AB}} A_I \, dv \quad , \quad \hat{b}_I = \frac{1}{v_{AB}} \int_{v_{AB}} B_I \, dv \quad . \tag{90}$$

Finally, we define the two parameters μ and μ_I such that

$$\int_{v_{AB}} AB \, dv = \mu \hat{a}\hat{b} v_{AB} \quad , \tag{91}$$

$$\int_{v_{AB}} A_I B_I \, dv = \mu_I \hat{a}_I \hat{b}_I v_{AB} \quad . \tag{92}$$

efforts to relate λ to indices of both of the chemical natures of the reacting species and of the turbulence and molecular diffusivity.

C. FORMULATION OF THE PARAMETERS ζ_A AND ζ_B

We consider three distinct situations, each of which illustrates to some degree the physical significance of these parameters and how each is related to properties of the flow.

1. Release of A into a Uniform Field of B

Suppose that a cloud of A particles of initial concentration A_0 and volume V_0 is released into a turbulent fluid in which particles of species B are uniformly distributed. We desire to estimate ζ_A.

In this situation, v_{AB}, and hence ζ_A, are initially zero. Although particles at the edge of the cloud are near particles of the other species, there is no region in which one species is immersed in the other. However, with the passage of time, particles of A, excited by molecular-scale agitations, migrate into the ambient fluid and thereby create a region v_{AB}. The flux of migrating particles at the cloud edge can be represented in the form

$$F = \kappa \frac{dA}{dn} \quad , \tag{101}$$

where κ is the molecular diffusivity of A and dA/dn is the gradient of concentration of A particles normal to the cloud surface. If S denotes the instantaneous surface area of the cloud, then at any instant the number of A particles moving into the ambient fluid is given by

$$\frac{dN}{dt} = \int_S \underset{\sim}{F} \cdot \underset{\sim}{n} \, ds \tag{102}$$

Since the portion v_A of the original cloud that is occupied only by A particles is completely surrounded by a region v_{AB} created by the migration of A particles into the ambient fluid, all particles that leave v_A move immediately into v_{AB}. Therefore,

$$\zeta_A = \frac{N_0 - N}{N_0} \quad , \tag{103}$$

where $N_0 = A_0 V_0$ is the total number of A particles released and N is the number still in v_A at any given time. From Eqs. (103) and (102), we obtain

$$\frac{d}{dt} A = \frac{1}{N_0} \int_S \underset{\sim}{F} \cdot \underset{\sim}{n} \, ds \tag{104}$$

The particle flux F averaged over the cloud surface can be expressed in the form

$$F = \kappa \frac{A}{\xi} \quad , \tag{105}$$

where A and ξ are concentration and length scales, respectively. We propose that the ratio A/ξ entering in Eq. (105) can be represented to good approximation using the following expressions for A and ξ:

$$A = \frac{N}{V_0} \quad , \tag{106}$$

$$\xi = \left(\frac{\kappa^3}{\varepsilon}\right)^{1/4} \quad , \tag{107}$$

where ε is the energy dissipation rate of the turbulence.

The quantity on the right side of Eq. (107) represents the smallest length scale associated with spatial variations in a scalar field in turbulent fluid (see Batchelor, 1967). It represents the length scale associated with the concentration gradient that is required to produce a molecular diffusive flux of particles that just balances the compressional fluxes arising from the strain rate field of the turbulence. This length scale is thus a logical choice for ξ, at least initially. With the passage of time, however, ξ increases, but in a manner that is not possible to describe exactly. We are proposing that the overall effect of this increase (and the simultaneous decrease in A) on the flux F can be accounted for by Eqs. (105) through (107); i.e.,

$$F = (\kappa\varepsilon)^{1/4} \frac{N}{V_0} \quad . \tag{108}$$

Here, V_0 is constant because it is the combined volume occupied by all particles that initially were of species A. Combining Eqs. (108), (103), and (104), we obtain

$$\frac{d\zeta_A}{dt} = (1 - \zeta_A)\left(\frac{S_\kappa{}^{1/4}\ \varepsilon^{1/4}}{V_0}\right) \quad . \tag{109}$$

It is not possible to obtain a precise description of the rate of change of surface area S of a cloud of marked particles in turbulent fluid. A reasonable approximation for the average surface area might be

$$S \sim \overline{\ell^2} \quad , \tag{110}$$

where ℓ is the distance between a pair of marked particles released a distance ℓ_0 apart where

$$\ell_0 \sim S_0{}^{1/4} \quad , \tag{111}$$

and S_0 is the initial surface area of the cloud. Batchelor (1950) showed that for particles whose separation ℓ is within the inertial subrange of a homogeneous turbulence,

$$\frac{\overline{d\ell^2}}{dt} \sim 2t(\varepsilon\ell_0)^{2/3} \quad .$$

Combining this result with Eqs. (110) and (111), we obtain the estimate

$$S = S_0(1 + \varepsilon^{2/3} S_0^{-2/3} t^2) \quad ; \tag{112}$$

and upon substituting this expression into Eq. (109) and solving the resulting differential equation, we obtain finally

$$\zeta_A = 1 - e^{-(at+bt^3)} \quad , \tag{113}$$

where

$$a = 3\kappa^{1/4} \varepsilon^{1/4} \ell_0^{-1} \quad , \tag{114}$$

$$b = \kappa^{1/4} \varepsilon^{11/12} \ell_0^{-7/3} \quad , \tag{115}$$

and ℓ_0 is the initial cloud diameter.

Under conditions of strong convection in the atmosphere with ε on the order of 10^{-2} m^2/sec^3, Eq. (113) predicts that for a cloud of material of Schmidt number on the order of 1 and initial diamter of roughly 1 meter, ζ_A will reach its limiting value of unity within about 20 seconds after release.

2. Release of Dilute Mixtures of A and B into a Homogeneous Turbulent Reactor

In view of its definition [Eq. (96)], ζ_A is equivalent, in a homogeneous system, to the probability that any inert particle of A will be found at time t within some distance ∂r, say, of a particle of B. In other words, implicit in our definition of v_{AB} is the condition that the smallest distance between particles of opposite species is on the average ∂r or smaller. The magnitude of ∂r is in turn an implicit function of the chemical reactivity of A and B because reactions are assumed to occur within and only within v_{AB}.

Let $E|A_0$ represent the event

$$E|A_0 = \text{given particle } A_0 \text{ is within a distance } \partial r \text{ of at least one B at time t} \quad . \tag{116}$$

If the concentrations of A and B are sufficiently dilute that the probability of finding more than one B particle with a distance ∂r of the given A is negligible, then clearly

$$\text{prob}\left\{E|A_0\right\} = \int_0^t \int_0^t \int\int_{\partial v} p(\underset{\sim}{r},t,\underset{\sim}{r}',t|\underset{\sim}{r}_{AO},t_{AO},\underset{\sim}{r}_{BO},t_{BO}) S_B(r_{BO},t_{BO})\, d\underset{\sim}{r}'\, d\underset{\sim}{r}\, dt_{BO}\, d\underset{\sim}{r}_{BO} \quad , \tag{117}$$

where $(\underset{\sim}{r}_{AO},t_{AO})$ is the release point of the given inert A particle, ∂v is a volume of radius ∂r centered at the location $(\underset{\sim}{r},t)$ of a particular inert B particle, and $S_B(\underset{\sim}{r}_{BO},t_{BO})$ is the number density of B particles released per unit time and volume at $(\underset{\sim}{r}_{BO},t_{BO})$.

Equation (117) gives the probability that a particular A particle experiences event E. However, ζ_A is equivalent to the event

E = any randomly chosen particle of A is within a distance δr of at least one B at time t.

If N_A particles of A have been released prior to time t, then there are N_A mutually exclusive ways in which E can be realized, and it follows that

$$\zeta_A = \text{prob}\{E\} = \frac{1}{N_A} \int_0^t \int \text{prob}\{E|A_0\}\, S_A(\underset{\sim}{r}_{A0}, t_{A0})\, dt_{A0}\, d\underset{\sim}{r}_{A0} \quad , \tag{118}$$

where $S_A(\underset{\sim}{r}_{A0}, t_{A0})$ is the number density of A particles released per time and volume at $(\underset{\sim}{r}_{A0}, t_{A0})$. Upon substituting Eq. (117) into Eq. (118), we obtain finally (see Lamb, 1974)

$$\zeta_A = \frac{1}{N_A} \iint_{\delta v} \overline{A_I(\underset{\sim}{r}', t)\, B_I(\underset{\sim}{r}, t)}\, d\underset{\sim}{r}'\, d\underset{\sim}{r} \quad . \tag{119}$$

If the volume δv is sufficiently small that $\overline{A_I(\underset{\sim}{r}', t)\, B_I(\underset{\sim}{r}, t)}$ is nearly constant for all r' in δv and for all $\underset{\sim}{r}$, then Eq. (119) reduces to

$$\zeta_A = \frac{\delta v}{N_A} \int \overline{A_I(\underset{\sim}{r}, t)\, B_I(\underset{\sim}{r}, t)}\, d\underset{\sim}{r} \quad . \tag{120}$$

If, moreover, the chemical reactor has volume V and the statistics of A_I and B_I are uniform throughout V--the homogeneity assumption--then Eq. (120) gives finally

$$\zeta_A = \overline{B}_I\, \delta v \hat{\Gamma}_{AB} \quad . \tag{121}$$

In the limit as A and B became thoroughly mixed, $\hat{\Gamma}_{AB} \to 1$ and $\zeta_A \to \overline{B}_I\ \delta v$. Since by definition $0 < \zeta_A \leq 1$, we see that Eq. (121) holds only if the concentrations are so dilute that

$$\overline{B}_I\ \delta v < 1 \quad . \tag{122}$$

3. Release of Rectangular Slugs of Reactants into a Hypothetical, One-Dimensional Reactor

Imagine a one-dimensional system such as that shown in Figure 20 in which the reacting clouds have rectangular shapes. In this hypothetical system, we see that

$$\zeta_A = \frac{A_0 \ell_{AB}}{A_0 \ell_A} = \frac{\ell_{AB}}{\ell_A} \quad , \quad \zeta_B = \frac{\ell_{AB}}{\ell_B} \quad , \tag{123}$$

where A_0 is the (uniform) concentration of inert particles in the cloud. The following mean values are thus defined:

$$\overline{A}_I = \frac{A_0 \ell_A}{L} \quad , \quad \overline{B}_I = \frac{B_0 \ell_B}{L}$$

$$\overline{A_I^2} = \frac{A_0^2 \ell_A}{L} \quad , \quad \overline{B_I^2} = \frac{B_0^2 \ell_B}{L}$$

$$\overline{A_I B_I} = \frac{A_0 B_0 \ell_{AB}}{L} \quad .$$

Solving these six equations for ℓ_{AB} and ℓ_A and substituting the result into Eq. (123), we obtain

$$\zeta_A = \frac{\hat{\Gamma}_{AB}}{\hat{\Gamma}_B} \quad , \tag{124}$$

and, similarly,

$$\zeta_B = \frac{\hat{\Gamma}_{AB}}{\hat{\Gamma}_A} \quad , \tag{125}$$

where

$$\hat{\Gamma}_A = \frac{\overline{A_I^2}}{\overline{A}_I^2} \quad ,$$

$$\hat{\Gamma}_B = \frac{\overline{B_I^2}}{\overline{B}_I^2} \quad .$$

$$\hat{\Gamma}_{AB} = \frac{\overline{A_I B_I}}{\overline{A}_I \overline{B}_I} \quad .$$

It turns out (as we show later) that when Eqs. (124) and (125) are used in the closure approximation [Eq. (95)], good agreement with observation results, even in turbulent pipe flow reactors. This suggests that Eqs. (124) and (125) may be sufficiently accurate for all general purpose applications of Eq. (125), but this remains to be definitely established.

D. FORMULATION OF THE PARAMETER λ

Being dependent upon the properties of both the turbulence and the chemical reaction, λ is more difficult to formulate than the mixing parameters ζ_A and ζ_B. By virtue of its definition, i.e.,

$$\lambda = \frac{\mu}{\mu_I} = \frac{\int_{v_{AB}} AB \, dv}{\int_{v_{AB}} A \, dv \int_{v_{AB}} B \, dv} \cdot \frac{\int_{v_{AB}} A_I \, dv \int_{v_{AB}} B_I \, dv}{\int_{v_{AB}} A_I B_I \, dv} \quad , \qquad (126)$$

λ is a measure of the effect of the chemical reaction on the correlation of the concentrations of A and B within the mixed zone v_{AB}. This can be seen more clearly in Figure 23, which compares profiles of the concentrations of inert species in v_{AB} with those that might be observed if the species were reactive. In interpreting this diagram, one should keep in mind that v_{AB} is defined for the inert rather than the reactive particles. As a consequence, portions of the zone defined as v_{AB} may contain only one of the species rather than a mixture of the two. In fact, if the reaction is extremely fast, no part of v_{AB} contains a mixture of the reactants except a very small zone where the reactant clouds merge. In this case, it is clear from Eq. (126) that $\lambda \to 0$. However, at the other extreme where the reaction is exceedingly slow, the concentration profiles within v_{AB} are nearly identical for both the reactive and inert materials, and it follows that $\lambda \to 1$.

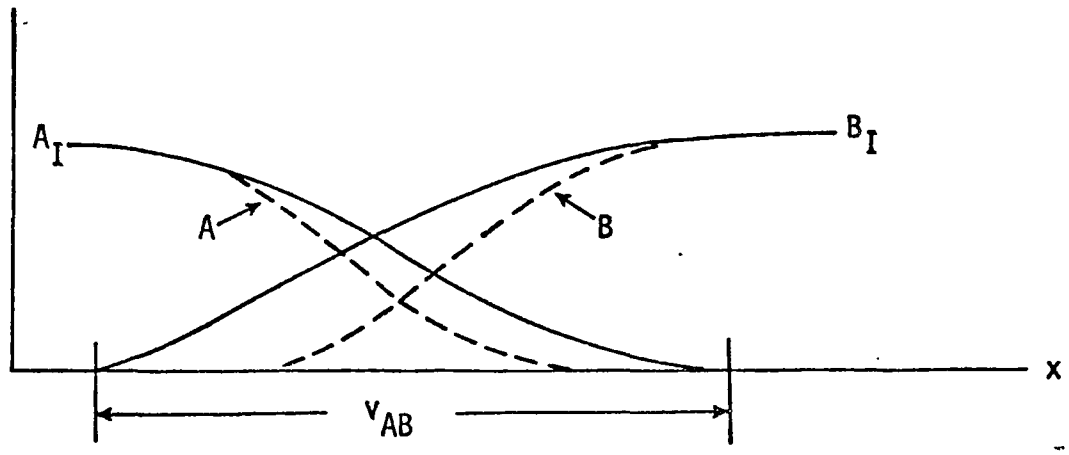

FIGURE 23. COMPARISON OF CONCENTRATION PROFILES IN THE MIXED ZONE v_{AB} FOR INERT AND REACTIVE SPECIES

The behavior of the parameter λ for reactions of intermediate speed has been studied by Shu (1975). In his analyses, the differential equations governing the combined reaction and molecular diffusion of two reacting species in one dimension were solved numerically, and the values of λ were calculated explicitly for a wide range of rate constants, molecular diffusivities, initial conditions, and the like. The model equations used were

$$\frac{\partial A}{\partial t} = D\frac{\partial^2 A}{\partial x^2} - kAB \quad , \tag{127}$$

$$\frac{\partial B}{\partial t} = D\frac{\partial^2 B}{\partial x^2} - knAB \quad , \tag{128}$$

$$\frac{\partial A_I}{\partial t} = D\frac{\partial^2 A_I}{\partial x^2} \quad , \tag{129}$$

$$\frac{\partial B_I}{\partial t} = D\frac{\partial^2 B_I}{\partial x^2} \quad , \tag{130}$$

where k is the reaction rate constant, D is the molecular diffusivity, and n is the stoichometric ratio. These equations were solved subject to the initial and boundary conditions

$$A(x,0) = A_I(x,0) = \begin{cases} A_0 \quad , & -\delta < x \leq 0 \quad ; \\ 0 \quad , & \text{otherwise;} \end{cases} \tag{131}$$

$$B(x,0) = B_I(x,0) = \begin{cases} B_0 \quad , & 0 < x \leq \delta \quad ; \\ 0 \quad , & \text{otherwise;} \end{cases} \tag{132}$$

$$\lim_{x \to \pm\infty} A, B = 0 \quad . \tag{133}$$

The computed functional form of $\lambda(t)$ is shown graphically in Figure 24 for several values of the dimensionless group

$$\alpha = \frac{t_D}{t_R} = \frac{k\delta^2 nA_0}{D} \quad , \tag{134}$$

where t_D is the characteristic time scale of the diffusion; i.e.,

$$t_D = \frac{\delta^2}{D} \quad , \tag{135}$$

and t_R is the (initial) characteristic time scale of the reaction, namely,

$$t_R = (knA_0)^{-1} \quad . \tag{136}$$

All curves in this figure are for the case of the feed ratio

$$\beta = \frac{B_0}{nA_0} \tag{137}$$

equal to unity.

It can be seen that in all cases both the initial value and the final values of λ are 1. Initially, before the reaction has had time to consume appreciable quantities of the reactants, the concentration profiles are virtually identical to those in the inert case. In the long time limit, the eventual total mixing of the species results in uniform spatial concentration distributions that, as is easily verified, are characterized by $\lambda = 1$, regardless of the value of k.

It is important to note that for $\alpha \lesssim 1$, the parameter λ has approximately unit value for all time (see Figure 24). This greatly simplifies the functional form of the closure scheme [Eq. (95)]. In contrast, significant temporal variations occur in λ as α becomes large compared with unity. A fortuitous and fortunate feature of this behavior is that for all values of α, λ reaches its minimum value λ_{min} at approximately $t = 0.5t_D$ and maintains this value for a period of about 100 t_D. Inasmuch as reacting species that are initially unmixed can be consumed only as fast as the molecular diffusion and turbulence can bring them together, for fast reactions ($\alpha >> 1$), the characteristic time scale must be t_D rather than t_R. In view of this, it appears from the behavior of $\lambda(t)$ described above (and shown in Figure 24) that a constant value of λ, namely,

$$\lambda = \lambda_{min} \quad , \tag{138}$$

should yield good results in Eq. (95) for all values of α. With this prospect in mind, Shu examined the relationship between λ_{min} and α and found that for $\beta = 1$,

$$\lambda_{min} = \frac{1}{1 + \frac{\alpha}{12}} \quad , \tag{139}$$

as shown graphically in Figure 25.

An interesting consequence of Eqs. (138) and (139) is that for large values of α, we have

$$\lambda = \frac{12}{\alpha} \quad .$$

Upon substituting this result into Eq. (95) and using the resulting expression for $\overline{AB}$ in the rate equation for $\overline{A}$, we obtain

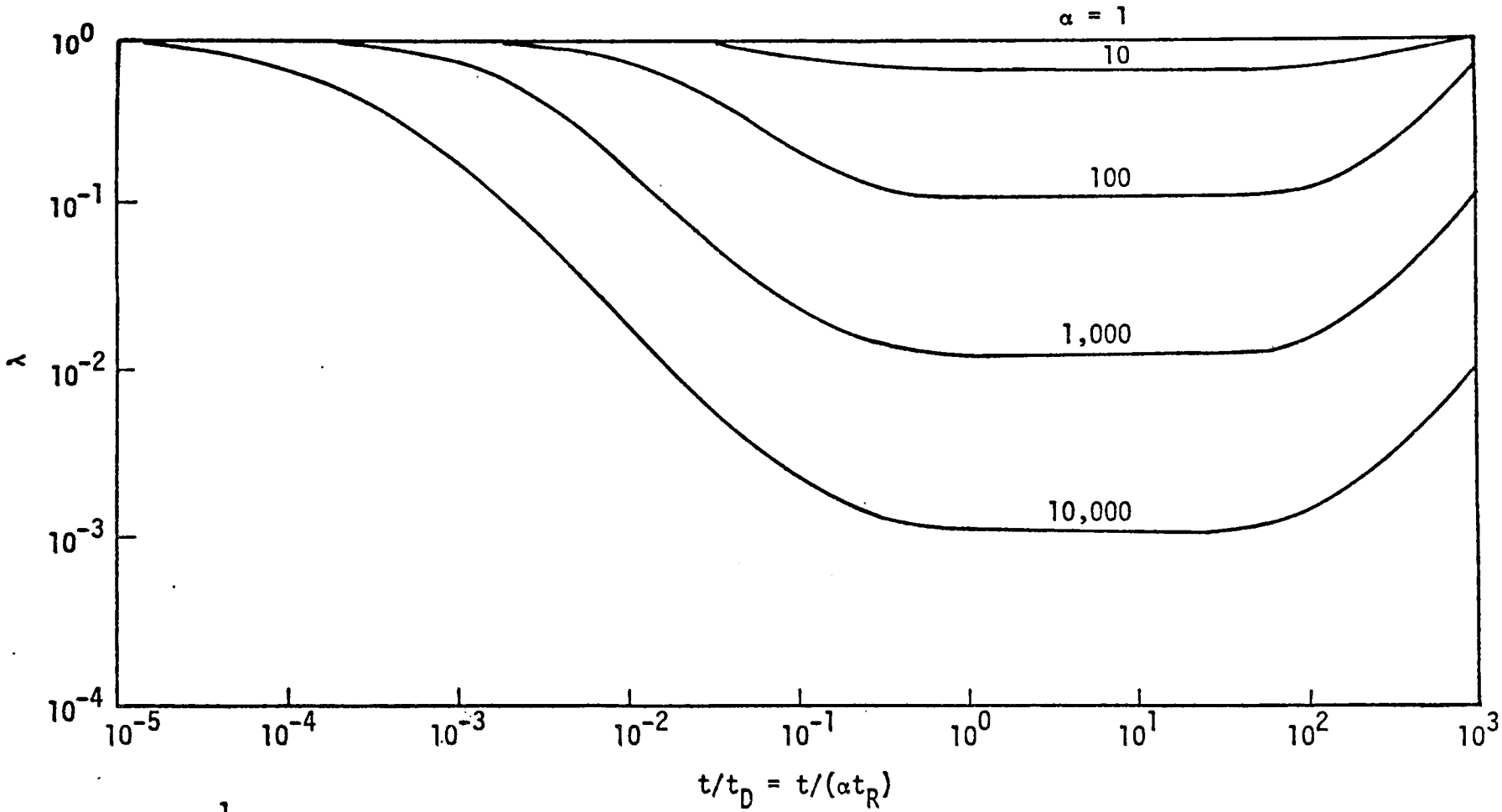

$t_K = (knA_0)^{-1}$

Source: Shu (1975).

FIGURE 24. FUNCTIONAL FORM OF $\lambda(t)$ FOR VARIOUS VALUES OF THE RATIO α OF THE DIFFUSIVE AND REACTIVE TIME SCALES t_D AND t_R

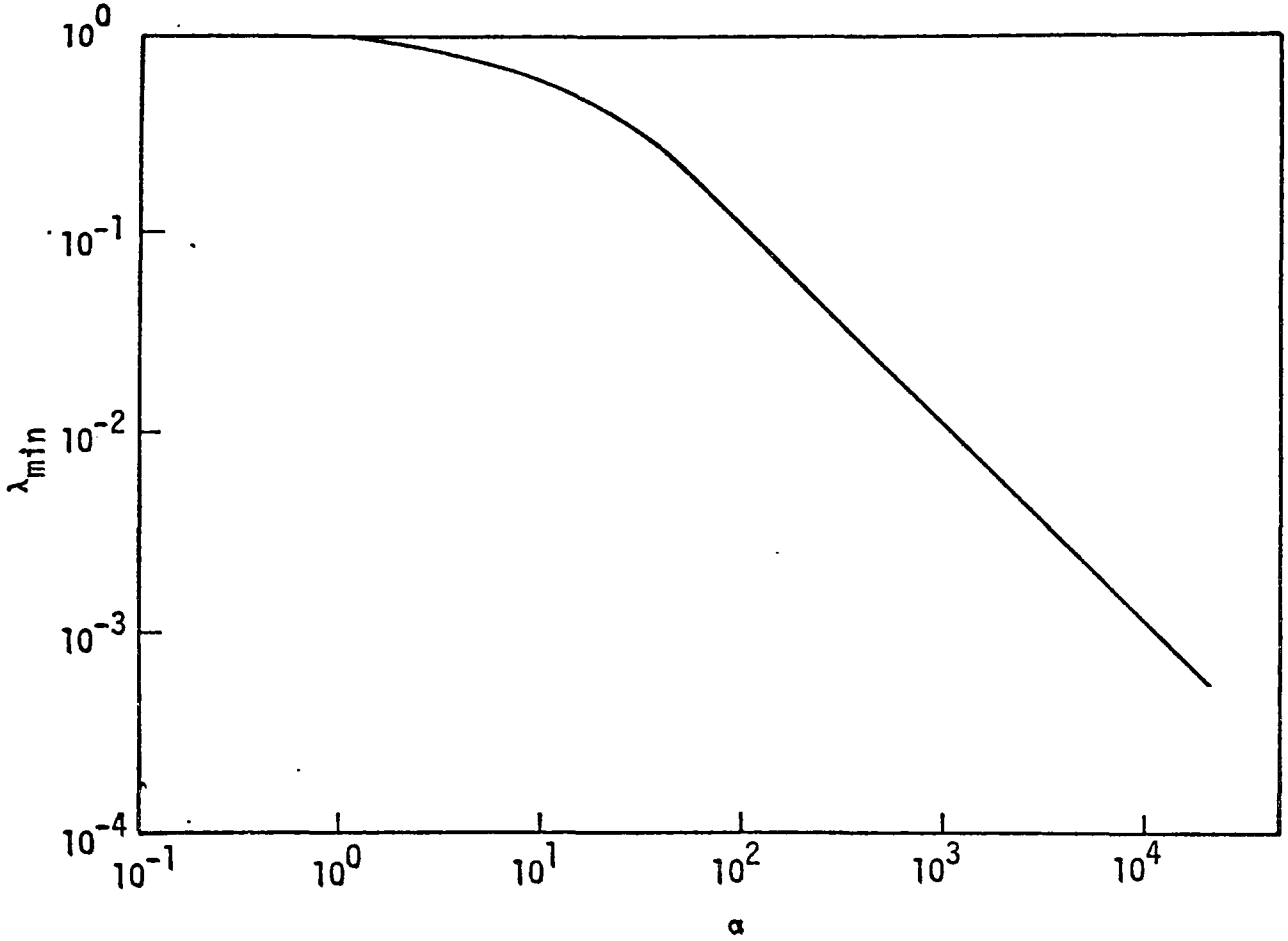

Source: Shu (1975).

FIGURE 25. DEPENDENCE OF λ_{min} ON α FOR THE CASE OF THE FEED RATIO $\beta = 1$

$$\frac{d\overline{A}}{dt} = - \frac{12D}{\delta^2 A_0 n} \frac{\hat{r}_{AB}}{\zeta_A \zeta_B} [\overline{A} - (1 - \zeta_A)\overline{A}_I] [\overline{B} - (1 - \zeta_B)\overline{B}_I] \quad . \quad (140)$$

The absence of the rate constant k from the right side of this equation emphasizes the fact that fast reactions are diffusion-limited processes.

Shu (1975) also considered the effects of variations in the feed ratio β and the number and initial separation of the slugs of reactants. Figure 26 shows how $\lambda(t)$ is affected by variations in β when α is held constant at 700. The most striking effect is the more rapid onset of the rise of λ toward its final value of 1. This behavior reflects the more rapid exhuastion of the species (in these cases A) that is present in a smaller quantity. Despite this behavior, the assumption

$$\lambda = \text{constant} = \lambda_{min}$$

should still prove accurate during the major part of the period in which the reaction is in progress. Figure 26 also shows that except for the case of $\beta \ll 1$, the order of magnitude of λ_{min} is unaffected by changes in β.

Figure 27 shows the influence on λ of changes in the number and separation of the initial slugs of reactants. In each of the three separate cases shown, the minimum value achieved by λ is of the same order of magnitude. These results, those presented above, and other experiments not described here suggest that Eqs. (138) and (139) are perhaps accurate even in general situations. In the next section, we examine this possibility in light of observational data.

E. TESTING THE CLOSURE SCHEME REPRESENTED BY EQ. (95) USING OBSERVATIONAL DATA

Few empirical studies of turbulent reactions have been reported in which all of the information required to apply and subsequently to test Eq. (95) has been measured. Usually, the data reported are not sufficient

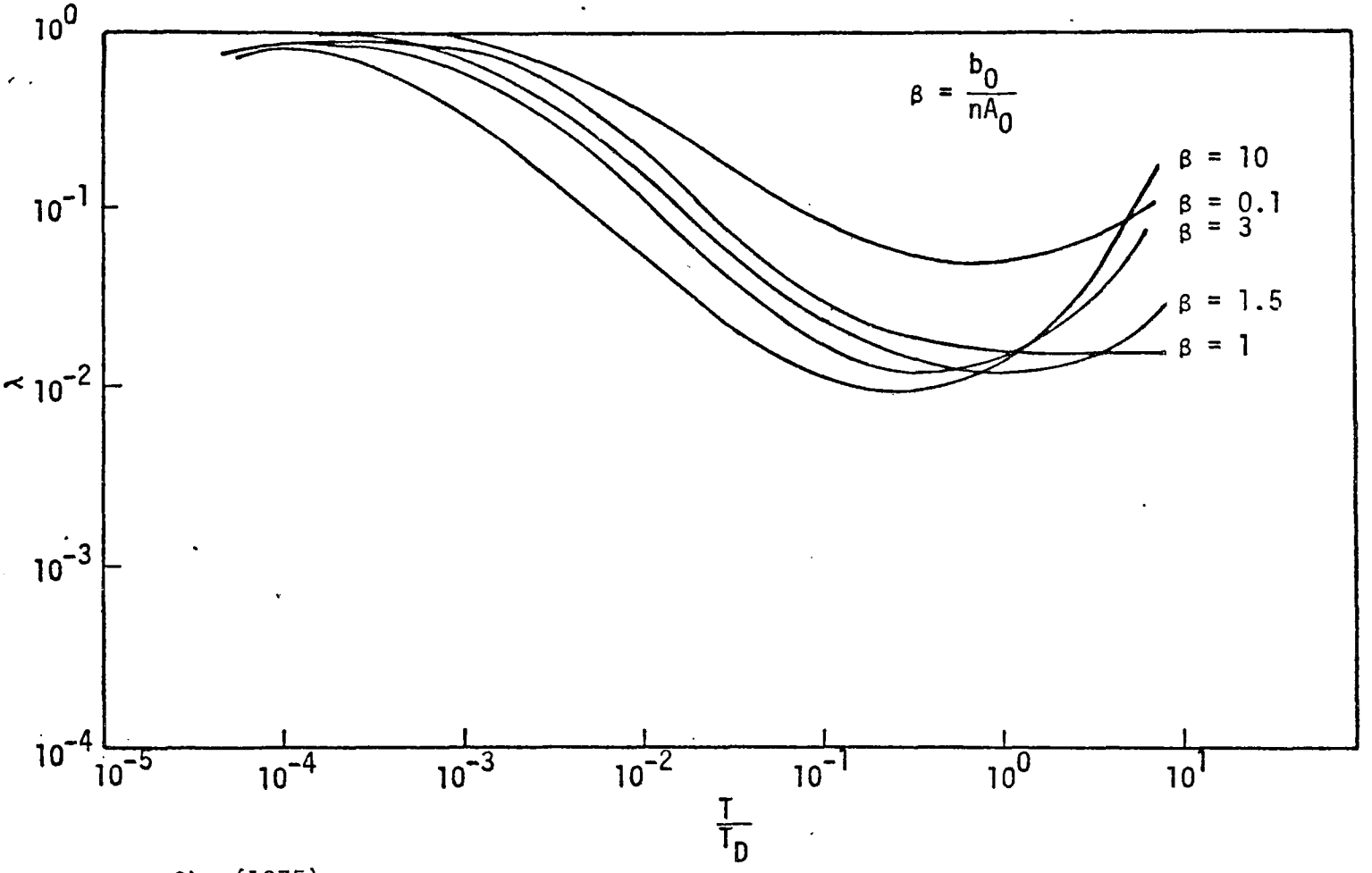

Source: Shu (1975).

FIGURE 26. IMPACT OF VARIATIONS IN THE FEED RATIO β ON THE FUNCTIONAL FORM OF λ(t) FOR α = 700

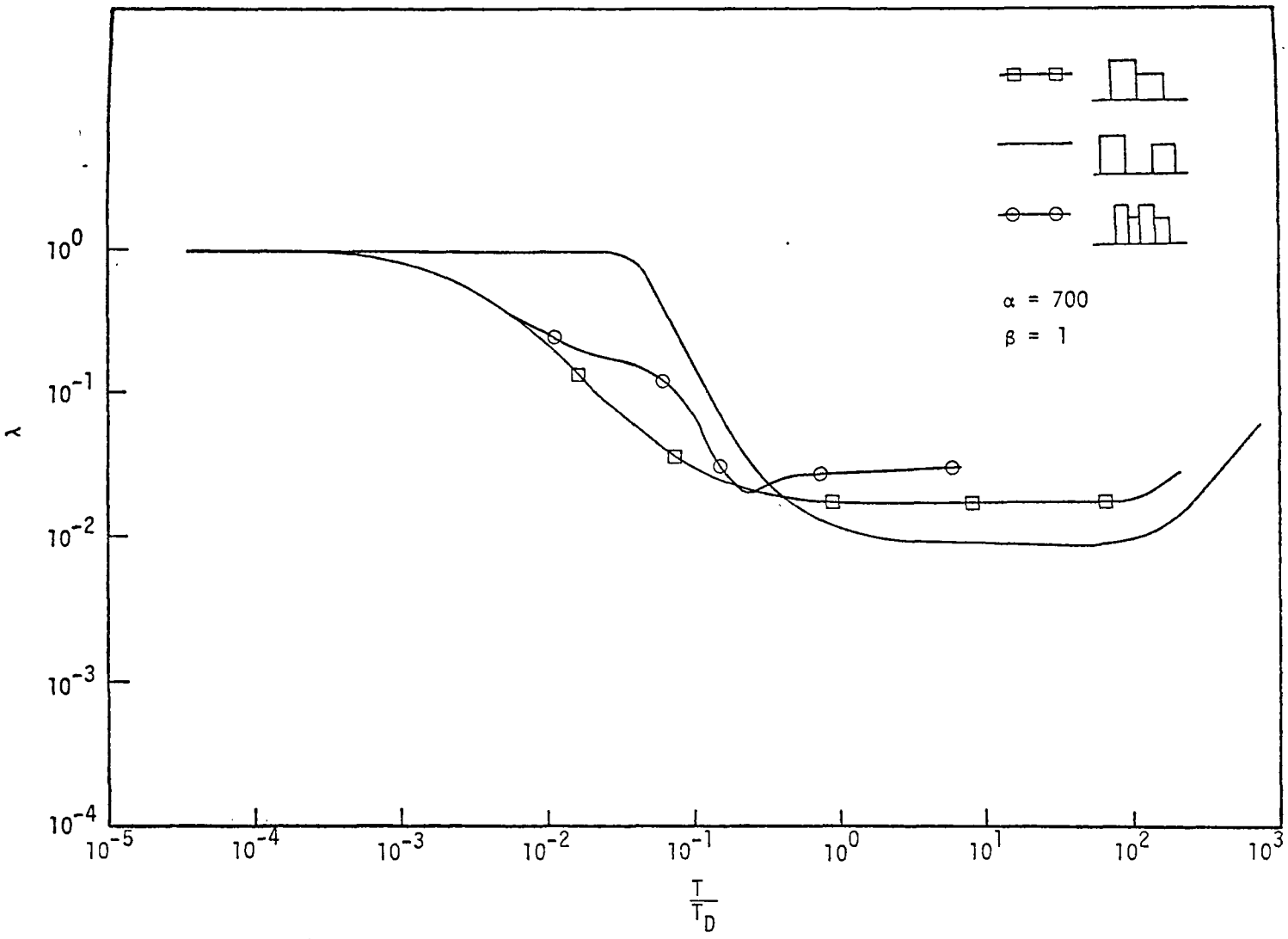

Source: Shu (1975).

FIGURE 27. INFLUENCE OF CHANGES IN THE INITIAL NUMBER AND SEPARATION OF REACTANT SLUGS ON THE FUNCTIONAL FORM OF λ

to permit estimations of the parameters $\hat{\Gamma}_{AB}$, ζ_A, and ζ_B that are properties of the inert species concentration statistics. However, using the theory of Toor (1962), which relates the concentration statistics of inert species to those of extremely fast reactants in the same turbulence, Shu (1975) succeeded in collecting experimental data from the literature that are adequate to apply and test Eq. (95). (See Appendix E for details.) We report some of his findings here. For more details, we refer the reader to Shu (1975)

All of the data used were gathered from the multijet reactor designed by Vassilatos and Toor (1965). In this system, the reactants, usually an acid and a base, are fed through alternate jets in a head consisting of 100 small jets at the end of a pipe several centimeters in diameter. Downstream from the jet head, the mean concentrations are constant on all planes normal to the pipe axis. Thus, this reactor approximates a one-dimensional system in which downstream distance corresponds to elapsed time.

Using Eq. (95) in the governing rate equations, Shu modeled this system by

$$\frac{dF_A}{dt} = - \frac{k\lambda\hat{\Gamma}_{AB}}{\zeta_A\zeta_B} \overline{A}_I\overline{B}_I \, [F_A - (1 - \zeta_A)] \, [F_B - (1 - \zeta_B)] \quad , \qquad (141)$$

where

$$F_A = \frac{\overline{A}}{\overline{A}_I} \quad , \qquad (142a)$$

$$F_B = \frac{\overline{B}}{\overline{B}_I} \quad , \qquad (142b)$$

and where $\overline{A}_I$ and $\overline{B}_I$ are constants. Since the reactions are of the form $A + nB \rightarrow$ products, and since the mean speed $\overline{u}$ of material down the pipe is constant, Eq. (141) can be written in the equivalent form

$$\frac{dF_A}{dx} = - \frac{k\lambda \hat{\Gamma}_{AB} n\bar{A}_I}{\bar{u}\zeta_A\zeta_B} [F_A - (1 - \zeta_A)] [F_A - 1 + \beta\zeta_B] \quad ; \qquad (143)$$

where x represents downstream distance and

$$\beta = \frac{\bar{B}_I}{n\bar{A}_I}$$

is the feed ratio of the inlet jets.

Shu used Eqs. (124) and (125) to approximate ζ_A and ζ_B. Subsequently, he determined the values of $\hat{\Gamma}_A$, $\hat{\Gamma}_B$, and $\hat{\Gamma}_{AB}$ entering into these expressions and into Eq. (143) by using Toor's theory, mentioned above, together with relevant measured data on extremely fast reactions in the multijet reactor (see Appendix E). We should add that although Toor's theory has been corroborated by several experiments, a more thorough and meaningful test could be performed if data were available that did not require this theory.

To apply the approximation [Eqs. (136) and (139)] for λ, Shu evaluated α using reported values of k, D, and other terms, and the measured scalar microscale for δ. In all cases, Shu found that $\alpha \leq 1$, and so he used the constant value $\lambda = 1$ throughout the model validation calculations.

Figure 28 presents the first set of comparisons between the observed values of F_A and those predicted by the model equation [Eq. (143)] for two different values of the feed ratio β. In both cases, the agreement between the model predictions (solid line) and the observations (circles) is very good. The degree to which the concentration fluctuations dominate the rate of change of the mean reactant concentrations is revealed by the discrepancy between the data points and the dashed lines shown in both panels of Figure 28. These lines show the predictions of the rate equations in which the concentration fluctuation term $\overline{A'B'}$ has been omitted. The comparisons show that the effect of the fluctuations is a retardation of the

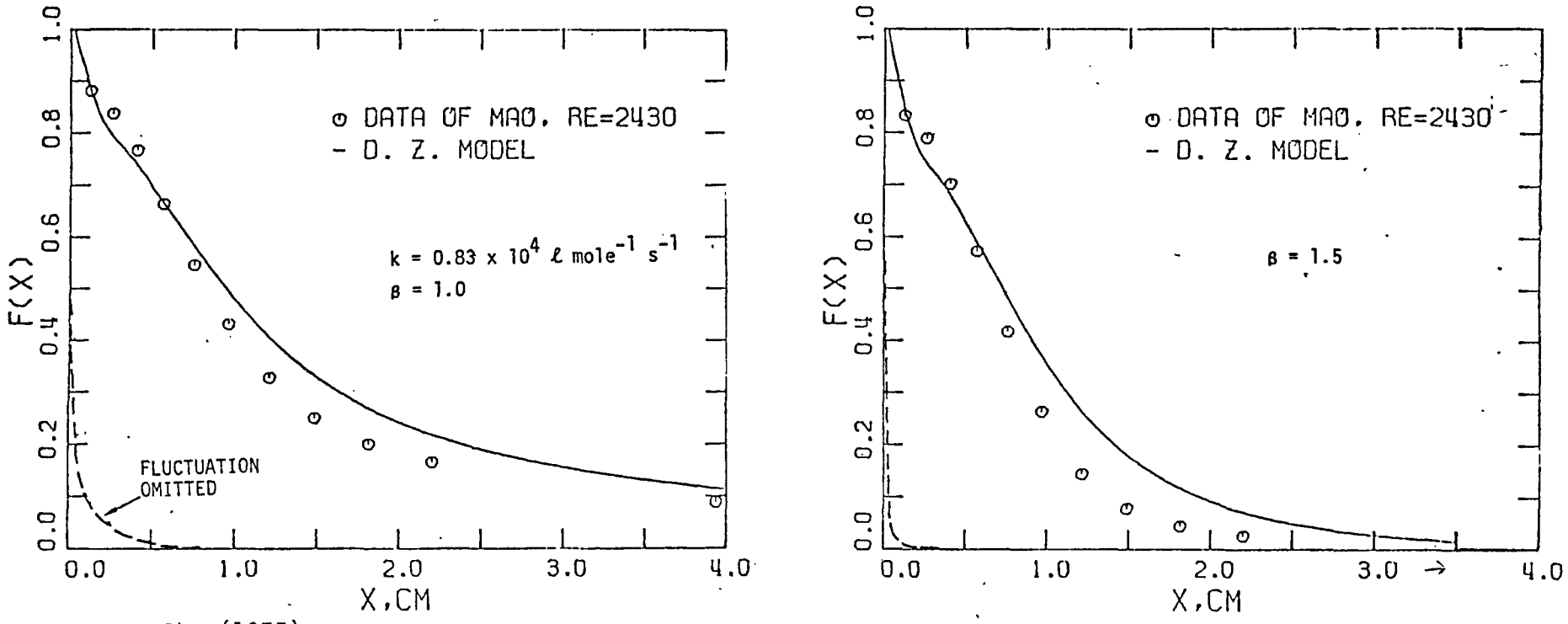

Source: Shu (1975).

FIGURE 28. FIRST COMPARISON OF CLOSURE MODEL PREDICTIONS WITH OBSERVATIONAL DATA

speed of the reaction. This result is caused by the segregation of the reactants initially and the finite time required for the turbulence and molecular diffusion acting together to bring the two materials into contact. As shown in Figure 29, this phenomenon cannot be described in terms of $\overline{A}$ and $\overline{B}$ alone. In this figure, we have plotted the solutions of the equation

$$\frac{d\overline{A}}{dt} = -\varepsilon k \overline{A}\overline{B} \tag{144}$$

for several values of the constant ε. Note that no value of ε exists that will bring the solution of Eq. (144) into even crude agreement with the observations.

Figure 30 shows a comparison of the theory and observations for a situation involving both a faster reaction and larger values of the feed ratio than those presented in Figure 28. As this figure indicates, the agreement between theory and observation is better than it was in the previous case. Additional comparisons can be found in Shu (1975).

The results reported above are very encouraging and provide the hope that our closure model will perform well under a wide range of conditions, both in the atmosphere and in the laboratory. Our immediate goal is to develop expressions for $\hat{\Gamma}_{AB}$, ζ_A, and ζ_B that permit Eq. (95) to be applied to reaction processes in the atmosphere. Toward this end, we are currently preparing a numerical experiment in which these functions will be estimated using the turbulence model of Deardorff. The procedure will be to release pairs of particles in the numerical fluid in each of many realizations of the turbulent flow and to calculate the mean square concentration field from the ensemble of particle-pair trajectories generated thereby. In this way, we plan to derive the forms of $\hat{\Gamma}_{AB}$, ζ_A, and ζ_B as functions of the atmospheric stability, wind speed, release height, surface roughness, and the like. Provided that the resulting expressions have universal features, the universal functional forms of these parameters can be used in conjunction with those of the diffusivities K_z presented in Chapter II to study reactive plumes of material in the planetary boundary layer. Progress on this project will be reported in Shu (1975) and in future reports on our EPA contract efforts.

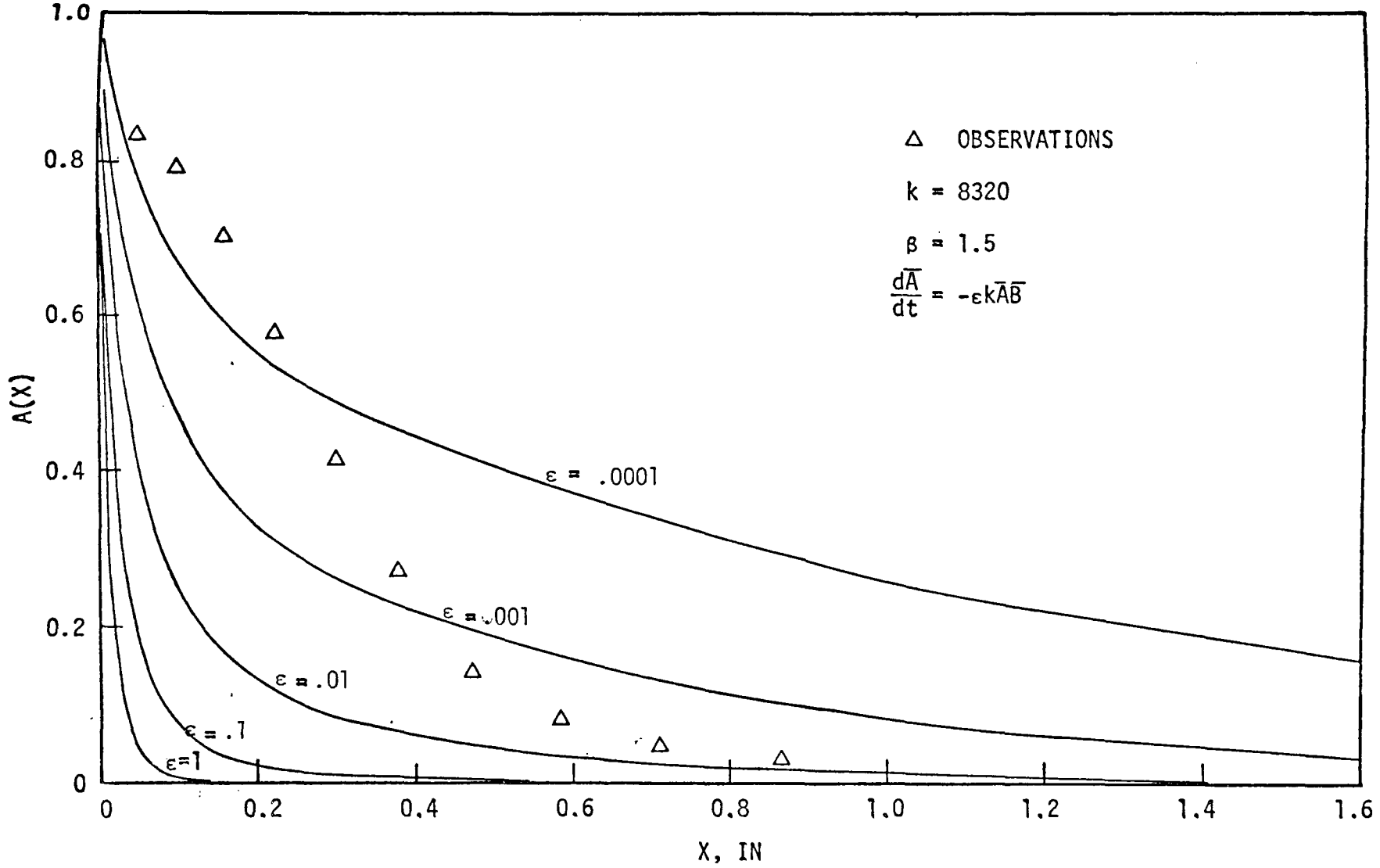

FIGURE 29. ATTEMPTS TO SIMULATE THE OBSERVATIONAL DATA USING A RATE EQUATION THAT OMITS CONCENTRATION FLUCTUATION EFFECTS

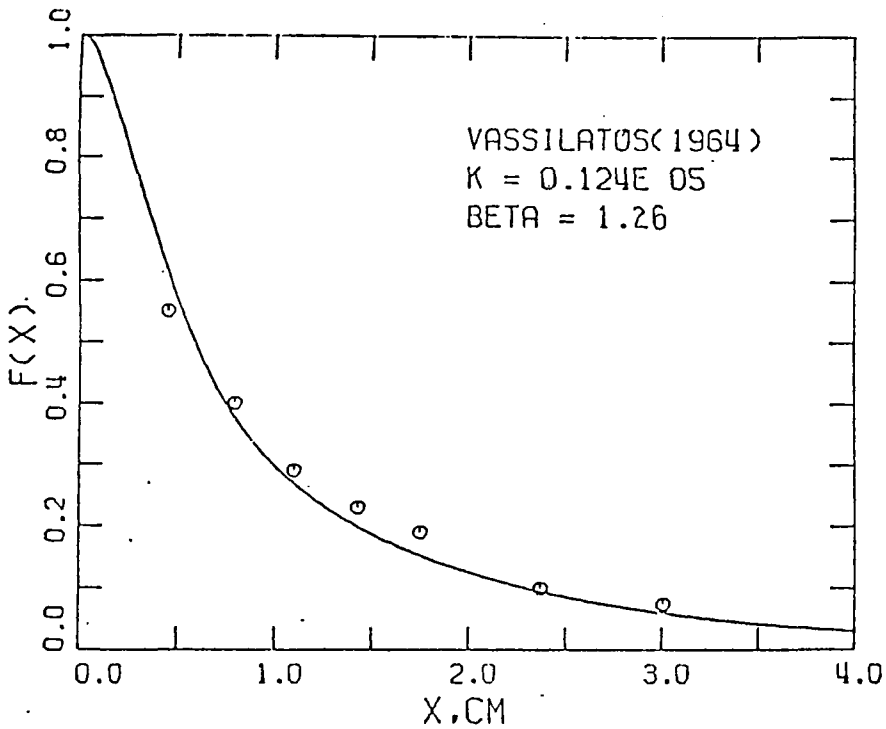

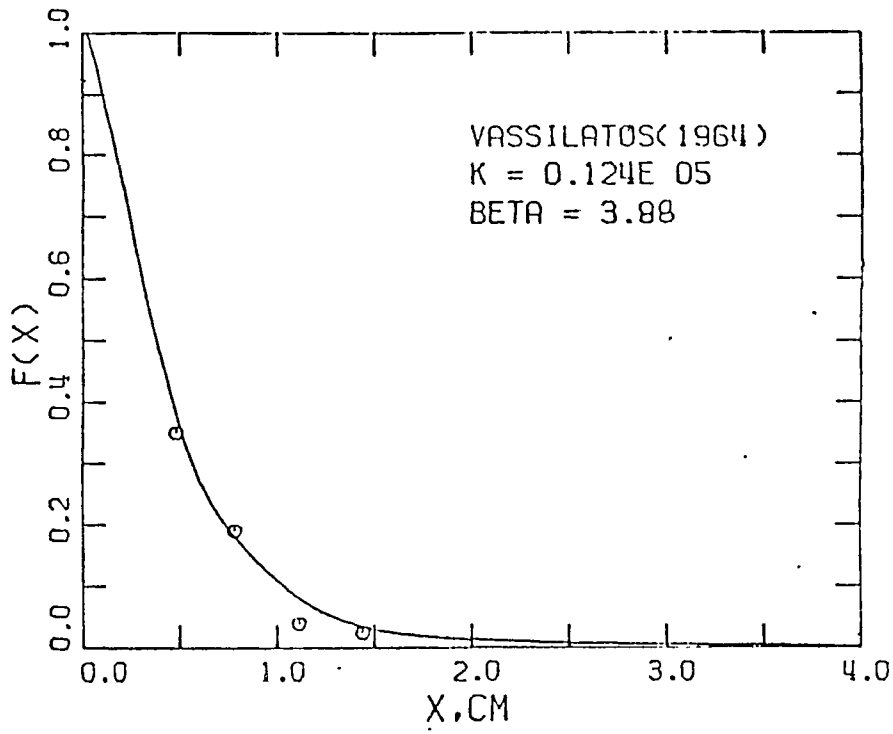

Source: Shu (1975).

FIGURE 30. SECOND COMPARISON OF CLOSURE MODEL PREDICTIONS WITH OBSERVATIONAL DATA

IV DEVELOPMENT OF A SCHEME FOR PARAMETERIZING THE EFFECT OF SUBGRID-SCALE CONCENTRATION VARIATIONS ON REACTION RATE

A. INTRODUCTION

The previous chapter dealt with the instantaneous concentration fluctuations produced by turbulence and the effect they have on the reaction rate of nonlinear chemical reactions. In this chapter, we treat the analogous problem of variations in the mean concentration that are of too small a scale to be resolvable by a grid model of an urban atmosphere. The similarity of this problem to that of the turbulent concentration fluctuation is so great that the closure scheme we developed in the last chapter can be used here as the basis of a parameterization scheme for the subgrid-scale effects.

Before proceeding with the development and application of the scheme, we briefly review the nature of the subgrid-scale variation (SSV) problem and then develop necessary conditions under which SSV is of negligible consequence. The last two sections of this chapter are devoted to the derivation of the SSV parameterization scheme and to the application of it to air pollution problems of applied interest.

B. STATEMENT OF THE PROBLEM

Consider two pollutants, A and B, that undergo the reaction

$$A + B \rightarrow D$$

to form a third product D. The equations governing the concentrations of these species in an urban atmosphere are generally taken to be (for modeling purposes)

$$\frac{\partial A}{\partial t} + \bar{u}_i \frac{\partial A}{\partial x_i} = \frac{\partial}{\partial x_i} K_{ij} \frac{\partial A}{\partial x_j} + S_A - kAB \qquad (145a)$$

where

A = some time averaged concentration of A,
$\bar{u}_i$ = the i-th component of the mean wind speed,
K_{ij} = the turbulent diffusivity tensor,
S_A = the distribution and strength of sources of A,
k = the rate constant for the above reaction.

An equation similar to Eq. (145) governs the concentration of B:

$$\frac{\partial B}{\partial t} + \bar{u}_i \frac{\partial B}{\partial x_i} = \frac{\partial}{\partial x_i} K_{ij} \frac{\partial B}{\partial x_j} + S_B - kAB \quad . \tag{145b}$$

Because the analytic solution of this system of equations is not available, Eq. (145) must be solved numerically. For reasons given in Chapter I, this necessitates the averaging of Eq. (145) over volumes equal to that of the grid cells into which space is discretized in the numerical technique. The spatial average is denoted by the tilde (~) and is defined by (using the concentration of A as an example)

$$\tilde{A}(\underset{\sim}{r},t) \equiv \frac{1}{8\Delta x\Delta y\Delta z} \int_{x-\Delta x}^{x+\Delta x} \int_{y-\Delta y}^{y+\Delta y} \int_{z-\Delta z}^{z+\Delta z} A(\underset{\sim}{r}',t)\, d\underset{\sim}{r}' \quad , \tag{146}$$

where $r = (x,y,z)$ and $(2\Delta x, 2\Delta y, 2\Delta z)$ denotes the dimension of the grid cells. Averaging Eqs. (145a) and (145b) in the manner of Eq. (146) and assuming that $\bar{u}$ and K are nearly constant over distances comparable to the grid cell dimensions, we obtain

$$\frac{\partial \tilde{A}}{\partial t} + \bar{u}_i \frac{\partial \tilde{A}}{\partial x_i} = \frac{\partial}{\partial x_i} K_{ij} \frac{\partial \tilde{A}}{\partial x_j} + \tilde{S}_A - k\widetilde{AB} \quad , \tag{147}$$

where $\tilde{S}_A$ and $\widetilde{AB}$ are defined as in Eq. (146). A similar equation can be derived for $\tilde{B}$. Equation (147) and the corresponding equation for $\tilde{B}$ are used as the basis of urban pollution models; therefore, it is $\tilde{A}$ and $\tilde{B}$, rather than the "point" values A and B that these models predict. The differences

$$A'' = A - \tilde{\tilde{A}} \quad ,$$

$$B'' = B - \tilde{\tilde{B}} \tag{148}$$

are the subgrid-scale variations. Using the definitions given by Eq. (148) and assuming that

$$\tilde{\tilde{\tilde{A}}} = \tilde{\tilde{A}} \quad ,$$

$$\tilde{\tilde{\tilde{B}}} = \tilde{\tilde{B}} \quad ,$$

and so forth, we can express Eq. (147), and the corresponding equation for B, in the more useful forms

$$\frac{\partial \tilde{A}}{\partial t} + L\tilde{A} = \tilde{S}_A - k\tilde{A}\tilde{B} - k\widetilde{A''B''} \quad , \tag{149a}$$

$$\frac{\partial \tilde{B}}{\partial t} + L\tilde{B} = \tilde{S}_B - k\tilde{A}\tilde{B} - k\widetilde{A''B''} \quad , \tag{149b}$$

where for brevity we have introduced the linear operator

$$L \equiv \tilde{u}_i \frac{\partial}{\partial x_i} - \frac{\partial}{\partial x_i} K_{ij} \frac{\partial}{\partial x_j} \quad . \tag{150}$$

The quantity $k\widetilde{A''B''}$ on the right side of Eqs. (149a) and (149b) represents the influence of the SSV on the rate of decay of $\tilde{A}$ and $\tilde{B}$. Until now, all models of urban pollution have tacitly ignored SSV effects, but as we show in the next section, this omission is generally unjustifiable.

C. CONDITIONS UNDER WHICH SSV EFFECTS ON REACTION SPEED ARE NEGLIGIBLE

If

$$\widetilde{A''B''} \ll \tilde{A}\tilde{B} \quad , \tag{151}$$

then it is clear from Eq. (149) that SSV has a negligible influence on $\tilde{A}$ and $\tilde{B}$ and can be ignored. To derive the condition under which Eq. (151) is satisfied, we begin by deriving the equations governing A" and B".

Subtracting Eq. (149a) from Eq. (145a) and using Eq. (148) to define A", we obtain

$$\frac{\partial A''}{\partial t} + \mathcal{L}A'' = S_A'' - k(\tilde{A}B'' + \tilde{B}A'' + A''B'' - \widetilde{A''B''}) \quad , \tag{152a}$$

and, similarly,

$$\frac{\partial B''}{\partial t} + \mathcal{L}B'' = S_B'' - k(\tilde{A}B'' + \tilde{B}A'' + A''B'' - \widetilde{A''B''}) \quad , \tag{152b}$$

where $S_A'' = S_A - \tilde{S}_A$ and $S_B'' = S_B - \tilde{S}_B$. Multiplying Eq. (152a) by B" and Eq. (152b) by A" and adding, we obtain

$$\frac{\partial}{\partial t}(A''B'') + \mathcal{L}(A''B'') = - K_{ij}\left[\frac{\partial A''}{\partial x_i}\frac{\partial B''}{\partial x_j} + \frac{\partial A''}{\partial x_j}\frac{\partial B''}{\partial x_i}\right] + B''S_A'' + A''S_B''$$

$$- k(\tilde{A}B''^2 + \tilde{B}A''B'' + A''B''^2 - B''\widetilde{A''B''}$$

$$+ \tilde{A}B''A'' + \tilde{B}A''^2 + A''^2B'' - A''\widetilde{A''B''}) \quad .$$

Upon averaging this equation in the manner of Eq. (146) and invoking assumptions such as $\tilde{A} = \tilde{A}$ made earlier, we obtain

$$\frac{\partial}{\partial t}\widetilde{A''B''} + \mathcal{L}\widetilde{A''B''} = - K_{ij}\left[\widetilde{\frac{\partial A''}{\partial x_i}\frac{\partial B''}{\partial x_j}} + \widetilde{\frac{\partial A''}{\partial x_j}\frac{\partial B''}{\partial x_i}}\right] + \widetilde{B''S_A''} + \widetilde{A''S_B''}$$

$$- k[\tilde{A}\widetilde{B''^2} + \tilde{B}\widetilde{A''^2} + \widetilde{A''B''}(\tilde{A} + \tilde{B}) + \widetilde{A''B''^2} + \widetilde{A''^2B''}] \quad . \tag{153}$$

The first term on the right side of this equation causes a decay of $\widetilde{A''B''}$, even in the absence of chemical decay, i.e., when k = 0. Thus, if A and B were inert and if $\widetilde{A''B''}$ were nearly uniform in space, the steady-state value of $\widetilde{A''B''}$ would be such that

$$K_{ij}\left[\widetilde{\frac{\partial A''}{\partial x_i}\frac{\partial B''}{\partial x_j}} + \widetilde{\frac{\partial A''}{\partial x_j}\frac{\partial B''}{\partial x_i}}\right] = \widetilde{B''S_A''} + \widetilde{A''S_B''} \quad . \tag{154}$$

Let the steady-state value prescribed by Eq. (154) be denoted by $(\widetilde{A"B"})_I$. It follows, therefore, that the conditions that result in the satisfaction of

$$(\widetilde{A"B"})_I << \tilde{\tilde{A}}\tilde{\tilde{B}} \tag{155}$$

are sufficient conditions for the realization of Eq. (151). Since these conditions are not difficult to derive, we use them as the measure that we seek of the importance of the SSV.

We note first that the left side of Eq. (155) can be expressed approximately in terms of known quantities using Eq. (154) and the equation corresponding to Eq. (153) that governs $\widetilde{A"^2}$, namely,

$$\frac{\partial \widetilde{A"^2}}{\partial t} + \mathcal{L}\widetilde{A"^2} = -2K_{ij}\widetilde{\frac{\partial A"}{\partial x_i}\frac{\partial A"}{\partial x_j}} + \widetilde{A"S"_A} - k(\widetilde{AA"B"} + \tilde{B}\widetilde{A"^2} + \widetilde{A"^2B"}) \quad . \tag{156}$$

In Appendix F, we show that the first term on the right side of Eq. (156) can be approximated by

$$2K_{ij}\widetilde{\frac{\partial A"}{\partial x_i}\frac{\partial A"}{\partial x_j}} \sim \frac{2K_\lambda}{\lambda^2}\widetilde{A"^2} \quad , \tag{157}$$

where λ is on the order of the smallest dimension of a grid cell and K_λ is the turbulent diffusivity in the corresponding coordinate direction. Also, it is not unreasonable to assume that $\widetilde{A"S"_A}$ is on the order of

$$\widetilde{A"S"_A} \sim (\widetilde{A"^2})^{\frac{1}{2}}(\widetilde{S"_A{}^2})^{\frac{1}{2}} \quad . \tag{158}$$

From this approximation and from Eq. (157), we conclude from Eq. (156) that in the steady state

$$(\widetilde{A"^2})^{\frac{1}{2}} \sim (\widetilde{S"_A{}^2})^{\frac{1}{2}}\frac{\lambda^2}{K_\lambda} \quad , \tag{159}$$

ignoring the chemical decay ($k = 0$) as before. Employing assumptions such as Eqs. (158) and (157) in Eq. (154), we conclude finally that

$$\widetilde{(A"B")}_I \sim \frac{\lambda^4}{K_\lambda^2} \widetilde{S"_A S"_B} \quad . \tag{160}$$

The quantities on the right side of Eq. (155) pertain to the concentrations of the reactive species A and B, rather than to their inert counterparts considered above in deriving Eq. (160). Since the decay rates of $\tilde{A}$ and $\tilde{B}$ are on the order of

$$\frac{d\tilde{A}}{dt} = \frac{d\tilde{B}}{dt} \sim -k\tilde{A}\tilde{B} \quad , \tag{161}$$

and since the production rates of these quantities are $\tilde{S}_A$ and $\tilde{S}_B$, respectively, we see that in the steady state

$$\tilde{A}\tilde{B} \sim \frac{\tilde{S}_B}{k} \frac{(\alpha\tilde{B} + \tilde{A})}{\tilde{B} + \tilde{A}} \quad , \tag{162}$$

where

$$\alpha = \frac{\tilde{S}_A}{\tilde{S}_B} \quad . \tag{163}$$

Assuming that

$$\frac{\tilde{A}}{\tilde{B}} \sim \frac{\tilde{S}_A}{\tilde{S}_B} \quad ,$$

we can reduce Eq. (162) to the form

$$\tilde{A}\tilde{B} \sim \frac{2\tilde{S}_A\tilde{S}_B}{k(\tilde{S}_A + \tilde{S}_B)} \quad .$$

Upon combining this result with Eq. (160), we conclude finally that a sufficient condition for ignoring SSV effects on the chemical decay of $\tilde{A}$ and $\tilde{B}$ is

$$\frac{\lambda^4 \widetilde{S_A'' S_B''}}{2K_\lambda^2 \tilde{S}_A \tilde{S}_B} k(\tilde{S}_A + \tilde{S}_B) \ll 1. \tag{164}$$

When this condition is not satisfied, SSV effects may or may not be important, depending on the particular physical situation. In the next section, we consider the derivation of a necessary condition under which subgrid-scale concentration variations significantly influence $\tilde{A}$ and $\tilde{B}$.

To demonstrate the quantitative significance of Eq. (164), let us consider a simple one-dimensional problem in which a series of sources of strength S and width W are distributed with separation ℓ along the x-axis, as shown in Figure 31. We might consider this problem to represent a cross section of a system of infinitely long, parallel streets.

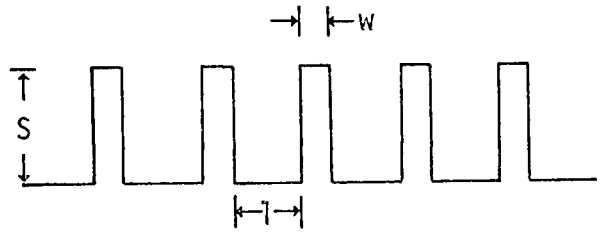

FIGURE 31. SYSTEM OF RECTANGULAR SOURCES

Suppose that S represents the emission rate of species B and that αS is the emission rate of species A. Suppose further that a grid model simulation of this problem is to be constructed using a grid mesh size Δx. We desire to know whether subgrid-scale concentration variations can be ignored in the grid model simulation of the concentrations $\tilde{A}$ and $\tilde{B}$.

Through a straightforward series of analyses, we find that in this problem

$$\widetilde{S_A'' S_B''} = \alpha\left[\frac{S^2 W}{\ell}\left(1 - \frac{W}{\ell}\right)\right] \tag{165}$$

and that

$$\tilde{S}_B = \frac{SW}{\ell} \quad , \quad \tilde{S}_A = \frac{\alpha SW}{\ell} \tag{166}$$

Substituting these results into Eq. (164), we find that SSV can be ignored if

$$kS \leq \frac{2K_\lambda^2}{\lambda^4(1+\alpha)(1-\frac{w}{\ell})} \quad . \tag{167}$$

Normally $\ell >> w$ and γ might be on the order of one. Under these conditions, Eq. (167) can be simplified to

$$kS \leq \frac{K_\lambda^2}{\lambda^4} \quad . \tag{168a}$$

For the hydrocarbon-ozone reaction, $k \sim 0.1$ ppm^{-1}min^{-1}. Also, hydrocarbon emissions from motor vehicles are on the order of 10 gm/mile. Using these values we find that for a roadway carrying 1000 vehicles per hour,

$$kS \sim 3 \times 10^{-5}\text{sec}^{-2} \quad . \tag{168b}$$

A typical value of K_λ in the atmosphere is 10 m^2/sec. Consequently, we find from Eq. (168a) that SSV effects are negligible in the present problem if

$$\lambda \leq 50 \text{ m} \quad . \tag{169}$$

In the problem shown in Figure 31, λ is on the order of ℓ. Thus, if the source configuration shown here represented a network of actual streets, ℓ would certainly exceed 50 m, and SSV effects could not be ignored. In cases where $\ell > \Delta x$, λ is on the order of Δx. In this case, SSV effects could be suppressed by making the mesh size Δx suitably small; but this is not practical in many cases, and one is left with a problem in which SSV effects might have to be parameterized to achieve meaningful estimates of the spatial averaged concentrations $\tilde{A}$ and $\tilde{B}$. In Section E, we develop a quantitative measure of whether parameterization is actually necessary.

D. PARAMETERIZATION SCHEME FOR THE SUBGRID-SCALE CONCENTRATION VARIATIONS

Having derived the conditions under which SSV effects are negligible in the modeling of nonlinear chemical reactions and having demonstrated that these conditions are frequently not realized in actual air pollution simulation studies, we turn now to the development of a mathematical scheme for representing SSV. The scheme we developed here is based on the closure approximation developed in Chapter III.

Let V denote the volume of any grid cell in the grid model of $\tilde{A}$ and $\tilde{B}$, and let v_A denote the total volume within V in which particles of species A are found alone. Similarly, let v_B denote the volume where B particles are found alone. The volumes v_A and v_B are distinguished from a third volume v_{AB} in which particles of A and B are mixed sufficiently for chemical reactions to occur. Figure 32 illustrates these three volumes. By definition, we thus have

$$\tilde{A} = \frac{1}{V}\left(\int_{v_A} A\, dv + \int_{v_{AB}} A\, dv\right) , \tag{170a}$$

$$\tilde{B} = \frac{1}{V}\left(\int_{v_B} B\, dv + \int_{v_{AB}} B\, dv\right) . \tag{170b}$$

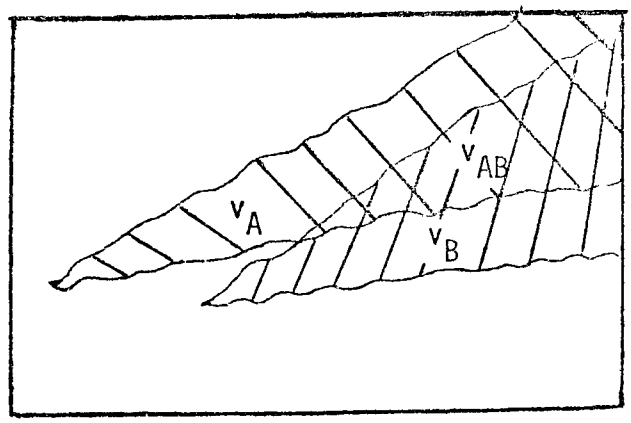

FIGURE 32. DESCRIPTION OF THE VOLUMES v_A, v_B, AND v_{AB}

It is clear from the definition of v_A and v_B that if A and B were chemically inert, the concentrations within these volumes would be the same as in the reactive case. It is only in the domain v_{AB} that the inert and chemically reactive systems differ. This fact is one of the key points upon which our parameterization scheme is based.

We define the following four variables:

$$\hat{A} \equiv \frac{1}{v_A} \int_{v_A} A \, dv \quad , \qquad \hat{B} \equiv \frac{1}{v_B} \int_{v_B} B \, dv \quad ;$$

$$\hat{a} \equiv \frac{1}{v_{AB}} \int_{v_{AB}} A \, dv \quad , \qquad \hat{b} \equiv \frac{1}{v_{AB}} \int_{v_{AB}} B \, dv \quad . \tag{171}$$

Let the subscript I denote the situation where the given particle species is chemically inert. Then analogous to Eq. (171), we define

$$\hat{a}_I \equiv \frac{1}{v_{AB}} \int_{v_{AB}} A_I \, dv \quad , \qquad \hat{b}_I \equiv \frac{1}{v_{AB}} \int_{v_{AB}} B_I \, dv \quad . \tag{172}$$

In terms of these variables, $\tilde{A}$, $\tilde{B}$, $\tilde{A}_I$, and $\tilde{B}_I$ become

$$\tilde{A} = \frac{1}{V}\left[\hat{A}v_A + \hat{a}v_{AB}\right] \tag{173a}$$

$$\tilde{B} = \frac{1}{V}\left[\hat{B}v_B + \hat{b}v_{AB}\right] \tag{173b}$$

$$\tilde{A}_I = \frac{1}{V}\left[\hat{A}v_A + \hat{a}_I v_{AB}\right] \tag{173c}$$

$$\tilde{B}_I = \frac{1}{V}\left[\hat{B}v_B + \hat{b}_I v_{AB}\right] \quad . \tag{173d}$$

Treating v_A, v_B, and v_{AB} as invariants in the inert and reactive systems as we have done above is permissible as long as the fluid motions, which control these volumes, are not perturbed by the chemical reactions. In the problems of interest to us, this condition is always satisfied.

Next, we define

$$\Gamma_{AB} \equiv \widetilde{A_I B_I} = \frac{1}{V}\int_{v_{AB}} AB \, dv = \frac{\mu AB}{V} \hat{a}_I \hat{b}_I v_{AB} \quad , \tag{174a}$$

$$\Gamma_A \equiv \widetilde{A_I^2} = \frac{1}{V}\left[\int_{v_A} A^2 \, dv + \int_{v_{AB}} A^2 \, dv\right] = \frac{1}{V}\left[\mu_A \hat{A} v_A + \mu_a \hat{a}_I^2 v_{AB}\right] \quad , \tag{174b}$$

$$\Gamma_B \equiv \widetilde{B_I^2} = \frac{1}{V}\left[\int_{v_B} B^2 \, dv + \int_{v_{AB}} B^2 \, dv\right] = \frac{1}{V}\left[\mu_B \hat{B}^2 v_B + \mu_b \hat{b}_I^2 v_{AB}\right] \quad . \tag{174c}$$

(We discuss the μ's later.) Just as $\tilde{A}_I$ and $\tilde{B}_I$ are determined completely by the fluid velocity field and source distribution, so too are Γ_{AB}, Γ_A, and Γ_B. Consequently, these five quantities can be regarded as known parameters that characterize the given problem.

Rather than parameterize the term $\widetilde{A"B"}$ explicitly, we shall instead treat the term

$$\tilde{A}\tilde{B} = \widetilde{A"B"} + \tilde{A}\tilde{B} \quad . \tag{175}$$

Using the variables introduced above, we can write

$$\tilde{A}\tilde{B} = \frac{1}{V}\int_{v_{AB}} AB \, dv = \frac{\lambda}{V} \hat{a}\hat{b} v_{AB} \quad , \tag{176}$$

where λ is a parameter that can vary with time. The desired parameterization is then obtained by examining $\hat{a}$, $\hat{b}$, and v_{AB} in terms of the seven known quantities given by Eqs. (173), (174), and by substituting the results into Eq. (176). To accomplish this, we must use two additional approximations because

there are two more variables in Eqs. (173) and (174) than there are equations. We therefore write

$$\hat{a}_I = \xi_A \hat{A} \tag{177a}$$

$$\hat{b}_I = \xi_B \hat{\hat{B}} \quad . \tag{177b}$$

In terms of the new parameters ξ_A and ξ_B, $\tilde{A}_I$ and $\tilde{B}_I$ become

$$\tilde{A}_I = \frac{\hat{A}}{V}(v_A + \xi_A v_{AB}) \quad , \tag{178a}$$

$$\tilde{B}_I = \frac{\hat{B}}{V}(v_B + \xi_B v_{AB}) \quad . \tag{178b}$$

In the manipulation of Eqs. (173), (174), and (177), several terms frequently appear together in a form that we call g; i.e.

$$g_B = \frac{\mu_{AB}\xi_B}{\mu_B} \frac{v_B + \xi_B v_{AB}}{v_B + \frac{\mu_b \xi_B^2 v_{AB}}{\mu_B}} \quad , \qquad g_A = \frac{\mu_{AB}\xi_A}{\mu_A} \frac{v_A + \xi_A v_{AB}}{v_A + \frac{\mu_A \xi_A^2 v_{AB}}{\mu_A}} \tag{179}$$

Using this parameter, we can write

$$\hat{\Gamma}_A = \frac{\hat{A}}{\tilde{A}_I} \frac{\mu_{AB}\xi_A}{g_A} \quad , \tag{180a}$$

$$\hat{\Gamma}_B = \frac{\hat{B}}{\tilde{B}_I} \frac{\mu_{AB}\xi_B}{g_B} \tag{180b}$$

$$\hat{\Gamma}_{AB} = \frac{v_{AB} g_A g_B}{\mu_{AB} V} \hat{\Gamma}_A \hat{\Gamma}_B \quad , \tag{180c}$$

where

$$\hat{\Gamma}_A = \frac{\Gamma_A}{\tilde{A}^2} \quad , \quad \hat{\Gamma}_B = \frac{\Gamma_B}{\tilde{B}^2} \quad , \quad \hat{\Gamma}_{AB} = \frac{\Gamma_{AB}}{\tilde{A}\tilde{B}} \quad . \tag{181}$$

Using all of the above expressions, we obtain finally

$$\widetilde{AB} = \frac{h}{\hat{\Gamma}_{AB}}\left[\hat{\Gamma}_B g_B \tilde{A} - \left(\hat{\Gamma}_B g_B - \hat{\Gamma}_{AB}\right)\tilde{A}_I\right]\left[\hat{\Gamma}_A g_A \tilde{B} - \left(\hat{\Gamma}_A g_A - \hat{\Gamma}_{AB}\right)\tilde{B}_I\right] \tag{182}$$

where

$$h = \frac{\lambda}{\mu_{AB}} \quad . \tag{183}$$

Except for the parameters h and g, which we discuss in more detail later, all of the terms on the right side of Eq. (182) are known quantities. The next step, therefore, in implementing this parameterization of AB is to express the right side of Eq. (182) in terms of the source distribution, fluid velocity, and other variables that characterize the given system.

This task is simplified somewhat in situations where the species A and B are released from the same sources, as is often the case in actual air pollution simulation studies. Under this condition, we have

$$v_A = v_B = 0 \quad ,$$

and g_A and g_B reduce to

$$g_A = \frac{\mu_{AB}}{\mu_a} \quad , \quad g_B = \frac{\mu_{AB}}{\mu_b} \quad . \tag{184}$$

Using these results, we find that

$$\hat{\Gamma}_B g_B - \hat{\Gamma}_{AB} = \frac{\mu_{AB}\hat{b}_I v_{AB}}{v\tilde{B}_I}\left(\frac{\hat{b}_I}{\tilde{B}_I} - \frac{\hat{a}_I}{\tilde{A}_I}\right) \quad , \tag{185}$$

A similar expression can be found for $\hat{\Gamma}_A g_A - \hat{\Gamma}_{AB}$. Now, from Eqs. (177) and (178), we conclude that the term in parentheses in Eq. (185) is identically zero. Thus,

$$\widetilde{AB} = \frac{h}{\hat{\Gamma}_{AB}} g_A g_B \hat{\Gamma}_A \hat{\Gamma}_B \tilde{A}\tilde{B} \quad ,$$

which reduces with the aid of Eqs. (180c), (174a), (178a), and (178b) to the final form

$$\widetilde{AB} = h\hat{\Gamma}_{AB}\tilde{\tilde{A}}\tilde{\tilde{B}} \quad . \tag{186}$$

This simple form of the parameterization is valid whenever the reacting species are emitted from the same source or in other terms, when the reactants are premixed. That most of the air pollution modeling problems of interest fall within this class of problems is justification for our continuing the analysis of the parameterization scheme with Eq. (186) rather than the general expression Eq. (182). Thus, in the next section, we consider h briefly and then derive expression relating $\hat{\Gamma}_{AB}$ to measurable parameters.

E. DERIVATION OF $\hat{\Gamma}_{AB}$ IN TERMS OF MEASURABLE PARAMETERS AND APPLICATION OF THE PARAMETERIZATION SCHEME TO SPECIFIC PROBLEMS

Before considering $\hat{\Gamma}_{AB}$, we should point out that h is also a function of the given system and ranges from a value of zero for infinitely fast reactions to a value of unity for inert materials. Chapter III further analyzes this parameter. In the present analysis, we assume that h is a known constant.

By virtue of its definition, $\hat{\Gamma}_{AB}$ pertains to the inert species A_I and B_I and can accordingly be derived from linear theory. That is,

$$\hat{\Gamma}_{AB} = \frac{\widetilde{A_I B_I}}{\tilde{\tilde{A}}_I \tilde{\tilde{B}}_I}$$

where A_I is the solution of Eq. (145a) with k = 0; i. e.,

$$\frac{\partial A_I}{\partial t} + \mathcal{L}A_I = S_A \quad , \tag{187a}$$

and, similarly,

$$\frac{\partial B_I}{\partial t} + \mathcal{L}B_I = S_B \quad . \tag{187b}$$

We assume that A and B are released from the same sources. Hence,

$$S_A = \alpha S_B \quad , \tag{188}$$

where α is the ratio of the emission rates of A and B. If the initial concentration of A_I and B_I are both zero, then it follows from Eqs. (187) and (188) that

$$A_I = \alpha B_I$$

and hence that

$$\hat{\Gamma}_{AB} = \frac{\tilde{B}_I^2}{\tilde{B}_I^2} = \frac{\tilde{A}_I^2}{\tilde{A}_I^2} \quad . \tag{189}$$

The solution of Eq. (187a) is of the form

$$A_I(\underset{\sim}{r},t) = \int\int_0^t p(\underset{\sim}{r},t|\underset{\sim}{r}',t')\, S(\underset{\sim}{r}',t')\, dt'\, d\underset{\sim}{r}' \quad , \tag{190}$$

where p is the Green's function of Eq. (187a) and where, for brevity, we have dropped the subscript from the source function S_A. All aspects of the transport, diffusion, and interactions of the particles with boundaries are embodied in the kernel p. If the turbulence is homogeneous, then p has the property

$$p(\underset{\sim}{r},t|\underset{\sim}{r}',t') = p(\underset{\sim}{r}-\underset{\sim}{r}',t,t') \quad , \tag{191}$$

which leads to the following simplifications of the expressions for $\tilde{A}_I$ and $\tilde{A}_I^2$:

$$\tilde{A}_I(\underset{\sim}{r},t) = \frac{1}{V}\int_{v(\underset{\sim}{r})}\iiint_0^t p(\underset{\sim}{r}_1-\underset{\sim}{r}',t,t')\, S(\underset{\sim}{r}',t')\, dt'\, d\underset{\sim}{r}'\, d\underset{\sim}{r}_1 \quad , \tag{192}$$

$$= \iiint_0^t p(\underset{\sim}{r}-\underset{\sim}{r}',t,t')\, \tilde{S}(\underset{\sim}{r}',t')\, dt'\, d\underset{\sim}{r}' \quad , \tag{193}$$

$$\tilde{A}_I^2(\underset{\sim}{r},t) = \frac{1}{V}\int_{v(\underset{\sim}{r})}\iiiint\int_0^t\int_0^t p(\underset{\sim}{r}_1-\underset{\sim}{r}',t,t')\, p(\underset{\sim}{r}_1-\underset{\sim}{r}'',t,t'')\, S(\underset{\sim}{r}',t')\, S(\underset{\sim}{r}'',t'')\, dt'\, dt''\, d\underset{\sim}{r}'\, d\underset{\sim}{r}''\, d\underset{\sim}{r}_1, \tag{194}$$

$$\tilde{A}_I^2(\underset{\sim}{r},t) = \iiint_0^t\int_0^t p(\underset{\sim}{r}-\underset{\sim}{r}',t,t')\, p(\underset{\sim}{r}-\underset{\sim}{r}'',t,t'')\, G(\underset{\sim}{r}',\underset{\sim}{r}'',t',t'')\, dt'\, dt''\, d\underset{\sim}{r}'\, d\underset{\sim}{r}'' \quad , \tag{195}$$

where

$$G(\underset{\sim}{r}',\underset{\sim}{r}'',t',t'') = \frac{1}{V}\int_{-\frac{\Delta x}{2}}^{\frac{\Delta x}{2}}\int_{-\frac{\Delta y}{2}}^{\frac{\Delta y}{2}}\int_{-\frac{\Delta z}{2}}^{\frac{\Delta z}{2}} S(\underset{\sim}{r}'+\underset{\sim}{\zeta},t')\, S(\underset{\sim}{r}''+\underset{\sim}{\zeta},t'')\, d\underset{\sim}{\zeta} \tag{196}$$

and $V = \Delta x \Delta y \Delta z$ is the volume of the grid cell $v(\underset{\sim}{r})$ centered at $\underset{\sim}{r}$. The derivations of Eqs. (193) and (195) are presented in Appendix B. Since p is the known Green's function of Eq. (187), the parameter $\hat{r}_{AB}$ can be evaluated using Eqs. (193) and (195) once the source correlation function G has been prescribed. (Note that $\tilde{S}$ is the source function that enters into the grid model of $\tilde{A}$ and $\tilde{B}$.) We consider below the forms that G acquires in three problems of practical interest.

1. Random Distribution of Point Sources in a Three-Dimensional Space

Consider the situation in which "Point" sources of (small) volume v are distributed at random in space, and suppose that each source has a constant emission rate $\dot{m}$. Let the number density of sources $D(\underset{\sim}{r})$ be sufficiently large that on scales comparable to that of the grid cells used in a numerical calculation, the density D can be treated as a continuous function. The problem just posed might serve as a model of emissions arising from home heating units, or, through proper choices of D, from clusters of major point sources of pollution.

The source strength function that describes this array of sources is

$$S(\underset{\sim}{r},t) = \frac{\dot{m}}{v} U(\underset{\sim}{r}) \quad , \tag{197a}$$

where

$$U(\underset{\sim}{r}) = \begin{cases} 1 \quad , & \text{if } \underset{\sim}{r} \text{ lies within any source} \quad ; \\ 0 \quad , & \text{otherwise} \quad . \end{cases} \tag{197b}$$

Thus,

$$\tilde{S}(\underset{\sim}{r}) = \frac{1}{V} \int_{z-\Delta z}^{z+\Delta z} \int_{y-\Delta y}^{y+\Delta y} \int_{x-\Delta x}^{x+\Delta x} S(\underset{\sim}{r}')\, dx'\, dy'\, dz' \quad ,$$

$$= \dot{m} D(\underset{\sim}{r}) \quad , \tag{198}$$

where we have taken the averaging volume V to have the dimensions $2\Delta z \cdot 2\Delta x \cdot 2\Delta y$ Similarly, we have

$$G(\underset{\sim}{r}',\underset{\sim}{r}'') = \frac{1}{V} \int_{-\Delta z}^{\Delta z} \int_{-\Delta x}^{\Delta x} \int_{-\Delta y}^{\Delta y} \frac{\dot{m}^2}{v^2} U(\underset{\sim}{r}' + \underset{\sim}{\zeta})\, U(\underset{\sim}{r}'' + \underset{\sim}{\zeta})\, d\zeta_y\, d\zeta_x\, d\zeta_z \quad . \tag{199}$$

Let

$$W(\underset{\sim}{r},\Delta\underset{\sim}{r}) \equiv U(\underset{\sim}{r})\ U(\underset{\sim}{r} + \Delta\underset{\sim}{r}) \quad . \tag{200}$$

It can be seen from the definition of U [Eq. (197b)] that W is a random variable whose value is either 1 or 0 depending on whether both $\underset{\sim}{r}$ and $\underset{\sim}{r} + \Delta\underset{\sim}{r}$ lie within sources. If we let

$$\Delta\underset{\sim}{r} = \underset{\sim}{r}' - \underset{\sim}{r}'' \quad , \tag{201}$$

Eq. (199) then can be written in the form

$$G(\underset{\sim}{r}',\underset{\sim}{r}'') = \frac{\dot{m}^2}{v^2}\left[\frac{1}{V}\int_{x''-\Delta x}^{x''+\Delta x}\int_{y''-\Delta y}^{y''+\Delta y}\int_{z''-\Delta z}^{z''+\Delta z} W(\underset{\sim}{r},\Delta\underset{\sim}{r})\ d\underset{\sim}{r}\right] \quad , \tag{202a}$$

or

$$G(\underset{\sim}{r}',\underset{\sim}{r}'') = \frac{\dot{m}^2}{v^2}\,\tilde{W}(\underset{\sim}{r}'',\Delta\underset{\sim}{r}) \quad , \tag{202b}$$

where W(r",Δr) is the Volume average of W at the point r".

Provided that the source density D in the vicinity of r" is sufficiently large, we can exploit the random variable nature of W described earlier to write

$$\tilde{W}(\underset{\sim}{r}'', \Delta r) = (1)\ P(1;\underset{\sim}{r}'') + (0)\ P(0;\ \underset{\sim}{r}'') \quad ,$$

$$= P(1;\underset{\sim}{r}'') \quad , \tag{203}$$

where $P(n;\underset{\sim}{r}'')$ is the probability that $W(\underset{\sim}{r}'',\Delta r)$ has the value n, where n = 0, 1. If $\Delta\underset{\sim}{r} = (\Delta r_x, \Delta r_y, \Delta r_z)$ is larger than the dimensions of the elemental sources, i.e.,

$$\begin{aligned} \Delta r_x &> v_x \quad , \\ \Delta r_y &> v_y \quad , \\ \Delta r_z &> v_z \quad , \end{aligned} \tag{204}$$

where $v = v_x v_y v_z$, then $P(1;r")$ is just the product of the probabilities that the vectors $\underset{\sim}{r}"$ and $\underset{\sim}{r}" + \Delta\underset{\sim}{r}$ fall within sources. This is a result of the statistical independence of the source positions. Simple reasoning is sufficient to show that the probability that a point chosen at random will lie within a source is just the fraction of the total volume occupied by sources in the vicinity of that point. Thus, we conclude that

$$\tilde{W}(\underset{\sim}{r}", \Delta\underset{\sim}{r}) = v^2 D(\underset{\sim}{r}")\ D(\underset{\sim}{r}" + \Delta\underset{\sim}{r}) \quad , \quad |\Delta\underset{\sim}{r}| > \text{dimensions of } v \quad , \tag{205}$$

and hence that

$$G(\underset{\sim}{r}', \underset{\sim}{r}") \equiv \dot{m}^2 D(\underset{\sim}{r}')\ D(\underset{\sim}{r}") \quad , \quad \text{if } |\underset{\sim}{r}' - \underset{\sim}{r}"| > \text{dimensions of } v \quad . \tag{206}$$

When $|r' - r"|$ has a value smaller than the source size, the determination of $\tilde{W}$ is slightly more difficult because the probabilities that $\underset{\sim}{r}'$ and $\underset{\sim}{r}"$ each fall within sources are no longer independent. Instead, we have

$$P(1;\underset{\sim}{r}") = P_{UU'}(1,1;\underset{\sim}{r}") \quad , \tag{207}$$

where $P_{UU'}(n,m)$ is the joint probability that $U(r")$ has value n and that simultaneously $U(\underset{\sim}{r}" + \Delta\underset{\sim}{r})$ has value m. By definition,

$$P_{UU'}(1,1;\underset{\sim}{r}") = P_{UU'}(1|1)\ P_{U'}(1) \quad , \tag{208}$$

where $P_{UU'}(n|m)$ is the conditional probability that $U(\underset{\sim}{r}") = n$ given that $U(\underset{\sim}{r}" + \Delta r) = m$, and where $P_{U'}(1)$ is the probability that $U(\underset{\sim}{r}" + \Delta\underset{\sim}{r}) = 1$. From this definition and from Figure 33, we conclude after some reasoning that

$$P_{UU'}(1|1;\underset{\sim}{r}") = \frac{v' + (v^2 - vv')\ D(\underset{\sim}{r}")}{v} \tag{209a}$$

where

$$v' = (v_x - |\Delta r_x|)(v_y - |\Delta r_y|)(v_z - |\Delta r_z|) \quad . \tag{209b}$$

To see this, note first that it is given that one point, say, $\underset{\sim}{r}''$, lies in a source, for example, the source marked v_1 in Figure 33. Since the separation vector $\Delta\underset{\sim}{r}$ is also given, the second point $\underset{\sim}{r}'' + \Delta\underset{\sim}{r}$ must lie somewhere in the volume denoted v_2 in Figure 33. If this second point happens to lie in the shaded volume, i.e., v', then both $U(\underset{\sim}{r}'')$ and $U(\underset{\sim}{r}'' + \Delta\underset{\sim}{r})$ will have unit value; but if the point falls outside the shaded region, then $U(\underset{\sim}{r}'' + \Delta\underset{\sim}{r})$ will have zero value, unless the point happens to fall within a neighboring source. The two events, $\underset{\sim}{r}'' + \Delta\underset{\sim}{r}$ lies in v' and $\underset{\sim}{r}'' + \Delta\underset{\sim}{r}$ lies outside v', are mutually exclusive. Thus, Eq. (209) follows immediately.

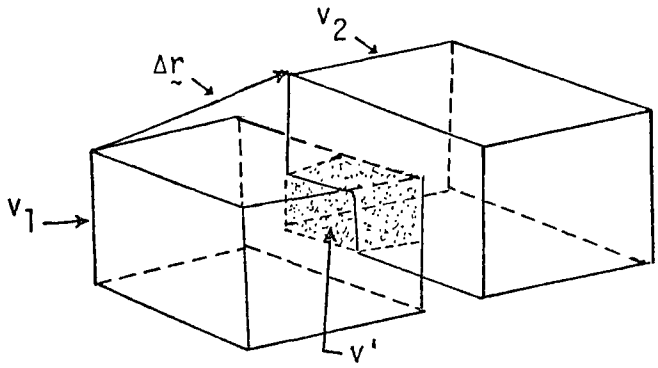

FIGURE 33. RANGES OF THE VECTORS $\underset{\sim}{r}''$ AND $\underset{\sim}{r}'' + \Delta\underset{\sim}{r}$ GIVEN $\Delta\underset{\sim}{r}$ AND GIVEN THAT $\underset{\sim}{r}''$ LIES IN v_1

We found earlier that

$$P_U'(1) = P_U(1;r'' + \Delta r) = vD(r'' + \Delta r) \quad ;$$

but since $|\Delta r| < v_x, v_y, v_z$ in the present analyses, we have

$$P_U'(1) = vD(\underset{\sim}{r}'') \quad . \tag{210}$$

Combining this result with Eqs. (209), (207), and (208), we obtain the information required to evaluate $\tilde{W}$, given by Eq. (203), and subsequently G:

$$G(r',r'') = \frac{\dot{m}^2}{v^2} D(r'')\left[v' - (v^2 - vv') D(r'')\right] \quad , \qquad |\Delta r| < \text{dimensions of } v \quad . \tag{211}$$

where v' is given by Eq. (209b). In summary,

$$G(\underset{\sim}{r}'\underset{\sim}{r}'') = \begin{cases} \dot{m}^2 D(\underset{\sim}{r}') D(\underset{\sim}{r}'') \quad , & \text{if any component of } \underset{\sim}{r}' - \underset{\sim}{r}'' \text{ is larger than the corresponding dimension of } v \quad ; \\ \dfrac{\dot{m}^2}{v^2} D(\underset{\sim}{r}'')\left[v' - (v^2 - vv') D(\underset{\sim}{r}'')\right] \quad , & \text{otherwise;} \end{cases} \tag{212}$$

$$\text{where } v' = (v_x - |\Delta r_x|)(v_y - |\Delta r_y|)(v_z - |\Delta r_z|) \quad ,$$

$$v = v_x v_y v_z \quad .$$

Upon substituting this expression into Eq. (195), we can solve for the mean square inert concentration distribution $\tilde{\tilde{A}}_I^2$ arising from the random array of point sources.

For simplicity, let us assume that

$$D(\underset{\sim}{r}) = D = \text{constant.} \tag{213}$$

If the diffusivities K_H and K_z are also uniform in space, then all spatially averaged quantities, such as $\tilde{A}_I$, $\tilde{\tilde{A}}_I^2$, and $\tilde{S}$, will be independent of spatial variables. Consequently, regardless of the speed of the mean wind, there can be no net advection of spatially averaged quantities, and we can therefore assume that $\tilde{u} = 0$ without any further loss of generality. In this case, we have

$$p(\underset{\sim}{r}-\underset{\sim}{r}',t,t') = \frac{1}{(2\pi)^{3/2}\sigma_H^2\sigma_z} \exp\left[-\frac{(x - x')^2 + (y - y')^2}{2\sigma_H^2} - \frac{(z - z')^2}{2\sigma_z^2}\right] \quad , \tag{214a}$$

$$\sigma_H^2 = 2K_H(t - t') \quad ,$$

$$\sigma_z^2 = 2K_Z(t - t') \quad . \tag{214b}$$

The problem thus posed is one of a uniform spatial density of continuous point sources acting in a homogeneous turbulence of arbitrary mean speed.

From Eq. (195), we now have

$$\tilde{A}_I^2(\underset{\sim}{r},t) = \dot{m}^2 \int_0^t \int \left\{ \int_\infty \int_{|\Delta\underset{\sim}{r}|>v^{1/3}} D^2 p(\underset{\sim}{r}-\underset{\sim}{r}'',t-t'')\, p(\underset{\sim}{r}-\underset{\sim}{r}''-\Delta\underset{\sim}{r},t-t')\, d\Delta\underset{\sim}{r}\, d\underset{\sim}{r}'' \right. \tag{215}$$

$$+ \int_\infty \int_{|\Delta\underset{\sim}{r}|\le v^{1/3}} \frac{D}{v^2}\left[v' - (v^2 - vv')D\right] p(\underset{\sim}{r}-\underset{\sim}{r}'',t-t'')$$

$$\left. \cdot\, p(\underset{\sim}{r}-\underset{\sim}{r}''-\Delta\underset{\sim}{r},t-t')\, d\Delta\underset{\sim}{r}\, d\underset{\sim}{r}'' \right\} dt'\, dt''$$

where we have assumed that

$$v_x = v_y = v_z = v^{1/3} \tag{216}$$

The Gaussian form [Eq. (214a)] of the kernels p permits a reduction of the first integral within the braces in Eq. (215) to

$$D^2\left[1 - \frac{v^{1/3}}{\sqrt{\pi}(\sigma_H'^2 + \sigma_H''^2)^{1/2}}\right]^2 \left[1 - \frac{v^{1/3}}{\sqrt{\pi}(\sigma_z'^2 + \sigma_z''^2)^{1/2}}\right] , \tag{217}$$

where

$$\sigma_H'^2 = 2K_H(t - t') \quad , \quad \sigma_H''^2 = 2K_H(t - t'') \quad ,$$

and so forth. The second integral within the braces in Eq. (215) reduces to

$$\frac{D(1 - 7vD)}{(2\pi)^{3/2}\,(\sigma_H'^2 + \sigma_H''^2)\,(\sigma_z'^2 + \sigma_z''^2)^{1/2}} \tag{218}$$

In deriving Eqs. (217) and (218), we had to assume that σ_H, σ_z, $>> v^{1/3}$. Furthermore, we assumed earlier that $vD << 1$. Consequently, Eq. (215) can be written in the form

$$\tilde{A}_I^2(\underset{\sim}{r},t) = \dot{m}^2 \int_0^t \int \left\{ D^2 + \frac{D}{(2\pi)^{3/2}\, 2K_H[(t-t') + (t-t'')]^{3/2}} \frac{}{(2K_z)^{1/2}} \right\} dt'\, dt''$$

$$= \dot{m}^2 D^2 t^2 + \frac{D\dot{m}^2 t^{1/2}}{(2\pi^3)^{1/2}\, K_H K_z^{1/2}} (\sqrt{2} - 1) \quad . \tag{219}$$

Similarly, we find that

$$\tilde{A}_I^2(\underset{\sim}{r},t) = \dot{m}^2 D^2 t^2 \quad . \tag{220}$$

Making use of this result and Eq. (219), we obtain from Eq. (189)

$$\hat{\Gamma}_{AB} = 1 + \frac{\sqrt{2} - 1}{Dt^{3/2}\, K_H K_z^{1/2}\, (2\pi^3)^{1/2}} \quad , \quad t >> \frac{v^{2/3}}{K_H^{2/3}\, K_z^{1/3}} \quad . \tag{221}$$

As indicated, Eq. (221) is not valid in the limit as $t \to 0$. This limiting value is easily obtained, however, when one notes that at small times the material is confined to a puff of volumes v equal to that of each source. Straightforward analyses then lead to the result

$$\lim_{t \to 0} \hat{\Gamma}_{AB} = \frac{1}{Dv} \quad . \tag{222}$$

The significance of these results to the behavior of $\tilde{A}$ and $\tilde{B}$ in the problem under study becomes clear once Eq. (221) is incorporated into our parameterization [Eq. (186)] and the result is used in Eq. (147). We obtain

$$\frac{\partial \tilde{A}}{\partial t} + L\tilde{A} = \dot{m}D - k'\tilde{A}\tilde{B} \quad , \tag{223}$$

where

$$k' = kh\left(1 + \frac{a}{DK_H K_z^{1/2}\, t^{3/2}}\right) \tag{224}$$

and

$$a = \frac{\sqrt{2} - 1}{(2\pi^3)^{1/2}} \quad .$$

The parameter k' is an effective rate "constant" whose departure from the nominal value k is a measure of the SSV effects on the chemistry of $\tilde{A}$ and $\tilde{B}$. In the case where $h \simeq 1$, we note that

$$\lim_{t\to\infty} k' = k, \tag{225a}$$

and that

$$k' \propto \frac{1}{DK_H K_z^{1/2}} \quad . \tag{225b}$$

The first of these indicates that SSV effects die out with time. From Eq. (222), we find that

$$\lim_{t\to 0} k' = \frac{k}{Dv} \quad . \tag{226}$$

In view of the second property, Eq. (225b), the importance of SSV effects diminishes as the source number density D, the turbulent diffusivity K, or both increase.

Let us examine the SSV effects quantitatively. Because of the constancy of S_A and S_B, $\tilde{A}$ is homogeneous in space. This fact results in

$$L\tilde{A} = 0 \quad .$$

Assume also that $S_A = S_B$ so that $\tilde{A} = \tilde{B}$. Equation (223) then reduces to

$$\frac{d\tilde{A}}{dt} = \dot{m}D - k'\tilde{A}^2 \quad , \tag{227}$$

the solution of which is

$$\tilde{A}(t) = \sqrt{\frac{\dot{m}D}{k'}}\ \frac{e^{2\gamma t} - 1}{e^{2\gamma t} + 1} \quad , \tag{228}$$

where

$$\gamma = \sqrt{\dot{m}Dk'} \quad .$$

It can be seen from Eqs. (228) and (225a) that the steady-state value of $\tilde{A}$ is independent of the SSV:

$$\tilde{A}_\infty = \lim_{t\to\infty} \tilde{A}(t) = \sqrt{\frac{\dot{m}D}{k}} \quad . \tag{229}$$

Using $\tilde{A}_\infty$, we can define a reaction time scale T_R:

$$T_R = (k\tilde{A}_\infty)^{-1} = (\dot{m}kD)^{-1/2} \quad . \tag{230}$$

This time scale is a rough measure of the time required for the chemical reaction A+B→D to achieve a rate equal to that of the source emission rate. Substituting T_R into Eq. (224), we find that by the time the chemical decay rate and the emission rate are in balance, the effective rate constant k' has a value

$$k' = k\left[1 + \frac{a(\dot{m}k)^{3/4}}{D^{1/4}K_H K_z^{1/2}}\right] \quad . \tag{231}$$

Since k' has a maximum at t = 0 and decreases thereafter, it follows from Eq. (231) that if

$$\mu \equiv \frac{(\dot{m}k)^{3/4}}{D^{1/4}K_H K_z^{1/2}} \gg 1 \quad , \tag{232}$$

then SSV effects will play a significant role in the behavior of $\tilde{A}$ and $\tilde{B}$ as they approach their steady-state values. This fact is illustrated graphically in Figure 34, where we have plotted the ratio

$$\rho(t) \equiv \frac{\tilde{A}_{SSV}}{\tilde{A}} \tag{233}$$

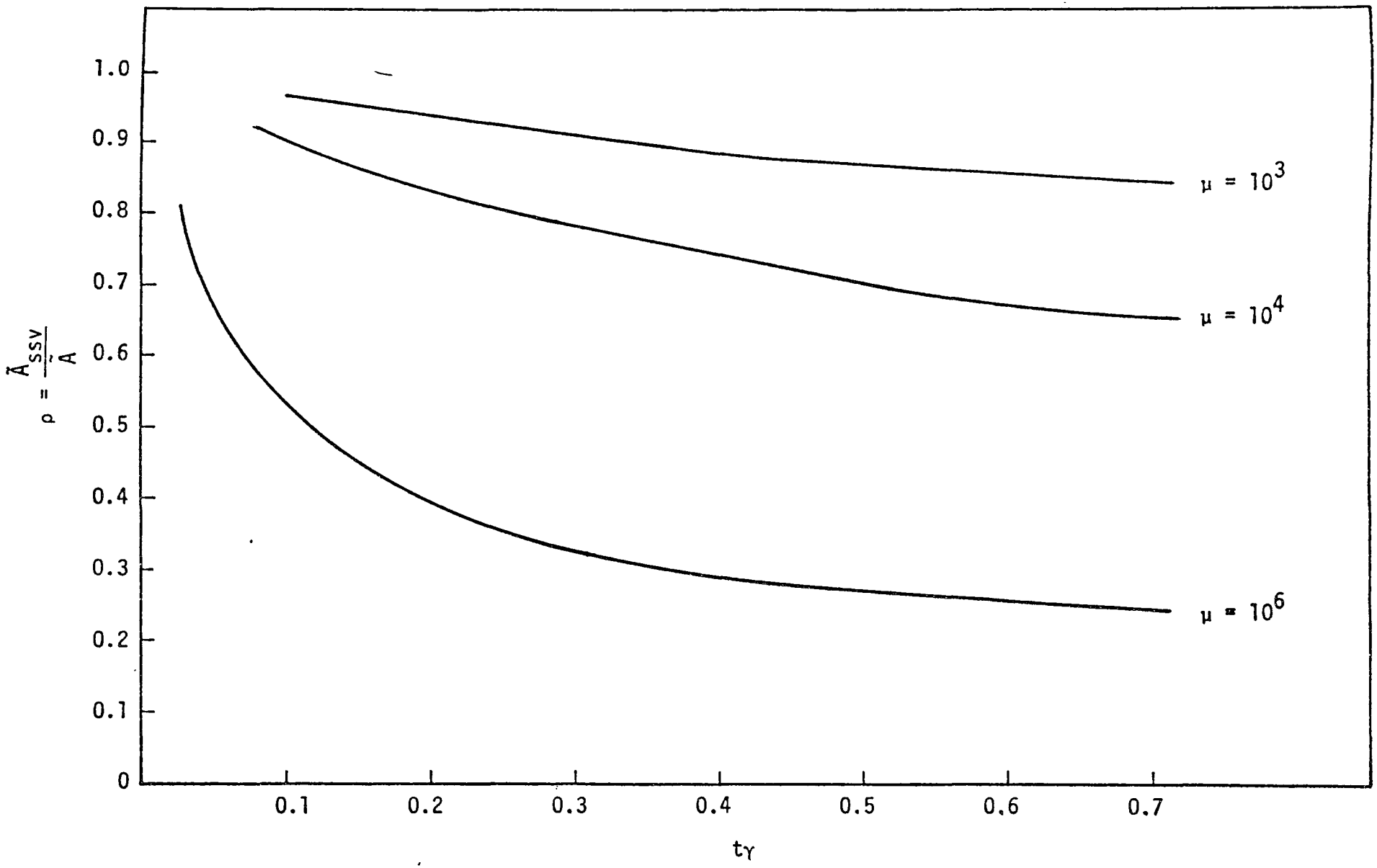

FIGURE 34. INFLUENCE OF SUBGRID-SCALE CONCENTRATION VARIATIONS ON THE CHEMICAL RATE OF CHANGE OF $\tilde{A}$

for several values of the dimensionless group μ. Here, $\tilde{A}_{SSV}$ denotes the mean value of A, which accounts explicitly for the SSV using k', and $\tilde{A}$ denotes the corresponding value obtained using k. According to Figure 34, μ must have a value comparable to or larger than about 10^3 before significant SSV effects are manifest in $\tilde{A}$.

It is of interest now to apply our criterion, Eq. (232), to an assessment of the SSV effects in actual problems encountered in pollution simulation studies. One such problem is the simulation of large urban areas containing strong point sources, such as power plants and refineries. The question here is whether such sources produce a significant SSV impact on the predictions of an airshed model.

To approximate the conditions of a problem of this type, we let D approach the value of one source per grid cell. In a typical case where the grid cell dimensions are $10^3 \times 10^3 \times 50$ m, we have

$$D = 2 \times 10^{-8}\ m^{-3} \quad .$$

We assume that the source emission rate in this case is 100 gm/sec. This is a rough value for the NO emission rate of power plants. We also consider here three conditions of atmospheric stability. These and the corresponding values assumed for K_H and K_z are as follows (in m^2/sec):

Condition	K_H	K_z
Stable	5	10^{-1}
Neutral	50	1
Unstable	50	25

Substituting the above values in Eq. (232), we obtain the curves of μ as a function of k shown in Figure 35.

Note that $\mu = 10^3$ is the smallest value of μ shown in the figure. Consequently, all combinations of rate constant and stability classification shown in this figure represent cases where significant SSV effects occur, at least in

problems of the type considered here. For reference, we have indicated the values of the rate constants for some of the important photochemical pollution reactions. We should add, however, that for some of these reactions, the value of μ cannot be read directly from the figure because we assumed that the concentration of the two reactants are approximately equal. In cases where the reactant concentrations are in the ratio α ($\alpha<1$), the value of μ read from Figure 35 should be multiplied by the factor $\alpha^{3/4}$.

According to Figure 35, the ozone-olefin reaction is too slow to be affected significantly by subgrid-scale concentration fluctuations. The same is probably true of the reactions involving atomic oxygen, in view of the extremely low concentrations of this species in urban air. Only the ozone-nitric oxide reaction appears likely to be affected by SSV, especially in cases where an elevated stack emits pollutants into a neutral or stable layer aloft. An investigation of the impact of SSV on the other important photochemical reactions is required before a thorough treatment of this phenomenon can be incorporated into air pollution models.

We should also note that for point sources of the space heating type whose emission rate $\dot{m}$ is much smaller and whose number density D is much larger than the values assumed in Figure 35, the resulting value of μ is very small, and SSV effects are insignificant for nearly all pollution reactions.

2. Nonrandom Distribution of Sources in Three Dimensions

Having considered the SSV effects produced by a homogeneous distribution of point sources, we look now at the effects produced by networks of streets. It is advantageous to reduce this problem to a system of small volume sources such as that of the random distribution just treated. With a constant width w for all streets and an effective source depth of h, the "point" source volume v becomes

$$v = w^2 h \quad . \tag{234}$$

The effective source population density D is defined, as before,

$$D = \frac{N}{\Delta x \Delta y \Delta z} \quad ,$$

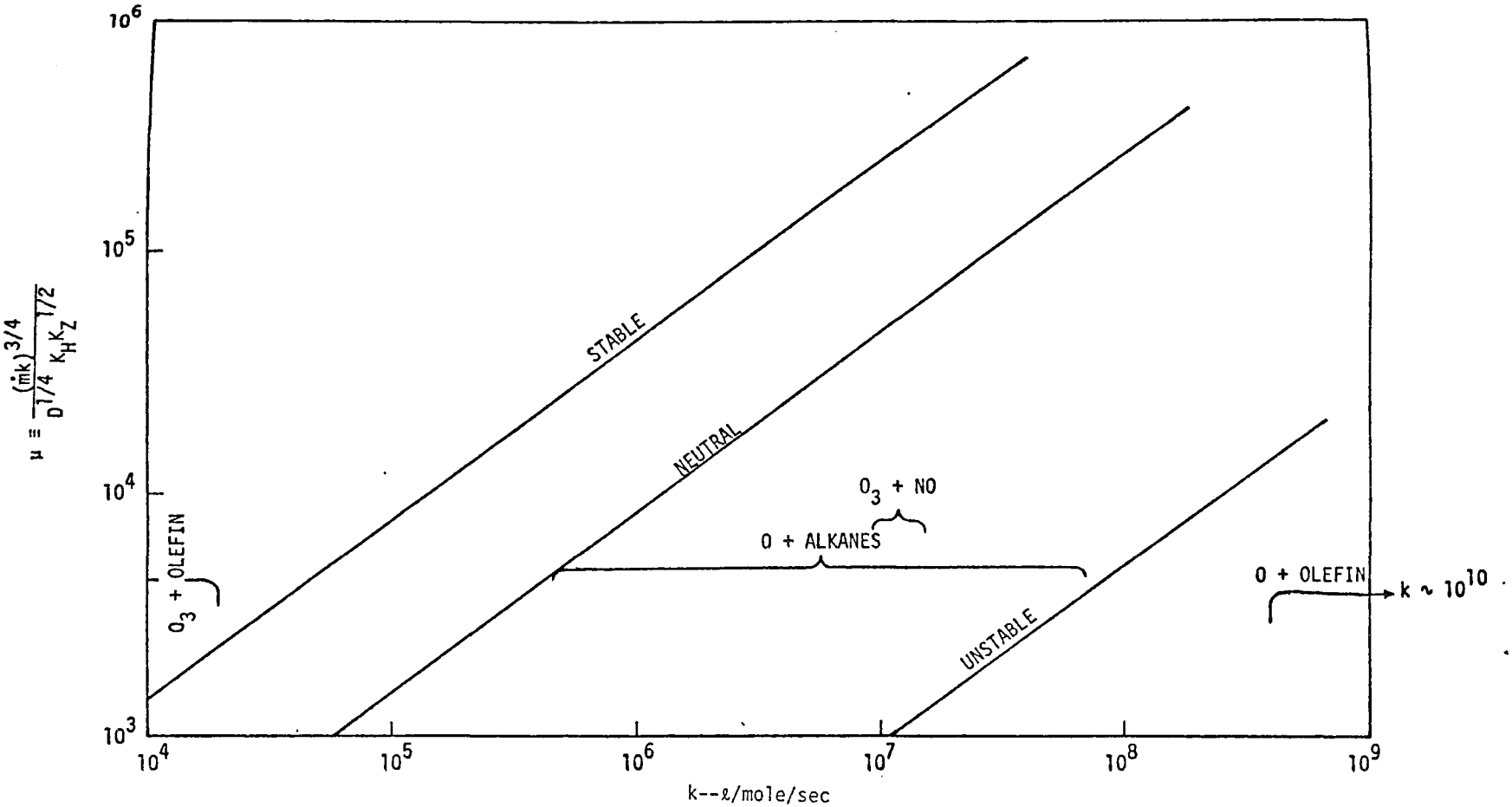

Note: $D = 2 \times 10^{-8}$ m^{-3} ,

$m = 10^2$ gm/sec ,

K_H and K_Z for source height of 10^2 m.

FIGURE 35. VARIATION OF THE DIMENSIONLESS PARAMETER μ AS A FUNCTION OF RATE CONSTANT k FOR VARIOUS ATMOSPHERIC STABILITIES

where N is the number of "point" sources in the averaging volume. Let λ_x and λ_y denote the separation distances between streets, and assume that

$$\Delta x >> \lambda_x >> w \quad ,$$

$$\Delta y >> \lambda_y >> w \quad .$$

Then we have

$$N = \left(\frac{\Delta x}{\lambda_x}\right)\left(\frac{\Delta y}{w}\right) + \left(\frac{\Delta y}{\lambda_y}\right)\left(\frac{\Delta x}{w}\right) \quad ,$$

$$= \left(\frac{\Delta x \Delta y}{w}\right)\left(\frac{\lambda_x + \lambda_y}{\lambda_x \lambda_y}\right) \quad .$$

Therefore,

$$D = \frac{\lambda_x + \lambda_y}{w \Delta z \lambda_x \lambda_y} \quad . \tag{235}$$

The source strength function S that describes the network of streets is

$$S(\underset{\sim}{r},t) = \frac{\dot{m}}{v} U(\underset{\sim}{r}) \quad , \tag{236}$$

where $\dot{m}$ is the mass emission rate of each "point" source that constitutes the network, v is the point source volume given by Eq. (234), and

$$U(\underset{\sim}{r}) = \begin{cases} 1, & \text{if r falls on a street,} \\ 0, & \text{otherwise.} \end{cases} \tag{237}$$

The source correlation function G [see Eq. (196)] is therefore given by

$$G(\underset{\sim}{r}',\underset{\sim}{r}'') = \frac{\dot{m}^2}{v^2 V} \int_{-\Delta z/2}^{\Delta z/2} \int_{-\Delta y/2}^{\Delta y/2} \int_{-\Delta x/2}^{\Delta x/2} U(\underset{\sim}{r}' + \underset{\sim}{\zeta})\, U(\underset{\sim}{r}'' + \underset{\sim}{\zeta})\, d\zeta_x\, d\zeta_y\, d\zeta_z \quad , \tag{238}$$

where $V = \Delta x \Delta y \Delta z$. Making the change of variables

$$\underset{\sim}{r}'' = \underset{\sim}{r}' + \Delta \underset{\sim}{r}$$

and using the fact that $G(\underset{\sim}{r}', \underset{\sim}{r}'+\Delta \underset{\sim}{r})$ is independent of $\underset{\sim}{r}'$ for all $\underset{\sim}{r}'$ lying in the slab $0 \leq z < h$ and is zero for all $\underset{\sim}{r}'$ outside this slab, we obtain

$$G(\underset{\sim}{r}', \underset{\sim}{r}'+\Delta \underset{\sim}{r}) = \frac{\dot{m}^2}{v^2 V} \int_V U(\underset{\sim}{r}')\, U(\underset{\sim}{r}' + \Delta \underset{\sim}{r})\, d\underset{\sim}{r}' \quad . \tag{239}$$

With the aid of Figure 36, we can be seen that

$$\int_V U(\underset{\sim}{r}')\, U(\underset{\sim}{r}' + \Delta \underset{\sim}{r})\, dr' = \begin{cases} 0 \text{ , if } |\Delta r_x| \neq n\lambda_x \quad , \quad n = 0, 1, 2, \ldots \\ \quad \text{and } |\Delta r_y| \neq m\lambda_y \quad , \quad m = 0, 1, 2, \ldots \quad ; \\ \dfrac{wh\Delta x\Delta y}{\lambda_x} \text{ if } |\Delta r_x| = n\lambda_x \quad , \\ \quad \text{and } |\Delta r_y| \neq m\lambda_y \quad ; \\ \dfrac{wh\Delta x\Delta y}{\lambda_y} \text{ if } |\Delta r_x| \neq n\lambda_x \quad , \\ \quad \text{and } |\Delta r_y| = m\lambda_y \quad ; \\ w^2 hDV \text{ if } |\Delta r_x| = n\lambda_x \quad , \\ \quad \text{and } |\Delta r_y| = m\lambda_y \quad . \end{cases} \tag{240}$$

Therefore,

$$G(\underset{\sim}{r}', \underset{\sim}{r}'+\Delta \underset{\sim}{r}) = G(\Delta \underset{\sim}{r}) = \frac{\dot{m}^2}{w^2 h} \left[\frac{\phi(\Delta r_x)}{w\lambda_x \Delta z} + \frac{\phi(\Delta r_y)}{w\lambda_y \Delta z} + D\phi(\Delta r_x)\, \phi(\Delta r_y) \right]$$

$$\text{if } \quad 0 \leq z' < h \quad , \quad \text{and } z' + \Delta z < h \quad ; \tag{241}$$

$$G(\Delta \underset{\sim}{r}) = 0 \quad \text{for all } z' \geq h \quad .$$

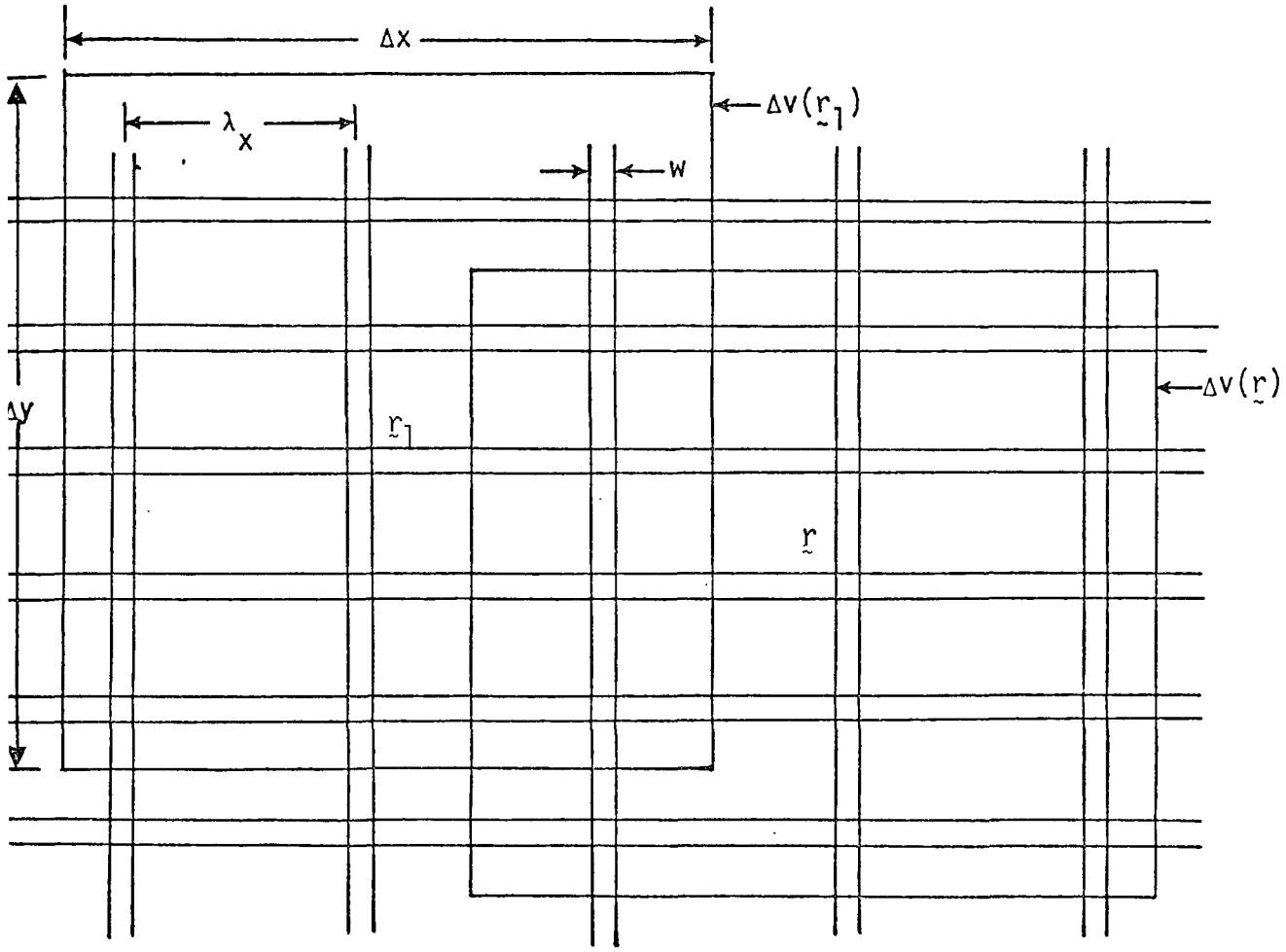

FIGURE 36. UNIFORM NETWORK OF STREETS ILLUSTRATING THE CALCULATION OF THE SOURCE CORRELATION FUNCTION G

In this expression,

$$\phi(\Delta r_x) = \begin{cases} 0 & , \text{ if } |\Delta r_x| \neq n\lambda_x \quad ; \\ 1 & , \text{ if } |\Delta r_x| = n\lambda_x \text{ and } |\Delta r_y| \neq m\lambda_y \quad ; \end{cases} \tag{242}$$

Similar values apply for $\phi(\Delta r_y)$. Substituting these results into Eq. (195), we obtain

$$t) = \int_0^t \int_0^t \iiint p(\underset{\sim}{r}-\underset{\sim}{r}',t,t')\, p(\underset{\sim}{r}-\underset{\sim}{r}'-\Delta\underset{\sim}{r},t,t'')\, G(\Delta\underset{\sim}{r},t't'')\, d\Delta\underset{\sim}{r}\, d\underset{\sim}{r}'\, dt'\, dt''$$

$$= \int_0^t \int_0^t \iiint p(\underset{\sim}{\xi},t,t')\, p(\underset{\sim}{\xi}+\Delta\underset{\sim}{r},t,t'')\, G(\Delta\underset{\sim}{r})\, d\Delta\underset{\sim}{r}\, d\underset{\sim}{\xi}\, dt'\, dt'' \tag{243}$$

$$= \int_0^t \int_0^t \left\{ \frac{wA_x\sqrt{2\pi}\sigma_H\dot{\sigma}_H}{(\sigma_H^2 + \sigma_H'^2)^{1/2}} \sum_{n=-\infty}^{\infty} \exp\left[-\frac{(n\lambda_x)^2}{2(\sigma_H^2 + \sigma_H'^2)} \right] \iint_{-\infty}^{\infty}{}' \exp\left[-\frac{\xi_y^2}{2\sigma_H^2} - \frac{(\xi_y + \Delta r_y)^2}{2\sigma_H'^2} \right] d\Delta ry\, d\xi_y \right.$$

$$\left. + \text{term in } \phi(\Delta r_y) + \text{term in } \phi(\Delta r_x)\phi(\Delta r_y) \right\} dt'\, dt'' \quad ,$$

where

$$A_x = \frac{\dot{m}^2 h}{w^3 \lambda_x \Delta z \sigma_H'^2 \sigma_H^2 \sigma_z' \sigma_z (2\pi)^3} \tag{244}$$

and

$$\sigma_H' = \sigma_H(t'') \quad ,$$

$$\sigma_H = \sigma_H(t') \quad ,$$

and so forth. Evaluating the expanded term in Eq. (243), we obtain

$$\text{term in } \phi(\Delta r_x) = \frac{wA_x(2\pi)\sigma_H^2\sigma_H'^2}{(\sigma_H^2 + \sigma_H'^2)^{1/2}} \left\{ \sum_{n=-\infty}^{\infty} \exp\left[- \frac{(n\lambda_x)^2}{2(\sigma_H^2 + \sigma_H'^2)} \right] \right\}$$

$$\cdot \left\{ \sqrt{2\pi} - \frac{w}{(\sigma_H^2 + \sigma_H'^2)^{1/2}} \sum_{m=-\infty}^{\infty} \exp\left[- \frac{(m\lambda_y)^2}{2(\sigma_H^2 + \sigma_H'^2} \right] \right\} \quad . \quad (245)$$

The term in $\phi(\Delta r_y)$ in Eq. (243) is symmetrical to that in $\phi(\Delta r_x)$ and has the form

$$\text{term in } \phi(\Delta r_y) = \frac{wA_y(2\pi)\sigma_H^2\sigma_H'^2}{(\sigma_H^2 + \sigma_H'^2)^{1/2}} \left\{ \sum_{m=-\infty}^{\infty} \exp\left[- \frac{(m\lambda_y)^2}{2(\sigma_H^2 + \sigma_H'^2)} \right] \right\}$$

$$\cdot \left\{ \sqrt{2\pi} - \frac{w}{(\sigma_H^2 + \sigma_H'^2)^{1/2}} \sum_{n=-\infty}^{\infty} \exp\left[- \frac{(n\lambda_x)^2}{2(\sigma_H^2 + \sigma_H'^2)} \right] \right\} \quad , \quad (246)$$

where

$$A_y = A_x \frac{\lambda_x}{\lambda_y} \quad . \quad (247)$$

On evaluating the product term in Eq. (243) and combining the result with Eqs. (245) and (246), we obtain finally

$$\tilde{A}_I^2(t) = \int_0^t \int_0^t \frac{\dot{m}^2 h}{w^2 \Delta z \sigma_z' \sigma_z (2\pi)^{3/2} (\sigma_H^2 + \sigma_H'^2)^{1/2}} \left\{ \left[\frac{1}{\lambda_x} \sum_{n=-\infty}^{\infty} \exp \frac{-(n\lambda_x)^2}{2(\sigma_H^2 + \sigma_H'^2)} \right] \right.$$

$$\left. + \left[\frac{1}{\lambda_y} \sum_{m=-\infty}^{\infty} \exp\left(\frac{-(m\lambda_y)^2}{2(\sigma_H^2 + \sigma_H'^2)} \right) \right] \right\} dt' \, dt'' \quad . \quad (248)$$

Determining the mean value $\tilde{A}_I$ is not quite as complex. We find through straightforward reasoning based on the homogeneity of $\tilde{A}_I$ that

$$\tilde{A}_I(t) = \frac{\text{Total Mass in } V}{V} \quad ,$$

$$= \frac{1}{V}\left[\frac{\dot{m}DVt}{\Delta x \Delta y \sigma_z}\, V\right] \quad ,$$

$$\tilde{A}_I(t) = \frac{\dot{m}t}{w\sigma_z}\,\frac{\lambda_x + \lambda_y}{\lambda_x \lambda_y} \quad . \tag{249}$$

Using this expression and Eq. (248), we can determine the variable $\hat{r}_{AB}$ [defined in the present instance by Eq. (189) that is required in the subgrid-scale parameterization scheme [Eq. (186)]. Unfortunately, Eq. (248) involves non-elementary integrals that can be evaluated only by numerical integration techniques. Such methods will therefore be necessary to implement the present scheme in an airshed model. For the present, however, it is useful to obtain an order-of-magnitude estimate of the effect of the subgrid-scale concentration variations on the chemistry.

According to our scheme, the measure of the importance of the subgrid-scale chemistry effect is the degree to which the parameter

$$\hat{r}_{AB} = \frac{\tilde{A}_I^2}{\tilde{A}_I^2}$$

differs from unity during the period when the generation of material by sources and the chemical decay are unbalanced. Through simple, straightforward analysis, we find that initially

$$\hat{r}_{AB} \sim \left(\frac{\Delta z}{h}\right)\left(\frac{\lambda}{w}\right) \quad , \tag{250}$$

assuming that $\lambda_x \sim \lambda_y \sim \lambda$. Note that $\hat{\Gamma}_{AB}$ is independent of the emission rate. Thus, assuming an effective emission depth h = 2 m, a street width w = 10 m, and an average street separation λ = 150 m, we find that in a diffusion model that employs a grid spacing Δz = 20 m in its lowest level,

$$\hat{\Gamma}_{AB} \sim 150 \quad .$$

We know from the work presented in the previous sections that $\hat{\Gamma}_{AB}$ decays because of turbulent diffusion and ultimately attains a constant value of unity. The time scale of this decay is given roughly by

$$T_\Gamma \sim \max \left\{ \frac{\Delta z^2}{K_z} \quad , \quad \frac{\lambda^2}{K_H} \right\} \quad , \tag{251}$$

where it is assumed that both σ_z and σ_H are proportional to $t^{1/2}$. Since $\hat{\Gamma}_{AB}$ is initially much larger than unity, significant subgrid-scale chemistry effects will arise if T_Γ turns out to be comparable to or larger than the time scale T_E, for example, required for the chemical decay and source emissions rates to reach an equilibrium. The time scale T_E is equivalent to the time required for

$$k\tilde{A}^2 \sim S \quad ,$$

where S denotes the source emission rate. In the present problem,

$$S = \dot{m}D = \frac{2\dot{m}}{w\lambda\Delta z} \quad ,$$

and

$$\tilde{A}^2 = \frac{4\dot{m}^2 t^2}{w^2\lambda^2\Delta z^2} \quad .$$

Thus,

$$T_E \sim \left(\frac{w\lambda\Delta z}{2\dot{m}k} \right)^{1/2} \quad . \tag{252}$$

In the present problem, we find that

$$T_\Gamma \sim \frac{\lambda^2}{K_H} \sim 400 \text{ sec} \tag{253}$$

(using $K_H \sim 60 m^2/sec$), and

$$T_E \sim \left(\frac{3 \times 10^4 \ m^3}{2\dot{m}k} \right)^{1/2} . \tag{254}$$

Subgrid-scale effects will be most pronounced for fast reactions in which T_E is small. For the case of the NO-O_3 reaction, we have $k \sim 10^7 \ell$/mole/sec. Thus, if vehicles emit about 1 gm of NO per kilometer, on a street network in which 10^4 vehicles pass each point per day,

$$T_E \sim 200 \text{ sec} . \tag{255}$$

From this estimate and from Eq. (253), we conclude that in areas with street network densities less than or comparable to that treated here (i.e., streets 150 m apart), and with traffic densities greater than or equal to 10^4 vehicles per day, subgrid-scale concentration variations will have a nonnegligible effect on the simulation of ozone and nitrogen oxide concentrations. To account for these effects, we must incorporate a scheme such as that developed here into the simulation model.

3. Isolated Point and Line Sources

The analyses presented in the last two subsections deal with homogeneous source distributions. The results of those analyses are therefore applicable only in portions of an urban region where sources are fairly uniformly distributed upwind of a given site. In this section, we briefly consider the magnitude of subgrid-scale effects arising from isolated point and line sources, such as power plants and major highways.

For the purposes of this study, we assume that, in a point source plume, the mean concentration is described with adequate accuracy by

$$c(x,y,z) = \frac{Q}{\bar{u}\sigma_z\sigma_y} \exp\left(-\frac{z^2}{2\sigma_z^2}\right) \exp\left(-\frac{y^2}{2\sigma_y^2}\right) \quad , \tag{256}$$

where Q is the emission rate,

$$\sigma_z^2 = K_z \frac{x}{\bar{u}} \quad ,$$

$$\sigma_y^2 = K_y \frac{x}{\bar{u}} \quad ,$$

and where the x-axis lies on the plume centerline with the mean wind parallel to the x-axis. Assuming that the grid volume $V = \Delta x \Delta y \Delta z$ has dimensions much larger than the y and z dimensions of the plume, we find after integrating Eq. (256) that

$$\hat{\Gamma}_{AB} = \frac{\bar{u}\Delta y \Delta z \ell n(\frac{\Delta x}{d})}{\Delta x K_y^{1/2} K_z^{1/2}} \quad , \tag{257}$$

where d is the effective source diameter. This value of $\hat{\Gamma}_{AB}$ pertains to the grid cell that contains the source. At a point $n\Delta x$ downstream from the source, $\hat{\Gamma}_{AB}$ can be found by replacing $\ell n(\Delta x/d)$ by $\ell n[n\Delta x/(n + 1)\Delta x]$. At each point in space, the value of $\hat{\Gamma}_{AB}$ is constant, because of the constancy of the source and meteorology, but the value that emitted material "sees" as it moves downstream decays with time.

In the context of the present problem, the effect of subgrid-scale concentration variations on reaction rate is accounted for in our parameterization scheme by replacing the true rate constant k by an effective value k' given by

$$k' = \hat{\Gamma}_{AB} k \quad . \tag{258}$$

The resulting perturbation in the space averaged concentration due to the subgrid-scale variations is therefore

$$\frac{dc}{c} = \frac{\hat{\Gamma}_{AB} - 1}{1 + (k\tilde{c}_I t)^{-1}} \quad , \tag{259}$$

where $t = \Delta x/\bar{u}$ is the residence time of material in each grid cell. With

$$\tilde{c}_I = \frac{\Delta x Q}{\bar{u} V} \quad ,$$

Eq. (259) reduces to (assuming that $k\tilde{c}_I t \geq 1$)

$$\frac{dc}{c} \sim \hat{\Gamma}_{AB} \sim \frac{\bar{u}\Delta y \Delta z}{\Delta x \sqrt{K_z K_y}} \quad . \tag{260}$$

Typically, $\Delta x = \Delta y$, $\Delta z \sim 20$ m, and $K_z K_y \sim 100$ m^4/sec^2. Recalling that our analysis assumes that the plume dimensions σ_z and σ_y are much smaller than Δz and Δy, respectively, we conclude that for sufficiently large $\bar{u}$,

$$\frac{dc}{c} \sim 2\bar{u} \quad . \tag{261}$$

This result indicates that the perturbation due to the subgrid scale is very large for reactions in which $(k\tilde{c}_I \Delta x/\bar{u}) \geq 1$. The NO-$O_3$ reaction in power plant plumes is one example of a situation that satisfies this criterion. When $k\tilde{c}_I(\Delta x/\bar{u})$ becomes much smaller than unity, the subgrid-scale effect diminishes. These results agree with the analyses of randomly distributed point sources presented in Section IV-E-1.

Turning finally to the subgrid-scale effects produced by isolated line sources, we assumed a line source plume concentration distribution of the form

$$c(x,y,z) = \frac{Q_L}{\bar{u}\sigma_z} \exp -\left(\frac{z^2}{2\sigma_z^2}\right) \tag{262}$$

where Q_L is the emission rate per unit length of source and

$$\sigma_z^2 = K_z \frac{x}{\bar{u}} \quad .$$

Integrating Eq. (262) and assuming that $\Delta z >> \sigma_2$, we obtain

$$\hat{\Gamma}_{AB} = \frac{\bar{u}^{1/2}\Delta z}{\Delta x^{1/2} K_z^{1/2}} \quad . \tag{263}$$

As in the case of the point source, the subgrid-scale-induced perturbation in the concentration will be on the order of

$$\frac{dc}{c} \sim \hat{\Gamma}_{AB} = \frac{\bar{u}^{1/2}\Delta z}{\Delta x^{1/2} K_z^{1/2}} \tag{264}$$

when

$$k\tilde{c}_I \frac{\Delta x}{\bar{u}} \geq 1 \quad . \tag{265}$$

Since the line source produces a mean concentration level $\tilde{c}_I$ of

$$\tilde{c}_I = \frac{Q_L}{\bar{u}\Delta z} \quad , \tag{266}$$

Eq. (265) is satisfied if

$$kQ_L \geq \frac{\bar{u}^2 \Delta z}{\Delta x} \quad . \tag{267}$$

For the NO-O_3 reaction with $k = 10^7$ ℓ/mole/sec, Eq. (267) reduces to

$$Q_L \geq 10^{-3} \text{ gm/sec/m} \tag{268}$$

when $\bar{u}$ = 3 m/sec, Δz = 20 m, and $\Delta x = 10^3$ m. If NO emissions are on the order of 1 gm/km, Eq. (268) is satisfied only by roadways carrying 10^5 or more vehicles per day. Few highways rank in this category. Even for those that do, $\hat{\Gamma}_{AB}$ is only on the order of unity; consequently, little if any subgrid-scale chemistry effect occurs.

We conclude that in contrast to the point sources, line sources of commonly encountered strengths produce negligible subgrid-scale chemistry effects, at least insofar as the NO-O_3 reaction is concerned. All other reactions that are explicitly treated in air pollution simulations are slower than this one and accordingly are less affected by subgrid-scale concentration variations.

V DEVELOPMENT OF A SUBMODEL FOR RESTORING POINT SPATIAL RESOLUTION TO GRID MODELS OF URBAN POLLUTION

A. INTRODUCTION

In Chapter I, we have discussed and explained the inability of grid models (i.e., those in which space and time are discretized) to resolve features in the concentration field smaller than the discretization interval. Generally speaking, urban diffusion models of the grid type employ grid networks with a horizontal mesh size of several kilometers and a vertical mesh several tens of meters in length. Since most major sources of air pollution, such as power plants, refineries, and highways, have scales much smaller than these, there is a great deal of fine structure in the concentration distribution that grid models cannot resolve. Indeed, the locations and intensities of concentration maxima, the extent and location of the zone of oxidant depression near roadways, and the pollutant exposures in street canyons are examples of important pollution phenomena about which urban-scale grid models can provide no information. Moreover, validation studies of grid models use monitoring station data that represent time averages at a fixed point rather than averages over the large volumes represented by each grid cell. Consequently, without an estimate of the amplitude of small-scale concentration variations in the vicinity of each monitoring station, the validation process can be hindered, because it would be difficult to ascertain whether discrepancies between the computed and observed concentrations were due to small-scale spatial variations or to errors in the model.

These weaknesses have been cited by some in arguments favoring the development of alternative pollution modeling approaches. Spectral methods are among the alternatives most often proposed. In this chapter, we develop

a "microscale model" (not based on spectral methods) that can be used in conjunction with an urban-scale grid model to achieve point spatial resolution of the concentration distribution at any specified point. In developing this microscale model, one fundamental constraint was imposed: The microscale model must operate totally independently of the urban-scale model. That is, we sought the capability of examining the near-source small-scale concentration distribution at any point without having to make multiple runs of the large-scale model. We also wanted the microscale model not to be structured around or coupled to the urban-scale model. If all of these conditions are met, the microscale model can be used with any grid model, and the required calculations can be performed with a minimum of time and effort.

Before proceeding with the mathematical development of the microscale model, we review, for orientation purposes, some of the basic concepts introduced in Chapter I.

Most air pollution models in current use are based on the premise that the processes governing the concentrations of each pollutant can be described by an equation of the form

$$\frac{\partial c}{\partial t} + \bar{u}_i \frac{\partial c}{\partial x_i} = \frac{\partial}{\partial x_i} K_{ij} \frac{\partial c}{\partial x_j} + S + R \quad , \tag{269}$$

where

$\bar{u}_i$ = the i-th coordinate component of the mean wind,

K_{ij} = the turbulent diffusivity tensor,

S = the strength of all systematic sources of the pollutant,

R = the time rate of change of the concentration due to chemical interactions among all of the pollutants present.

In adopting Eq. (269), one tacitly assumes that if all of the parameters in this equation were known precisely, then the solution $c(\underset{\sim}{r},t)$ of the resulting equation (and initial and boundary conditions) would correspond exactly to an error-free measurement of the concentration at the point $(\underset{\sim}{r},t)$.

{Actually, c in Eq. (269) represents a mean value, which we can think of as a time average over an interval of several minutes, say, depending on the nature of the diffusivities used [see Lamb (1971)].}

If Eq. (269) is to be solved by numerical methods executed on a digital computer, this equation must first be "filtered" to remove all small-scale variations that the grid network cannot resolve. One way to achieve such filtering is to space average the equation at each point over a volume V equal to that of the grid mesh. Thus, if the grid network has mesh dimensions of Δx by Δy by Δz, then it can be shown that any space averaged variable defined by

$$\tilde{\zeta}(\underset{\sim}{r},t) \equiv \frac{1}{8\Delta x\Delta y\Delta z} \int_{x-\Delta x}^{x+\Delta x}\int_{y-\Delta y}^{y+\Delta y}\int_{z-\Delta z}^{z+\Delta z} \zeta(\underset{\sim}{r}',t)\, d\underset{\sim}{r}' \tag{270}$$

is essentially free of spatial variations unresolvable by the grid network. [In Eq. (270), $\underset{\sim}{r} = (x,y,z)$.] Similar definitions can be written for $\tilde{S}$ and $\tilde{R}$. Averaging Eq. (269) in the manner of Eq. (270) and assuming that $\bar{u}$ and K are nearly constant on scales comparable to the grid dimensions, we obtain

$$\frac{\partial \tilde{c}}{\partial t} + \bar{u}_i \frac{\partial \tilde{c}}{\partial x_i} = \frac{\partial}{\partial x_i} K_{ij} \frac{\partial \tilde{c}}{\partial x_j} + \tilde{S} + \tilde{R} \quad . \tag{271}$$

Numerical methods can then be applied to this equation to obtain an approximate solution for $\tilde{c}$.

Thus, a grid model yields the quantity $\tilde{c}(\underset{\sim}{r},t)$ rather than the point value $c(\underset{\sim}{r},t)$. The difference between these quantities, which we denote by

$$c''(\underset{\sim}{r},t) = c(\underset{\sim}{r},t) - \tilde{c}(\underset{\sim}{r},t) \quad , \tag{272}$$

is what we refer to as the subgrid-scale variations (SSV). Upon subtracting Eq. (271) from Eq. (269), we obtain the equation governing the SSV:

$$\frac{\partial c''}{\partial t} + \bar{u}_i \frac{\partial c''}{\partial x_i} = \frac{\partial}{\partial x_i} K_{ij} \frac{\partial c''}{\partial x_j} + S'' + R'' \quad , \tag{273}$$

where

$$S''(\underset{\sim}{r},t) = S(\underset{\sim}{r},t) - \tilde{S}(\underset{\sim}{r},t) \quad ,$$
$$R''(\underset{\sim}{r},t) = R(\underset{\sim}{r},t) - \tilde{R}(\underset{\sim}{r},t) \quad . \tag{274}$$

Since R is not a function of any spatially variable parameter other than the concentration, it is clear from Eq. (273) that subgrid-scale variations c" can arise only from subgrid-scale variations S" in the source strength. Given the usual dimensions of grid meshes used in airshed models (see the earlier discussion), there are no urban areas in which S", and hence c", is everywhere identically zero.

It is the mean value $c(\underset{\sim}{x},t)$, rather than the space averaged mean $\tilde{c}(\underset{\sim}{x},t)$ given by the grid model, that possesses the point spatial resolution and hence all of the information that we require in air pollution studies. According to Eq. (272), we can acquire this information from the grid model by calculating in addition the subgrid-scale field c". Thus, our approach to the restoration of point resolution to the grid model is simply to develop a microscale, or subgrid-scale, model based on Eq. (273) whose output $c''(\underset{\sim}{x},t)$ can be combined with that of the grid model $\tilde{c}(\underset{\sim}{x},t)$ to describe the point field $c(\underset{\sim}{x},t)$ at any arbitrary point.

To illustrate an important property of the subgrid-scale variation c" and to give the reader a better physical feel for the nature of c", we examine this field quantitatively in an elementary example in the next section.

B. QUANTITATIVE ILLUSTRATION OF THE SUBGRID-SCALE VARIATIONS $c''(\underset{\sim}{r},t)$

For simplicity, we consider a one-dimensional problem governed by the equation

$$\frac{\partial c}{\partial t} = K \frac{\partial^2 c}{\partial z^2} + \delta(z)\ \delta(t) \tag{275}$$

with initial and boundary conditions

$$c(z,0) = 0 \quad , \tag{276a}$$

$$\lim_{z\to\pm\infty} c(z,t) = 0 \quad , \tag{276b}$$

where K is the turbulent diffusivity, assumed to be a constant, and δ is the delta function. The solution of Eqs. (275)and (276) is

$$c(z,t) = (4\pi Kt)^{-1/2} \exp\left(-\frac{z^2}{4Kt}\right) \quad . \tag{277}$$

Now let

$$\tilde{c}(z,t) \equiv \frac{1}{2\Delta z} \int_{z-\Delta z}^{z+\Delta z} c(z',t)\, dz' \quad . \tag{278}$$

Averaging Eq. (277) in this manner, we obtain

$$\tilde{c}(z,t) = \frac{1}{4\Delta z} \left[\operatorname{erf}\left(\frac{z + \Delta z}{\sqrt{4Kt}}\right) - \operatorname{erf}\left(\frac{z - \Delta z}{\sqrt{4Kt}}\right)\right] \quad , \tag{279}$$

where

$$\operatorname{erf}(x) = \frac{2}{\sqrt{\pi}} \int_0^x e^{-\lambda^2}\, d\lambda$$

is the standard error function. Note that Eq. (279) is the solution of the equation obtained by averaging Eq. (275); i.e.,

$$\frac{\partial \tilde{c}}{\partial t} = K \frac{\partial^2 \tilde{c}}{\partial z^2} + \frac{1}{2\Delta z} U(z)\, \delta(t) \quad , \tag{280}$$

where

$$u(z) = \begin{cases} 1 & , \quad -\Delta z \leq z < \Delta z \\ 0 & , \quad \text{otherwise} \end{cases} .$$

Let us assume that Eq. (280) is a grid model representation of Eq. (275) and that $\tilde{c}$, as given by Eq. (279), is the model's output. The subgrid-scale variations are therefore [from Eqs. (277) and (279)]

$$c''(z,t) = \frac{1}{\sqrt{4\pi Kt}} \exp\left(-\frac{z^2}{4Kt}\right) - \frac{1}{4\Delta z}\left[\operatorname{erf}\left(\frac{z+\Delta z}{\sqrt{4Kt}}\right) - \operatorname{erf}\left(\frac{z-\Delta z}{\sqrt{4Kt}}\right)\right] . \tag{281}$$

We can see from this expression that the amplitude of the SSV decreases as the discretization interval Δz in the grid model is made smaller. Moreover, for fixed Δz, the SSV in this example decreases with time. The latter effect is shown graphically in Figure 37. The figure also shows $\tilde{c}$ for comparison. It can be seen that for the earlier travel time (i.e., $t = 0.031\Delta z^2/K$), c'' is up to three times as large as $\tilde{c}$ and is therefore not a negligible variation.

To obtain a more concise description of the relative magnitude of the subgrid-scale variation c'', we note first that c'' is largest at the source location (i.e., $z = 0$). Thus, the maximum amplitude of c'' relative to $\tilde{c}$ can be expressed by

$$\rho(t) \equiv \frac{c''(0,t)}{\tilde{c}(0,t)} . \tag{282}$$

From the expressions for c'' and $\tilde{c}$, we obtain

$$\rho(t) = \frac{2}{\sqrt{\pi}}\left[\sigma^* \operatorname{erf}\left(\frac{1}{\sigma^*}\right)\right]^{-1} - 1 , \tag{283}$$

where

$$\sigma^* = \frac{\sqrt{4Kt}}{\Delta z} . \tag{284}$$

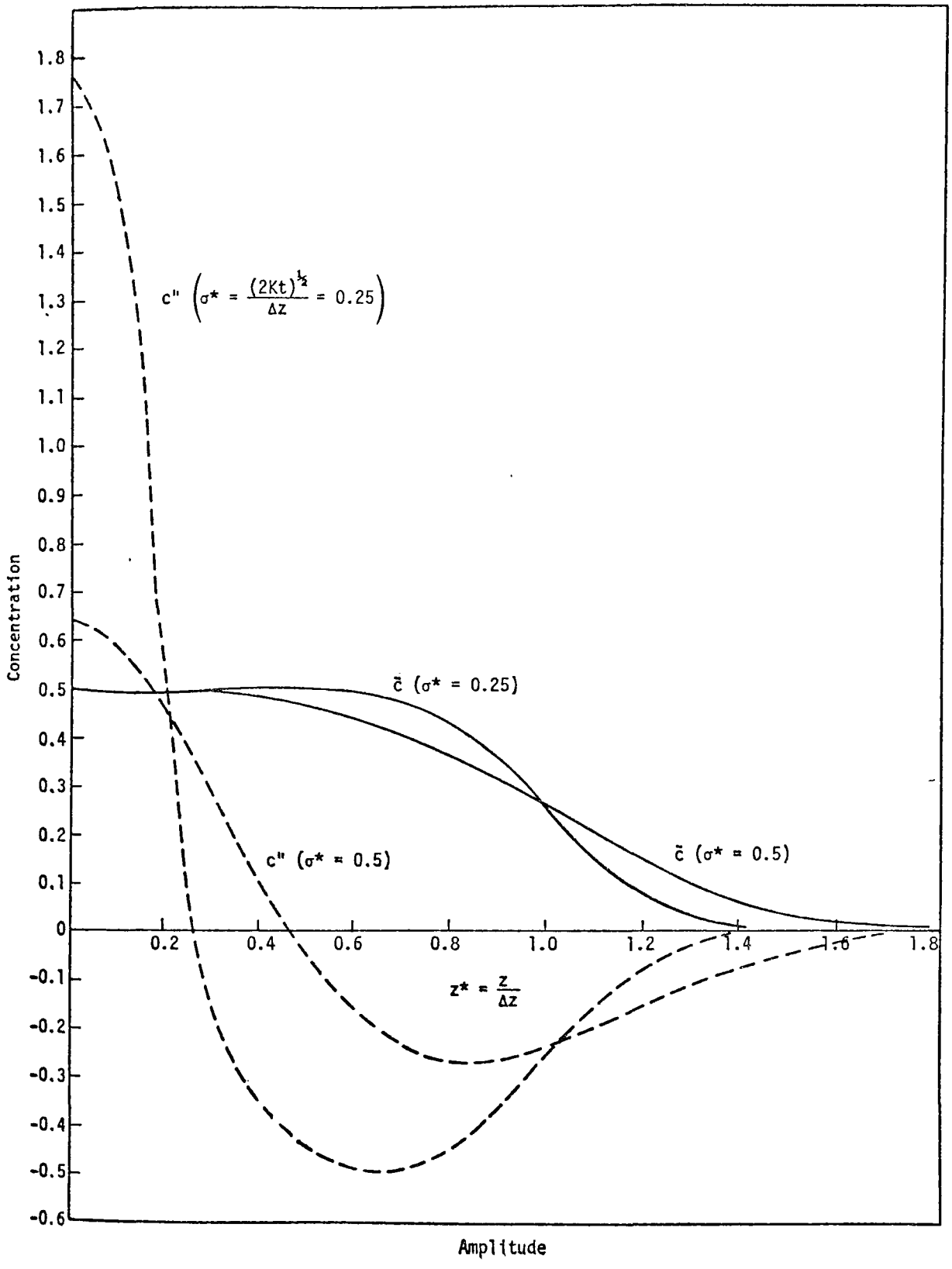

FIGURE 37. ILLUSTRATION OF THE SUBGRID-SCALE CONCENTRATION VARIATIONS ARISING FROM AN INSTANTANEOUS POINT SOURCE

That is, σ^* is the approximate half-width of the pollutant cloud at time t normalized by the grid mesh size Δz. It is evident from Eq. (283) that σ^* is the key parameter that determines the relative size of the SSV in this instance. Upon evaluating Eq. (283) for several values of σ^*, we obtain $\rho = 10$ when $\sigma^* = 0.1$, $\rho = 0.34$ when $\sigma^* = 1$, and $\rho = 0.08$ when $\sigma^* = 2$. From these values, we conclude that, in the case of a point source, the SSV can be neglected relative to $\tilde{c}$ after the pollutant cloud has grown to a width of about four grid intervals.

These results take on added meaning when one realizes that the one-dimensional equation considered here is an approximate model of a two-dimensional steady-state plume. In this case, time is related to the downwind distance x from the plume source by the relationship

$$x = \bar{u}t \quad , \tag{285}$$

where $\bar{u}$ is the mean wind speed (directed along the x-axis). Translated into terms of the two-dimensional plume, the conclusions reached above regarding the relative magnitude of the SSV indicate that SSV effects will be significant within a distance of approximately

$$x = \frac{\bar{u}\Delta z^2}{K} \tag{286}$$

from the plume source. In the grid model, this distance x will represent

$$N = \frac{x}{\Delta z} = \frac{\bar{u}\Delta z}{K} \quad \text{e.} \tag{287}$$

grid intervals from the source. Thus, for fixed $\bar{u}$ and K, the number of grid cells affected by SSV actually increases as the grid size Δz is increased, albeit both c" and $\tilde{c}$ become insignificant sufficiently far from the source.

Although we considered only the maximum value of c" (i.e., c"(0,t) in the analysis above, we can expect (see Figure 37) that the SSV will become negligible everywhere in space on the same time scale as that of the maximum.

C. DERIVATION OF A SUBMODEL OF c" FOR LINEARLY REACTIVE POLLUTANTS

1. Discussion of General Operational Problems

As stated in the introduction to this chapter, we seek to obtain c" from its governing equation [Eq. (273)] and to use this result along with that given by the grid model to obtain the point mean field $c(\underline{x},t)$. Since our earlier discussion of the equation governing c", i.e., Eq. (273), was very general, it did not reveal several of the operational problems that arise in solving this equation in given situations. We discuss these below, within the context of a simple problem, before proceeding with the development of specific models.

To keep the mathematics as simple as possible, we consider here only a single pollutant that decays at a nonlinear rate. The equation governing the concentration of this pollutant in the urban atmosphere is assumed to be

$$\frac{\partial c}{\partial t} + Lc = -kc^2 - k\langle c'^2\rangle + S \quad , \tag{288}$$

where L is the operator

$$L \equiv \bar{u}_i \frac{\partial}{\partial x_i} - \frac{\partial}{\partial x_i} K_{ij} \frac{\partial}{\partial x_j} \quad , \tag{289}$$

$\bar{u}_i$ is the mean wind speed, K_{ij} is the turbulent diffusivity tensor, and $\langle c'^2\rangle$ is the turbulent concentration fluctuation term discussed in Chapter III. Although this example is mathematically much simpler than that for photochemical air pollution, which involves a system of coupled nonlinear equations, the problem posed by Eq. (288) has many of the essential characteristics of the more complicated real situation. Thus, techniques developed for a pollutant that undergoes a second-order reaction can be applied to more general situations through straightforward extensions.

Suppose that a grid model for the pollutant cited above is to be developed. As outlined earlier, the procedure for deriving the working equation of the model is to perform at each point a spatial average of

Eq. (288) over a volume V equal to that of the grid cells. In this way, we obtain the working equation

$$\frac{\partial \tilde{c}}{\partial t} + L\tilde{c} = -k\tilde{c}^2 - k\widetilde{c''^2} - k\widetilde{\langle c'^2 \rangle} + \tilde{S} \quad , \tag{290}$$

where c and S are spatial averages and c" is the subgrid-scale concentration variation. Note that it is the spatial average mean square turbulent fluctuation term $\widetilde{\langle c'^2 \rangle}$ that enters into the grid model equation. Upon subtracting Eq. (290) from Eq. (288), we obtain the equation governing c":

$$\frac{\partial c''}{\partial t} + Lc'' = -kc''^2 - 2k\tilde{c}c'' + k\widetilde{c''^2} - k\widetilde{\langle c'^2 \rangle}'' + S'' \quad , \tag{291}$$

where $\langle c'^2 \rangle''$ represents the subgrid-scale portion of the mean square fluctuation field $\langle c'^2 \rangle$. The second term on the right side of Eq. (291) represents the chemical interaction of the subgrid-and supergrid-scale concentration fields. Since the latter is a known quantity at each point (it is given by the grid model), Eq. (291) contains only one dependent variable, c" (after $\widetilde{c''^2}$ and $\langle c'^2 \rangle$ have been parameterized), and this equation can thus in principle be solved.

The nonlinearity of Eq. (291) dictates that its solution can be approximated only by using numerical integration techniques. It is to be expected, however, that the implementation of these techniques will require the solution of operational problems unlike those associated with the modeling of $\tilde{c}$. This requirement arises because point and line type sources give rise in S" to delta functions, which are not amenable to treatment using discrete grid numerical methods. We could, of course, attempt to evaluate Eq. (291) on a fine grid, but this would only create new subgrid-scale problems. To circumvent these problems, we develop a new technique later in this chapter.

In contrast, in cases where the pollutant is linearly reactive, the implementation of the microscale model is quite simple because the governing equation, Eq. (291), reduces to the much simpler form

$$\frac{\partial c''}{\partial t} + Lc'' = -kc'' + S'' \quad , \tag{292}$$

and if the pollutant is inert, the equation reduces further to

$$\frac{\partial c''}{\partial t} + Lc'' = S'' \quad . \tag{293}$$

In the remainder of this section, we develop the known analytic solution of Eq. (292) into a working model of c" that can be used with any grid model of CO, SO_2, or other essentially linear pollutants.

2. Derivation of the Working Equations for a Microscale Model of Linearly Reactive Pollutants

Consider a pollutant that decays linearly at a rate described by

$$\frac{dc}{dt} = -kc \quad , \tag{294}$$

where k is the rate constant. (Note that inert pollutants are represented by k = 0.) The equation governing c" in this case is Eq. (292), the solution of which is of the form [see Lamb and Neiburger (1971)]

$$c''(\underset{\sim}{r},t) = \int\int_{t_0}^{t} p(\underset{\sim}{r},t|\underset{\sim}{r}'t') \exp\left[-k(t - t')\right] S''(\underset{\sim}{r}',t') \, dt' \, d\underset{\sim}{r}'$$

$$+ \int p(\underset{\sim}{r},t|\underset{\sim}{r}'t_0) \exp\left[-k(t - t_0)\right] c''(\underset{\sim}{r}',t_0) \, d\underset{\sim}{r}' \quad , \tag{295}$$

where p denotes the Green's function of Eq. (292) and its boundary conditions. For simplicity, we assume that $c''(\underset{\sim}{r},t_0) = 0.$ in which case the last term in Eq. (295) vanishes. Our aim now is to derive formulas for c" pertinent to general source configurations S" in conditions of open terrain where the form of p is rather simple. Consider first the source function S".

The source distribution S can be expressed in the general form

$$S(\underset{\sim}{r},t) = \sum_{\alpha=1}^{N} S_{p\alpha}(t)\ \delta(\underset{\sim}{r} - \underset{\sim}{r}_{\alpha}) + \sum_{\beta=1}^{M} S_{L\beta}(t)\ \delta(z - z_{\beta})\ \delta[y - s_{\beta}(x)] \quad , \tag{296}$$

where $S_{p\alpha}$ denotes the emission rate (mass/time) of the α-th point source (of which N are present), $\underset{\sim}{r}_{\alpha}$ is the position of the α-th source, and δ is the delta function. The line sources represented by the last term in Eq. (296) have strengths S_{Lp} per unit length and lie along the curves $y = S_{\beta}(x)$ at elevation Z_{β}. From Eqs. (296), (274), and (270), we obtain

$$S''(\underset{\sim}{r},t) = \sum_{\alpha=1}^{N} S_{p\alpha}(t)\ \delta(\underset{\sim}{r} - \underset{\sim}{r}_{\alpha}) + \sum_{\beta=1}^{M} S_{L\beta}(t)\ \delta(z - z_{\beta})\ \delta[y - s_{\beta}(x)] \quad ,$$

$$- \frac{Q_{ijk}}{\Delta x \Delta y \Delta z}\, U_{ijk}(\underset{\sim}{r}) \quad , \tag{297}$$

where Q_{ijk} is the total mass of pollutant emitted per unit time in the grid cell (i,j,k) and

$$U_{ijk}(\underset{\sim}{r}) = \begin{cases} 1, & \text{if } \underset{\sim}{r} \text{ lies in the grid cell } (i,j,k); \\ 0, & \text{otherwise.} \end{cases} \tag{298}$$

Upon substituting Eq. (297) into Eq. (295), we obtain an expression for c'' of the form

$$c''(\underset{\sim}{r},t) = \sum_{\alpha=1}^{N} P_{\alpha}(\underset{\sim}{r},t) + \sum_{\beta=1}^{M} L_{\beta}(\underset{\sim}{r},t) - \sum_{\gamma=1}^{L} V_{\gamma}(\underset{\sim}{r},t) \quad , \tag{299}$$

where P_{α} is the contribution to c'' from the α-th point source, L_{β} is the contribution to c'' from the β-th line source, and where V_{γ} is the collective contribution of all sources in the γ-th grid cell. Below we derive the functional form of each of these terms, assuming that in the open terrain and quasi-steady flow regimes of interest to us here the kernel p in Eq. (295) has the Gaussian form

$$p(\underset{\sim}{r},t|\underset{\sim}{r}',t') = \left[(2\pi)^{3/2}\sigma_x\sigma_y\sigma_z\right]^{-1} \exp\left[-\frac{(x - x' - \bar{u}\tau)^2}{2\sigma_x^2} - \frac{(y - y' - \bar{v}\tau)^2}{2\sigma_y^2}\right]$$

$$\cdot\left\{\exp\left[-\frac{(z - z')^2}{2\sigma_z^2}\right] + \exp\left[-\frac{(z + z')^2}{2\sigma_z^2}\right]\right\} \quad , \tag{300}$$

where

$$\tau = t - t', \tag{301a}$$

$$\sigma_x, \sigma_y, \sigma_z = F(\tau), \tag{301b}$$

$$\bar{u}, \bar{v} \quad = \text{constants}, \tag{301c}$$

$$\bar{w} \quad = 0. \tag{301d}$$

This form of p contains the implicit assumptions that the earth acts as a reflective barrier to the pollutant particles, that the turbulence is homogeneous, and that no low-level inversions exist. Assumptions (301c) and (301d) are not generally valid, but are acceptable approximations over the relative small areas, comparable to a grid cell, in which c" is finite. To maximize the accuracy of Assumption (301b), we plan to use the "optimal" $\sigma_x(t)$ and $\sigma_z(t)$ profiles developed in Chapter II.

a. The Point Source Contribution, P_α

Using the delta function's property

$$\int_a^b f(x)\,\delta(x - x_0)\,dx = f(x_0) \quad , \quad a<x_0<b \quad ,$$

we find immediately from Eqs. (295) and (297) through (300) that the point source term P_α entering in Eq. (299) is of the form

$$P_\alpha(\underset{\sim}{r},t) = S_{p\alpha}(t)\int_0^t p_{xy}(x,y,x_\alpha,y_\alpha,\tau)\; p_z(z,z_\alpha,\tau)\; d\tau \quad , \tag{302}$$

where

$$p_{xy}(x,y,x_\alpha,y_\alpha,\tau) = \left[2\pi\sigma_x(\tau)\;\sigma_y(\tau)\right]^{-1} \exp\left[-\frac{(x - x_\alpha - \bar{u}\tau)^2}{2\sigma_x^2(\tau)}\right.$$

$$\left. - \frac{(y - y_\alpha - \bar{v}\tau)^2}{2\sigma_y^2(\tau)} - k\tau\right] \tag{303}$$

and

$$p_z(z,z_\alpha,\tau) = \left[\sqrt{2\pi}\;\sigma_z(\tau)\right]^{-1}\left\{\exp\left[-\frac{(z - z_\alpha)^2}{2\sigma_z^2(\tau)}\right] + \exp\left[-\frac{(z + z_\alpha)^2}{2\sigma_z^2(\tau)}\right]\right\} \quad . \tag{304}$$

We should mention that the assumptions of a reflective earth and the absence of an upper level inversion can be relaxed by substituting the appropriate expression for p_z in Eq. (302). Equation (302) is the first of the set that we need to model c".

b. Line Source Terms

We first assume that all line source segments are straight lines lying at ground level (i.e., $z_\beta = 0$, $\beta = 1,2, \ldots, M$) and that the strength of each segment is constant along its length. Suppose that the β-th line source has length ℓ_β, that it is centered at (x_β, y_β), and that it makes an angle Θ_β with the y-axis as shown in Figure 38.

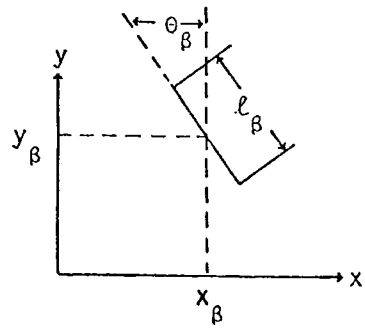

FIGURE 38. PARAMETERS REQUIRED TO SPECIFY A FINITE LINE SOURCE

The line source term L_β, which represents this source in the c" formula [Eq. (299)], can be shown to be [see Lamb and Neiburger (1971)]

$$L_\beta(\underset{\sim}{r},t) = S_{L\beta}(t) \int_0^t \exp\left\{ - \frac{\left[(x - \bar{u}\tau - x_\beta)\cos\theta_\beta + (y - \bar{v}\tau - y_\beta)\sin\theta_\beta\right]^2}{2\sigma^2} - k\tau \right\}$$

$$\cdot (2\sqrt{2\pi}\sigma)^{-1} \left\{ \operatorname{erf}\left[\frac{(y - \bar{v}\tau - y_\beta)\cos\theta_\beta - (x - u\tau - x_\beta)\sin\theta_\beta + \frac{\ell_\beta}{2}}{\sqrt{2}\,\sigma} \right] \right.$$

$$\left. - \operatorname{erf}\left[\frac{(y - \bar{v}\tau - y_\beta)\cos\theta_\beta - (x - \bar{u}\tau - x_\beta)\sin\theta_\beta - \frac{\ell_\beta}{2}}{\sqrt{2}\,\sigma} \right] \right\}$$

$$\cdot p_z(z,0,\tau)\, d\tau \quad , \tag{305}$$

where $\sigma = \sigma_x = \sigma_y$ and where p_z is given by Eq. (304), with $z_\beta = 0$. This is the general line source term needed to compute c".

c. Volume Source Terms

The volume source terms V_γ arise from $\tilde{S}$, each volume source having the dimensions $\Delta x \cdot \Delta y \cdot \Delta z$ of the grid cells in the urban-scale model. It is not difficult to show that the volume source term V_γ is given by

$$V_\gamma(\underset{\sim}{r},t) = \frac{Q_\gamma}{8\Delta v} \int_0^t \left[\operatorname{erf}\left(\frac{x - x_\gamma - \bar{u}\tau + \frac{\Delta x}{2}}{\sqrt{2}\,\sigma} \right) - \operatorname{erf}\left(\frac{x - x_\gamma - \bar{u}\tau - \frac{\Delta x}{2}}{\sqrt{2}\,\sigma} \right) \right]$$

$$\cdot e^{-k\tau} \cdot \left[\operatorname{erf}\left(\frac{y - y_\gamma - \bar{v}\tau + \frac{\Delta y}{2}}{\sqrt{2}\,\sigma} \right) - \operatorname{erf}\left(\frac{y - y_\gamma - \bar{v}\tau - \frac{\Delta y}{2}}{\sqrt{2}\,\sigma} \right) \right]$$

$$\cdot \left[\operatorname{erf}(A) - \operatorname{erf}(B) + \operatorname{erf}(D) - \operatorname{erf}(c) \right] d\tau \quad , \tag{306}$$

where

$$A = \frac{z - z_\gamma + \frac{\Delta z}{2}}{\sqrt{2}\,\sigma_z} \quad , \qquad C = \frac{z + z_\gamma - \frac{\Delta z}{2}}{\sqrt{2}\,\sigma_z} \quad ,$$

$$B = \frac{z - z_\gamma - \frac{\Delta z}{2}}{\sqrt{2}\,\sigma_z} \quad , \qquad D = \frac{z + z_\gamma + \frac{\Delta z}{2}}{\sqrt{2}\,\sigma_z} \quad , \tag{307}$$

and $(x_\gamma, y_\gamma, z_\gamma)$ denotes the center of the γ-th grid cell. Equation (306) is the volume source term required in Eq. (299) to calculate c".

3. Design of the c" Model Computer Program--Interaction with the Source Inventory Data Bank

We have derived the basic equations required to calculate c". The next step is to put these results into the form of a subroutine that the airshed model can call to compute concentrations c at any given point. As previously stated, the c" model must not interfere with the operation of the full urban-scale model, and it must not require the latter to perform special calculations In short, the c" subprogram must be capable of calculating c" given only the following information (which is always available in the grid model itself):

$(\bar{u}, \bar{v})$	= horizontal components of the mean wind in the vicinity of the receptor,
z_i/L	= local stability parameter,
$\Delta x, \Delta y, \Delta z$	= dimensions of the grid cells,
u_*	= local friction velocity,
z_i	= mixing depth in the vicinity of the receptor,
$\tilde{c}$	= value computed by the grid model for the receptor point,
(x,y,z)	= coordinates of the receptor.

Thus, if MICRO is the name of the c" model, the call for it by the grid model might look something like the following:

```
CALL MICRO (X,Y,Z,T,ZIOVL,USTAR,ZI,UBAR,VBAR,
            DELTAX,DELTAY,DELTAX,CTILDE,CPP)    ,
```

where CPP = c"(x,y,z,T).

The MICRO program must also have access to the source inventory, where each point and line source segment, or link, is stored separately. In particular, the following source data are needed to compute c":

XPS(I), YPS(I), ZPS(I) = (x,y,z) coordinates of I-th point source.

XLS(J), YLS(J) = (x,y) coordinates of the center of the J-th line line source (ZLS = 0 assumed).

THETA(J) = angle of the J-th line source (see Figure 38).

XLNGTH(J) = length of the J-th line source.

SP(I) = strength (mass/time) of the I-th point source.

SL(J) = strength (mass/length/time) of the J-th line source.

Using all of the above information, MICRO computes c" in a manner described roughly by the flow chart shown in Figure 39. We have completed the steps labeled SIGMA and CALC in the flow chart; Appendix C presents listings of their source programs. Steps SEARCH, SORT, and DOMAIN have not been completed, and without these modules, the MICRO subprogram lacks the capability of searching the source inventory itself. However, if the user provides the relevant source information, the existing steps SIGMA and CALC can compute c" at any given point.

In its present form, SIGMA consists of two FORTRAN functions, SIGMAX(T) and SIGMAZ(T), which are used by the subprogram CALC. The SIGMA functions calculate σ_x and σ_z for a given travel time T and for given stability, mixing depth, and friction velocity conditions (which are passed through common blocks to the function programs). To evaluate the integrals entering in the equations derived earlier for c", the CALC subprogram uses a Monte Carlo quadrature technique, described theoretically in Appendix D. This technique allows infinite flexibility in the ability of the CALC program to evaluate c" both near

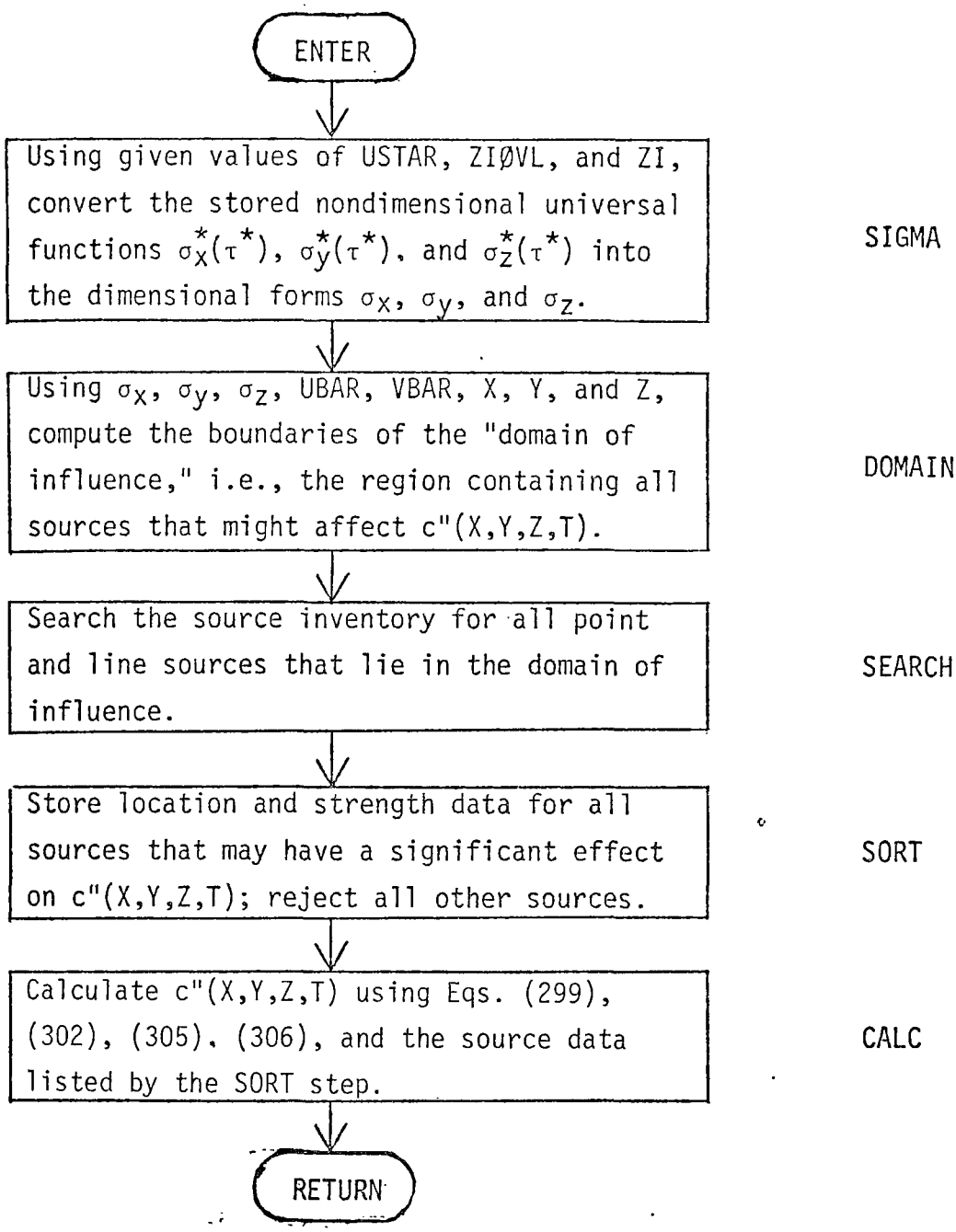

FIGURE 39. FLOW DIAGRAM OF THE c"-MODEL ROUTINE MICRO

and far from point and line sources. It also requires minimal complexity in programming and permits control over the accuracy of the integral evaluation.

Test calculations performed with the MICRO model in its present form for the problem portrayed in Figure (40a) are presented in Figures (40b) and (40c). Although these figures are self-explanatory, we wish to call attention to the size of c" in the immediate vicinity of the line source in this calculation: It is over two orders of magnitude larger than $\tilde{c}$ at the same point [cf. Figures (40b) and (40c)].

One of the main problems that we anticipate in the implementation of microscale models such as MICRO into full-scale urban diffusion models is the incompatability of the source inventory data bases that the two kinds of models require. That is, in grid models, such as that developed by SAI, the source inventory consists of total emissions from each grid cell rather than emissions from each point and line source within a cell. The MICRO model requires data in the latter form, which is not derivable from the existing source inventory.

A logical solution to this problem is to collect raw data in the form of point and line source emissions and to store it in this form. It is then a simple matter to compute total emissions from any grid cell network for use in a grid model. This approach was employed in a pollution modeling study of the Los Angeles basin conducted by Lamb and Neiburger (unpublished). Data from this study consist of the coordinates and strengths of each of approximately 6000 roadway links in the Los Angeles area for the year 1966. These data are stored on discs and can be converted, using simple programs, into emissions from any desired grid cell network. We have procured this data bank and will use it in the final developmental phases of the MICRO program. Our chief interest is in using this data to test the DOMAIN, SEARCH, and SORT modules, which will allow the MICRO program to interact with the data bank for the purposes of computing c" at any desired point.

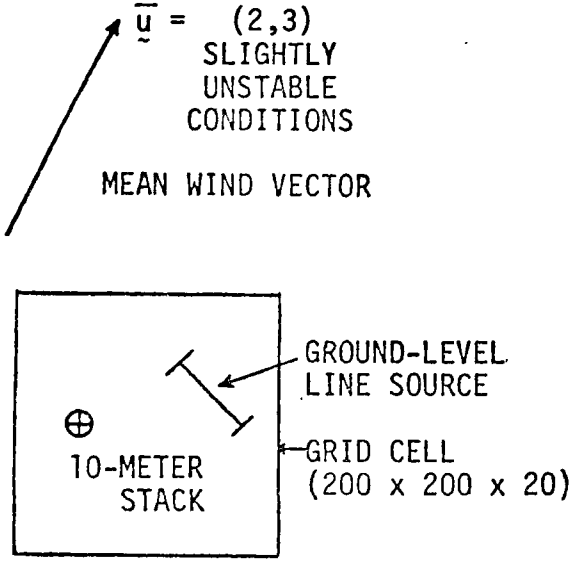

(a) Source Configuration Showing the Conditions of a Test Problem for Solution Using the CALC Routine Listed in Appendix C.

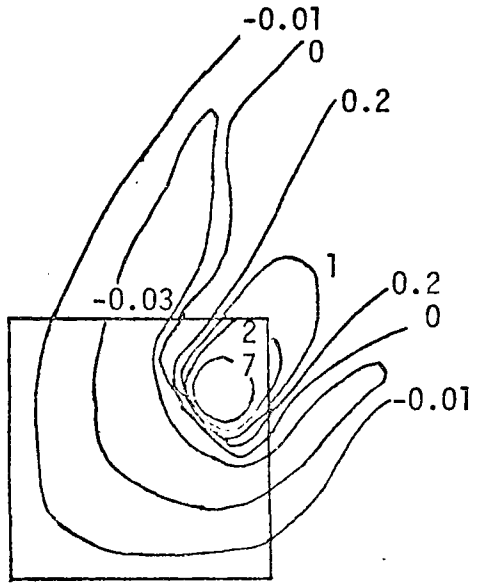

(b) c" (x 10^3) Computed by CALC for the Problem Given in Part (a). Note the large magnitude of c" near the line source. The elevation of the point source results in positive c" only at large distances.

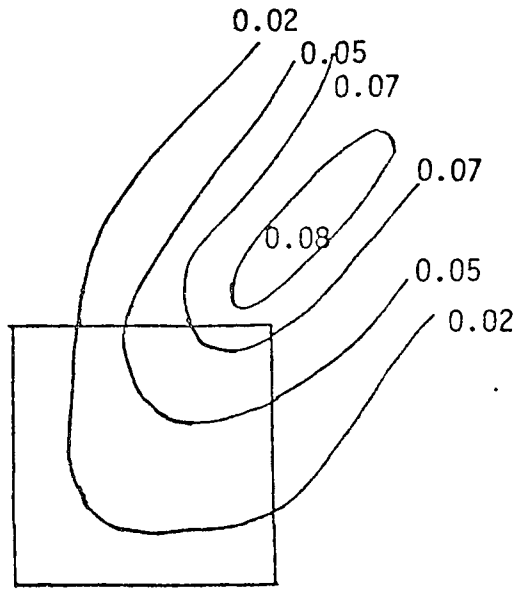

(c) $\tilde{c}$ (x 10^3) as a Perfect Grid Model Would Compute It for the Problem Shown in Part (a).

FIGURE 40. THE CONTOURS OF c" ARISING FROM A SINGLE POINT AND LINE SOURCE, AS COMPUTED BY CALC

The final version of MICRO will enable the user of a grid model to restore point-scale spatial resolution to his diffusion model at any desired point. The following sections describe the DOMAIN, SEARCH, and SORT modules that we are presently developing.

a. DOMAIN

We demonstrated analytically in Section V-B that c" decays with travel time, even in the absence of chemical decay. Let the characteristic time scale of this decay be T. Thus, sources located a distance

$$\ell \geq [\bar{u}^2 + \bar{v}^2]^{1/2} T \qquad (308)$$

upwind of the receptor point (XR,YR,ZR) have a negligible effect on c". Furthermore, because of the limited horizontal and vertical dispersion rates, all sources downwind of (XR,YR,ZR) and those outside a wedge-shaped sector upwind of (XR,YR,ZR) have negligible effect on c". By ignoring all such sources, the MICRO program can optimize its calculation speed.

We showed in Section V-B that the decay time scale T of c" is approximately equal to the time required for a point source cloud to grow to the size of a grid cell. Thus, if $\sigma_x = a_x t^{b_x}$, $\sigma_y = a_y t^{b_y}$, and $\sigma_z = a_z t^{b_z}$, we have

$$T = \max\left\{\left(\frac{\Delta x}{a_x}\right)^{1/b_x}, \left(\frac{\Delta y}{a_y}\right)^{1/b_y}, \left(\frac{\Delta z}{a_z}\right)^{1/b_z}\right\} . \qquad (309)$$

The upwind dimension ℓ of the domain of influence is therefore

$$\ell = VT , \qquad (310)$$

and T is given by Eq. (310).

The width of the domain of influence is proportional to $\sigma_y(t)$, assuming that $\sigma_x \simeq \sigma_y$. We conclude that the domain of influence is the wedge-shaped region shown in Figure 41.

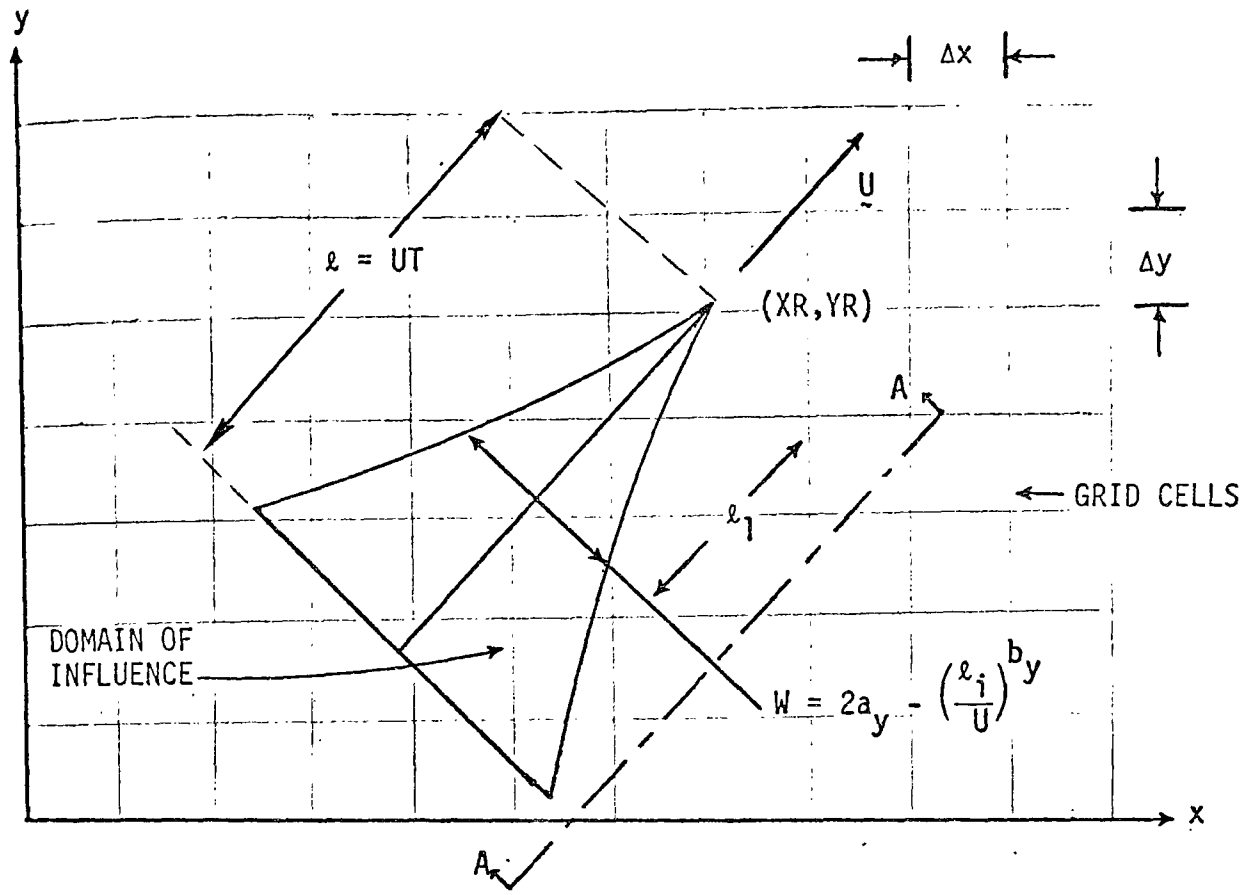

(a) Horizontal View of the Domain of Influence

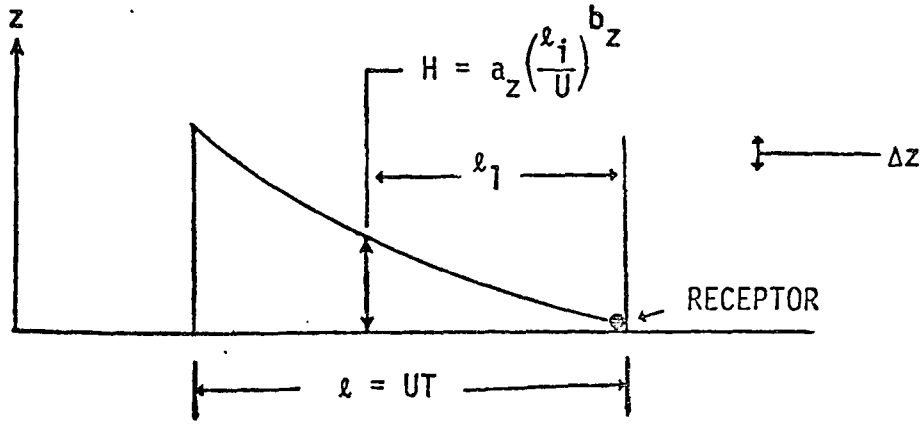

(b) Vertical Cross Section View A-A of the Domain of Influence

FIGURE 41. HORIZONTAL AND VERTICAL CROSS SECTIONS OF THE DOMAIN OF INFLUENCE ON c"(XR,YR)

b. SEARCH

Once the boundaries of the domain of influence have been established, the next step is to find and list all point, line, and volume sources that lie within it. As indicated earlier, the coordinates of the i-th point source are stored in the data bank as XPS(I), UPS(I), ZPS(I). Four parameters are stored for each line source. By testing the coordinates of each source, we can determine whether that source lies wholly or partially within the domain of influence.

The speed of the point- and line-source searching operation can be optimized if sources in the data bank are catalogued according to the grid cell in which they lie. If this is the case, only those blocks of data filed in locations corresponding to grid cells within the zone of influence need be examined. Determining the volume sources within the domain of influence is a simple matter, since these correspond to the grid cells. Note that even if only the edge of a volume source (grid cell) falls within the domain of influence, the entire source must be treated. The extent to which that source affects c" at the receptor is automatically accounted for in the c" equation.

c. SORT

The efficiency of the c" calculation can be increased by considering only those sources that together have the largest influence on c" at the receptor. For example, the SEARCH step may find a total of 10 point and line sources within the domain of influence, but only three of these together may be responsible for 90 percent of the observed magnitude of c". In this case, neglecting the other seven sources would cut computation time by 70 percent at the cost of only a 10 percent error in c".

Because the SORT process itself consumes computing time, the usefulness of this step is limited to those cases where there are many point and line sources within the domain of influence. To determine which sources to neglect, we need an algorithm that permits rapid estimates of the approximate effect on c" of a given source. The following is such an algorithm.

To each point and line source, we assign a number RANK. For the i-th point source, RANK is given by

$$\text{RANK} = \frac{\text{SP(I)}}{\left[a_{LAT} a_z \left(\frac{d}{U}\right)^{b_{LAT}} \left(\frac{d}{U}\right)^{b_z}\right]} \quad , \tag{311}$$

where

$$d = [(\text{XPS(I)} - \text{XR})^2 + (\text{YPS(I)} - \text{YR})^2]^{1/2} \quad . \tag{312}$$

For the j-th line source,

$$\text{RANK} = \frac{\text{SL(J)} * \text{XLNGTH(J)}}{a_z \left(\frac{d}{U}\right)^{b_z} \left[w + a_{LAT} \left(\frac{d}{U}\right)^{b_{LAT}}\right]} \quad , \tag{313}$$

where

$$d = [(\text{XLS(J)} - \text{XP})^2 + (\text{YLS(J)} - \text{YP})^2] \quad , \tag{314}$$

$$w = \text{XLNGTH(J)} * \text{SIN}\left[\text{THETA(J)} + \text{TAN}^{-1}\left(\frac{\text{UBAR}}{\text{VBAR}}\right)\right] \quad . \tag{315}$$

With a value of RANK assigned to each point and line source, we now form the sum

$$\text{RANKT} = \Sigma \text{RANK} \quad , \tag{316}$$

where the summation is over all point and line sources and where we arrange the sources in order of decreasing values of RANK, with point and line sources mixed as their values of RANK dictate.

In the CALC step, the sources are treated in order of their RANK values, the largest being treated first. As we proceed through the list of sources, we keep a running sum of the RANK values of the sources treated. Let this sum be denoted by

$$\text{RUNSUM}(K) = \sum_{k=1}^{K} \text{RANK}(k) \quad , \tag{317}$$

where K represents the number of sources out of the total of KMAX point and line sources in the domain of influence that have been treated. Note that, by definition, RUNSUM (KMAX) = RANKT. Thus, when

$$\frac{\text{RUNSUM}(K)}{\text{RANKT}} \geq \beta \quad , \tag{318}$$

where $0<\beta\leq 1$, we terminate the calculation of the point and line sources contributions to c" and neglect all sources with labels between K and KMAX. The value assigned to β depends largely on the estimated overall accuracy of the model; it is generally unnecessary to set $\beta = 1$ because errors in the model itself do not warrant the added computing time required.

A print-out of the list of the sources actually treated and their RANK values will also be of aid in assessing the polluting potential of each source in the vicinity of the receptor.

D. DEVELOPMENT OF MATHEMATICAL METHODS FOR MODELING SUBGRID-SCALE CONCENTRATION VARIATIONS c" OF NONLINEAR POLLUTANTS

In the last section, we derived solutions of Eq. (292), which governs the c" distribution of linear pollutants. Needless to say, obtaining solutions of the more general equation [Eq. (291)], which governs nonlinear species, is a much more difficult process. And modeling the complete system of photochemical pollutants is even more complex. We have only begun to consider the nonlinear problem. We outline here a method that we have developed and are considering for constructing a microscale model of nonlinear pollutant species. We demonstrate the method in the context of Eq. (291) because it is mathematically much simpler than the equations describing the complete kinetic mechanism, but yet it retains the essential nonlinear property of those equations.

The obvious approach to solving Eq. (291) is to express the equation in finite difference form and to integrate the resulting expression numerically. However, this method only creates a new subgrid-scale problem: because due to the presence in S" of delta functions arising from point and line sources, subgrid-scale concentration variations will exist in any discrete analogue of Eq. (291). Even if it were possible to achieve a grid network fine enough to resolve the major variations in the concentration field, operational problems would still remain. For example, because of the arbitrariness of the locations and orientations of point and line sources, a variable grid network would be required to optimize the accuracy of the numerical integration process. But this might lead to difficulties with computational stability, boundary conditions, truncation error, and the like, and would certainly complicate the computer program.

To circumvent all of the problems, we develop in this section a relatively new type of pollution modeling equation. This model is not based on any radically new theory. Rather, it is based on an equation that is an intermediate step in a sequence of mathematical operations that leads from the general Lagrangian equation of turbulent diffusion Eq. (16), through the well-known Gaussian puff and plume formulas, to the classical diffusion equation [Eq. (291)]. One of the unique features of the new equation that enables it to avoid the problems listed above is that it is continuous in space (like the diffusion equation), but discrete in time. In the remainder of this section, we derive the new model, briefly discuss its place in the scheme of existing modeling equations, and outline a set of ways in which this model can be implemented in the calculation of c" of nonlinear pollutants. The actual implementation process will be undertaken in a later study.

1. Derivation of a Discrete-Time, Continuous-Space Diffusion Equation

The starting point of the derivation is the Lagrangian form of the diffusion equation introduced in Chapter II, i.e. ,

$$\langle c(\underset{\sim}{r},t)\rangle = \iint_{t_0}^{t} p(\underset{\sim}{r},t|\underset{\sim}{r}',t')\, S'(\underset{\sim}{r}',t')\, dt'\, d\underset{\sim}{r}' + \int p(\underset{\sim}{r},t|\underset{\sim}{r}',t_0)\langle c(\underset{\sim}{r}',t_0)\rangle\, d\underset{\sim}{r}' \quad , \tag{319}$$

where S is the source strength function. In cases where linear chemical decay occurs at a rate

$$\frac{dc}{dt} = -k(t)c \quad , \tag{320}$$

where k(t) is the rate "constant," it can be shown [see, for example, Lamb (1971)] that the proper form of the kernel p entering in Eq. (319) is

$$p(\underset{\sim}{r},t|\underset{\sim}{r}',t') = p'(\underset{\sim}{r},t|\underset{\sim}{r}',t') \exp\left[-\int_{t'}^{t} k(t'')\, dt''\right] \quad , \tag{321}$$

where p' is the probability density that the fluid will advect a particle from $(\underset{\sim}{r}',t')$ to $(\underset{\sim}{r},t)$. Note that p' is a property of the fluid motions alone and is independent of the chemistry. Through a series of assumptions and mathematical operations, it can be shown that the Gaussian plume formula, the puff model, and the classical diffusion equation are all derivable from Eq. (319). It is in the derivation of the diffusion equation that the discrete-time, continuous-space model arises.

Thus, let the time axis be divided into equal intervals of length Δt, and let t_n denote the time $t = n\Delta t$. For brevity, we omit the reference to time in the derivation by writing, for example,

$$p(\underset{\sim}{r},t_n|\underset{\sim}{r}',t_0) = p(\underset{\sim}{r}_n|\underset{\sim}{r}_0) \quad .$$

Consider now the conditional probability density

$$p(\underset{\sim}{r}_n|\underset{\sim}{r}_{n-1}, \underset{\sim}{r}_{n-2},\ldots,\underset{\sim}{r}_0) \quad . \tag{322}$$

that a particle is at $\underset{\sim}{r}_n$ at time t_n given that it was at $\underset{\sim}{r}_{n-1}$ at time t_{n-1}, at $\underset{\sim}{r}_{n-2}$ at time t_{n-2}, and so forth. If an interval Δt exists such that

$$p(\underset{\sim}{r}_n|\underset{\sim}{r}_{n-1},\underset{\sim}{r}_{n-2},\ldots,\underset{\sim}{r}_0) = p(\underset{\sim}{r}_n|\underset{\sim}{r}_{n-1}) \quad , \tag{323}$$

then the particle motions are said to consitute a Markov process in the discrete time frame because any stochastic process whose probability density satisfies a relationship of the form of Eq. (323) is called a Markov process. An important property of a Markov sequence is that its probability density $p(\underset{\sim}{r}_n|\underset{\sim}{r}_m)$ satisfies the Chapman-Kolmogoroff equation

$$p(\underset{\sim}{r}_n|\underset{\sim}{r}_m) = \int p(\underset{\sim}{r}_n|\underset{\sim}{r}_\ell)\ p(\underset{\sim}{r}_\ell|\underset{\sim}{r}_m)\ d\underset{\sim}{r}_\ell \quad , \tag{324}$$

where $n>\ell>m$ are any integers.

The physical significance of the Markov process in the context of a turbulent diffusion problem warrants comment. Suppose that the turbulent eddies that are responsible for the random motions of the pollutant particles have a time scale T. A reasonable estimate for T is the Lagrangian integral time scale of the turbulence defined by

$$T_L \equiv \frac{1}{v'^2} \int_0^\infty \overline{v'(t)\ v\ (t+\xi)}\ d\xi \quad , \tag{325}$$

where v'(t) is the velocity component at time t of a fluid particle. (If the turbulence is stationary, then T_L is independent of the time t.) The time scale T_L can be regarded as a rough measure of the lifetime of the so-called energy-containing eddies.

Suppose now that a particle is released in the turbulence and that its velocity is recorded at intervals $\Delta t = T_L/10$ apart. We can expect that if the velocity is, say, positive at times t_n, t_{n+1}, and t_{n+2}, then there is a greater chance of observing a positive velocity at time t_{n+3} than a negative velocity; and conversely, if the velocity is negative at the first three times,

then it is more likely to be negative than positive at time t_{n+3}. In contrast, if the particle velocity is recorded at intervals $\Delta t = 10_{L}$ apart, then we can expect the velocity at time t_{n+3} to be independent of that at t_{n+2} and all previous times. The idea here is simply that a particle has a "memory" of some length T in the sense that the behavior of the particle at any time t is seemingly influenced by its history during the interval T just prior to the time t. This apparent memory is imparted to the particles by the organized or systematic behavior that each eddy exhibits during its lifetime. It is the randomness of the birth and death processes of the eddies and of the transferral of a particle from one eddy to another that causes a particle ultimately to "forget" its distant past history. This type of reasoning leads us to expect that the probability density of the particle positions will satisfy the Markov condition [Eq. (323)] if the discretization time interval Δt is chosen such that

$$\Delta t >> T_L \quad , \tag{326}$$

where T_L is given by Eq. (325).

For reference, we rewrite here the general equation [Eq. (319)] using the notation adopted above:

$$\langle c(\underset{\sim}{r},t_n)\rangle = \int p(\underset{\sim}{r}_n|\underset{\sim}{r}_0)\langle c(\underset{\sim}{r}_0,t_0)\rangle \, d\underset{\sim}{r}_0 + \iint_{t_0}^{t_{n-1}} p(\underset{\sim}{r}_n|\underset{\sim}{r}') \, S(\underset{\sim}{r}',t')dt' \, d\underset{\sim}{r}'$$

$$+ \iint_{t_{n-1}}^{t_n} p(\underset{\sim}{r}_n|\underset{\sim}{r}') \, S(\underset{\sim}{r}',t') \, dt' \, d\underset{\sim}{r} \quad . \tag{327}$$

The reason for the split integral in this equation will become clear later.

For any time $t' \leq t_{n-1}$, we have from the Markov assumption

$$p(\underset{\sim}{r}_n|\underset{\sim}{r}_{n-1},\underset{\sim}{r}') = p(\underset{\sim}{r}_n|\underset{\sim}{r}_{n-1}) \quad . \tag{328}$$

Thus, from the general relationship

$$f(X_n|X_m) = \int f(X_n|X_\ell, X_m)\ f(X_\ell|X_m)\ dX_\ell \quad , \tag{329}$$

where X_n, X_ℓ, and X_m are any three random variables with probability density functions f, it follows from Eq. (328) that

$$p(\underset{\sim}{r}_n|\underset{\sim}{r}') = \int p(\underset{\sim}{r}_n|\underset{\sim}{r}_{n-1})\ p(\underset{\sim}{r}_{n-1}|\underset{\sim}{r}')\ d\underset{\sim}{r}_{n-1} \quad . \tag{330}$$

Thus, $p(\underset{\sim}{r}_n|\underset{\sim}{r}')$ satisfies a Chapman-Kolmogoroff type of equation, even through $\underset{\sim}{r}'$ can be the particle position anywhere on the continuous time axis prior to t_{n-1}.

Using Eq. (324), we can express the first term in Eq. (327) in the form

$$\int p(\underset{\sim}{r}_n|\underset{\sim}{r}_0)\ \langle c(\underset{\sim}{r}_0,t_0)\rangle\ d\underset{\sim}{r}_0 = \int p(\underset{\sim}{r}_n|\underset{\sim}{r}_{n-1}) \int p(\underset{\sim}{r}_{n-1}|\underset{\sim}{r}_0)\ \langle c(\underset{\sim}{r}_0,t_0)\rangle\ d\underset{\sim}{r}_0\ d\underset{\sim}{r}_n \quad . \tag{331}$$

Similarly, Eq. (330) permits the second term in Eq. (327) to be written as

$$\iint_{t_0}^{t_{n-1}} p(\underset{\sim}{r}_n|\underset{\sim}{r}')\ S(\underset{\sim}{r}',t')\ dt'\ d\underset{\sim}{r}' = \int p(\underset{\sim}{r}_n|\underset{\sim}{r}_{n-1}) \cdot \iint_{t_0}^{t_{n-1}} p(\underset{\sim}{r}_{n-1}|\underset{\sim}{r}')\ S(\underset{\sim}{r}',t')\ dt'\ d\underset{\sim}{r}'\ d\underset{\sim}{r}_{n-1} \quad . \tag{332}$$

Combining Eqs. (331) and (332) and comparing the result with Eq. (327) for $\langle c(\underset{\sim}{r},t_{n-1})\rangle$, we conclude finally that, by virtue of the Markov property, Eq. (327) is equivalent to

$$\langle c(\underset{\sim}{r},t_n)\rangle = \int p(\underset{\sim}{r},t_n|\underset{\sim}{r}',t_{n-1})\,\langle c(\underset{\sim}{r}',t_{n-1})\rangle\, d\underset{\sim}{r}' + \iint_{t_{n-1}}^{t_n} p(\underset{\sim}{r},t_n|\underset{\sim}{r}',t')\, S(\underset{\sim}{r}',t')\, dt'\, d\underset{\sim}{r}' \quad . \tag{333}$$

This is the discrete-time, continuous-space diffusion equation.

From the modeling standpoint, Eq. (333) has several very useful assets. The first is that it allows concentrations at time t to be calculated from those at time t-Δt and from the source emissions that have occurred during the interval Δt just prior to t. This is in contrast to Eq. (319) or to the puff model, for example, which requires an integration over the entire period t_0 - t to obtain the concentrations at time t. The second advantage of Eq. (333) is that it possesses unlimited spatial resolution. As we pointed out earlier, this property is essential in modeling the microscale concentration distribution. The third advantage of Eq. (333) is that finite differencing techniques are not required to evaluate it. In fact, all of the integrals in this equation can be evaluated analytically when the concentration distribution $\langle c(\underset{\sim}{r},t_{n-1})\rangle$ is expressed in series form. This advantage circumvents the problems, often associated with differencing techniques, of computational stability and of the imposition of artificial boundary conditions.

2. Development of A Microscale Model of Nonlinear Pollutants Based on The Discrete-Time, Continuous-Space Equation

Our aim is to use Eq. (333) as the basis of a microscale model. In this section, we demonstrate how this might be accomplished, using as the example a single nonlinear species c whose microscale variations c" are governed by Eq. (291). The formal relationship between Eqs. (333) and (291) is quite complicated, and since the details are not important to the present analyses, we outline the relationship only briefly below.

First, we note that Eq. (219) is of the form

$$\frac{\partial c''}{\partial t} + Lc'' = -k\left(a + bc'' + c''^2\right) + S'' \quad , \tag{334}$$

where

$$a = -\widetilde{c''^2} + \langle c'^2 \rangle'' \quad , \tag{335a}$$

$$b = 2\tilde{c} \quad . \tag{335b}$$

Consequently, if S" were zero and if c" were initially uniformly distributed in space (so that $\mathcal{L}c'' = 0$), then the chemistry alone would cause c" to change in time, and we would have

$$c''(t) = -\tilde{c} + q\left[\frac{d + 1}{1 - d}\right] \quad , \tag{336}$$

where

$$q = (\tilde{c}^2 - 4a)^{1/2} \tag{337a}$$

$$d = e^{-2kqt}\left[\frac{c_0'' + \tilde{c} - q}{c_0'' + \tilde{c} + q}\right] \tag{337b}$$

and where $c_0'' = c''(0)$. Recall the form [Eq. (321)] that the kernel p acquires in situations where the scalar quantity decays at the linear rate

$$\frac{dc}{dt} = -k(t)c.$$

We anticipate, therefore, that if a nonlinear decay of the form found in Eq. (334) occurs, then the kernel p entering in Eq. (335) can be approximated by

$$p(\underset{\sim}{r},t|\underset{\sim}{r}',t') = p'(\underset{\sim}{r},t|\underset{\sim}{r}',t')\left[-\frac{\tilde{c}}{c_0''} + \frac{q}{c_0''}\left(\frac{d + 1}{1 - d}\right)\right] \quad , \tag{338}$$

where, as in the case of Eq. (321), p' is the solution of the equation

$$\frac{\partial p'}{\partial t} + \mathcal{L}p' = \delta(\underset{\sim}{r} - \underset{\sim}{r}')\,\delta(t - t') \quad . \tag{339}$$

We now state without proof that the equation

$$c''(\underset{\sim}{r},t_n) = \int p'(\underset{\sim}{r},t_n|\,\underset{\sim}{r}',t_{n-1})\left[-\tilde{c}(\underset{\sim}{r}',t_{n-1}) + q\left(\frac{d+1}{1-d}\right)\right]d\underset{\sim}{r}'$$

$$+\iint_{t_{n-1}}^{t_n} p'(\underset{\sim}{r},t_n|\,\underset{\sim}{r}',t')\,S(\underset{\sim}{r}',t')\left[-\tilde{c}(\underset{\sim}{r}',t')\right.$$

$$\left. + q\left(\frac{d+1}{1-d}\right)\right]\left[c''(\underset{\sim}{r}',t')\right]^{-1} dt'\,d\underset{\sim}{r}' \qquad (340)$$

becomes equivalent to Eq. (291) in the limit as $\Delta t = t_n - t_{n-1}$ approaches zero. In Eq. (340), q and d are functions of the time and space variables that appear to the right of the vertical bar in the kernel p. Thus, we can say that Eq. (340) provides a consistent representation of Eq. (291) inasmuch as the solution of Eq. (340) can be made arbitrarily close to that of Eq. (291) by making the time step Δt suitably small. We should hasten to add, however, that the size of Δt is restricted by Eq. (326); so the equivalence of Eqs. (340) and (291) can be realized only by scaling the time axis with some value T and then making $\Delta t^* = \Delta t/T$ suitably small by making T sufficiently large. The implication of this is that temporal resolution is lost as Eq. (340) is made to approach Eq. (291). Nevertheless, for all practical purposes, Eq. (340) will serve well as the working equation for a model of c".

Consider now the evaluation of Eq. (340). We demonstrate our proposed technique for solving this equation by considering only the first integral on the right side. To simplify the analysis further, we assume homogeneous, stationary turbulence and restrict our attention to a one-dimensional problem. Albeit highly simplified, this case is adequate to demonstrate the essential features of our technique.

Under the conditions that we have imposed upon the turbulence characteristics, the kernel p' becomes

$$p'(x,t_n|x',t_{n-1}) = \left[(2\pi)^{1/2}\right]^{-1} \exp\left[-\frac{(x-\bar{x})^2}{2\sigma^2}\right] , \tag{341}$$

where

$$\bar{x} = x' + \bar{u}\Delta t \tag{342}$$

and $\bar{u}$ and σ are functions of x' and t_{n-1}.

Turning next to the definition [Eq. (337a)] of the parameter q that enters in Eq. (340), we see that two of the variables upon which it depends, namely, $\tilde{c}$ and c''^2, spatially averaged quantities. Since the spatial region of concern to us in the microscale model is only as large as several grid cells, it is not unreasonable to treat these two quantities as constants. This assumption is also supported by observational studies of mean concentration variations in both the horizontal and vertical directions. The third quantity entering into the definition of q--namely, $\langle c'^2 \rangle''$--is variable over the microscale region, but for simplicity we also regard it as essentially constant. Combining all of the above assumptions in Eq. (340), we obtain

$$c''(x,t_n) = -\int \tilde{c}(x',t_{n-1})\, p'(x,t_n|x',t_{n-1})\, dx'$$

$$+ q\int\left[(2\pi)^{1/2}\sigma\right]^{-1} \exp\left[-\frac{(x-\bar{x})^2}{2\sigma^2}\right]\left(\frac{c''_{n-1}{}^{\alpha} + \tilde{c}_{\alpha} + q}{c''_{n-1} + \tilde{c} + q_{\alpha}}\right) dx' , \tag{343}$$

where

$$c''_{n-1} = c''(x',t_{n-1}) , \tag{344a}$$

$$\alpha = \frac{e^{-2kq\Delta t} + 1}{1 - e^{-2kq\Delta t}} . \tag{344b}$$

The first term on the right side of Eq. (343) is clearly equal to $\tilde{c}(x,t_n)$ [Eq. (333)].

Now let $c''(x,t_n)$ be represented by the power series

$$c''(x,\, t_n) = \sum_{m\,=\,0}^{\infty} a_{n,m} x^m \quad . \tag{345}$$

The last term in parentheses in Eq. (343) can now be written in the form

$$\left(\cdots\right) = \frac{1}{\beta_0} \sum_{m\,=\,0}^{\infty} d_{n-1,m} x'^m \quad , \tag{346}$$

where

$$\beta_0 = a_{n-1,0} + \tilde{c} + q\alpha \quad , \tag{347}$$

$$d_{n-1,0} = \alpha a_{n-1,0} + \alpha\tilde{c} + q \quad , \tag{348}$$

$$d_{n-1,m} = \alpha a_{n-1,m} - \frac{1}{\beta_0} \sum_{k\,=\,1}^{m} d_{n-1,m-k} a_{n-1,k} \quad . \tag{349}$$

Substituting Eq. (346) into Eq. (343), we obtain

$$c''(x,t_n) + \tilde{c}(x,t_n) = c(x,t_n) = \frac{q}{\beta_0 \sqrt{2\pi}\,\sigma} \sum_{m\,=\,0}^{\infty} d_{n-1,m} \cdot \int x'^m \exp\left(-\frac{(x - x' - \bar{u}\Delta t)^2}{2\sigma^2}\right) dx' \quad . \tag{350}$$

Changing the integration variable to

$$\xi = x' + \bar{u}\Delta t - x \quad ,$$

we obtain

$$c(x,t_n) = \frac{q}{\beta_0\sqrt{2\pi}\,\sigma} \sum_{m=0}^{\infty} d_{n-1,m} \int (\xi - \bar{x})^m \, e^{-\xi^2/2\sigma^2} \, d\xi \quad , \tag{351}$$

where

$$\bar{x} = \bar{u}\Delta t - x \quad . \tag{352}$$

Equation (351) can be written in the equivalent form

$$c(x,t_n) = \frac{q}{\beta_0\sqrt{2\pi}\,\sigma} \sum_{m=0}^{\infty} d_{n-1,m} \sum_{k=0}^{m} \frac{m!(-\bar{x})^{m-k}}{k!(m-k)!} \int \xi^k \, e^{-\xi^2/2\sigma^2} \, d\xi \quad . \tag{353}$$

Evaluating the integral in this expression, we obtain

$$c(x,t_n) = \frac{q}{\beta_0} \sum_{m=0}^{\infty} d_{n-1,m} \sum_{k=0}^{m/2} \frac{m!(-\bar{x})^{m-2k}\sigma^{2k}}{(2k)!(m-2k)!}(2k-1)!! \quad , \tag{354}$$

where

$$(2k-1)!! = 1\cdot3\cdot5\ldots(2k-1)$$

and where $\Sigma_{k=0}^{m/2}$ denotes summation over all k that do not exceed m/2. Upon expanding the right side of Eq. (354) and collecting like powers of x, and upon writing the left side of this equation, i.e., $c(x,t_n)$, in its series form

$$c(x,t_n) = \sum_{m=0}^{\infty} d_{n,m} x^m + \tilde{c}(x,t_n)$$

and grouping these terms with those of the right side of Eq. (354), we obtain the set of equations for the coefficients $d_{n,m}$. The desired mircoscale field $c''(x,t_n)$ is now in the form

$$c''(x,t_n) = \sum_{m=0}^{M} a_{n,m} x^m$$

where

$$a_{n,m} = f_m (a_{n-1,m})$$

and the f_m are known functions. The modeling of c" is thus reduced simply to the algebraic manipulation of coefficients in a series expansion. No differential equations or integrals require manipulation.

As we mentioned earlier, this modeling approach has not been developed or tested heretofore. Consequently, considerable work remains to be done in producing a working microscale model for photochemical pollutants. We hope, however, to make considerable progress toward that goal in our continuing model development program.

VI SIMULATION OF BUOYANT PLUMES IN THE PLANETARY BOUNDARY LAYER

A. INTRODUCTION

Up to this point, all of the work presented in this volume has pertained to passive scalar quantities, that is, to scalars that do not interact dynamically with the fluid. Under this condition, the mathematical problems of diffusion modeling are greatly simplified because the effects of the turbulence on the scalar can be described in terms of quantities, (namely, the turbulent diffusivity) that are properties of the flow. It is this assumption that made it possible for us in Chapter II to derive profiles for the diffusivity K_z that were independent of the character of the diffusing substance.

In air pollution studies involving emissions from power plants, oil refineries, and other sources in which large quantities of both heat and pollutants are discharged simultaneously, the "passive scalar" assumption is not valid on the microscale, i.e., over distances up to about 1 km from the source. The reason for this is that the heat exhausted along with the pollutants produces buoyancy forces, which enchance the vertical transport of the pollutant material. The result is the so-called plume rise phenomenon, which has been studied analytically by Briggs (1968) and others. In most of these investigations, attempts were made to describe the plume rise using semi-empirical formulas. Some of these formulas were found to work reasonably well under certain special circumstances, but not in others. Apparently, there is no formulation that is applicable to a wide range of conditions. In this chapter, we outline a model that we hope will fill this need.

The starting point of our simulation is the Lagrangian diffusion equation introduced in Chapter II [Eq. (16)]:

$$\langle c(\underset{\sim}{r},t)\rangle = \iint_0^t p(\underset{\sim}{r},t|\underset{\sim}{r}',t)\, S(\underset{\sim}{r}',t')dt'd\underset{\sim}{r}' \quad .$$

Our approach is to use the planetary boundary layer model or Deardorff in conjunction with our own model of buoyant particle motions in turbulent fluid to derive the probability density junction $p(\underset{\sim}{r},t|\underset{\sim}{r}',t')$ that would be required in Eq. (16) to describe the mean concentration disturbation in a buoyant plume. In this chapter, we outline our particle model and describe how it will be used with Deardorff's calculations to achieve the desired results.

B. CALCULATION OF THE PROBABILITY DENSITY $p(\underset{\sim}{r},t|\underset{\sim}{r}',t')$

The density function p describes the ensemble properties of particle displacements in the turbulent fluid. To obtain this function from Deardorff's data, which represent only a single realization of an infinitely large ensemble, we must invoke ergodic theory. The details of this theory are not presented here. Suffice it to say that the stationarity and homogeneity (in horizontal planes) of the turbulence simulated by Deardorff's model are amenable to the application of ergodic theory in the manner we require.

An additional consequence of stationarity and homogeneity is that p has the property

$$p(\underset{\sim}{r},t|\underset{\sim}{r}',t') = p(\xi,\eta,z,z',\tau) \quad , \tag{355}$$

where

$$\xi = x - x',$$
$$\eta = y - y',$$
$$\tau = t - t',$$
$$\underset{\sim}{r} = (x,y,z).$$

Thus, p is a function of the horizontal projection of the distance to the release point--but not of the positions of the source or receptor separately--and of the travel time τ--but not of the clock time t or release time t' separately. Consequently, we can calculate p in the following way.

For a given release height z', say $z' = z_1$, we release a particle from each grid point on the horizontal plane at height z_1 at the initial instant t_0 when the data begin. If there are N grid points in each horizontal plane, then N particles will be released. We allow each particle to move forward in time under the action of the forces exerted upon it by the turbulent fluid. By tracking each particle, we create an ensemble of N particle trajectories, each of duration T, from which the density function $p(\xi,\eta,z,z_1,\tau)$, $0 < \tau < T$, can be computed by conventional techniques [see, for example, Bendat and Piersol (1968)]. Here, T denotes the length of the interval during which data from Deardorff's model are available. In our early work, T corresponds roughly to 1 hour in real time.

For the function p derived by this process to be applicable to a given dispersion problem--for example, the diffusion and transport of pollutants from a stack of height H, diameter D, exhaust velocity V_x, and temperature θ_s--the ensembel of particle trajectories on which the function p is based must adequately reflect the behavior of particles released under such conditions. In the example just cited, it is clear that wind shear, buoyancy, and other phenomena have strong effects on the particle motions. Furthermore, as a result of the proximity of the particles to one another at their time of release, particle interactions affect drag forces, heat exchange between the particles, and the atmosphere, and similar factors. Thus, unless all of these mechanisms are properly modeled in the simulation of the ensemble of particle trajectories, the density function p based on this ensemble will lead to erroneous estimates of the mean concentration when used in the $\langle c \rangle$ equation.

Hinze (1959) has reveiwed the theory relevant to the prediction of the motion of discrete, bouyant particles in a turbulent fluid. In the remaining sections, we use this theory to formulate a model that, using Deardorff's data as input, can simulate the trajectory ensembeles required

to study the diffusion of any type of pollutant (e.g., heat, moisture, gases) released under any conditions in the planetary boundary layer.

C. MATHEMATICAL BASIS OF THE TRAJECTORY SIMULATION MODEL--PRELIMINARY DESIGN

1. The Particle Momentum Equation

Let (u,v,w) represent the velocity $\underset{\sim}{V}$ of the scalar (pollutant) particle with respect to a fixed Eulerian frame, and let (u_e,v_e,w_e) represent the average (spatial) velocity $\underset{\sim}{V}_e$ of the fluid in the immediate vicinity of the given particle, i.e., the local environmental velocity. We distinguish between the "environmental" velocity $\underset{\sim}{V}_e$ and the ambient fluid velocity $\underset{\sim}{V}_f$, because, as a result of the presence of large numbers of scalar particles, the local velocity of the fluid that a particular particel "sees" will generally differ from $\underset{\sim}{V}_f$. Also, let T and T_e represent the particle and environment temperatures, respectively. Provided that the particles are sufficiently small, the momentum equation governing their motion can be written in the form [see Hinze (1959)]

$$\frac{d}{dt}\underset{\sim}{V}(\underset{\sim}{a},t) = -\alpha\left[\underset{\sim}{V}(\underset{\sim}{a},t) - \underset{\sim}{V}_e\left(X(\underset{\sim}{a},t),t\right)\right] - \beta\underset{\sim}{g} + \gamma\frac{d}{dt}\underset{\sim}{V}_e\left(X(\underset{\sim}{a},t),t\right) \quad , \tag{356a}$$

where

$$\alpha = \frac{9\nu}{r^2\left[2\left(\frac{\rho}{\rho_e}+1\right)\right]} \quad , \tag{356b}$$

$$\beta = \frac{\frac{\rho}{\rho_e}-1}{\frac{\rho}{\rho_e}+\frac{1}{2}} \quad , \tag{356c}$$

$$\gamma = \frac{3}{\frac{2\rho}{\rho_e}+1} \quad , \tag{356d}$$

and

r = the particle radius,
ρ = the particle density,
ν = the kinematic viscosity of the environmental fluid,
ρ_e = the density of the environmental fluid,
$\underset{\sim}{a}$ = the release points of the particle in ouestion,
$\underset{\sim}{X}(\underset{\sim}{a},t)$ = the position of the particle at time t
$\underset{\sim}{g}$ = the gravity vector,

and

$$\frac{d}{dt} = \frac{\partial}{\partial t} + \underset{\sim}{V} \cdot \nabla \quad . \tag{357}$$

The second term on the right side of Eq. (356a) represents a Stokes drag force on the particle. For this approximation to be valid, the Reynolds number of the particle with respect to the particle radius r and relative velocity $|\underset{\sim}{V} - \underset{\sim}{V}_e|$ must be on the order of unity or smaller.

The last term on the right side of Eq. (356a) represents the acceleration of the environmental fluid relative to the axis of the moving particle. In cases such as those of interest to us, where the scalar and fluid particles are dynamically quite similar, accelerations of the one relative to the other are sufficiently small that the last term in Eq. (356a) can be neglected. We assume further that the response time α^{-1} of the particle is so small relative to the time scale of changes in $\underset{\sim}{V}_e$ that the quasi-steady-state relation

$$\frac{d}{dt}\underset{\sim}{V}(\underset{\sim}{a},t) \simeq 0 \tag{358}$$

holds at all times. Under these two assumptions, we obtain from EQ. (356a)

$$u = u_e \quad , \tag{359a}$$

$$v = v_e \quad , \tag{359b}$$

$$w = w_e - \frac{2r^2 g}{9\nu}\left(\frac{\rho}{\rho_e} - 1\right) \quad . \tag{359c}$$

In view of the absence of horizontal forces on the particles other than those exerted by the fluid, we assume that the horizontal components of the velocities of all particles are equal at all times to the corresponding velocities of the local ambient fluid. That is, we assume that

$$\begin{aligned} u &= u_f \quad , \\ v &= v_f \quad , \end{aligned} \tag{360}$$

where u_f and v_f are the velocities given by Deardorff's data.

It is more convenient to work with potential temperature than with densities because the former are given for the fluid by Deardorff's data. Using the gas law and the definition of potential temperature, i.e.,

$$\theta = T\left(\frac{1000}{p}\right)^{R/c_p} \quad ,$$

where p is pressure in millibars, we can convert Eq. (359c) into the form

$$w = w_e + \frac{2r^2 g}{9\nu}\left(\frac{\theta - \theta_e}{\theta}\right) \quad . \tag{361}$$

Later, we derive the equation governing the particle temperature θ that can be used in conjunction with Eq. (361) to obtain the particle's vertical velocity component w. However, to render Eq. (361) solvable, we must first express w_e in terms of the known ambient fluid velocity component w_f.

Toward this end, we consider two limiting cases. First, in the limit as the travel time becomes large and the initial cloud of scalar particles becomes so dispersed that each particle is surrounded mainly by ambient fluid particles, we have

$$\lim_{t\to\infty} w_e = w_f \quad . \tag{362}$$

Recall that w_e represents the velocity of the environmental fluid, composed of both scalar and ambient fluid particles, in the immediate vicinity of the given scalar particle. At the other extreme, where the travel time τ is near zero, the entire collection of scalar particles can be envisaged as a buoyant jet of diameter D (equal to that of the source diameter) issuing into the ambient fluid. The velocity of each particle can be assumed to be equal to that of the jet and can be approximated by empirical and theoretical means. For the present, however, we assume that initially the particles form a spherical cloud of diameter D. This approximation might apply under very unstable conditions. The initial velocity of each particle is now assumed to be equal to that of the entire cloud and is to be calculated by assuming a drag force on the cloud of the form

$$|D| = \frac{\frac{1}{2}\pi C_D \rho \left(\frac{D^2}{4}\right) u_\infty^2}{\frac{4}{3}\pi\rho\left(\frac{D^3}{8}\right)}$$

$$= \frac{3}{4}\left(\frac{C_D}{D}\right) u_\infty^2 \quad , \tag{363}$$

where C_D is the drag coefficient of the spherical cloud and u_∞ is the speed of the cloud relative to the ambient fluid. Invoking the quasi-steady-state assumption as before, we can equate the drag force D and the buoyancy force B, where

$$|B| = g\,\frac{\Theta - \Theta_e}{\Theta_e} \quad , \tag{364}$$

to obtain

$$(w - w_f)^2 = \frac{4D}{3C_D} |B|$$

or

$$w = w_f + \text{sign}(B) \left(\frac{4D|B|}{3C_D}\right)^{1/2} \quad . \tag{365}$$

Upon substituting this expression into the left side of Eq. (361), we can find the effective environmental velocity w_e in the limit as $\tau \to 0$. We obtain

$$\lim_{\tau \to 0} w_e = w_f + \text{sign}(\theta - \theta_e)\left(\frac{4Dg|\theta - \theta_e|}{3C_D\theta_e}\right)^{1/2} - \frac{2r^2 g}{9\nu}\left(\frac{\theta - \theta_e}{\theta}\right) \quad . \tag{366}$$

This, then, is the environmental velocity component w_e in the initial instance where the cloud of scalar particles behaves as a sphere moving through the ambient fluid. From the two limiting cases given in Eqs. (362) and (366), we surmise that w_e can be expressed in the general form

$$w_e = w_f + \phi(\tau)\, G(\theta,\theta_e) \quad , \tag{367}$$

where

$$G(\theta,\theta_e) = \text{sign}(\theta - \theta_e)\left(\frac{4Dg|\theta - \theta_e|}{3C_D\theta_e}\right)^{1/2} - \frac{2r^2 g}{9\nu}\left(\frac{\theta - \theta_e}{\theta}\right) \tag{368}$$

and where $\phi(0) = 1$, $\lim_{\tau \to \infty} \phi(\tau) = 0$. (In the general case, $G(\theta,\theta_e)$ represents the velocity of the buoyant plume as it emerges from its source.) The rate at which $\phi(\tau)$ change with travel time depends on how rapidly the initial

cloud of particles becomes dispersed, or, in other terms, how rapidly the population of particles surrounding any given scalar particle becomes saturated with ambient fluid particles. We attempt in a later section to derive an explicit expression for ϕ based on turbulence properties. Thus, from Eqs. (361) and (367), we arrive at the final form of the expression for w:

$$w = w_f + \phi(\tau)\, G(\theta,\theta_e) + \frac{2r^2 g}{9\nu\theta}\,(\theta \quad \theta_e) \quad . \tag{369}$$

The next task is to derive the equation governing the temperature θ.

2. The Particle Temperature Equation for Dry Plumes

As long as there is a difference between the particle temperature θ and the ambient fluid temperature θ_f, not only is a buoyancy force exerted on the particle, but also a heat exchange between the particle and fluid acts to eliminate any temperature differences. This heat flux can be expressed quantitatively by

$$q = -\bar{h}A(\theta - \theta_e) \quad , \tag{370}$$

where $\bar{h}$ is the heat transfer coefficient of the particle and A is the particle's surface area. The temperature change resulting from the heat flux q is

$$\frac{d\theta}{dt} = -\frac{\bar{h}A(\theta - \theta_e)}{\rho V_p C_p} \quad , \tag{371}$$

where V_p is the particle volume and C_p is the specific heat capacity (in units of energy/mass/^{o}K). For spheres in the Reynolds number range $1 < R_e < 25$, $\bar{h}$ has the form (Kreith, 1966)

$$\bar{h} = aC_p u_\infty \rho_e \quad , \tag{372}$$

where

$$a = \frac{2.2\nu}{2u_\infty r} + \frac{0.48\nu^{1/2}}{(2u_\infty r)^{1/2}} \quad . \tag{373}$$

Combining Eqs. (372) and (371), we obtain

$$\frac{d\Theta}{dt} = \frac{3a}{r}(w - w_e)\left(\Theta - \frac{\Theta^2}{\Theta_e}\right) \quad . \tag{374}$$

Here it is necessary to express Θ_e in terms of Θ_f. For this purpose, we consider the two limiting cases that we considered earlier in relating w_e to w_f. First, in the limit, as the travel time becomes very large, Θ_e approaches Θ_f because each scalar particle "sees" an environment composed almost totally of ambient fluid particles. We can therefore write

$$\lim_{\tau\to\infty} \Theta_e = \Theta_f \quad . \tag{375}$$

In the other limit, when $\tau \approx 0$, we envisage as before that the entire collection of scalar particles comprise a spherical cloud of diameter D and that this cloud exchanges heat with its environment at the same rate as a rigid sphere would under identical conditions. (In the general case, we envisage the particles as comprising a buoyant jet, but we do not consider this case here.) Moreover, we assume that internal mixing in the cloud is sufficient to result in an equi-partitioning among all of the particles of the total heat exchanged. In this case, we have

$$\lim_{\tau\to 0} \frac{d\Theta}{dt} = -\bar{h}\,\frac{\left(\frac{4\pi D^2}{4}\right)(\Theta - \Theta_f)}{\rho c_p\left(\frac{4}{3}\right)\left(\frac{\pi D^3}{8}\right)} \quad , \tag{376}$$

or

$$\lim_{\tau \to 0} \frac{d\Theta}{dt} = - \frac{6\bar{h}(\Theta - \Theta_f)}{\rho C_p D} \quad . \tag{377}$$

For spheres with Reynolds numbers in the range $25 < R_e < 10^5$, the heat transfer coefficient is given to good approximation by (Kreith, 1966)

$$\bar{h} = \frac{0.37 k_f}{D} \left(\frac{u_\infty D}{\nu} \right)^{0.6} \quad , \tag{378}$$

where k_f is the thermal conductivity of the fluid (units of energy/time/meter/$^\circ$K). Combining Eqs. (377) and (378), we obtain

$$\lim_{\tau \to 0} \frac{d\Theta}{dt} = - \frac{2.2 k_f u_\infty^{0.6} (\Theta - \Theta_f)}{\rho C_p D^{1.4} \nu^{0.6}} \quad ; \tag{379}$$

and by equating this expression and Eq. (374), we obtain the effective environmental temperature Θ_e at the initial instant of release:

$$\lim_{\tau \to 0} \Theta_e = \Theta \left[1 + \frac{2.2 r k_f (\Theta - \Theta_f)}{3 a \rho C_p \Theta (w - w_f)^{0.4} D^{1.4} \nu^{0.6}} \right]^{-1} \quad . \tag{380}$$

Since both w_e and Θ_e are uniquely determined once the populations of scalar and ambient fluid particles surrounding any given scalar particle have been prescribed, we assume that the transition of Θ_e from its initial value [Eq. (380)] to its final form [Eq. (375)] is describable in terms of the function ϕ used earlier with w_e. In particular, we assume that

$$\Theta_e = \Theta \phi(\tau) \left[1 + \frac{2.2 r k_f (\Theta - \Theta_f)}{3 a \rho C_p \Theta (w - w_f)^{0.4} D^{1.4} \nu^{0.6}} \right]^{-1} + [1 - \phi(\tau)] \Theta_f \quad . \tag{381}$$

This equation, together with Eqs. (374), (367), and (369), forms a closed system of equations that can be solved for the temperature Θ of the particle and vertical velocity component w as a function of travel time τ and the ambient fluid conditions Θ_f and w_f described by Deardorff's data. In short, we now have model equations that we can use to simulate the trajectories of dry particles of any type in a turbulent fluid. (The derivation of the corresponding equations for vapor plumes is currently in progress.) All that remains to complete the model is to derive a suitable functional form for $\phi(\tau)$.

3. The $\phi(\tau)$ Equation

As defined, $\phi(\tau)$ has the limiting values

$$\lim_{\tau \to 0} \phi(\tau) = 1 \quad , \tag{382a}$$

$$\lim_{\tau \to 0} \phi(\tau) = 0 \quad . \tag{382b}$$

In physical terms, $\phi(\tau)$ represents the fractional population of scalar particles within a distance of several radii of a given scalar particle. This suggests that ϕ is equivalent to the mean particle concentration in an expanding cluster. Under the action of turbulence in the inertial subrange, a cluster of particles expands at a rate given by

$$\frac{d\langle \ell^2 \rangle}{d\tau} = \frac{20}{3} \varepsilon^{2/3} \ell_0^{2/3} \tau \quad , \tag{383}$$

where ε is the energy dissipation rate per mass of fluid, ℓ_0 is the initial diameter of the cluster, τ is the travel time, and $\langle \ell^2 \rangle$ denotes the mean square cluster diameter after a travel time τ. Equation (383) is valid only as long as $\langle \ell^2 \rangle^{1/2}$ is within the range of eddy sizes that comprise the inertial subrange and only as long as a true inertial subrange exists.

The latter condition may not always be fulfilled in some problems of interest to us where significant turbulent energy is created by the particle cloud itself. Indeed, observations reveal that under neutral and stable atmospheric conditions, the turbulent energy within the plumes produced by large power plants is often significantly greater than that in the atmosphere just outside the plume. Under these conditions, it will be necessary to resort to the available empirical and theoretical knowledge of buoyant jets to derive a saitable approximation for $\phi(\tau)$. Nevertheless, in those cases in which Eq. (383) holds, the mean cloud diameter d at time τ is given by

$$d(\tau) = \left[D^2 + \frac{10}{3}\,\varepsilon^{2/3}\,D^{2/3}\,\tau^2\right]^{1/2} \quad , \tag{384}$$

where D denotes the initial cloud diameter. This expression holds only as long as $d \lesssim 10D$.

If the initial concentration of particles in the cloud is unity, it follows from the considerations presented above that

$$\phi(\tau) = \frac{\frac{4}{3}\,\pi\,\frac{D^3}{8}}{\frac{4}{3}\,\pi\left(D^2 + \frac{10}{3}\,\varepsilon^{2/3}\,D^{2/3}\,\tau^2\right)^{3/2}} \quad ,$$

$$= \left(1 + \frac{10}{3}\,\varepsilon^{2/3}\,D^{-4/3}\,\tau^2\right)^{-3/2} \quad . \tag{385}$$

We assume that by the time $\langle \ell^2 \rangle^{1/2}$ is outside the inertial subrange, or $d > 10D$, and Eq. (385) ceases to hold, either the mignitude of ϕ has fallen to a value near zero or $\langle \ell^2 \rangle^{1/2} \sim \Delta X$, where ΔX is a measure of the grid size in Deardorff's model. In the latter case, the growth rate of the cloud can be estimated explicitly from the computed particle trajectories.

VII SUMMARY

For the reader's convenience, we summarize here the major points presented in each of the six previous chapters.

A. CHAPTER I

In this chapter, we introduced the term "microscale" to refer to all phenomena whose space or time scales are too small to be resolvable explicitly and deterministically in grid models of urban pollution. Such small features result because of turbulence and finite differencing techniques. Those produced by the former include the turbulent velocity fluctuations themselves, usually denoted by $\underset{\sim}{u}'$, and the concentration flucutations c' generated by $\underset{\sim}{u}'$. Both of these microscale features affect the spatial and temporal behavior of the evolution of the mean concentrations of photochemical pollutants. No exact mathematical expressions have yet been found that can describe these effects in generalized situations. Consequently, an important problem in pollution modeling is the development of an approximate description of these phenomena that, under most conditions of interest, will be as accurate as the data upon which the model calculations are to be based. Chapters II, III, and VI address these problem areas.

The use of finite differencing techniques in diffusion modeling gives rise to the microscale phenomenon that we have termed the SSV, or subgrid-scale concentration variation. This feature occurs because the spatial variations that exist in the concentration distribution near point and line sources, such as power plant stacks or highways, are of much too small a scale to be resolved by the grid meshes used in urban pollution models. We showed that the SSV can affect the grid-averaged concentrations of photochemical pollutants in much the same way that the turbulence-induced concentration fluctuations can influence the time mean concentration. We also pointed out that the SSV can complicate the use

of pollutant concentration values predicted by a simulation model: The concentration levels observed at a fixed point will differ from the spatially averaged concentration predicted at that point as long as the SSV is not zero. Model validation studies and concentration extrema forecasts are two examples of applications in which this problem arises. Chapters IV and V addressed all aspects of the SSV microscale effects.

B. CHAPTER II

In this chapter, we demonstrated how Lagrangian diffusion theory can be implemented using numerical turbulence models. Using this technique, we were able to derive expressions for the distribution of the mean concentration of passive material issuing from a continuous point source in the planetary boundary layer. We referred to these distributions, shown in Figures 8(a) and 9(a), as the numerico-empirical (NE) solutions of the Lagrangian equation. Inasmuch as the data sets on which these solutions were based were rather small, the results presented in Chapter II are only tentative. Future studies will attempt to achieve greater accuracy and will address the important questions of how the concentrations are affected by changes in source height and atmospheric stabilities (other than those treated here) and by changes to other source types, such as area or line sources.

Proceeding under the assumption that the accuracies of the present NE solutions are at worst comparable to those of available empirical data, we used these solutions as standards for assessing the accuracies of the three major diffusion models: the diffusion equation and the Gaussian puff and plume formulas. We devoted subsequent work to optimizing the performances of these models by adjusting the functional forms of the free parameters in each model such that the resulting predictions were in closest overall agreement with the NE solutions. These "optimal" parameters, i.e., diffusivities K_z and dispersion coefficients σ_z and σ_x, are summarized in functional form in Table 2. With regard to the accuracies of the optimal models, we note the following:

- Of the three models, the diffusion equation is by far the superior one. Errors are generally on the order of 20 percent, except at points near the source under neutral conditions in which case much larger discrepancies are observed [see Figures 8(b) and 9(b)].
- Relative to the plume formula, the Gaussian puff equation is a slightly superior model; but, in quantitative terms, neither provides an acceptable description of atmospheric diffusion under neutral stability conditions, at least in the problem considered in Chapter II. Both models tend to overpredict ground-level concentrations arising from elevated sources. Errors of 100 percent are prevalent, and in isolated areas they are much larger. In the particular problem treated, the accuracies of the optimal models were acceptable under unstable conditions (see Figures 18 and 19).

Considering the Gaussian puff and plume models in general, we note the following points:

- Spatial concentration distributions in the planetary boundary layer are decidedly non-Gaussian.
- The Pasquill-Gifford data commonly used in the plume forumla are not applicable to emissions from elevated sources unless some allowance is made for wind shear effects. When such modifications are made, they greatly improve the accuracy of the plume formula for elevated sources [see Figure 13(b), as compared with Figure 18(b)].

The optimal diffusivity, dispersion coefficient, and wind shear profiles presented in Table 2 were implemented in the form of FORTRAN function routines. These routines can be used in place of the corresponding variable names in existing diffusion models to achieve results that are compatible with the predictions of Deardorff's boundary layer model.

C. CHAPTER III

Using empirical data, we showed (see Figure 28) that concentration fluctuations generated by turbulence can dominate the temporal behavior of the mean concentration of materials that undergo nonlinear chemical reactions. Although several previous investigators have suggested approximate mathematical expressions for describing these effects, none of these equations is well suited to pollution modeling studies because each introduces too many additional differential euqations into the system to be solved. For this reason, we set for ourselves the task of developing a new approximation that does not entail multiple equations. The results of our efforts for the case of a bimolecular reaction are represented by Eq. (95) for the generalized case, and by Eq. (99) for the case where the reactants are premixed.

In Section C of Chapter III, we develop for various situations approximate functional forms of the parameters ζ_A and ζ_B, which enter into the generalized closure scheme expressed by Eq. (95). [See Eqs. (113), (121), (124), and (125).] Tests--based on empirical data--of the accuracy of the overall scheme produced excellent results (see Figures 28 and 30).

D. CHAPTER IV

Just as turbulent concentration fluctuations can affect the mean rates of nonlinear chemical reactions, so can subgrid-scale variations in the concentration fields simulated by numerical models. In Chapter IV, we derived a test of the significance of these effects [see Eq. (164)]. When this condition is satisfied, SSV effects are negligible and can be ignored; but, when it is violated, SSV effects may or may not be important, depending on the particular physical situation. To handle these cases, we used the concepts that we employed in Chapter III to treat turbulent concentration fluctuation effects to develop a scheme for parameterizing the SSV influences. In its most general form, this scheme is described mathematically by Eq. (182); and in cases where the reactants are emitted from the same sources, it takes the form of Eq. (186).

We applied the latter to three problems of practical interest:

- A random spatial distribution of point sources, such as building heating emissions.
- A network of streets of arbitrary separation.
- Strong, isolated point and line sources.

From these applications, we derived a dimensionless number μ, defined by Eq. (232), that provides a quantitative measure of the magnitude of SSV effects on nonlinear reactions simulated in urban pollution models. As portrayed in Figure 34, the magnitude of the SSV impact grows as the value of μ increases. Using representative rate constants, source strengths, diffusivities, and the like, we evaluated the parameter μ for several of the important photochemical pollutants (see Figure 35). From this study, we drew the following conclusions:

- The NO-O_3 reaction is the only reaction explicitly treated in the current SAI model that is affected by subgrid-scale concentration variations. In this case, the SSV suppresses the effective rate of ozone depletion.
- Effects from freeways carrying 10^5 or more vehicles per day are significant when the wind is parallel to the freeway, but not when it is perpendicular. Smaller traffic volumes produce proportionately smaller effects, and larger volumes produce proportionately larger ones.
- SSV effects from networks of city streets carrying 10^4 or more vehicles per day are significant when (1) the streets are 150 meters or more apart and (2) the meteorology or source emission rates are in a state of transition. Under steady-state conditions, the SSV effects from uniform street networks become negligible, but those arising from strong isolated sources do not, as described in the second point above.

These findings are only tentative. In future work, we will attempt to corroborate them through numerical experiments.

E. CHAPTER V

An objection frequently raised against grid point diffusion models is that in spreading emissions from point and line sources uniformly throughout the local grid cell, such models produce distorted descriptions of the time concentration field within the immediate vicinity of point and line sources. This effect complicates the tasks of model validation and concentration extrema predictions. In Chapter V, we developed a so-called microscale model that can be used as a subprogram in any grid model of CO, SO_2, or other inert or first-order reactant to resolve the detailed concentration field at a given point. This submodel has been implemented in FORTRAN and tested in several preliminary calculations, as shown in Figure 41.

The chief weaknesses of this microscale model in its present form are its inability to handle pollutants that react nonlinearly and its use of Gaussian kernels. The latter precludes applications to problems of the following types:

- Those in which aerodynamic effects are important, such as downwash in the lee of an elevated roadway or building.
- Calculations of pollutant levels in street canyons.
- Estimations of pollutant levels on a roadway where vehicle wake turbulence is primarily responsible for the initial pollutant dispersal.

For the purpose of developing a microscale model for pollutants that react nonlinearly, we derived a special discrete-time continuous-space diffusion equation [Eq. (333)]. We showed that, when the concentration field is expressed in a series form and line and point sources are represented in the usual delta function forms, the nonlinear microscale model reduces to a simple set of algebraic equations (see the last equation in Chapter V). Tests of this equation and attempts to relax the Gaussian kernel assumption implicit in the current microscale model versions will be undertaken in the next phase of the EPA contract work.

F. CHAPTER VI

In this chapter, we outlined a method whereby the boundary layer model of Deardorff and the equation governing fluid particle dynamics can be combined to simulate buoyant plumes and cooling tower exhaust in the planetary boundary later. The idea was to create an ensemble of particle trajectories from which the probability density function p that enters into the general Lagrangian diffusion equation [Eq. (16)] can be derived. The analyses presented in Chapter VI are intended primarily as an illustration of the technique we are planning to use to simulate buoyant plumes. Further theoretical analyses will be required to develop the final form of the model equations.

VIII FUTURE EFFORTS

The work reported in this volume has attempted both to emphasize the aspects of pollution modeling that are affected by microscale phenomena and to develop mathematical tools for describing these effects. However, two basic aspects of this project are still incomplete:

> A thorough and systematic evaluation of the magnitude of microscale effects in specific problem areas of pollution modeling interest.
> A thorough testing of the accuracies of the various tools that we have developed for treating microscale phenomena.

This last deficiency can be remedied by means of a series of straightforward numerical experiments in which each of the microscale modeling techniques is examined and exercised under controlled conditions. We reported the results of a few such studies--the tests of the closure scheme presented in Chapter III is one example--and others are planned for the next phase of our work. It is the evaluation of the magnitude of the actual microscale problem area itself that will require further planning and careful study. Indeed, the outcome of these evaluations may well alter the future course of our microscale modeling work. We foresee three basic steps in the design of these evaluative studies, as discussed in the sections below.

A. SPECIFICATION OF THE DEGREE OF SPATIAL RESOLUTION REQUIRED IN URBAN POLLUTION MODELING STUDIES

Air quality standards are currently expressed in terms of certain time-averaged concentrations, but no mention is made of the extent of the spatial areas to which these criteria apply. Considering the fact that air quality standards are intended primarily as safeguards of public

health, one can infer that these standards apply to all points where plants or animals vulnerable to pollution damage are found. Thus, for assessments of air quality relative to cropland, livestock, hospital patients, and so forth, or for validations of a diffusion model using data gathered by a pollution monitoring station, an urban-scale pollution model possessing point spatial resolution (as described in Chapter V) should be adequate. However, to assess the pollutant dosages received by highway patrolmen , bus and truck drivers, road maintenance men, and other similar occupational groups, a model should have not only the capability of providing line-integrated concentrations, but also the ability to simulate pollutant concentrations on the sources themselves. The last feature is outside the scope of present urban diffusion models, because on the urban scale highways can be treated as line sources of zero width within which concentrations are infinite. Moreover, on a highway or within a street canyon, the initial dispersion and the rates of fast nonlinear chemical reactions are controlled by vehicle wake turbulence and other aerodynamic effects that are not described by the conventional Gaussian puff and plume models or by the commonly used diffusion equation.

These considerations and the likelihood of observing intolerable highway-integrated pollutant dosages point to the need for special microscale models that can simulate pollutant levels in the motorist's frame of reference. One of the goals of the next phase of our microscale work will be to develop such a model to supplement the capabilities of our urban-scale model. We also plan to examine further the resolution required for various types of modeling studies.

B. EVALUATION OF THE ACTUAL SPATIAL VARIABILITY OF CONCENTRATIONS AT RECEPTOR SITES OF INTEREST

Having established the locations at which pollutant concentration calculations are needed and the degree of spatial resolution required at each site, one is faced next with the following question: Are local

spatial variations in the concentration field so large that an urban-scale model alone is incapable of providing a representative estimate of the true pollutant levels at those sites? In the case of the fixed-point dosage estimates, this question is essentially one of whether local sources are responsible for a significant fraction of the pollution observed; and in the case of the roadway-integrated dosage calculations, the question is whether background concentrations are so small--compared with those on and produced by the roadway--that the urban-scale model itself is needed.

Continuous pollutant measurement data can help resolve these questions. For example, suppose that such a record is available for a ground-level traverse of a city. If moving averages of this record were made to remove all variations that a grid model of that pollutant could resolve, then the residual concentrations would represent the microscale variations in question. If these microscale deviations in populous areas turn out to be only a small fraction of the total concentration observed at those same locations, then urban-scale models alone, i.e., without a supplementary microscale module, should be adequate for assessing urban air quality.

Analyses of the type just described have been performed on unpublished oxidant measurements made by Lamb and Neiburger in the Los Angeles basin in 1967. Preliminary results of this work indicate that significant microscale oxidant variations occur on freeways themselves. However, the amplitude of these perturbations decreases very rapidly with distance, both upwind and downwind, from the freeway. Microscale variations in oxidant levels also occur on heavily traveled city streets and in street canyons, but the amplitudes are less than those observed on freeways. Finally, on all streets with little or no traffic, microscale oxidant variations are negligible.

These preliminary findings emphasize the need for a microscale model applicable to roadways themselves. They also suggest that, except for sites on streets or freeways, it should be possible to obtain accurate fixed-point assessments of oxidant levels using an urban-scale model alone (one in which subgrid-scale concentration variations have been properly parameterized). We plan to continue these empirical studies so that we can determine where the true microscale modeling problems lie.

C. ASSESSMENT OF THE NEED FOR REFINED MICROSCALE TRANSPORT AND DIFFUSION FORMULAS

The foregoing discussions point toward the need for pollution simulation models applicable to both freeway and street canyon environments. Since within such regions transport, diffusion, and concentration fluctuation effects are controlled by vehicle wake turbulence and other aerodynamic effects not normally considered in conventional pollution modeling theories, the question arises of whether refined diffusion formulations will be required to develop the microscale models needed. We have already begun to develop a model of wake turbulence that can be used in conjunction with the theory presented in Chapter III of this report to simulate chemical reactions in the wakes of motor vehicles. We also plan to develop expressions for the kernel p, which enters in the Lagrangian diffusion equation [see, for example, Eq. (295)], to render this equation applicable to situations where aerodynamic effects, such as building and elevated roadway wakes, are important. This work will be described in subsequent phases of our EPA contract effort.

APPENDIX A

FORTRAN PROGRAMS FOR USTAR, DKZ, AND UBAR

USTAR = u_* ROUTINE

U10 = wind speed at anemometer height,
Z10 = anemometer height, in meters,
ZI = inversion height, in meters,
Z0 = surface roughness, in meters,
ZIØVL = ZI/L = stability parameter.

```
   FUNCTION USTAR (U10,Z0,ZIØVL,ZI,Z10)

              IF (ZIØVL)  10,20,30

10              Z10=Z10/ZI
                Z0=Z0/ZI
              IF (Z10.GT.0.025.AND.Z0,LT.0.004) GC TO 15
                X=(1.-15.*Z10+Z0)*ZIØVL)**0.25
                X0=(1.-15.*Z0*ZIØVL)**0.25
                A1=ATAN(X)-ATAN(X0)
                A2=ALOG((X-1.)/(X0-1.))-ALOG((X+1.)/(X0+1.))
                U10BAR=(2.*A1+A2)/0.35
                USTAR=U10/U10BAR
   RETURN
15              IF (Z10.GT.0.3)Z10=0.3
                UU=26.22+153.2*Z10-1428.*Z10**2+5541.*Z10**3
                     -7523.*Z10**4-ALOG(Z0*6.8E6)/0.35
                USTAR=U10/UU
   RETURN
20              USTAR=0.35*U10/ALOG((Z10+Z0)/Z0)
   RETURN
C  EXPRESSIONS BELOW FROM RAGLAND PAPER
30              ZZ=Z10*ZIØVL/ZI
              IF (ZZ.GT.1.0) GO TO 35
                USTAR=0.35*U10/(ALOG((Z10+Z0)/Z0)+5.2*ZZ)
   RETURN
35              USTAR=0.35*U10/(ALOG((Z10+Z0/Z0)+5.2)
   RETURN
   END
```

VERTICAL DIFFUSIVITY ROUTINE

Z = height of level where KZ is wanted,
ZI = inversion height,
USTAR = friction velocity,
F = Coriolis parameter = 2Ω sin Ø,
ZIØVL = ZI/L = stability parameter.

```
      FUNCTION DKZ(Z,ZI,USTAR,F,ZIØVL)

                IF (ZIØVL) 10,20,30

10              Z=Z/ZI
                IF (Z.GT.1.0) GO TO 15
                  DK=-6.934E-3+0.6113*Z+3.297*Z**2
                       -6.442*Z**3+3.153*Z**4
                IF (DK.LT.0.0) DK=0.0
                  DKZ=DK*USTAR*ZI
     RETURN
15              DKZ=0.6123*EXP(-(Z-1.)**2/.02)
     RETURN
20              Z=Z*F/USTAR
                IF (Z.GT.0.45) GO TO 25
                  DK=7.396E-4+6.082E-2*Z+2.532*Z*Z
                       -12.72*Z**3+15.17*Z**4
                  DKZ=DK*USTAR*USTAR/F
   RETURN
25              DK=3.793E-3*EXP(-(Z-0.45)**2/2./4.E-2)
                DKZ=DK*USTAR*USTAR/F
   RETURN
30              XL=ZI/ZIOVL
                IF (Z.GT.085*XL) GO TO 35
                  DKZ=.35*USTAR*Z/(1.+4.7*Z/XL)
   RETURN
35              DKZ=0.0
   RETURN
   END
```

WIND SPEED PROFILE ROUTINE

```
      FUNCTION UBAR (Z,ZO,ZI,ZIØVL,F,USTAR)

                IF (ZIØVL) 10,20,30
   10             ZO=ZO/ZI
                  Z=Z/ZI
                IF (Z,GT.0.025.AND.ZO.GT.0.004) GO TO 14
                  X=(1.-15.*(Z+ZO)*ZIØVL)**0.25
                  XO=(1.-15.*ZO*ZIØVL)**0.25
                  A1=ATAN(X)-ATAN(XO)
                  A2=ALOG((X-1.)/(XO-1.))-ALOG((X+1.)/(XO+1.))
                  UBAR=(2.*A1+A2)*USTAR/0.4
      RETURN
   14           IF (Z.GT.0.3) GO TO 15
                  UU=26.22+153.2*Z-1428.*Z**2+5541.*Z**3
                       -7523.*Z**4-ALOG(ZO*6.8E6)/0.35
                  UBAR=UU*USTAR
      RETURN
   15             UBAR=USTAR*(32.33-ALOG(ZO*6.8E6)/0.35)
      RETURN
   20             ZO=ZO*F/USTAR
                  Z=Z*F/USTAR
                IF (Z.GT.0.055.AND.ZO.LT.0.006) TO TO 25
                  UBAR=USTAR*ALOG((Z+ZO)/ZO)/0.37
      RETURN
   25           IF (Z.GT.0.21) Z=0.21
                  UU=29.82+213.2*Z-1989.*Z**2+8743.*Z**3
                       -14670.*Z**4-ALOG(ZO*1.5E7)/0.37
                  UBAR=UU*USTAR
      RETURN
   30             ZZ=Z*ZIØVL/ZI
                IF (ZZ.GT.1.0) GO TO 35
                  UBAR=USTAR*(ALOG((Z+ZO)/ZO)+5.2*ZZ)/0.37
      RETURN
   35           IF (ZZ.GT.6.0) ZZ=6.0
                  Z=ZZ*ZI/ZIØVL
      WRITE (6,1000)
                  UBAR=USTAR*(ALOG((Z+ZO)/ZO)+5.2)/0.37
      RETURN
 1000 FORMAT (1HO, 'NO ACCURATE WIND DATA ABOVE SURFACE LAYER IN STABLE CASE')
      END
```

Appendix B
DERIVATION OF EQS. (193) AND (195)

APPENDIX B
DERIVATION OF EQS. (193) AND (195)

Equation (193) states that

$$\tilde{A}_I(\underset{\sim}{r},t) = \int_0^t \int p(\underset{\sim}{r} - \underset{\sim}{r}',t,t') \, \tilde{S}(\underset{\sim}{r}',t') \, dt' \, d\underset{\sim}{r}' \quad ,$$

and Eq. (195) reads as follows:

$$\tilde{\tilde{A}}_I^2(\underset{\sim}{r},t) = \int_0^t \int_0^t \iint p(\underset{\sim}{r}-\underset{\sim}{r}',t,t') \, p(\underset{\sim}{r}-\underset{\sim}{r}'',t,t'') \, G(\underset{\sim}{r}',\underset{\sim}{r}'',t',t'') \, dt' \, dt'' \, d\underset{\sim}{r}' \, d\underset{\sim}{r}'' \quad .$$

In the derivation of these equations, we first want to show that

$$\frac{1}{v} \int_{\Delta v(\underset{\sim}{r})} \left[\int p(\underset{\sim}{r} - \underset{\sim}{r}') \, C(\underset{\sim}{r}) \, D(\underset{\sim}{r}') \, d\underset{\sim}{r}' \right] d\underset{\sim}{r} = \int p(\underset{\sim}{r} - \underset{\sim}{r}') \, \overbrace{C(\underset{\sim}{r}) \, D(\underset{\sim}{r}')} \, d\underset{\sim}{r}' \quad , \tag{B-1}$$

where

$$\overbrace{C(\underset{\sim}{r}) \, D(\underset{\sim}{r}')} = \frac{1}{8\Delta x \Delta y \Delta z} \int_{-\Delta x}^{\Delta x} \int_{-\Delta y}^{\Delta y} \int_{-\Delta z}^{\Delta z} C(\underset{\sim}{r} + \underset{\sim}{\varsigma}) \, D(\underset{\sim}{r}' + \underset{\sim}{\varsigma}) \, d\varsigma_z \, d\varsigma_y \, d\varsigma_x \quad . \tag{B-2}$$

Since each of the three integrals in $\int d\underset{\sim}{r}'$ in Eq. (B-1) are similar, we consider the one-dimensional case only, i.e.,

$$\int_{X-\Delta X}^{x+\Delta x} \int p(x'' - x') \, C(x'') \, D(x') \, dx' \, dx'' = \iint_{X-\Delta X}^{x+\Delta x} p(x'' - x') \, C(x'') \, D(X') \, dx'' \, dx' \quad .$$

Let

$$x'' = x - x_1 + x' \Rightarrow dx'' = -dx_1 \quad .$$

Then

$$\int\int_{x'-\Delta x}^{x'+\Delta x} p(x - x_1)\, C(x - x_1 + x')\, D(x')\, dx_1\, dx'$$

$$= \int p(x - x_1) \int_{x_1-\Delta x}^{x_1+\Delta x} C(x - x_1 + x')\, D(x')\, dx'\, dx_1 \quad .$$

Now let

$$\zeta = x' - x_1 \Rightarrow dx' = d\zeta \quad ,$$

$$= \int p(x - x_1) \int_{-\Delta x}^{\Delta x} C(x + \zeta)\, D(x_1 + \zeta)\, d\zeta\, dx_1 \quad .$$

Upon repeating for the y and z integrals, we obtain Eq. (B-1).

Now we want to show that

$$\frac{1}{V} \int_{\Delta V} \left[\iint p(\underset{\sim}{r} - \underset{\sim}{r}')\, p(\underset{\sim}{r} - \underset{\sim}{r}'')\, S(\underset{\sim}{r}')\, S(\underset{\sim}{r}'')\, d\underset{\sim}{r}'\, d\underset{\sim}{r}'' \right] d\underset{\sim}{r}$$

$$= \iint p(\underset{\sim}{r} - \underset{\sim}{r}')\, p(\underset{\sim}{r} - \underset{\sim}{r}'')\, \overbrace{S(\underset{\sim}{r}')\, S(\underset{\sim}{r}'')}\, d\underset{\sim}{r}'\, d\underset{\sim}{r}'' \quad ,$$

where the product mean value in the right integral is defined as in Eq. (B-2). To prove this, we start with the one-dimensional problem as before:

$$\int_{x-\Delta x}^{x+\Delta x} \iint p(\zeta - x')\, p(\zeta - x'')\, S(x')\, S(x'')\, dx'\, dx''\, d\zeta$$

$$= \frac{1}{2\Delta x} \int_{x-\Delta x}^{x+\Delta x} \int p(\zeta - x')\, S(x')\, F(\zeta)\, dx'\, d\zeta \quad , \qquad \text{(B-3)}$$

where $F(\zeta) = p(\zeta - x'')S(x'')dx''$. We can use Eq. (B-1) to write Eq. (B-3) in the form

$$p(\zeta - x')\, S(x')\, F(\zeta)\, dx' \quad , \qquad \text{(B-4)}$$

where

$$\overbrace{S(x')\, F(\zeta)} - \frac{1}{2\Delta x} \int_{-\Delta x}^{\Delta x} \int p(\zeta - x'' + \xi)\, S(x' + \xi)\, S(x'')\, dx''\, d\xi \quad .$$

Now let

$$x'' = x'' + \xi \Rightarrow dx'' = dx'' \quad .$$

Then

$$\overbrace{S(x')\, F(\zeta)} = \frac{1}{2\Delta x} \int_{-\Delta x}^{\Delta x} \int p(\zeta - x'')\, S(x' + \xi)\, S(x'' + \xi)\, dx''\, d\xi$$

$$= \int p(\zeta - x'')\, \overbrace{S(x')\, S(x'')}\, dx'' \quad ,$$

where the tilde average here is defined as in Eq. (B-2). Using this result in Eq. (B-4), we obtain

$$\frac{1}{V}\int_{\Delta V}\left[\iint p(\underset{\sim}{r}-\underset{\sim}{r}')\,p(\underset{\sim}{r}-\underset{\sim}{r}'')\,S(\underset{\sim}{r}')\,S(\underset{\sim}{r}'')\,d\underset{\sim}{r}'\,d\underset{\sim}{r}''\right]d\underset{\sim}{r}$$

$$= \iint p(\underset{\sim}{r}-\underset{\sim}{r}')\,p(\underset{\sim}{r}-\underset{\sim}{r}'')\,\overbrace{S(\underset{\sim}{r}')\,S(\underset{\sim}{r}'')}\,d\underset{\sim}{r}'\,d\underset{\sim}{r}'' \quad .$$

APPENDIX C

FORTRAN LISTINGS OF THE CALC, SIGMAX, AND SIGMAZ FUNCTIONS

```
      SUBROUTINE CALC(XALPHA,YALPHA,ZALPHA,XR,YR,ZR,ISTYPE,XLNGTH,THETA,
     *     DELTAX,DELTAY,DELTAZ,UBAR,VBAR,RESULT)
      COMMON/MICRO/ITRMAX,NCHECK,NSAMP,XSAMP,EPSLON,IX,RITE,SIGFAC
      COMMON/TABLE/ ERFT(1505),EXPT(2005),NERF,NEXP,ERFLIM,DERF,DEXP,
     *     EXPLIM
      DIMENSION TEST(50)
      LOGICAL HALT,RITE,CALL1
                  IOUT = ITRMAX/NCHECK + 1
                  SQ2 = 1.4142135
                  SQ2PI = 2.5066283
                  T2PI = 6.2831853
                  DELTA=0.0
                IF (ISTYPE) 20,10,15
   10             COSTH = COS(THETA)
                  SINTH = SIN(THETA)
                  XLO2 = XLNGTH/2.
                  DELTA=XLO2
                GO TO 20
   15             DXO2 = DELTAX/2.
                  DYO2 = DELTAY/2.
                  DZO2 = DELTAZ/2.
                  DELTV8 = DELTAX*DELTAY*DELTAZ*8.
                  DELTA=DXO2
   20             XMXA = XR-XALPHA
                  YMYA = YR-YALPHA
                  ZMZA = ZR-ZALPHA
                  ZPZA = ZR+ZALPHA
                  ZMZA22 = ZMZA**2/2.
                  ZPZA22 = ZPZA**2/2.
                  R = SQRT(XMXA*XMXA+YMYA*YMYA)
                  VEL = SQRT(UBAR*UBAR+VBAR*VBAR)
                  T0 = R/VEL
                  SIGX=SIGMAX(T0)
                  SGDELT=SIGFAC*SIGX+DELTA
                  TUP=(R+SGDELT)/VEL
                  TLO=(R-SGDELT)/VEL
                  IF (TLO.LT.0.0) TLO=0.0
                  TRNGE = TUP-TLO
                IF(TRNGE.NE.0.0) GO TO 25
              WRITE(6,1030)
                  RESULT=1.0E75
      RETURN
   25             SUM=0.0
            WRITE(6,1028) XMXA,YMYA,ZMZA,VEL,TLO,TRNGE,SIGX
          DO 200 ITROUT=1,IOUT
                  ITRS = ITROUT*NCHECK
        DO 90 ITRINR=1,NCHECK
C     RANDOM ROUTINE
                  IY = IX*65539
                IF (IY) 50,51,51
   50             IY = IY+2147483647+1
   51             ZFL = IY
                  TT=ZFL*0.4656613E-9
                  T=TT*TRNGE+TLO
                  IX = IY
C     END RANDOM ROUTINE
                IF(T.NE.0.0) GO TO 55
                  PXPY=0.0
C     THIS ASSUMES THAT THE RECEPTOR IS NOT ON A SOURCE...THUS PXPYPZ=0.
                GO TO 90
   55             SIGX=SIGMAX(T)
                  SIGX2=SIGX*SIGX
                  SIGZ=SIGMAZ(T)
                  SIGZ2 = SIGZ*SIGZ
                  XUBART=XMXA-UBAR*T
                  YVBART=YMYA-VBAR*T
                  SQ2SGX=SQ2*SIGX
                  SQ2SGZ=SQ2*SIGZ
                IF(ISTYPE) 60,65,70
```

```
   60                EXPARG=(XUBART*XUBART+YVBART*YVBART)/2.0/SIGX2
                     PXPY=EXPO(EXPARG)/SIGX2/T2PI
                   GO TO 75
   65                EX=(XUBART*COSTH+YVBART*SINTH)**2/2./SIGX2
                     A1=(YVBART*COSTH-XUBART*SINTH+XL02)/SQ2SGX
                     A2=(YVBART*COSTH-XUBART*SINTH-XL02)/SQ2SGX
                     PXPY=EXPO(EX)*(ERROR(A1)-ERROR(A2))/2./SQ2PI/SIGX
                   GO TO 75
   70                A1=(XUBART+DX02)/SQ2SGX
                     A2=(XUBART-DX02)/SQ2SGX
                     A3=(YVBART+DY02)/SQ2SGX
                     A4=(YVBART-DY02)/SQ2SGX
                     PXPY=(ERROR(A1)-ERROR(A2))*(ERROR(A3)-ERROR(A4))/
     *                    DELTV8
   75              IF(ISTYPE) 80,80,85
   80                PZ=(EXPO(ZMZA22/SIGZ2)+EXPO(ZPZA22/SIGZ2))/SQ2PI/SIGZ
                     GO TO 90
   85                A=(ZMZA+DZ02)/SQ2SGZ
                     B=(ZMZA-DZ02)/SQ2SGZ
                     C=(ZPZA-DZ02)/SQ2SGZ
                     D=(ZPZA+DZ02)/SQ2SGZ
                     PZ=ERROR(A)-ERROR(B)+ERROR(D)-ERROR(C)
   90                SUM=SUM+PXPY*PZ
                     T22=SUM/FLOAT(ITRS)
                     TEST(ITROUT)=T22
                   IF(ITROUT-NSAMP.LT.0) GO TO 200
C        CONVERGENCE ROUTINE
                     SUMJ=0.0
                     JMIN=ITROUT-NSAMP+1
              DO 150 J=JMIN,ITROUT
  150                SUMJ=SUMJ+TEST(J)
                     SBAR=SUMJ/XSAMP
                     SUMJ=0.0
              DO 160 J=JMIN,ITROUT
  160                SUMJ=SUMJ+(TEST(J)-SBAR)**2
                     HALT=SQRT(SUMJ/XSAMP).LE.EPSLON*SBAR
                   IF(HALT) GO TO 205
  200           CONTINUE
  205                RESULT=TRNGE*T22
                   IF(.NOT.RITE) RETURN
              DO 280 JTEST=1,ITROUT
                     ITRN=JTEST*NCHECK
  280              WRITE(6,1042) ITRN,TEST(JTEST)
        RETURN
 1028   FORMAT(1H0,7E13.5)
 1030   FORMAT(1H0,'RECEPTOR LIES ON A POINT SOURCE')
 1042   FORMAT(1H ,'AFTER',I6,2X,'ITERATIONS--TEST=',E12.5)
        END


        SUBROUTINE TABLET
        COMMON/TABLE/ERFT(1505),EXPT(2005),NERF,NEXP,ERFLIM,DERF,DEXP,
     *          EXPLIM
                     Y=0.0
                     NO2=NERF/2
                     NO2P1=NO2+1
                     DERF=ERFLIM/FLOAT(NO2)
                     ERFT(NO2P1)=0.0
              DO 15 N=1,NO2
                     Y=Y+DERF
                     ERE=ERF(Y)
                     ERFT(NO2P1+N)=ERE
   15                ERFT(NO2P1-N)=-ERE
                     DEXP=EXPLIM/FLOAT(NEXP)
                     X=-DEXP
              DO 20 N=1,NEXP
                     X=X+DEXP
   20                EXPT(N)=EXP(-X)
        RETURN
        END
```

```
      FUNCTION EXPO(ARG)
      COMMON/TABLE/ ERFT(1505),EXPT(2005),NERF,NEXP,ERFLIM,DERF,DEXP,
     *        EXPLIM
                    IE=IFIX(ARG/DEXP)+1
                    IF(IE.GT.NEXP) IE=NEXP
                    EXPO=EXPT(IE)
      RETURN
      END

      FUNCTION ERROR(ARG)
      COMMON/TABLE/ ERFT(1505),EXPT(2005),NERF,NEXP,ERFLIM,DERF,DEXP,
     *        EXPLIM
                    IERF=IFIX((ARG+ERFLIM)/DERF)+1
                    IF(IERF.LT.1) IERF=1
                    IF(IERF.GT.NERF) IERF=NERF
                    ERROR=ERFT(IERF)
      RETURN
      END


      FUNCTION SIGMAZ(T)
      COMMON WSTAR,USTAR,H,F
                    IF(WSTAR) 30,20,10
   10                 TS= T*WSTAR/H
                    IF(TS.GT.0.525) GO TO 15
                      SIGMAZ=H*(0.65*TS-1.89*TS*TS+5.32*TS**3)
      RETURN
   15               IF(TS.GT.1.1) GO TO 16
                      SIGMAZ=H*(-1.111*TS*TS+2.344*TS-0.334   )
      RETURN
   16                 SIGMAZ=H*0.9
      RETURN
   20                 TS=T*F/0.45
                      USTARF=USTAR/F
                    IF(TS.GT.0.05) GO TO 2
                      SIGMAZ=0.45*USTARF*0.64*TS
      RETURN
   21               IF(TS.GT.0.175) GO TO 22
                      SIGMAZ=0.45*USTARF*(0.01+0.4*TS)
      RETURN
   22                 SIGMAZ=0.45*USTARF*(0.058+0.129*TS)
                      IF(SIGMAZ.GT.0.31*USTARF) SIGMAZ=0.31*USTARF
C     THIS LIMIT DUE TO MAX(SIGZ/H)=.9 IN UNSTABLE CASE AND H=.35USTAR/F I
C          NEUTRAL CASE.
      RETURN
   30             WRITE(6,1003)
                    SIGMAZ=0.1*(USTAR/F)
      RETURN
 1003 FORMAT(1H0,'NO SIGMA DATA FOR STABLE CASE')
      END

      FUNCTION SIGMAX(T)
      COMMON WSTAR,USTAR,H,F
                    IF(WSTAR) 30,20,10
   10                 TS=T*WSTAR/H
                    IF(TS.GT.0.05) GO TO 15
                      SIGMAX=2.2*TS*H
      RETURN
   15                 SIGMAX=H*(0.045+1.307*TS)
      RETURN
   20                 TS=T*F/0.45
                    IF(TS.GT.0.1) GO TO 22
                      SIGMAX=(.45*USTAR/F)*1.85*TS
      RETURN
   22                 SIGMAX=(.45*USTAR/F)*(0.1+0.92*TS)
      RETURN
   30             WRITE(6,1003)
                    SIGMAX=0.5*(USTAR/F)
      RETURN
 1003 FORMAT(1H0,'NO DATA FOR STABLE CASE')
      END
```

APPENDIX D

THE MONTE CARLO TECHNIQUE USED BY THE CALC SUBPROGRAM

APPENDIX D
THE MONTE CARLO TECHNIQUE USED BY THE CALC SUBPROGRAM

We propose to use a Monte Carlo technique to evaluate the integrals entering in Eqs. (302), (305), and (306). The technique is best described by the mathematical analyses that are required to prove its validity.

Consider a function f(t) defined in the interval $t_0 < t \leq t_0 + T$ as shown in Figure D-1. Suppose we pick a sequence of numbers t_i, $i = 1,2,\ldots,n$, at random in the interval $t_0 \leq t \leq t_0 + T$. We choose the numbers by a random process such that each number in the interval is equally likely to occur. For each number t_i in the sequence, there is a corresponding unique number f_i:

$$f_i = f(t_i 0 \quad .$$

Thus, the probability of observing a value f in the range $f_i < f \leq f_i + \ f$ is by definition

$$p(f_i) = \text{prob}(f_i < f \leq f_i + \ f) = \frac{m(e_i)}{T} \quad , \qquad \text{(D-1)}$$

where $m(e_i)$ is the measure of the set e_i in which $f_i < f(t) \leq f_i + \ f$ (see Figure D-2) in the domain (t_0, t_0+T).

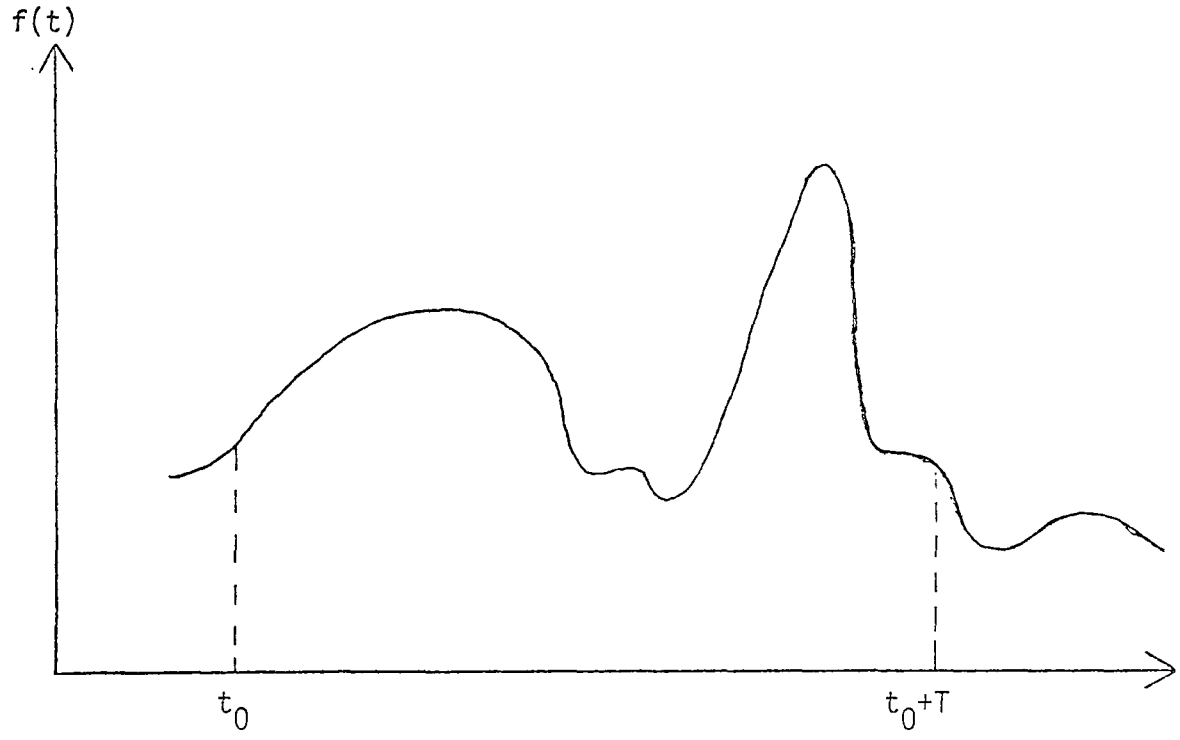

FIGURE D-1. A FUNCTION f(t) DEFINED IN THE INTERVAL $t_0 < t \leq t_0 + T$

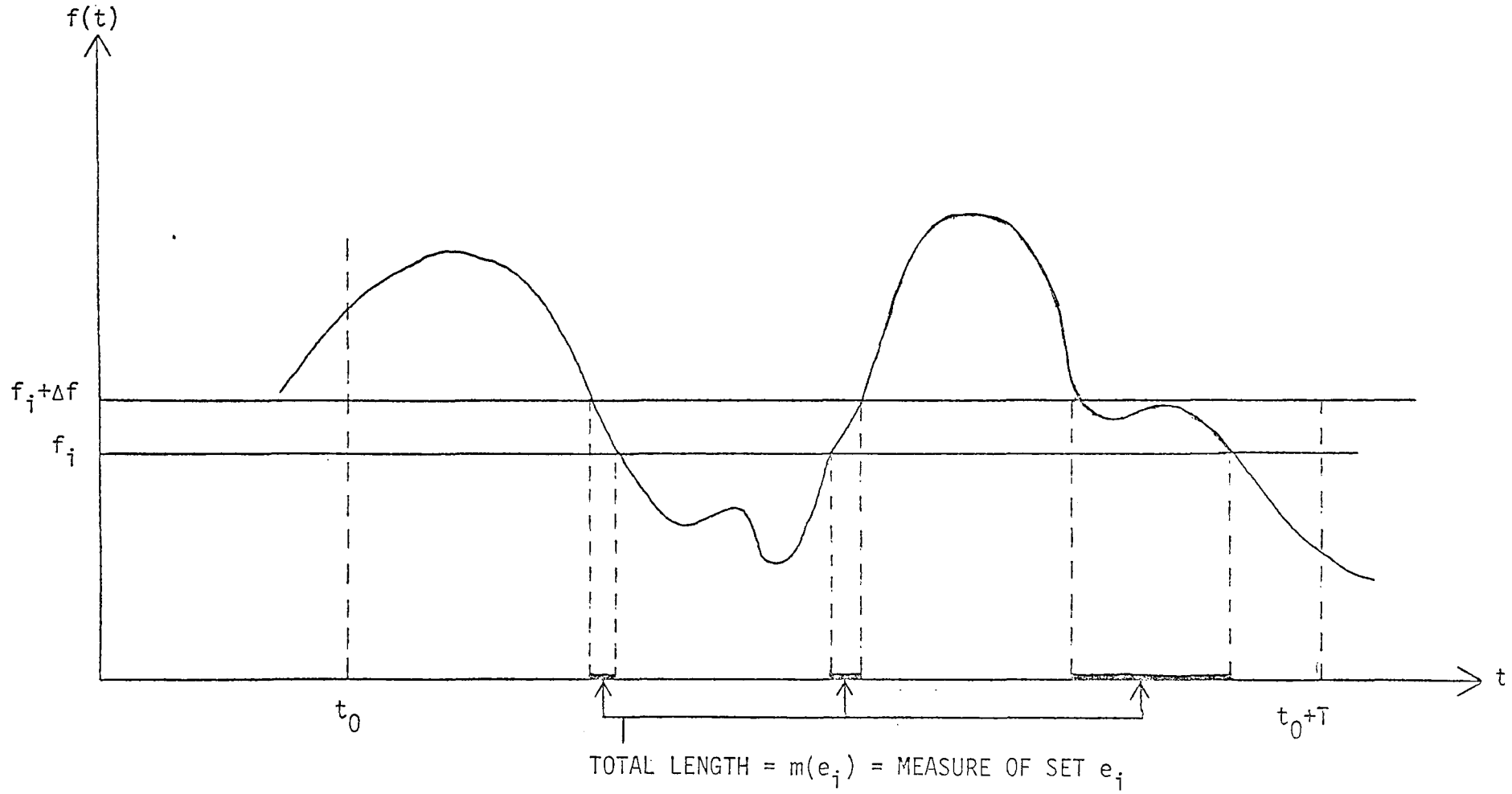

FIGURE D-2. ILLUSTRATION OF THE PROBABILITY THAT f(t) OCCURS IN THE INTERVAL f_i TO $f_i + \Delta f$ OVER THE TIME t_0

Now, by definition of the Lebesque integral, we have

$$\int_{t_0}^{t_0+T} f(t)\,dt = \lim_{\Delta f \to 0} \sum_j f_j m(e_j) \quad , \tag{D-2}$$

where the summation is over all intervals f_j in the range $-\infty < f < \infty$. Let the mean value of the random sequence $f(t_i)$, $i = 1,2,\ldots,m$, generated above be noted by

$$\overline{f}_n = \frac{1}{n} \sum_{i=1}^{n} f(t_i) \quad . \tag{D-3}$$

Then by definition the ensemble mean value of the random variable $f(t_i)$ is

$$\overline{f} = \lim_{n \to \infty} \overline{f}_n = \lim_{\Delta f \to 0} \sum_j f_j p(f_j) \quad , \tag{D-4}$$

where $p(f_j) = \text{prob}(f_j < f \leq f_j + \Delta f)$ and the summation is over all intervals f_j in the infinite range of f values. From Eqs. (D-1) and (317), we obtain

$$\overline{f} = \lim_{\Delta f \to 0} \sum_j f_j \frac{m(e_j)}{T} \quad .$$

Comparing this with Eq. (D-2), we see finally that

$$\int_{t_0}^{t_0+T} f(t)\,dt = T \lim_{n \to \infty} \left[\frac{1}{n} \sum_{i=1}^{n} f(t_i) \right] \quad . \tag{D-5}$$

This result means that we can approximate the integral of any function $f(t)$ over any domain by simply multiplying the length of the domain T by the mean value of the random variable $f(t_i)$ formed by picking points t_i at random in the domain of integration.

The speed of execution of this Monte Carlo integration technique can be increased greatly by tabulating the exponential and error functions that appear in the integrands of several of the integrals of interest. That is, rather than use the EXP and ERF FORTRAN routines to compute the function value each time it is required, we create a table of the values of each function initially and look the value up in the table as needed. This procedure has been found to reduce computation time by about one-third. The subroutines and functions TABLET, EXPO, and ERROR listed in the CALC program replace the EXP and ERF functions.

APPENDIX E
DERIVATION OF $\hat{\Gamma}_{AB}$, $\hat{\Gamma}_{A}$, AND $\hat{\Gamma}_{B}$ FROM MULTIJET REACTOR DATA AND TOOR'S THEORY

APPENDIX E
DERIVATION OF $\hat{\Gamma}_{AB}$, $\hat{\Gamma}_{A}$, AND $\hat{\Gamma}_{B}$ FROM MULTIJET REACTOR DATA AND TOOR'S THEORY

The purpose of this appendix is to give a brief description of the multijet reactor data and how we used the data to calculate the inert correlation functions ($\hat{r}_{AB}$, $\hat{r}_{A}$, and $\hat{r}_{B}$) used in Chapter III.

As noted in Chapter III, Toor (1962) developed a theory that relates the concentration statistics of two species undergoing a very rapid irreversible reaction in a turbulent mixer to the concentrations of inert species in an identical mixer. To test the theory experimentally, Vassilatos and Toor (1965) designed an ideal one-dimensional tubular reactor having a head made of some 100 small nozzles (Figure E-1). Reactants are fed through alternate jets to simulate a cross-sectionally uniform concentration profile. A modified version of this reactor was later made and used by Mao (1969). Extensive measurements covering a wide range of reaction speeds were made in these reactors. However, the results provided only a partial test of Toor's theory because no inert mixing data were taken. Later measurements of inert concentration statistics in the same reactors by McKelvey (1968) and Zakanycz (1971) have corroborated Toor's theory.

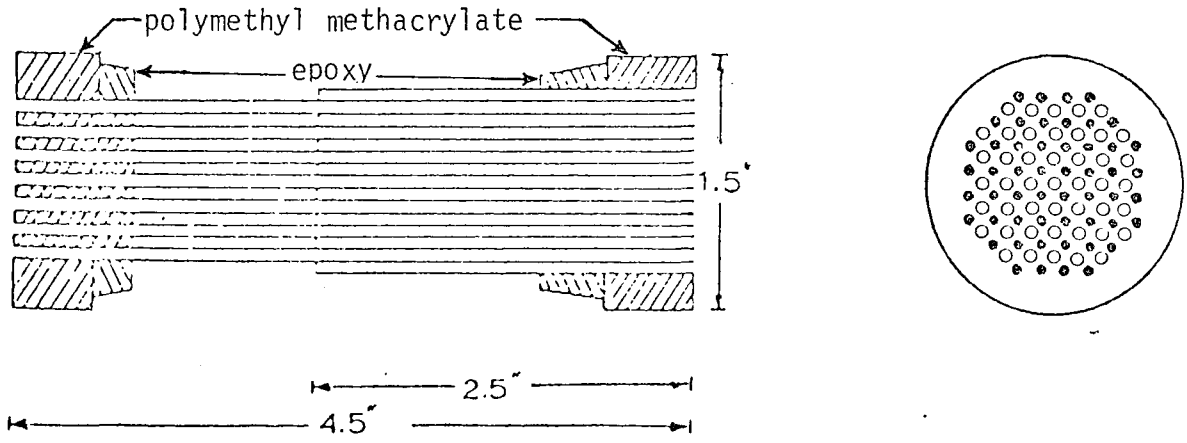

FIGURE E-1. SIDE AND END VIEWS OF TUBULAR REACTOR

The theory presented by Toor (1962) states that for very rapid reactions with stoichiometric feed,

$$F_\infty(x) \equiv \frac{\langle A(x)\rangle}{\langle A(x_0)\rangle} = \frac{\langle A_I' B_I'(x)\rangle^{\frac{1}{2}}}{\langle A_I' B_I'(x_0)\rangle^{\frac{1}{2}}} \qquad \text{(E-1)}$$

where $x = \langle u(x)\rangle t$ is the axial position along the reactor length and x_0 is some reference point where the reactor has reached the state of cross-sectional homogeneity. Toor and his coworkers designed the multijet reactor so that homogeneity is achieved virtually at the inlet of the reactor. Thus, we set $x_0 = 0$. Toor (1969) further derived a relationship between the concentration fluctuations of two unpremixed inert species fed into this reactor:

$$\frac{\langle A_I' B_I'(x)\rangle}{\langle A_I' B_I'(0)\rangle} = \frac{\langle A_I'^2(x)\rangle}{\langle A_I'^2(0)\rangle} = \frac{\langle B_I'^2(x)\rangle}{\langle B_I'^2(0)\rangle} \quad . \qquad \text{(E-2)}$$

Since the concentration field is assumed to be cross-sectionally homogeneous, the initial concentration fluctuations can be obtained theoretically by cross-sectional averaging. If one-half of the nozzles feed inert species A and the other half feed B (which is true for Mao's reactor and approximately true for Vassilatos'), it is easy to show that

$$\begin{aligned} \langle A_I'^2(0)\rangle &= \langle A_I\rangle^2 \\ \langle B_I'^2(0)\rangle &= \langle B_I\rangle^2 \quad . \end{aligned} \qquad \text{(E-3)}$$

Since the species are not premixed,

$$\langle A_I' B_I'(0)\rangle = -\langle A_I\rangle \langle B_I\rangle \quad . \qquad \text{(E-4)}$$

Combining Eqs. (E-1) through (E-4), we obtain

$$\Gamma_{AB}(x) \equiv \frac{\langle A_I B_I(x)\rangle}{\langle A_I\rangle\langle B_I\rangle} = 1 + \frac{\langle A_I' B_I'(x)\rangle}{\langle A_I\rangle\langle B_I\rangle} = 1 - F_\infty^2(x) \qquad \text{(E-5)}$$

$$\Gamma_A(x) \equiv \frac{\langle A_I^2(x)\rangle}{\langle A_I\rangle^2} = 1 + \frac{\langle A_I'^2(x)\rangle}{\langle A_I\rangle^2} = 1 + F_\infty^2(x) = \Gamma_B \qquad \text{(E-6)}$$

where $\langle A_I\rangle$ and $\langle B_I\rangle$ are independent of x due to homogeneity. Equations (E-5) and (E-6) are used to convert $F_\infty(x)$, the concentration decay of very rapid stoichiometric reactions, to the inert concentration correlations $\hat{\Gamma}_{AB}$, $\hat{\Gamma}_A$, and $\hat{\Gamma}_B$.

Conversion data of reactions with rate constants greater than 10^7 l/g·mole·sec are not distinguishable from one another in the chemical reactors of Vassilatos and Mao. Therefore, these data represent very fast, diffusion-limited reactions and may be used for F_∞ in Eqs. (E-5) and (E-6). Figures E-2, E-3, and E-4 show the data of F_∞ for three different flow conditions. Since data do not extend to the inlet of the reactor, we used a cubic spline function to extrapolate the first data point back to the reactor inlet. The reader is referred to Shu (1975) for further information regarding these data.

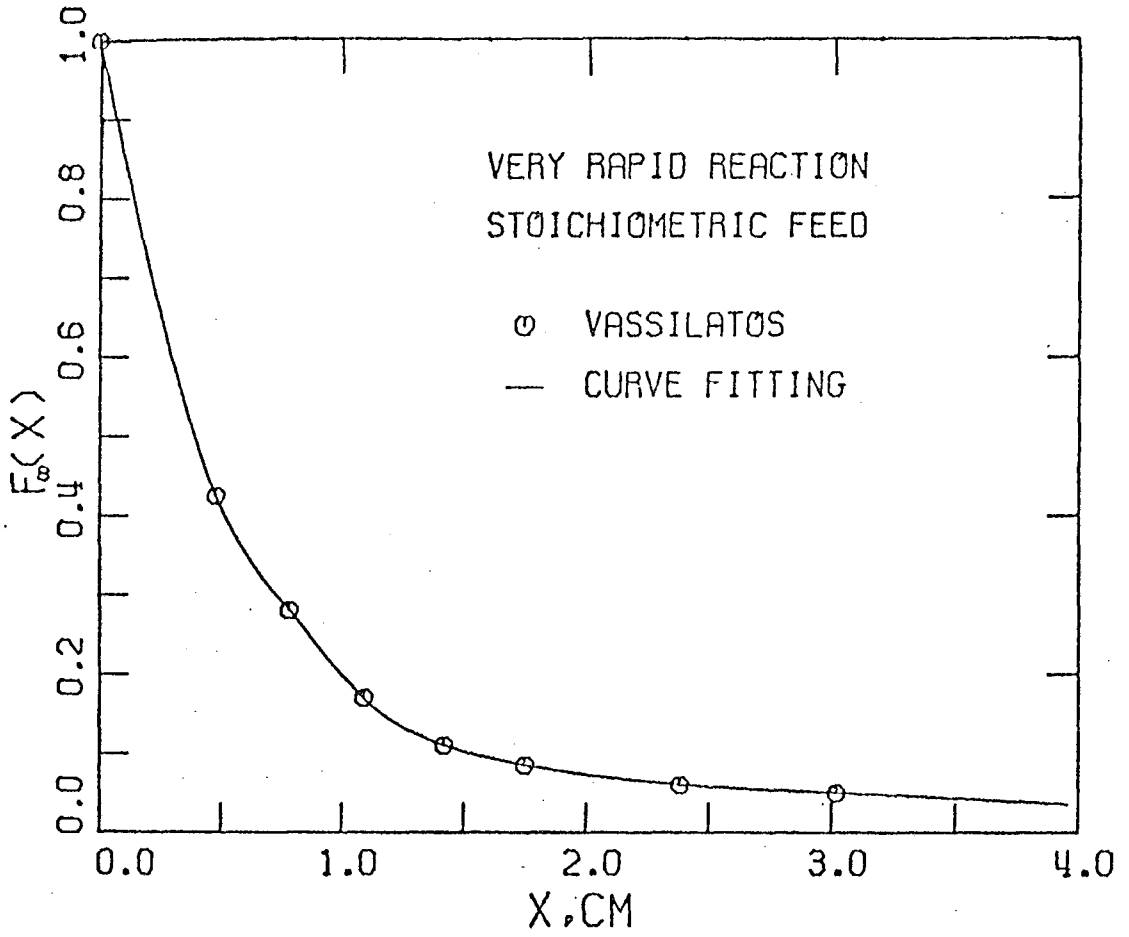

FIGURE E-2. DECAY OF CONCENTRATION WITH DISTANCE IN VASSILATOS' REACTOR

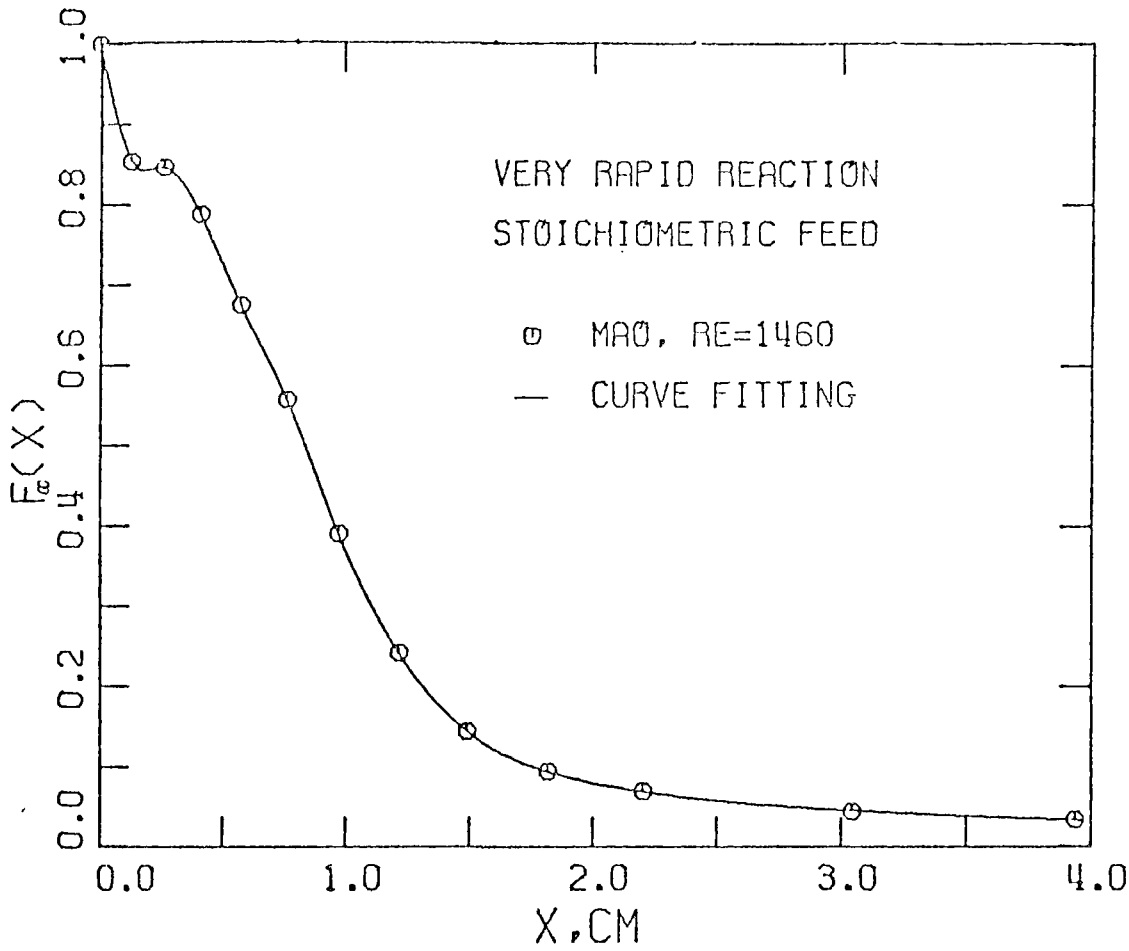

FIGURE E-3. DECAY OF CONCENTRATION WITH DISTANCE IN MAO'S REACTOR

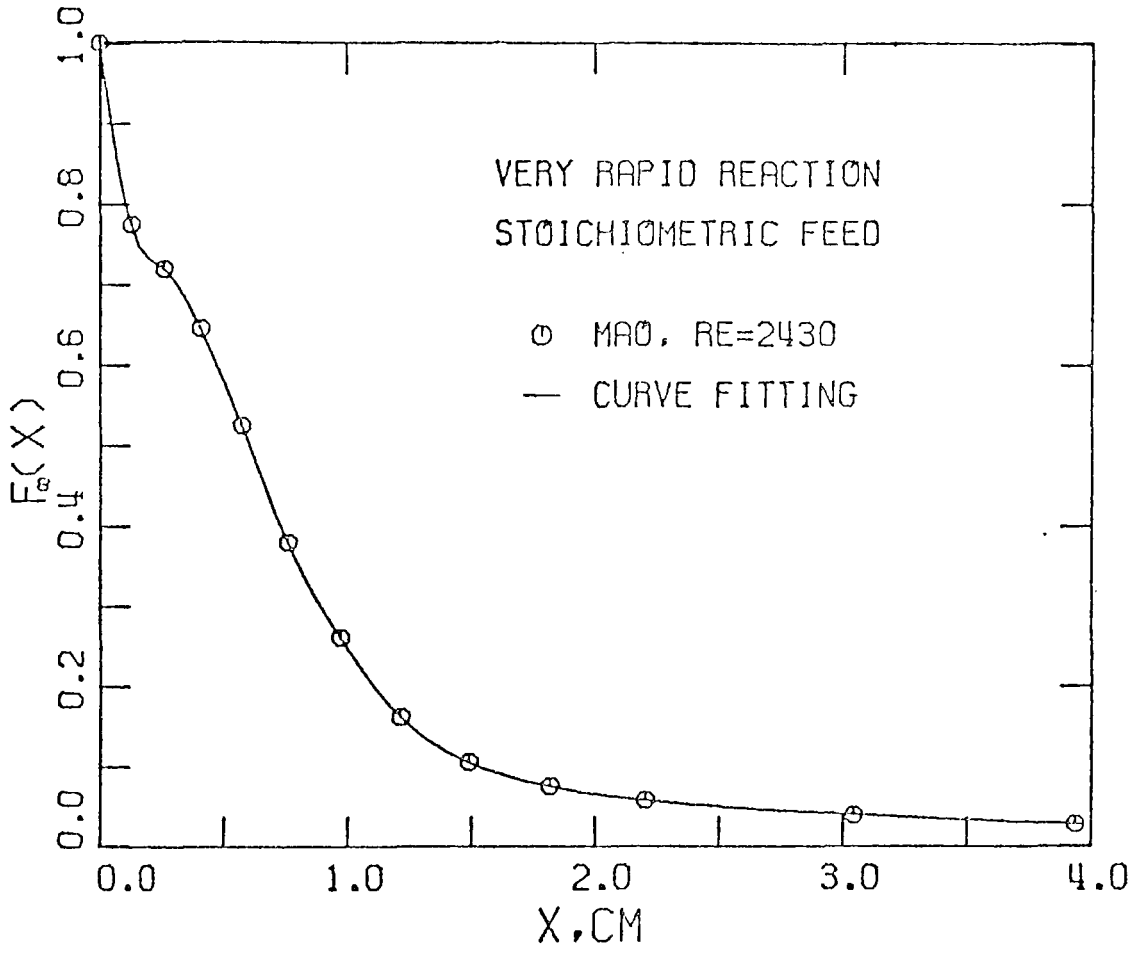

FIGURE E-4. DECAY OF CONCENTRATION WITH DISTANCE IN MAO'S REACTOR

APPENDIX F

ESTIMATION OF THE ORDER OF MAGNITUDE OF THE TIME SCALE OF DECAY OF $\overline{A''^2}$

APPENDIX F

ESTIMATION OF THE ORDER OF MAGNITUDE OF THE TIME SCALE OF DECAY OF $\widetilde{A''^2}$

When the first term on the righthand side of Eq. (156) is expressed in the form (157), we find that, in the absence of any mean transport, chemical decay, or sources of subgrid-scale concentration fluctuations, an initially present mean square fluctuation field $\widetilde{A''^2}$ decays according to

$$\frac{\partial \widetilde{A''^2}}{\partial t} = \frac{-2K_\lambda}{\lambda^2} \widetilde{A''^2} \quad , \tag{F-1}$$

where λ is some length scale and K_λ is the eddy diffusivity. In other words, the time scale of decay of $\widetilde{A''^2}$ due to turbulent diffusion is of the order of

$$T \sim \frac{\lambda^2}{K_\lambda} \quad . \tag{F-2}$$

We wish to show from an estimate of T that λ is of the order of the size of the grid mesh upon which the mean concentration field $\widetilde{A}$ is defined.

For simplicity we consider a one-dimensional problem governed by the equation

$$\frac{\partial c}{\partial t} = K \frac{\partial^2 c}{\partial z^2} + \delta(z)\delta(t) \tag{F-3}$$

with initial and boundary conditions

$$c(z,0) = 0 \tag{F-4a}$$

$$\lim_{z \to \pm\infty} c(z,t) = 0 \quad , \tag{F-4b}$$

where K is the turbulent diffusivity, assumed to be a constant, and δ is the delta function. The solution of (F-3) and (F-4a,b) is found to be

$$c(z,t) = (4\pi Kt)^{-1/2} \exp\left(-\frac{z^2}{4Kt}\right) \quad . \tag{F-5}$$

Now let

$$\tilde{c}(z,t) \equiv \frac{1}{2\Delta z} \int_{z-\Delta z}^{z+\Delta z} c(z',t)dz' \quad . \tag{F-6}$$

Averaging (F-5) in this manner we obtain

$$\tilde{c}(z,t) = \frac{1}{4\Delta z} \left[\text{erf}\left(\frac{z+\Delta z}{\sqrt{4Kt}}\right) - \text{erf}\left(\frac{z-\Delta z}{\sqrt{4Kt}}\right) \right] \quad , \tag{F-7}$$

where

$$\text{erf}(x) = \frac{2}{\sqrt{\pi}} \int_0^x e^{-\lambda^2} d\lambda$$

is the standard error function. Note that Eq. (F-7) is the solution of the equation obtained by averaging Eq. (F-3), that is

$$\frac{\partial \tilde{c}}{\partial t} = K \frac{\partial^2 \tilde{c}}{\partial z^2} + \frac{1}{2\Delta z} U(z)\delta(t) \quad , \tag{F-8}$$

where

$$U(z) \begin{cases} = 1, & -\Delta z \leq z < \Delta z; \\ = 0, & \text{otherwise.} \end{cases}$$

Let us assume that Eq. (F-8) is a grid model representation of Eq. (F-3) and that $\tilde{c}$, as given by Eq. (F-7), is the model's output. The subgrid-scale variations are therefore [from Eqs. (F-5) and (F-7)]

$$c''(z,t) = \frac{1}{\sqrt{4\pi Kt}} \exp\left(-\frac{z^2}{4Kt}\right) - \frac{1}{4\Delta z}\left[\text{erf}\left(\frac{z+\Delta z}{\sqrt{4Kt}}\right) - \text{erg}\left(\frac{z-\Delta z}{\sqrt{4Kt}}\right)\right] \quad . \quad \text{(F-9)}$$

We can see from this expression that the amplitude of the SSV decreases as the discretization interval Δz in the grid model is made smaller. Moreover, for fixed Δz the SSV in this example decrease with time.

To obtain a more concise description of the relative magnitude of the subgrid-scale variation c", we note first that c" is largest at the source location (i.e., z = 0). Thus, the maximum amplitude of c" relative to $\tilde{c}$ can be expressed by

$$\rho(t) \equiv \frac{c''(0,t)}{\tilde{c}(0,t)} \quad . \quad \text{(F-10)}$$

From the expressions for c" and $\tilde{c}$ we obtain

$$\rho(t) = \frac{2}{\sqrt{\pi}}\left[\sigma^* \text{erf}\left(\frac{1}{\sigma^*}\right)\right]^{-1} - 1 \quad , \quad \text{(F-11)}$$

where

$$\sigma^* = \frac{\sqrt{4Kt}}{\Delta z} \quad . \quad \text{(F-12)}$$

In words, σ^* is the approximate half-width of the pollutant cloud, normalized by the grid mesh size Δz, at time t. It is evident from Eq. (F-11) that σ^*

is the key parameter which determines the relative size of the SSV in this instance. On evaluating Eq. (F-11) for several values of σ^*, we obtain $\rho = 10$ when $\sigma^* = 0.1$; $\rho = 0.34$ when $\sigma^* = 1$; and $\rho = 0.08$ when $\sigma^* = 2$. Thus, the time scale of decay of ρ is of the order

$$T_\rho \sim \frac{4\Delta z^2}{4K} = \frac{\Delta z^2}{K} \quad . \tag{F-13}$$

Now since $\tilde{c}$ (0,t), which enters in the definition of ρ [in Eq. (F-10)], also decays with time, the decay rate of c"(0,t) can be no faster than that of ρ. Furthermore, since c"(0,t) represents the maximum amplitude of $\tilde{c}$"(z,t), it is not unreasonable to assume that the time scale of decay of $c"^2$ is comparable to that of c"(0,t). From all of these considerations we conclude that

$$T \sim T_\rho \sim \frac{\Delta z^2}{K} \quad , \tag{F-14}$$

and hence that the length scale λ, defined in the beginning of this appendix, is of the order of Δz.

REFERENCES

Batchelor, G. K. (1967), "Small Scale Variation of Convected Quantities Like Temperature in a Turbulent Fuel, Part I," J. of Fluid Mech., Vol. 5, p. 113.

_____ (1950), "Application of the Similarity Theory of Turbulence to Atmospheric Diffusion," Quart. J. of the Royal Meteor. Soc., Vol. 76, pp. 133-146.

Bendat, J. S., and A. G. Piersol (1968), "Measurement and Analysis of Random Data," John Wiley and Sons, New York, New York.

Briggs, G. A. (1968), in Meteorology and Atomic Energy, David Slade, ed.

Chen, W. H., and J. H. Seinfeld (1974), "Estimation of Spatially Varying Parameters in Partial Differential Equations," Int. J. Control, Vol. 15, pp. 487-495.

Deardorff, J. (1972), "Numerical Investigation of Neutral and Unstable Planetary Boundary Layers," J. Atmos. Sci., Vol. 29, pp. 91-115.

_____ (1970), "A Three-Dimensional Numerical Investigation of the Idealized Planetary Boundary Layer," Geophys. Fluid Dyn., Vol. 1, pp. 377-410.

Donaldson, C. duP., et al. (1973), "Atmospheric Turbulence and the Dispersal of Atmospheric Pollutants," Report EPA-R4-73-016a-c, Environmental Protection Agency, Research Triangle Park, North Carolina.

Donaldson, C. duP. (1969), J. of AIAA, Vol. 7, pp. 271-278.

Golder, D. (1972), "Relations Among Stability Parameters in the Surface Layer," Boundary Layer Meteorology, Vol. 3, pp. 47-58.

Hanjalic, K., and B. E. Launder (1972), "A Reynolds Stress Model of Turbulence and Its Application to Thin Shear Flows," J. Fluid Mech., Vol. 52, pp. 609-638.

Hilst, G. R., et al. (1973), "A Coupled Two-Dimensional Diffusion and Chemistry Model for Turbulent and Inhomogeneously Mixed Reaction Systems," Report RA-73-016C, Environmental Protection Agency, Research Triangle Park, North Carolina.

Hinze, J. O. (1959), Turbulence, McGraw-Hill Book Company, New York, New York.

Kreith, F. (1966), Principles of Heat Transfer, Second Edition (International Textbook Company, Scranton, Pennsylvania).

Lamb, R. G. (1974), "Lagrangian Analysis of a Passive Scalar in Turbulent Fluid, Part 1: General Theory," J. Fluid Mech., submitted for publication.

_____ (1971), "Numerical Modeling of Urban Air Pollution" PhD. dissertation. Department of Meteorology, University of California, Los Angeles, California.

Lamb, R. G. (1973), "Note on the Application of K-Theory to Diffusion Problems Involving Nonlinear Chemical Reactions," Atmos. Env., Vol. 7, pp. 257-263.

Lamb, R. G., and J. H. Seinfeld (1973), "Mathematical Modeling of Urban Air Pollution--General Theory," Environ. Sci. Technol., Vol. 7, pp. 253-261.

Lamb, R. G., and M. Neiburger (1971), "An Interim Version of a Generalized Urban Air Pollution Model," Atmos. Environ., Vol. 5, pp. 239-264.

Lettau, H. H. (1959), "Wind Profile, Surface Stress, and Geostrophic Drag Coefficients in the Atmospheric Surface Layer," Advances in Geophysics, Vol. 6, pp. 241-256.

Lions, J. L. (1971), Optimal Control of Systems Governed by Partial Differential Equations (Springer-Verlag, New York, New York) 396 pages.

Lumley, J. L. (1970), "Toward a Turbulent Constitutive Relation," J. Fluid Mech., Vol. 41, pp. 413-434.

Lumley, J. L., and B. Khajeh-Nouri (1973), "Computational Modeling of Turbulent Transport," Second IUTAM-IUGG Symposium on Turbulent Diffusion and Environmental Pollution, Charlottesville, Virginia.

Mao, K. (1969), "Chemical Reactions with Turbulent Mixing," Ph.D. thesis, Carnegie-Mellon University, Pittsburg, Pennsylvania (173 pages).

McElroy, J. L. (1969), "A Comparative Study of Urban and Rural Dispersion," J. Appl. Meteor., Vol. 8, pp. 19-31.

McKelvey, K. N. (1968), "Turbulent Mixing with Chemical Reactions," Ph.D. thesis, Ohio State University, Columbus, Ohio (123 pages).

Monin, A. S., and A. M. Yaglom (1971), Statistical Fluid Mechanics, MIT Press, Cambridge, Massachusetts.

O'Brien, E. E. (1968), "Closure for Stochastically Distributed Second-Order Reactants," Physics of Fluids, Vol. 11, p. 1883.

Orszag, S., and M. Israeli (1974), "Numerical Simulation of Viscous Incompressible Flows," Ann. Rev. of Fluid Mech., Vol. 6, p. 281.

Ragland, K. W. (1973), "Multiple Box Model for Dispersion of Air Pollutants from Area Sources," Atmos. Environ., Vol. 7, pp. 1017-1032.

Shir, C. C., and L. J. Shieh (1973), A Generalized Urban Air Pollution Model and Its Application to the Study of SO_2 Distributions in the St. Louis Metropolitan Area," Report RJ 1227, IBM, San Jose, California.

Shu, W. R. (1975), Ph.D. dissertation, in progress.

Toor, H. L. (1969) Ind. Eng. Chem. Fundam., Vol. 8, pp. 655-659.

_____ (1962), "Mass Transfer in Dilute Turbulent and Nonturbulent Systems with Rapid Irreversible Reactions and Equal Diffusivities," A.I.Ch.E. Journal, Vol. 8, pp. 70-78.

Turner, D. B. (1969), "Workbook of Atmospheric Dispersion Estimates," Publication AP-26, Environmental Protection Agency, Research Triangle Park, North Carolina.

Vassilatos, G., and H. L. Toor (1965), "Second-Order Chemical Reaction in a Nonhomogeneous Turbulent Fluid," A.I.Ch.E. Journal, Vol. 11, pp. 666-673.

Zakanycz, S. (1971), "Turbulence and the Mixing of Binary Gases," Ph.D. thesis, Ohio State University, Columbus, Ohio (172 pages).

TECHNICAL REPORT DATA
(Please read Instructions on the reverse before completing)

EPA-600/4-76-016 c	2.	3. RECIPIENT'S ACCESSION NO.
4. TITLE AND SUBTITLE: CONTINUED RESEARCH IN MESOSCALE AIR POLLUTION SIMULATION MODELING. VOLUME III. Modeling of Microscale Phenomena		5. REPORT DATE: May 1976 6. PERFORMING ORGANIZATION CODE
7. AUTHOR(S): R. G. Lamb		8. PERFORMING ORGANIZATION REPORT NO.: EF75-25
9. PERFORMING ORGANIZATION NAME AND ADDRESS: SYSTEMS APPLICATIONS, INC. 950 NORTHGATE DRIVE SAN RAFAEL, CALIFORNIA 94903		10. PROGRAM ELEMENT NO.: 1AA009 11. CONTRACT/GRANT NO.: 68-02-1237
12. SPONSORING AGENCY NAME AND ADDRESS: ENVIRONMENTAL SCIENCES RESEARCH LABORATORY OFFICE OF RESEARCH AND DEVELOPMENT U.S. ENVIRONMENTAL PROTECTION AGENCY RESEARCH TRIANGLE PARK, N.C. 27711		13. TYPE OF REPORT AND PERIOD COVERED: FINAL REPORT 6/74-6/75 14. SPONSORING AGENCY CODE: EPA-ORD

15. SUPPLEMENTARY NOTES

16. ABSTRACT

This report develops mathematical techniques that influence the development of urban air pollution but are not resolvable by grid networks used in airshed simulation models. These phenomena include turbulence-generated fluxes of pollutants, turbulence-induced fluctuations in the contaminant concentrations, and subgrid-scale variations in the mean concentration distribution. In addition, the report examines the problem of resolving the spatial details that exist in the mean concentration fields in the vicinity of point and line sources. The analysis concludes with a discussion of the problem of accounting for pollutant dispersion effects caused by buoyancy forces in hot stack exhausts.

17. KEY WORDS AND DOCUMENT ANALYSIS

a. DESCRIPTORS	b. IDENTIFIERS/OPEN ENDED TERMS	c. COSATI Field/Group
*Air Pollution *Mathematical Models *Atmospheric Diffusion *Chemical Reactions		13B 14B 04A 07D

18. DISTRIBUTION STATEMENT: RELEASE TO PUBLIC	19. SECURITY CLASS *(This Report)*: UNCLASSIFIED	21. NO. OF PAGES: 232
	20. SECURITY CLASS *(This page)*: UNCLASSIFIED	22. PRICE

EPA Form 2220-1 (9-73)